Probing Supersymmetry signatures at the Large Hadron Collider.

A Thesis

Submitted to the
Tata Institute of Fundamental Research,Mumbai
for the degree of Doctor of Philosophy
in Physics

by

Dipan Sengupta

School of Natural Sciences,
Tata Institute of Fundamental Research,
1, Homi Bhabha Road, Mumbai-400 005, India

Declaration.

This thesis is a presentation of my original research work. Wherever contributions of others are involved, every effort is made to indicate this clearly, with due reference to the literature and collaborative research with discussions.

This work was done under the guidance of Prof. Monoranjan Guchait at the Tata Institute of Fundamental Research,Mumbai.

[Dipan Sengupta]

In my capacity as supervisor of the candidate's thesis, I certify that the above statements are true to the best of my knowledge.

[Monoranjan Guchait]

Dedicated to my parents.

"A multitude of rulers is not a good thing. Let there be one ruler, one king."
The Iliad, Homer.

Acknowledgements

This thesis owes its gratitude to a multitude of people whose help and goodwill has carried me forward through this arduous but enjoyable journey. First of all I would like to thank the Tata Institute of Fundamental Research in general for the scintillating atmosphere, both academically and non academically, and for the wonderful facilities which I have been privileged to utilize during the time of my graduate school. No institute can boast such a wonderful campus on the shores of the Arabian sea, and undoubtedly that lifts the gloom engulfing you in hard times. A novella titled " The life and times in TIFR" would have been an apt way of describing the most rewarding years of my life till date.

The constant support of my family has been one of the primary reasons for me to carry on during this time. Unfortunately my mother did not live long enough to see this whole process completed; however I am sure she would have been extremely glad to witness the graduation. My father has defied all odds and mental trauma during this period to stand by my side, and this thesis is dedicated to my parents for their staunch and unconditional support.

This thesis would not have been possible without the constant support of my supervisor Prof. Monoranjan Guchait, who has stood thick and thin by my side, and tolerated my incompetence for a long time, and did not give up on me. I was advised that the relationship of a supervisor and his student is complex, and has to be handled with care. However I did not experience this burden, as I never felt out of sync. If anything, I have taken advantage most of the time, having felt the comfort of doing so. I have come to realize that the job was a supervisor is one of the hardest tasks in academics, and I can safely say that he did a splendid job with me.

All my collaborators during the period of my graduate school have been wonderfully supportive of me; and my heartfelt thanks to all of them for all the help to ensure my progress as a researcher. I have had the privilege of working with some of the stellar names of particle physics in India and abroad, and I take this opportunity to thank Prof. D.P. Roy (HBCSE, Bombay), Prof. Rohini Godbole (IISC, Bangalore), Prof. Sreerup Raychaudhuri (TIFR, Bombay), Prof. Genevieve Belanger (LAPth, Annecy) and Prof. Dilip K. Ghosh(IACS, Calcutta). I would also like to thank Prof. Christophe Grojean (IFAE, Barcelona and CERN, Geneva) for being the host during my trip to CERN in the summer of 2012. Additionally I would like thank Prof. Sabine Kraml for hosting me at LPSC, Grenoble during the summer of 2013. I have learnt a lot from them over the last few years. The fellow graduate students across the country who I have worked with also deserves special mention here. They have been friends more than collaborators and therefore merely thanking them would not be enough. I would instead offer them my best wishes in their academic careers. The whole list of people who deserves mention include Dr. Diptimoy Ghosh (INFN Roma II, Rome), Mr. Rajdeep Chatterjee (TIFR, Bombay), Mr. Kirtimaan Mohan (IISC, Bangalore) and Mr. Amit Chakraborty (IACS, Calcutta).

One of the most refreshing and pleasant experiences has been the office environment. The academic discussions with Sanmay Ganguly and Rajdeep Chatterjee have been thrilling to say the least, and we have argued over all things pertaining to science. The non academic discussions and the sheer energy oozing out of the one room, where we worked, slept and ate have been absolutely fascinating. At times the office ambience has been nothing short of madness, and I am going to spare myself the embarrassment of describing the anecdotes. I can only thank them for making the whole journey extremely comforting. A huge vote of thanks goes out to all my friends in TIFR. Special mention must be made of Mr. Sambuddha Sanyal, Mr. Nirupam Hatui, Dr. Shamasish Sengupta (now at Univ. of Paris Sud.), Dr. Sayantan Sharma (now at Bilefeld, Germany), Mr.

Sumanta Pal, Mr. Anirban Pal, Mr. Amlan Mukherjee Dr. Sayan Chakraborty (now at Harvard), Mr. Nairit Sur, Mr. Soureek Mitra, Mr. Saurabh Shandilya, Mr. Vipin Gaur, Mr. Sanjeev Kumar, Mr. Saranya Ghosh, Mr. Umesh Yadav, Mr. Rahul Dandekar, Mr. Nikhil Karthik, Mr. Nilay Kundu, Mrs. Madhvi Chand. I would also like to acknowledge the entire non academic staff of the Department of High Energy Physics.

The entire faculty of the Department of Experimental High Energy Physics have been extremely helpful in all things academic and non academic, and I am extremely thankful to them. I am indebted to Prof. Gobinda Majumdar, Prof. Kajari Majumdar, Prof. B.S Acharya, Prof. Gagan Mohanty, Prof. Sudeshna Bannerjee, Prof. Tariq Aziz. Additionally I would also like to thank Prof. Amol Dighe, Prof. Nilmani Mathur, Prof. Subrata Pal who were part of synopsis committee.

There are a few seniors who deserves my whole hearted appreciation. I would like to thank Dr. Devdatta Majumder (NTU,Taiwan), who has always been the best host during my visits to CERN, Geneva (A resounding thumbs up to his culinary skills), Dr. Anirban Saha (INFN Perugia, Italy), the best timepass senior I have encountered, Dr. Debashish Bannerjee (Albert Einstein center,Bern), who has been absolutely wonderful to me during graduate years. I have had some truly wonderful moments with them in India and in Europe, and I am indebted to them for everything.

Contents

I Conventions, Notations and Abbreviations **i**

II Synopsis **iv**
II.1 Introduction . . . iv
II.2 Supersymmetry at the Large Hadron Collider . . . vi
II.3 Tools used for analysis . . . viii
II.4 Event shape variables in SUSY searches . . . ix
II.5 Constraints on CMSSM . . . xiii
II.6 Implications of the Higgs boson in SUSY . . . xv
II.7 Supersymmetry with third generation squarks . . . xvii
II.8 Conclusion and Outlook . . . xix
II.9 List of Publications . . . xx

1 Introduction **1**

2 The Standard Model **4**
2.1 The Standard Model Lagrangian . . . 4
2.2 The Higgs boson in the Standard Model . . . 6
2.2.1 Requirement of a Higgs scalar in the theory . . . 6
2.2.2 The Higgs mechanism and its interactions . . . 6
2.3 Global symmetries and the Yukawa sector of the Standard Model. . . . 11
2.4 Theoretical constraints on the Higgs boson . . . 12
2.5 Standard Model at LEP and Tevatron . . . 14
2.6 The discovery of the Higgs boson at the LHC . . . 17
2.7 Beyond Standard Model and supersymmetry . . . 18
2.7.1 Shortcomings of the Standard Model . . . 18
2.7.2 Motivation for supersymmetry . . . 19

3 The Minimally Supersymmetric Standard Model **21**
3.1 Formal Aspects . . . 21
3.2 The Minimally Supersymmetric Standard Model(MSSM) . . . 27
3.2.1 Field and particle content . . . 27
3.3 SUSY breaking . . . 31
3.3.1 General aspects of SUSY breaking . . . 31
3.3.2 The general mass sum rule . . . 32
3.3.3 Soft SUSY breaking . . . 33

3.4 Hidden Sector models . . . 34
3.4.1 Minimal Supergravity(mSUGRA)/Constrained MSSM(CMSSM) . . . 34
3.5 Masses and mixing in MSSM . . . 37
3.5.1 Gaugino-higgsino-mixing . . . 37
3.5.2 Sfermion mixings . . . 39
3.6 The Higgs sector of MSSM . . . 40
3.6.1 The potential and stability . . . 40
3.6.2 Masses for the Higgs sector . . . 41
3.7 Interactions in MSSM . . . 43

4 Direct and indirect constraints on the SUSY parameter space 46
4.1 Constraints from flavor physics . . . 47
4.2 Dark matter relic density constraints . . . 50
4.3 Constraints from collider experiments . . . 52

5 Constraining the CMSSM parameter space with LHC data 54
5.1 Constraints on the model . . . 54
5.2 Update on the CMSSM parameter space . . . 57

6 The Large Hadron Collider: Kinematics and Jets 65
6.1 The Large Hadron Collider . . . 65
6.2 Kinematics at LHC . . . 65
6.3 Jets . . . 68
6.4 Monte carlo, jet finding and matrix element generator tools . . . 71

7 Probing generic SUSY signals at the LHC 74
7.1 Signatures of SUSY at the LHC . . . 74
7.2 The event shape analysis for 7 TeV LHC energy . . . 79
7.3 The updated event shape analysis at 7 TeV and 8 TeV LHC energy. . . . 84

8 Higgs signatures in MSSM 91
8.1 Higgs signal from electroweak gaugino decays . . . 91
8.1.1 The production and decay of electroweak gauginos . . . 92
8.1.2 Collider strategy and analysis of the signal . . . 94
8.2 Probing signatures of an invisible Higgs decay . . . 99
8.2.1 The invisible decay width of the Higgs in MSSM . . . 100
8.2.2 Signatures of an invisibly decaying Higgs . . . 101
8.2.3 Invisible Higgs signal via VBF . . . 102
8.2.4 Invisible Higgs signal via *ZH* . . . 105
8.2.5 Summary . . . 108

9 Supersymmetry with third generation squarks 110
9.1 Motivation for third generation squarks . . . 110
9.2 Probing the left handed lightest sbottom in the four lepton channel . . . 113
9.2.1 The left handed sbottom parameter space . . . 113
9.2.2 Signal and Background . . . 116
9.2.3 Summary and Conclusion . . . 118

9.3 Probing the flavor violating decay of the stop quark 119
9.3.1 CMSSM and PMSSM 120
9.3.2 Constraining CMSSM 120
9.3.3 Stop decay and benchmarks 121
9.3.4 Signal and background 123
9.3.5 Implications for dark matter 130
9.3.6 Conclusion 132

10 Conclusion **134**

Chapter I

Conventions, Notations and Abbreviations

Notations and Conventions

- Natural Units, $\hbar$=c=1.
- Cross section in units of barn. 1 barn= $10^{-28}m^2$.
- In natural mass units 1 GeV= 10^9 eV. 1 TeV = $10^{12}eV$.
- Metric: $\eta_{\mu\nu} = \text{diag}(1,-1,-1,-1)$.
- Levi-Civita tensor: $\varepsilon_{\mu\nu\rho\sigma}$ with $\varepsilon_{0123} = 1$.
- Pauli spin matrices = τ^a.
- Commutator: $[X,Y] = XY - YX$, Anti-commutator : $\{X,Y\} = XY + YX$.
- Coupling constants : g_1, g_2, g_3 for U(1),SU(2),SU(3).
- Fine structure constant =α.
- Strong coupling constant : $\alpha_s = \frac{g_3^2}{4\pi}$.
- Fermi constant= G_μ.
- Structure constants : f^{abc} for SU(3). and ε^{abc} for SU(2).
- Generators of SU(N) algebra. T^a, a=1..N.
- Q = Electric charge, T_3= weak isospin, Y=hypercharge.
- v= electroweak vacuum expectation value. Weinberg angle =θ_W. Yukawa couplings: λ_i.
- P_μ and $M_{\mu\nu}$ are the generators of translation and angular momentum respectively.
- Grassmann variables = θ^a with a=1,2 in two component notation.
- (a,b) = Spinor indices in $(\frac{1}{2},0)$ notation. $\dot{a},\dot{b}$= Spinor indices in $(0,\frac{1}{2})$ notation.
- Projection operators : Left $P_L = \frac{1}{2}(1-\gamma_5)$ and right $P_R = \frac{1}{2}(1+\gamma_5)$.
- Two component Levi-Civita : $\varepsilon^{12} = \varepsilon_{21}$=1. $\varepsilon^{21} = \varepsilon_{12}$=-1

- $\partial_a = \frac{\partial}{\partial\theta^a}$, $\partial^a = \frac{\partial}{\partial\theta_a}$. $\partial_{\dot{a}} = \frac{\partial}{\partial\theta^{\dot{a}}}$, $\partial^{\dot{a}} = \frac{\partial}{\partial\theta_{\dot{a}}}$
- Supercharges : Q_a=- $i(\partial_a + i\sigma^{\mu}_{a\dot{b}}\theta^{\dagger\dot{b}}\partial_\mu)$. $Q^{\dot{a}}$=+ $i(\partial^{\dagger\dot{a}} - i\sigma^{\mu\dot{a}b}\theta_b\partial_\mu)$
- Superfield co-ordinates : $z = (x, \theta, \theta^\dagger)$.
- Superfields : General= $\mathscr{F}$. Chiral = Φ, Vector=V. Auxiliary fields : F,D.
- Super covariant derivative : $\mathscr{D}_a = \partial_a + i\sigma^{\mu}_{a\dot{b}}\theta^{\dagger\dot{b}}\partial_\mu$.
- Integral measures : $d^4\theta = d^2\theta d^2\theta^\dagger$.
- Chiral field strengths : Left chiral : $W_a = -\frac{1}{4}\mathscr{D}^\dagger\mathscr{D}^\dagger\mathscr{D}_a V$, Right Chiral $W_a^\dagger = -\frac{1}{4}\mathscr{D}\mathscr{D}\mathscr{D}_a^\dagger V$.
- Rapidity=y= $\frac{1}{2}\ln\frac{\mathrm{E}+\mathrm{p_z}}{\mathrm{E}-\mathrm{p_Z}}$, pseudorapidity=$|\eta| = \frac{1}{2}ln\frac{|p|+p_z}{|p|-p_Z}$.

Abbreviations

- ATLAS : A Toroidal LHC apparatus.
- BR: Branching ratio.
- BSM : Beyond Standard Model.
- CERN: Organization for European Nuclear Research.
- CKM : Cabibo Kobayashi Maskawa.
- c.m : Center of mass.
- CMS : Compact Muon Solenoid
- CMB : Cosmic Microwave Background.
- CMSSM : Constrained Minimal Supersymmetric Standard Model.
- EM : Electromagnetic.
- EW : Electroweak.
- FCNC : Flavor Changing Neutral Current
- FSR : Final State Radiation
- GMSB : Gauge Mediated Supersymmetry Breaking
- GUT : Grand Unified Theory.
- IRC : Infrared and Colinear.
- ISR : Initial State Radiation.
- LEP : Large Electron Positron Collider.
- LHC : Large Hadron Collider.
- LSP : Lightest Supersymmetric particle.

- LO : Leading Order.
- Λ_{QCD} : QCD scale.
- MSSM: Minimal Supersymmetric Standard Model.
- mSUGRA : Minimal Supergravity.
- NLSP : Next to Lightest Supersymmetric particle.
- NLO : Next to Leading Order.
- QCD : Quantum Chromodynamics.
- QED : Quantum Electrodynamics.
- R_p: R-parity.
- RGE : Renormalization Group Evolution.
- SLC : Stanford Linear Collider.
- SM : Standard Model.
- SSB : Spontaneous symmetry breaking.
- SUSY : Supersymmetry.
- VEV : Vacuum Expectation Value.
- WIMP : Weakly Interacting Massive Particle.
- WZ : Wess Zumino.

Chapter II

Synopsis

II.1 Introduction

The standard model (SM) of particle physics, based on the principle of gauge invariance described by the gauge group ($SU(3)_c \times SU(2)_L \times U(1)_Y$), has been extremely successful in describing physics at the electroweak scale, and has been well tested to remarkable precision at the LEP, Tevatron and now at the LHC. The discovery of the Higgs like boson at 125 GeV [1, 2], an integral part of the SM that breaks the above symmetry down to $SU(3)_c \times U(1)_{em}$ and generates masses for the leptons, quarks and the gauge bosons of the theory has certainly vindicated the model. However the discovery of the Higgs like boson has thrown up intriguing questions in this context.

One of the primary concerns is the problem of self energy corrections of the Higgs mass (M_h), which develops quadratic divergences from SM particles running in the one loop diagrams, as one tries to extrapolate the SM to the Planck scale (10^{18} GeV). The loop correction is dominated by the top quark and can be expressed as $\delta M_h^2 \sim \frac{3\Lambda^2}{8\pi^2 v^2} m_t^2$ (where m_t is the mass of the top quark, and Λ is the cut off scale, taken at 10^{18} GeV). This requires a fine cancellation of parameters between the bare and the re-normalized mass to achieve the correct Higgs mass at the electroweak scale [3]. The problem of quadratic divergence is tackled by introducing new particles that differ by spin half to that of SM particles. This symmetry namely supersymmetry(SUSY) has been one of the prime candidates of a BSM theory for the last three decades. These new particles cancel the divergent contributions from the SM particles. The unification of the three gauge couplings in SUSY at a scale of 10^{16} GeV is an added motivation to consider it as a prime candidate for BSM physics. Additionally, SUSY also offers a suitable candidate for dark matter abundantly present in the universe.

As noted earlier SUSY introduces partners to the SM particles which differ in spin by half. The minimal version of SUSY, termed as the minimally supersymmetric standard model(MSSM), is a straightforward extension of the SM by the following prescription:

- Introduction of sfermions, the superpartners of fermions. This includes sleptons and squarks differing from their partners quarks and by leptons by spin half. The left handed supermultiplet contains the doublet squarks(Q) and sleptons(L), while the right handed singlets contain (U,D,E).
- Introduction of gaugino fields, namely Bino ($\tilde{B}$), Wino ($\tilde{W}^i$), and the gluino ($\tilde{g}^a$), which transform under $U(1)$ and the adjoint representations of SU(2) and SU(3) respectively. These are superpartners of the hypercharge gauge boson (B_μ), the weak gauge bosons (W_μ^i), and the

gluon (g^a_μ) respectively.

- Along with these, there are two Higgs doublets as compared to a single Higgs doublet in SM. This is required to cancel anomalies in the theory. After electroweak symmetry breaking we have 5 Higgs bosons, with 2 charged ($H^\pm$) and 3 neutral bosons (h, H, A), along with the corresponding superpartners termed as higgsinos ($\tilde{H}^0_i, \tilde{H}^\pm_i$). The ratio of the vacuum expectation values(VEV) of the neutral components of the two Higgs doublets is parametrized by $\tan\beta$.

The full SUSY particle content is as summarized in Table 3.1.

The Lagrangian of the MSSM is invariant under the SM gauge symmetry $SU(3)_c \times SU(2)_L \times U(1)_Y$. Furthermore one imposes a Z_2 symmetry termed as R parity defined as $R_p = (-1)^{3B-L+2S}$, where B is the baryon number, L the lepton number and S the spin of the particle. SM particles are even under this symmetry while their SUSY counterparts are odd. This ensures that the lightest SUSY particle(LSP), which is generally the lightest neutralino (χ^0_1) is stable, and hence is an ideal candidate for dark matter. Supersymmetry cannot be an exact symmetry as it implies equal masses for sferimons and the corresponding fermions which is not realized in nature. SUSY therefore has to be broken. Low energy SUSY is manifested as "soft" SUSY breaking terms. The term "soft" implies that no terms with mass dimension greater than 3 appear in the soft SUSY Lagrangian, such that the quadratic divergences do not reappear in the theory. The soft SUSY Lagrangian can be written as,

$$\mathscr{L} = (\frac{1}{2} M_a \bar{\lambda_a} \lambda_a + m_i |\phi_i|^2 + A_{ijk}\phi_i\phi_j\phi_k + + B_{ij}\phi_i\phi_j) + h.c, \tag{II.1.1}$$

where λ_a denotes the gauginos transforming under the the gauge groups U(1) ($\tilde{\mathrm{B}}$), and the adjoint representations of SU(2) ($\tilde{\mathrm{W}}^{\mathrm{i}}$) and SU(3) ($\tilde{\mathrm{g}}^{\mathrm{a}}$) respectively. The scalar mass terms include the squarks ($\tilde{\mathrm{u}}_\mathrm{L}, \tilde{\mathrm{d}}_\mathrm{L}$...), sleptons ($\tilde{\nu}_\mathrm{L}, \tilde{\mathrm{e}}_\mathrm{L}$..), and the Higgs fields (H_i). $\mathrm{A_{ijk}}$, and $\mathrm{B_{ij}}$ denotes the trilinear and the bilinear couplings. The MSSM Lagrangian, once expanded has 124 parameters including masses, phases and mixing angles as free parameters.

The exact nature of breaking is not well established and various models have been proposed to this end. The general understanding is that SUSY is spontaneously broken in a hidden sector of fields that is singlet to the SM gauge group. The effects of the breaking is transmitted to the visible sector by one or a group of fields known as mediators. In models of SUSY breaking like minimal supergravity (mSUGRA)/constrained MSSM (CMSSM), the breaking takes place in the hidden sector by higher dimensional operators. The CMSSM model is specified by universal parameters at the GUT scale, and includes $\mathrm{m_0}, \mathrm{m_{1/2}}, \mathrm{A_0}$, the universal scalar mass, the universal fermion mass and universal trilinear coupling respectively. Along with this one has to specify $\tan\beta$, the ratio of the vacuum expectation value(VEV) of the two Higgs doublets and the sign of μ. The sparticle spectrum at the electroweak scale is determined by renormalization group evolution (RGE) from the GUT scale to the electroweak scale.

After SUSY and electroweak symmetry is broken, sfermions and gauginos mix generically. The left and right handed squarks and sleptons mix, and thus the resulting mass eigen states are a combination of left and right handed components. This drives the phenomenology and decay rates, and hence is important from the perspective of collider studies.

While mixing in the first two generation of squarks and sleptons are small due to the smaller Yuakawa couplings, the third generation squarks and sleptons mix to a much larger extent owing to the larger Yukawa couplings of the third generation. This has a significant impact from the point of view of Higgs mass in SUSY, as we shall discuss later.

	Superfield	Particle	Spin	Superpartner	Spin
Matter Fields	Q	$(u,d)_L$	$\frac{1}{2}$	$(\tilde{u}_L, \tilde{d}_L)$	0
	U^c	$\bar{u}_R$	$\frac{1}{2}$	$\tilde{u}^*_R$	0
	D^c	$\bar{d}_R$	$\frac{1}{2}$	$\tilde{d}^*_R$	0
	L	$(\nu, e)_L$	$\frac{1}{2}$	$(\tilde{\nu}_L, \tilde{e}_L)$	0
	E^c	$\bar{e}_R$	$\frac{1}{2}$	$\tilde{e}^*_R$	0
Gauge Fields	V_1	B_μ	1	$\tilde{B}$	$\frac{1}{2}$
	V_2	W^i_μ	1	$\tilde{W}^i$	$\frac{1}{2}$
	V_3	G^a_μ	1	$\tilde{g}^a$	$\frac{1}{2}$
Higgs Fields	H_1	(H^0_1, H^-_1)	0	$(\tilde{H}^0_1, \tilde{H}^-_1)$	$\frac{1}{2}$
	H_2	(H^+_2, H^0_2)	0	$(\tilde{H}^+_2, \tilde{H}^0_2)$	$\frac{1}{2}$

Table II.1: Field content of the MSSM.

The charged gaugino and higgsino mix, generating charged mass eigen states called charginos ($\chi^{\pm}_{1,2}$). The neutral gauginos and the higssinos mix, with the mass eigen states termed as neutralinos ($\chi^0_{1,2,3,4}$).

The constitution of the charginos and the neutralinos as a function of their component fields is is also an important factor in driving the phenomenology of SUSY at colliders. Along with this the higgsino mass parameter μ also plays an important role in the phenomenology of SUSY.

The manifestation of SUSY is twofold. Firstly as direct production of sparticles at colliders, and secondly in effects through loops in low energy flavor physics processes. Both of the above can be used to constrain the SUSY parameter space. The Higgs boson, which has indeed been found also has a profound implication in SUSY.

The motivation of this work is to probe signatures of supersymmetry at the Large Hadron Collider. While a significant amount of work has already been done in the literature in this regard [4,5], we try to investigate if such strategies can be improved. Indeed as discussed in section 4 we find that with the use of the technique of event shape variables, which we introduce for the first time for SUSY searches, the efficiencies of SUSY searches can be significantly improved at the LHC. In section 6, the constraints on the SUSY parameter space in the model framework of CMSSM from flavor physics, collider search data and dark matter is discussed. In section 7, Higgs signatures in the context of SUSY and our work in probing Higgs signals in SUSY cascade decays with the help of the novel method of jet substructure is discussed. We also discuss our work on the possibility of the Higgs decaying invisibly. In section 5, the issue of third generation squarks and its connection with the Higgs mass in SUSY is discussed. In this context we discuss our work in probing signatures of third generation squarks. Finally in section 8 we conclude.

II.2 Supersymmetry at the Large Hadron Collider

The Large Hadron Collider(LHC), a proton proton collider at the European Organization for Nuclear Research (CERN), Geneva, started its operation in 2009 and has recently concluded its 8 TeV center of mass energy run delivering about 20 fb^{-1} of data. The early run of 7 TeV energy also

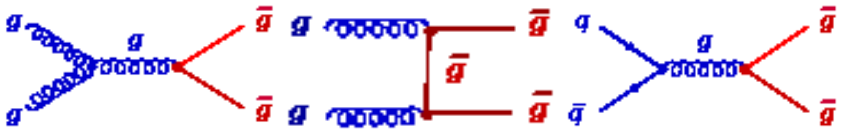

Figure II.1: Examples of diagrams for gluino pair production via the strong interactions.

concluded in 2011 collecting about 5 fb^{-1} data. Being a proton proton collider the interactions at the LHC are dominated by strong interaction processes mediated by quarks and gluons governed by the theory of quantum chromodynamics (QCD), characterized by the strong coupling constant α_s.

The principal production for strongly interacting SUSY particles like squarks($\tilde{q}$) and gluinos($\tilde{g}$) can be expressed as,

$$PP \rightarrow \tilde{g}\tilde{g},\ \tilde{q}\tilde{g},\ \tilde{q}\tilde{\bar{q}} \tag{II.2.1}$$

In the intermediate step, the squarks can decay to the higher chargino($\chi_2^{\pm}$) and neutralino states($\chi_{3,4}^0$) (if kinematically allowed) or to the lighter chargino/neutralino ($\chi_1^{\pm}$,χ_2^0). At the final stage of the cascade decay the charginos ($\chi_1^{\pm}$) and heavier neutralinos (χ_2^0) decay via the gauge bosons ($\chi_1^{\pm} \rightarrow \chi_1^0 W$) or via sleptons to the lightest stable particle (LSP), which is generally the lightest neutralino, along with quarks and leptons. Note that Eq. II.2.1 is only a generic chain. The exact decay will depend on the nature of squarks, mass differences among other factors. As the lightest neutralino is extremely weakly interacting, it evades detection and thus the resultant imbalance in momentum shows up as missing transverse momentum ($\not{p}_T$).

The generic SUSY signature is thus often designated by,

$$\mathrm{n-jets + m-leptons + } \not{p}_T,\ \ \mathrm{n,m} = 0,1,2.... \ . \tag{II.2.2}$$

At the LHC the total leading order (LO) cross section is given by,

$$\sigma(PP \rightarrow A\,B) = \sum_{a,b} \int dx_a \int dx_b\, f_{a/P}(x_a,\mu_f^2)\, f_{b/P}(x_b,\mu_f^2)\hat{\sigma}(\alpha_s(\mu_R))(ab \rightarrow A\,B). \tag{II.2.3}$$

The functions $f_{a/P}(x_a,\mu_f^2)$, $f_{b/P}(x_b,\mu_f^2)$, known as the parton density functions (PDF), represent the probability of finding a parton "i" a inside the proton target with momentum fraction x_i at a scale μ_f. Here μ_R, μ_f are the renormalization and factorization scales respectively and in general set to the hard scattering scale Q where $Q^2 = \hat{s}$. The sample Feynman diagrams for the gluino production are shown in Fig. 7.1.

Note however that the next to leading order (NLO) cross sections can be significantly larger than the LO cross section and hence can affect the mass exclusions significantly and reduce the uncertainties in predictions. The inclusive SUSY cross sections at 8 TeV energy can be as large 50 pb for squarks and gluino masses of 400 GeV to 10 fb for squarks and gluino masses of 1 TeV.

In order to probe SUSY signals a huge suppression of the enormous SM background is required. For a generic SUSY signature the principal background processes that mimic the SUSY signal is as described below,

- **QCD**: The QCD background, which includes copious productions of quarks and gluons in the final state is the largest SM background in terms of cross section of about 10^8 pb at 8

TeV. Thus this background should be estimated as one of the principal backgrounds to SUSY search. The $\not{p}_T$ in this case is generated from semileptonic B-meson decays, as well as from detector mis-measurements. In this thesis we do not take detector effects into account.

- $t\bar{t}+jets$: The $t\bar{t}$ production process can have semi-leptonic and fully hadronic final state. Since the cross section is significantly large ($\sim$ 220 pb at 8 TeV) and there is a significant amount of $\not{p}_T$ from the neutrinos in case of semi-leptonic decays this too is a significant background for SUSY searches.

- **Z+jets** :This eletroweak background comprises of the irreducible part of the background in SUSY searches for fully hadronic searches when the Z boson decays to a pair of neutrinos. The cross section for this process is quite large ($\sim 10^5$ pb at 8 TeV) and hence this background is one of the most severe backgrounds to SUSY searches.

- **W+jets** : This eletroweak background can be significantly large for leptonic and fully hadronic searches as the cross section is enormously large ($\sim 10^6$ pb at 8 TeV).

- **WW/WZ/ZZ** : The SM electroweak backgrounds, although low on cross sections, as compared to the previous ones can be serious backgrounds for a variety of SUSY searches.

Since the cross sections of SUSY production are miniscule in comparison to the SM background, a huge suppression of background cross section ($\sim 10^8 pb$) is required while retaining a significant fraction of the signal for discovery, which is a challenging task.

II.3 Tools used for analysis

Monte Carlo event generators and other software tools are an integral part of any collider study and here the essential tools are summarized. The monte carlo generators are used for two purposes. Firstly it is used to calculate cross sections of hard scattering processes, by the monte carlo integration of the hard parton level process and then convoluting it with the PDF. Secondly it is used for a realistic simulation of an actual experimental process where the hard scattering process is followed by showering to include initial and final state radiation(QCD and QED) effects and finally hadronization of the parton level objects. For SUSY signal processes, we generate events using the software PYTHIA6 [6]. Note that PYTHIA6 computes only leading order matrix elements, and for most purposes this suffices to make a prediction. The generation of leading order events in PYTHIA6 is followed by showering and and hadronization implemented in PYTHIA6. Note that although PYTHIA6 computes only leading order matrix elements, initial and final state radiation (ISR/FSR) can generate additional quarks, gluons and photons.

Quarks and gluons finally hadronize to form color singlet objects (baryons and mesons), which are ultimately clustered in detectors to form objects called jets. The procedure of defining a jet is varied, and is sometimes subject to the requirement of a physics process. However one would like to construct a jet such that it is infra-red and co-linear divergence safe, i.e, do not give unreliable results when soft and co-linear gluons are present in the system. To this end modern recombination algorithms to find jets are used as compared to the old cone algorithms which were infra-red and co-linear unsafe. The most popular algorithm in current use in most experimental analysis is known as anti-K_T [7] which forms circular jets. We use the FastJet [8] package to find jets with a size parameter of R=0.5.

For background processes this however may not be enough, as multijet processes like $t\bar{t}$ + jets, and W/Z + jets contribute a significant fraction to the total cross section. These however, are not well modelled in PYTHIA as multijet processes in PYTHIA only occur via ISR/FSR and hence may not be a correct manifestation of the actual matrix element amplitude. Hence it is advisable to generate proper matrix element events for the hard scattering process for these processes and subsequently use PYTHIA for showering and hadronization. As a caution however one must keep in mind not to double count events where parton showering and subsequent jet reconstruction mimics an actual matrix element generated configuration and hence these events must be discarded. In these studies we use ALPGEN [9] and Madgraph [10] to generate multijet background processes wherever applicable with the double counting of matrix element and parton showering avoided by a prescription termed as MLM matching [11].

To summarize, in the simulations as described below, all signal processes and backgrounds like QCD,WW,WZ,ZZ and $t\bar{t}$ with no additional hard jets at parton level are simulated using PYTHIA6. For background processes like Z+jets,W+jets, $t\bar{t}$ + jets, ALPGEN or Madgraph is used with subsequent showering and hadronization performed by PYTHIA. For parton distribution functions the package LHAPDF [12] is used with CTEQ6L [13] used as the PDF set.

To generate SUSY spectrums one needs to evolve a generic high scale SUSY model defined at the GUT scale down to the electroweak scale by renormalization group evolution (RGE). SUSY spectrums and branching ratios are calculated using SUSPECT [14] with subsequent decay computed using SUSYHIT [15]. SUSPECT implements two loop RGE while evolving from a generic high scale SUSY breaking model to the electroweak scale where the all the masses and couplings are computed. Flavor physics observables like the branching ratio(BR) of $B_s \to \mu^+\mu^-, B \to X_s\gamma$ are computed using the public domain software SUPERISO [16].

For cross sections we use the software package PROSPINO [17] to calculate NLO cross sections for various SUSY production processes.

II.4 Event shape variables in SUSY searches

The search for SUSY signatures started from the era of the early $p\bar{p}$ colliders, and continued during the running of LEP, and various strategies have been devised to effectively suppress the SM backgrounds to find a signal. Some of the earliest phenomenological works in SUSY searches at the start of the LHC run at 7 TeV was performed in [4,5]. These search strategies worked in the jets + $\not{p}_T$ scenario as well as single and dilepton channels in association with jets and $\not{p}_T$. In general these studies relied on the imposition of a hard $\not{p}_T$ cut as a way to suppress the SM background. Using their strategy they showed that they could probe squark and gluino masses up to $\sim$ 900 GeV when they are degenerate with each other.

As was the case with early phenomenological studies of SUSY searches we work in the framework of the CMSSM as discussed earlier.

The signal in our case consists of the process mentioned in Eq.II.2.1, with the generic signature given by Eq.II.2.2. The signal is characterized by hard jets and $\not{p}_T$. The CMSSM parameter space can be characterized in two regions with respect to our search strategy, firstly $m_0 \sim m_{1/2}$, where the gluino and the squark masses are close to each other, and secondly $m_0 >> m_{1/2}$, when the gluino mass is much smaller than the squark mass. The number of hard jets in the latter case are expected to be larger than the former.

The background process consists of the entire set as described in section 2. The most severe background in our case consists of the $t\bar{t} + jets$ and the irreducible $Z(\to \nu\bar{\nu} + jets)$.

To analyze the signal and background we use the strategy based on event shape variables. The concept of event shape variables emerged with e^+e^- colliders, with the aim of defining the "shape" of an event, whether it is planar, spherical or pencil like, etc. These variables are defined to be infrared safe against soft or co-linear gluon emission and invariant under the branching $\vec{p}_i \to \vec{p}_j + \vec{p}_k$, whenever the momenta are parallel or one of them is small. Quantities made of linear sums of momenta always meet this criteria. The event shape variable we put to use is transverse thrust defined as [18],

$$T = max \frac{\sum_j |\vec{p}_T^{\,j}.\vec{n}_T|}{\sum_j |p_T^j|}, \tag{II.4.1}$$

where $\vec{p}_T^{\,j}$ is the jet j with momenta in the transverse direction, and $\vec{n}$ is an arbitrary unit vector in the transverse plane over which the maximization is performed. If the momenta $\vec{p}_T^{\,j}$ form co-linear jets , the thrust axis after maximization lies parallel to the jet and hence the value of the T is equal to 1. For a di-jet event with jets in the back to back configuration the value of T is again equal to 1, as can be readily seen from Eq.7.2.2. For an isotropically distributed configuration of jets, the value is $2/\pi$. The tail of the distribution is dominated by multi-jet events.

We use this feature to good use for SUSY searches. We realize that SUSY processes where the heaviest particle (gluino or squark) cascades down to the lightest supersymmetric particle (LSP), the final state can have a large number of jets along with a significant amount of $\not{p}_T$ from the LSP. A typical region of interest which produce these kind of events is in the region of moderate to high m_0 and relatively low $m_{1/2}$, leading to a low gluino mass and a high squark mass. In this case the gluino ($\tilde{g}$) decay mode proceeds as $\tilde{g} \to tb\chi_1^{\pm}$ via off-shell squarks. The largest SM background namely QCD produces mostly di-jet events, and therefore the thrust distribution in this case lies close to 1. Along with these leptonic decays of the top quark which yield a di-jet configuration in the final state , Z $(\to \nu\bar{\nu})$/W $(\to l\nu) + 1,2$ jets, which produce di-jet configurations also has values of T ($\tau = 1 - \mathrm{T}$) close to 1(0). Thus putting a cut of $\tau > 0.1$ suppresses a huge amount of SM background leaving the signal mostly unaffected. The thrust distribution expressed in terms of τ is presented in Fig. 7.3. We can thus observe a clear distinction between signal and background processes [19] particularly QCD which lies close to 0.

The $\not{p}_T$ in QCD is generated from semileptonic B meson decays resulting in neutrinos at the final state.

To supplement the above we use the following variables to suppress the remaining SM background.

Since the parent SUSY particle gluino or squark is fairly massive, the resulting jets and missing energy are hard. Additionally the fact that the process consists of multi-jets motivates us to construct a ratio of the transverse momenta called R_T [19] and defined as,

$$R_T = \frac{\sum_1^{n_j^{min}} p_T^{j_i}}{H_T}, \tag{II.4.2}$$

where the numerator runs over a minimum number of pre-selected jets ($\mathrm{n_j^{min}}$) depending on the signal topology. The denominator $\mathrm{H_T}$ is the scalar sum of the transverse momenta of all jets in a given event. For events which peak at 1, $\mathrm{n_j = n_j^{min}}$, while values less than 1 are for events where the number of jets are greater than $\mathrm{n_j^{min}}$. In our study we choose $\mathrm{R_{T4}}$, implying $\mathrm{n_j^{min} = 4}$.

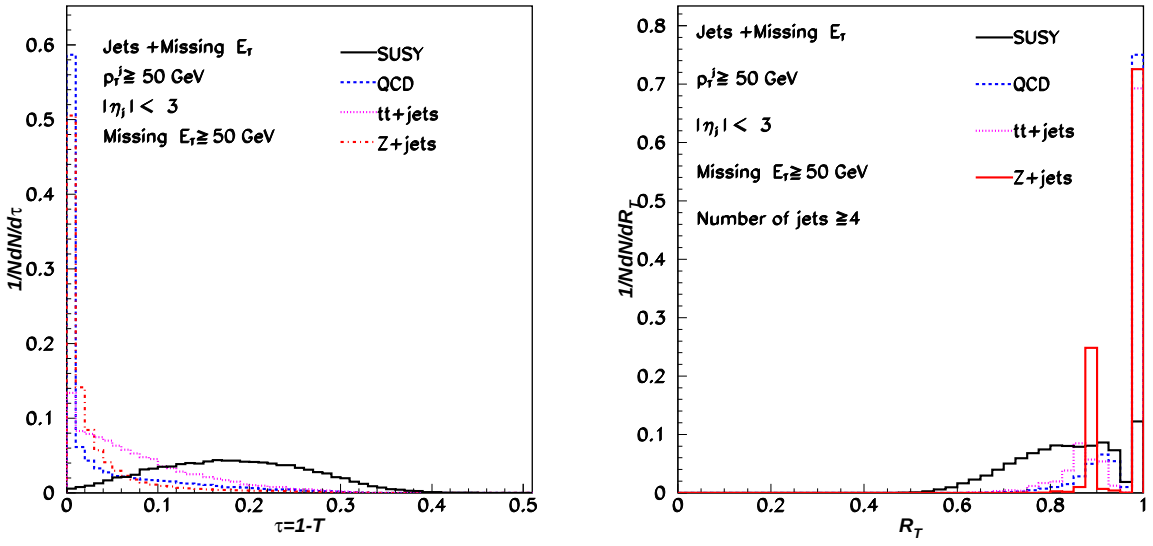

Figure II.2: The $\tau = 1 - T$ distribution(left panel) and the R_T distribution(right panel) for 7 TeV LHC energy. The benchmark signal point is in the CMSSM framework for $m_0 = 1500, m_{1/2} = 200, \tan\beta = 45, A_0 = 0, \mathrm{sgn}(\mu) > 0$. The jet p_T threshold is chosen to be 50 GeV within $|\eta| < 3$.

This is more than a naive implementation of a cut on the total number of jets, as this cut also utilizes the hardness of the final state objects. This variable is most effective in suppressing the W + jets and the irreducible Z($\rightarrow \nu\bar{\nu}$)+jets background. For SM backgrounds the sub leading jets are expected to be much softer than the corresponding SUSY processes. Hence the tail of R_T distribution in expected to fall to much lower values for the signal process as compared to the background process. This is illustrated in the right hand panel of the Fig. 7.3 where we put a cut of 0.85.

This reduces most of the background coming from Z/W + jets processes. Finally the remaining background consists of $t\bar{t}$ + jets which can have a significantly high number of jets along with $\not{p}_T$. To suppress this we construct the variable with the leading two jets in the event as,

$$M_T^{jj} = \sqrt{2p_t^{j1} \times p_T^{j2}(1 - cos\phi)}, \tag{II.4.3}$$

where ϕ is the angle between the leading two jets in the transverse direction. We note two facts about this variable which helps us to suppress the large $t\bar{t}$ + jets background. First of all note that the leading two jets in $t\bar{t}$ production are relatively softer than that of the SUSY process where the leading jets come from a relatively massive particle. Secondly for $t\bar{t}$ process the opening angle between the leading jets is much larger as compared to the signal process where the jets are isotropically distributed.

Finally a significant $\not{p}_T$ cut helps us to remove the remainder of the backgrounds.

After all cuts the background level was found to be negligible while retaining a significant proportion of the signal events. The efficiency of the signal varies from 10% for low gluino squark masses to 25% at 1 TeV for the case of low gluino and high squark masses. The details of the event summary of signal and background can be found in [19, 20] for 7 and 8 TeV LHC energy. We deem a parameter space point to be discoverable if the total number of signal (S) events and

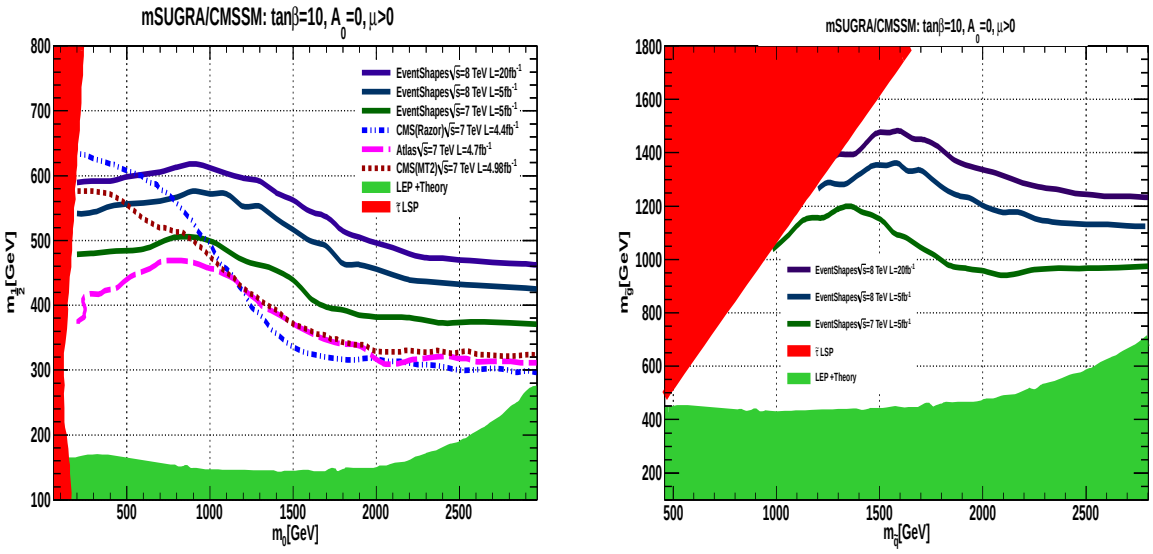

Figure II.3: The discovery region in the $m_0 - m_{1/2}$(left panel) and the squark gluino plane(right panel) for tanβ=10, $A_0 = 0$, The CMS M_{T2}, razor and ATLAS exclusion plots [21–23] are also overlayed at 95 % confidence level. The green shaded region is excluded by theory and LEP constraints and red region is excluded by $\tilde{\tau}$ LSP condition.

the background (B) events at a particular luminosity and energy is such that $\frac{S}{\sqrt{B}} > 5$. Here we present our results as a parameter space scan in the m_0-$m_{1/2}$ plane for the CMSSM parameter space for tanβ=10, $A_0 = 0$ and sgn$(\mu) > 0$, in Fig. II.3 at 8 TeV for 5 and 20 fb^{-1} and 7 TeV for 5 fb^{-1} luminosity. As a comparison we also present the exclusion curves from ATLAS and CMS collaborations [21–23]. With our strategy we observe that for the CMSSM parameter space we can discover gluino masses up to 1.4 TeV for degenerate squarks and gluinos and upto about 1.2 TeV when the gluino is much lighter than the squark at 8 TeV center of mass energy with 20 fb^{-1} luminosity.

As mentioned earlier, our strategy works best for regions with high multiplicity of hard jets, which is reflected in the Fig. II.3, where we observe that our discovery reach is better than that of CMS and ATLAS exclusion curves. In this region the gluino decays via off shell squarks as $\tilde{g} \to tb\chi_1^{\pm}$ yielding hard multi-jets. It must be mentioned that we do not explicitly impose a lepton veto as is generally done by ATLAS and CMS collaborations.

Also it has to be noted that the ATLAS and CMS exclusion plots are at 95% C.L with systematic uncertainities taken into account while our discovery plots are at 5σ without any systematic effects taken into account.

Note that our study does not include detector effects. However since our variables (Thrust and R_T) are dimensionless ratios, the systematic errors are expected to be small.

We also emphasize that our strategy is not just limited to CMSSM but works whenever hard multi-jets are present in the system. As a follow up we implemented our strategy for a non universal gaugino mass model motivated by dark matter considerations at 7 TeV LHC and showed that it was possible to probe a significant fraction of parameter space with 5 fb^{-1} luminosity with our search strategy [24].

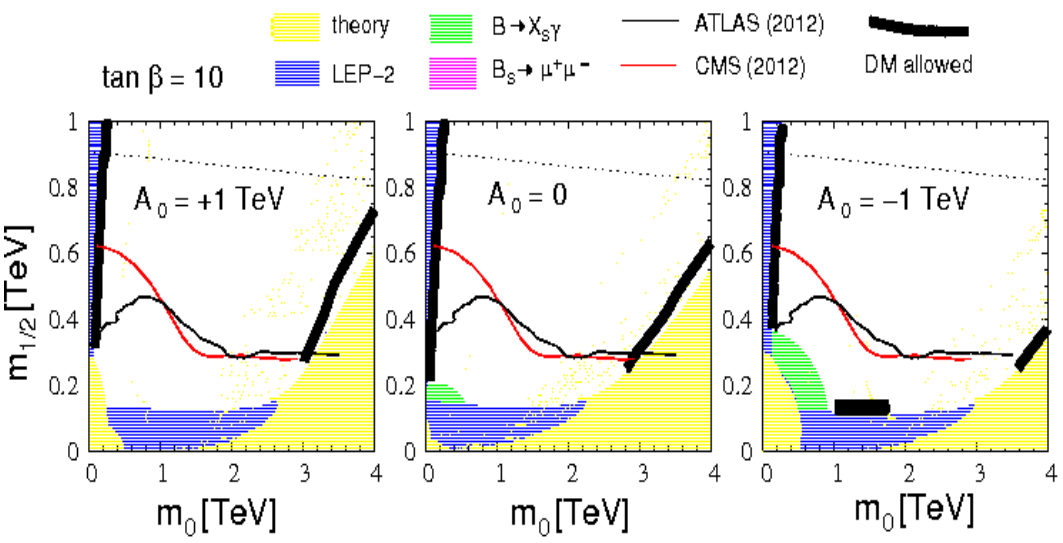

Figure II.4: The constraints on the CMSSM parameter space for tanβ=10. The different constraints are depicted in different colors as quoted above.

II.5 Constraints on CMSSM

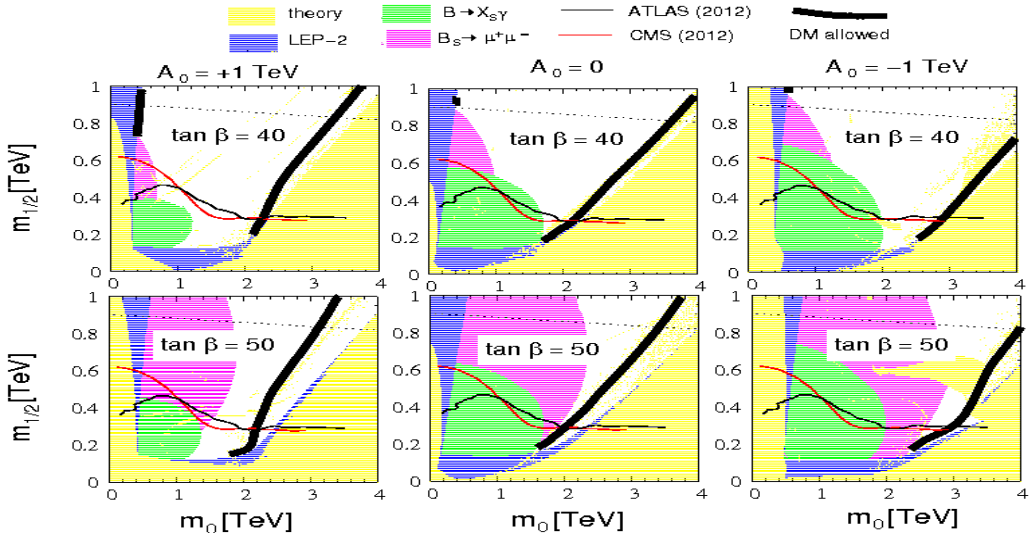

Figure II.5: Same as Fig. II.4 but for tanβ=40 and 50.

At the end of the 7 TeV run, it was imperative to look at the constraints from direct collider searches and indirect constraints specially from flavor physics along with dark matter to identify the CMSSM parameter space allowed by various observables.

The criteria that we considered to constrain the CMSSM parameter space are as follows [25],

- The first kind of constraints are from theoretical considerations. For tanβ, we require that the Yukawa couplings of the top and the bottom quark remain perturbative between 1.2 $<$tanβ $<$ 65. Moreover very low values of m_0 and $m_{1/2}$ are not allowed as then the RGE would drive

electroweak symmetry breaking to occur too close to the GUT scale. For larger values of m_0 and $m_{1/2}$, we require that under RGE running, the scalar potential remain bounded from below and hence stable. The second requirement requires that the LSP should be neutral , which is demanded if it is to be the major component of the dark matter. This rules out the lightest stau ($\tilde{\tau}_1$) to be the LSP. The lighest neutralino is the favored LSP to satisfy the dark matter requirements.

- The second kind of constraint is where SUSY can affect low energy flavor processes when heavy superparticles enter at the loop level. The first type comes in the form where the observed and expected SM processes match with each other and hence no SUSY induced enhancement is expected. Such a constraint is Br($B \to X_s\gamma$) where the measured value $(3.55 \pm 0.24 \pm 0.09) \times 10^{-4}$ [26] is rather close to the SM prediction of $(3.15 \pm 0.23) \times 10^{-4}$ [27]. The CMSSM contribution must satisfy,

$$-0.55 \times 10^{-4} \leq \mathrm{BR}(B \to X_s\gamma) \leq 1.35 \times 10^{-4} \, .$$

  The second kind is where experimental measurements are away from SM leaving enough room for SUSY contributions to produce an actual enhancement or suppression. [1] A prime example is the recently measured BR($B_s \to \mu^+\mu^-$). In MSSM the branching ratio is enhanced by $\tan^6\beta$. Thus at large $\tan\beta$, a deviation from the SM expected value is predicted. While this study was being conducted the measured experimental upper limit was set to 4.5×10^{-9} [28], against the SM prediction of $(3.2 \pm 0.2) \times 10^{-9}$ [29].

  While conducting this study we set the numerical upper limit to be 5.0×10^{-9}. The CMSSM contributon should thus satisfy,

$$\mathrm{BR}(B_s \to \mu^+\mu^-) \leq 1.8 \times 10^{-9} \, .$$

- We also look at direct searches on gluino and squark from ATLAS and CMS collaborations that put bounds on the CMSSM parameter space. Here we take the limits for 7 TeV energy 5 fb^{-1} luminosity run [21, 30].

- At the time of this work the Higgs boson was not discovered and hence we did not impose a condition on the lightest Higgs mass apart from LEP lower bound of 93 GeV for $\tan\beta \geq 6$ and the chargino ($\chi_1^{\pm}$) lower bound of 94 GeV [31].

- Finally we consider dark matter constraints that requires that the dark matter relic density of the universe to be within $0.1053 \leq \Omega_d h^2 \leq 0.1193$ [2] [32]. In CMSSM which conserves R-parity, the dark matter candidate is the lightest neutralino.

With the above constraints we analyzed the CMSSM parameter space. This is summarized in the Fig. II.4 and Fig. II.5. We find that for low $\tan\beta$ (10-30) the most stringent constraints come from direct SUSY searches at the LHC. However at large $\tan\beta$ the biggest constraint, as expected, come from the flavor observable $B_s \to \mu^+\mu^-$, which rules out a large swath of CMSSM parameter space. Hence the bulk of parameter space allowed at large $\tan\beta$ in CMSSM with R parity conservation is generally out of reach of the LHC even at 14 TeV, unless very high luminosity is obtained.

[1] We do not consider the value of the anomalous magnetic moment of the muon $(g-2)_\mu$. This is primarily because of the large uncertainties in theoretical calculations in this number.

[2] h is the Hubble constant, not to be confused with the Higgs boson.

	$m_{1/2}$	μ	m_h	$m_{\tilde{g}}$	$m_{\tilde{q}}$	$m_{\tilde{t}_1}$	$m_{\chi_1^0}$	$m_{\chi_2^0}$	$m_{\chi_1^\pm}$
P1	300	1541	122.4	865	3000	1305	133	265	265
P2	380	1660	122.8	1046	3060	1335	168	332	332
P3	450	1653	123.2	1200	3096	1370	198	390	390

Table II.2: Masses of some of the sparticles for three benchmark points for [34]. In all the cases $m_0 = 3000$, $\tan\beta$=30 and A_0=-4500. All mass units are in GeV.

II.6 Implications of the Higgs boson in SUSY

As mentioned in the previous section, the Higgs mass which was not considered in the previous work has indeed been found. This puts severe constraints on the SUSY parameter and in particular the CMSSM parameter space.

At tree level the lightest Higgs mass (M_h) in SUSY is totally determined by M_A and $\tan\beta$. At tree level the lightest Higgs mass is bounded from above by the mass of the Z boson and is given by the expression $M_h^2 \leq M_Z^2 \cos^2 2\beta$. Loop corrections can however increase the Higgs mass bound significantly. The dominant contribution to the increase in Higgs mass comes from top-stop loops and is given by the expression [33],

$$\Delta M_h^2 \simeq \frac{3G_F}{\sqrt{2}\pi^2} m_t^4 \left[\log \frac{M_{SUSY}^2}{m_t^2} + \left\{ \frac{X_t^2}{M_{SUSY}^2} \left(1 - \frac{X_t^2}{12 M_{SUSY}^2} \right) \right\} \right], \tag{II.6.1}$$

where $M_{SUSY} = \sqrt{m_{\tilde{t}_1} m_{\tilde{t}_2}}$, the geometric mean of the two stop masses, and $X_t = A_t - \mu \cot\beta$, the mixing parameter in the stop mass matrix. Thus to increase the Higgs mass either heavy scalars, (so as to increase M_{SUSY}) or large negative values of A_t are required. Note that the above expression is maximized for $X_t = \sqrt{6} M_{SUSY}$ and can lead to an enhancement of Higgs mass in SUSY up to 140 GeV. This may however be unsuitable from the perspective of fine tuning which do not prefer unnaturally high values of the parameters of the theory.

A 125 GeV Higgs boson in the framework of SUSY can be analyzed from a variety of perspectives. Here we discuss the prospects of the lightest Higgs in MSSM in two different scenarios.

A lightest Higgs in SUSY can be produced through the decay of heavier SUSY particles. We investigate the decay mode,

$$\chi_1^\pm \chi_2^0 \rightarrow (W\chi_1^0)(\chi_1^0 h) \rightarrow 1 - lepton + b\bar{b} + \not{p}_T, \tag{II.6.2}$$

where leptons come from the W boson decay and the Higgs decays as $h \rightarrow b\bar{b}$. For situations where the μ parameter is fairly high, the lighter chargino ($\chi_1^\pm$) and the neutralinos ($\chi_{1,2}^0$) are gaugino like and if the decay mode $\chi_2^0 \rightarrow \chi_1^0 h$ is kinematically allowed, this mode dominates over $\chi_2^0 \rightarrow \chi_1^0 Z$. This is particularly true for CMSSM, where RGE effects drive the μ parameter to large values. As a demonstration we choose certain benchmark points for our simulation as shown in Table 9.4.

As the primary decay mode of the lightest Higgs is to a pair of b-quarks, one can observe a peak at the Higgs mass by reconstructing the invariant mass of the $b\bar{b}$ system. The largest background to this process comes from $t\bar{t}$ production where the presence of two b-quarks in the final state can lead to a similar fake mass peak. Since the $t\bar{t}$ cross section is quite large this is the most significant background, along with the standard model processes Wh and Zh which has a similar signature.

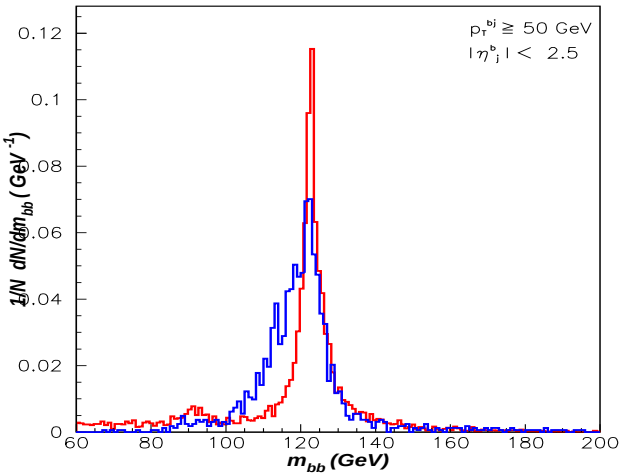

Figure II.6: The Higgs Mass reconstruction for two methods of mass reconstruction. The red curve for substructure method while the blue curve for b-like jet identification. The signal process is for the benchmark point P2 in Table 9.4.

We probe the decay channel in Eq.II.6.2 by reconstructing the Higgs mass from the di-jet final state in two ways. First, by identifying the b-like jets by matching b-quarks with jets within a cone of $\Delta R(b, j) = 0.5$, where the jets are reconstructed using FastJet with $p_T^j \geq 50\ GeV$ and $|\eta| \leq 3$. The resulting b-like jets are used to reconstruct the invariant mass, and we demand that the invariant mass should be within the Higgs mass window of 110-130 GeV. In the second case we use the method of jet substructure prescribed by [35] to identify b-like subjets from a fatjet to reconstruct the invariant mass. In Fig. II.6 the two methods of Higgs mass reconstruction are presented and clearly show that the method of jet substructure works better. It can be observed that the $t\bar{t}$ background can be reduced by a huge amount by applying the method of substructure; the details of the simulations can be found in [34]. We also use the previously defined variable R_T [19] to good use to suppress some of the backgrounds. Our analysis shows that it is possible to find a signal for the channel in Eq.II.6.2 with 8 and 14 TeV LHC energy at 100 fb^{-1} with a signal significance of $S/\sqrt{B} \geq 7$, for chargino and neutralino masses in the range of 250-450 GeV [34].

We also realize that the Higgs can decay to a pair of LSPs in SUSY. Since the LSP is extremely weakly interacting it will evade the detector and hence will show up as $\not{p}_T$. The invisible decay will be manifested in the total decay width of Higgs. ATLAS and CMS has constrained the invisible branching ratio of the Higgs to less than 0.64 from global fits [36]. The prospects of an invisible Higgs signature at the LHC has been studied previously in a number of works [37]. In this work we investigated the prospect of determining the invisible Higgs branching ratio by looking at the Higgs production via vector boson fusion (VBF) process and the associated production of the Higgs at the LHC. The VBF channel is probed in the final state,

$$pp \to qqh \to di-jet + \not{p}_T.$$

The VBF process is characterized by two jets moving in forward directions with large rapidity gaps and hence a central jet veto is useful to suppress a huge amount of SM background. The largest background to this decay mode is the Z ($\to \nu\bar{\nu}$)+ 2 jet process. To suppress the backgrounds we use the criteria of large dijet invariant mass along with the central jet veto. We observed that it

is possible to probe an invisible Higgs branching ratio down to 79 % at 8 TeV and down to 25 % with 300 fb^{-1} luminosity at 14 TeV [38].

Along with this we revisited the di-lepton + missing energy signature in the $pp \to Z(\to l^+l^-)h$ channel for 8 and 14 TeV LHC previously studied in [39]. We however use a better optimization of cuts as compared to the previous analysis and show that it is possible to observe a signal for 14 TeV LHC energy with a luminosity of 50 fb^{-1} with a significance of $S/\sqrt{B} = 8$ [38] corresponding to an invisible Higgs branching ratio down to 62.5%.

Finally we also probed the possibility of detecting an invisible branching fraction in the associated production $pp \to Z(\to b\bar{b})h$ by identifying b-jets and using jet substructure methods as before. We however find that since the jets are not boosted enough this procedure is not promising, and only high luminosity options at 14 TeV can probe this channel in this decay mode.

II.7 Supersymmetry with third generation squarks

While the Higgs boson was found to the joy of particle physicists, no hint of SUSY was observed at the end of the 8 TeV run. The non observation of SUSY signatures, particularly the first two generation of squarks and the gluino in the sub-TeV range lead to the emergence of natural SUSY as the motivating factor to approach SUSY. This is inspired by the observation that the most relevant particles for the cancellation of quadratic divergences in SM that are third generation squarks, and in particular stops. The second observation is that a Higgs mass of 125 GeV requires a large triliner coupling A_t (Eq.3.6.20), and hence even if the first two generation squarks are heavy, a large A_t term will result in a large splitting in the stop mass eigen states resulting in the fact that one of the stops could be light(200-500 GeV). Hence the light stop production cross section could be significantly large and its decay modes could be accessible at LHC energies. The emphasis has been to move away from the framework of CMSSM and consider simplified models in the phenomenological MSSM(pMSSM), which is specified by 19 parameters with simplified assumptions.The third generation phenomenology at colliders have been studied in the literature both from the point of view of naturalness and collider searches extensively. ATLAS and CMS has also probed light third generation squarks in a variety of final states [40–42].

In our work we study some of the decay modes of stop and sbottom. In a variety of situations a light 3rd generation also implies a light sbottom along with a light stop. Since sbottom cross sections are comparable to stop cross sections this too should be given equal priority. The sbottom phenomenology at colliders has been dealt with by a variety of works most of which concentrate on the sbottom co-annihilation scenario $\tilde{b}_1 \to b\chi_1^0$ [43], which is important also from the dark matter perspective. This requires either a small mass gap between the lightest sbottom (in this case the next to leading supersymmetric particle (NLSP)) and the LSP, or an entirely right handed sbottom. However there can be a large region of parameter space where the sbottom is predominantly left handed and decays via the mode,

$$pp \to \tilde{b}_1^*\tilde{b}_1 \to b\bar{b} + 2\chi_2^0 \to b\bar{b} + 2\chi_1^0 + 2Z \to b\bar{b} + 4l + \not{p}_T. \tag{II.7.1}$$

The branching ratio of $\tilde{b}_1 \to b\chi_2^0 \to \chi_1^0 Z$ is close to 100 % in this case, assuming that $\chi_2^0 \to \chi_1^0 h$ is kinematically closed. In this study we worked in the framework of pMSSM to find the appropriate parameter space which produces such a scenario. Thus from an sbottom pair production for Eq.II.7.1, one can obtain as many as 4 leptons from the Z boson decay along with b-jets. Since a 4 lepton +2 b-jets $+\not{p}_T$ signal is rather clean, this can be a strong probe of the left handed sbottom scenario. We analyzed the above decay mode and observed that although the backgrounds

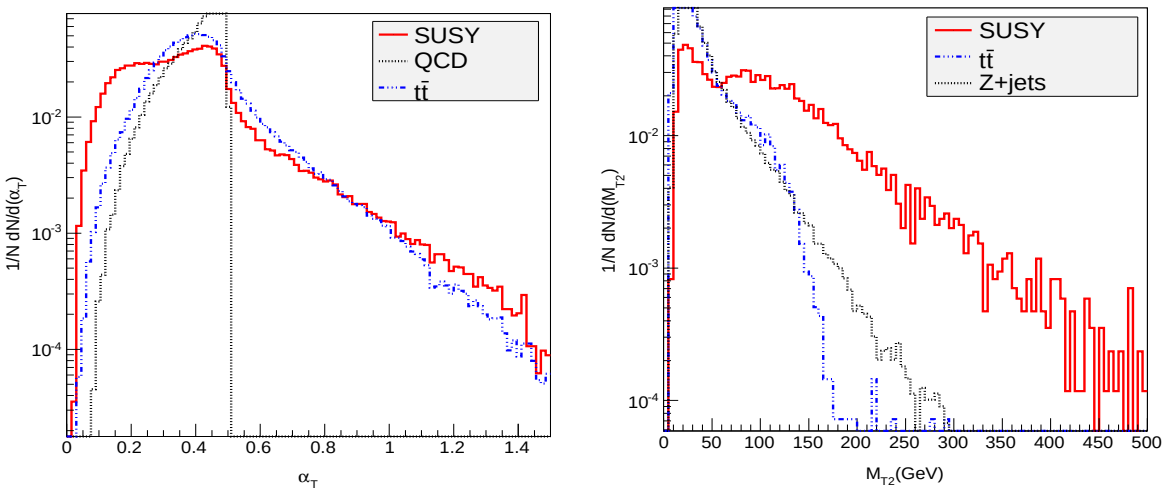

Figure II.7: The α_T(left) and the M_{T2}(right) distribution for signal and background for 13 TeV LHC. The benchmark point is for CMSSM parameter space $m_0 = 2589$, $m_{1/2} = 695$, $A_0 = -5849$, tanβ=10 $\mu > 0$. All energy units are in GeV.

were negligibly small, the low branching ratio of the Z boson to 4 leptons meant that our discovery reach is cross section limited rather than being background limited. We find that with our discovery strategy we can probe sbottom masses up to 550 GeV at 14 TeV with 100 fb^{-1} luminosity [44].

We also attempt to probe the lightest stop in the flavor violating channel $\tilde{t}_1 \to c\chi_1^0$. This channel is important from the perspective of dark matter related to the stop co-annihilation scenario. This flavor violating decay depends on the mass difference between the stop and the lightest neutralino and is dominant for small mass differences ($\sim$ 10-40 GeV). A competing mode to this channel is the four body decay mode $\tilde{t}_1 \to bff'\chi_1^0$. This channel however depends on tanβ, with the two body decay preferred over the four body decay for larger values of tanβ [45]. We probe the decay channel,

$$pp \to \tilde{t_1}\tilde{t_1^*} \to c\bar{c} + 2\chi_1^0 \to di - jet + \not{p}_T. \tag{II.7.2}$$

In this study we performed our analysis the framework of both CMSSM and pMSSM.

The challenging aspect of analyzing this channel is the low mass difference between $\tilde{t}_1$ and χ_1^0, which implies that the jets and missing energy are soft. One of the major backgrounds to this channel is the QCD process, which, due to its large cross section is quite problematic. The second major background to this process is the irreducible Z ($\to \nu\bar{\nu}$) + 2 jet. To suppress the QCD background, we use the variable $\alpha_T = p_T^{j2}/m_{jj}$ [46], where p_T^{j2} is the second hardest jet, and m_{jj} is the invariant mass of the di-jet system. It can be shown that for QCD processes dominated by back to back di-jet configuration without a significant $\not{p}_T$ this variable has an end point at 0.5. For processes like SUSY with a di-jet with a substantial $\not{p}_T$ in the final state, the tail of the distribution for this variable can extend well beyond 0.5, and therefore we can put a selection cut of 0.55 to suppress the QCD background. A plot of α_T for the signal and background is presented in the left panel of Fig. 9.8. Note that $t\bar{t}$ process is not significantly affected by this variable as there is a sufficient amount of $\not{p}_T$.

To suppress the $t\bar{t}$ and the Z($\to \nu\bar{\nu}$) + 2 jet background we use the kinematic variable M_{T2} [47] defined as,

$$M_{T2}(j_1, j_2, \not{p}_T) = \min\,[\max\{M_T(j_1, \chi), M_T(j_2, \chi)\}], \tag{II.7.3}$$

where the minimization is performed over $\not{p}_T^{\prime 1} + \not{p}_T^{\prime 2} = \not{p}_T^{\prime}$, where $\not{p}_T^{\prime 1}$, $\not{p}_T^{\prime 2}$ are all possible partitions of $\not{p}_T^{\prime}$. Here χ is the invisible particle whose mass (M_χ) is an undetermined parameter. The kinematic variable M_T is defined as,

$$M_T^2 = M_j^2 + M_\chi^2 + 2(E_T^j E_T^\chi - \tilde{p}_T^j . \tilde{p}_T^\chi),$$

where $\tilde{p}_T^j$ is the transverse momentum vector of the jet and E_T^j the corresponding energy, while $\tilde{p}_T^\chi$ is the missing transverse momentum ($\not{p}_T^{\prime}$) vector. Since we expect the standard model processes to have an end point at the respective parent masses, we set M_χ to 0 [48]. SUSY processes where the parent particle ($\widetilde{t}_1$) is heavier, the tail is expected to extend to higher values. In Fig. 9.8, the signal and background distribution for M_{T2} is displayed for 13 TeV LHC(right panel) for the choice of benchmark point as described in the caption of the figure. We observe that a cut of 250 GeV is effective in suppressing a huge amount of background from the Z ($\rightarrow \nu\bar{\nu}$) + jets and $t\bar{t}$ background.

We observed that with our choice of kinematic cuts it is possible to probe stop masses upto 450 GeV with 100 fb^{-1} data at 13 TeV LHC. We are also investigating the possibility of tagging charm-like jets. The preliminary studies show that the signal significance can be drastically improved if charm-like jets could be identified [49].

II.8 Conclusion and Outlook

In the works described in this synopsis the emphasis has been to probe various signatures of SUSY at the LHC. We developed a new technique based on event shape variables to probe SUSY signals which proved to be extremely useful in a large part of SUSY parameter space dominated by hard multi-jets. In the above works we also constrained the SUSY parameter space in the framework of CMSSM from flavor, dark matter and direct collider searches. After the discovery of the Higgs boson, we analyzed the possibility of signatures of the Higgs boson in the framework of SUSY and decays of SUSY particles. We used jet substructure methods to look for a Higgs signal in neutralino decays at the LHC. We also looked at the potential of the Higgs decaying invisibly into a pair of stable weakly interacting particles, which is well motivated in the context of SUSY. We probed the possibility of detecting such an invisible branching fraction. Finally we analyzed SUSY signatures of third generation squarks which are well motivated from the point of view naturalness. We probed third generation signatures in third generation NLSP scenarios and showed that a large part of the third generation squarks can be discovered with our strategy at 13/14 TeV center of mass energy.

The possibility of a SUSY signature is thus very much alive even if the early LHC run did not produce any SUSY signal. Arguments of naturalness and third generation squarks are expected to drive SUSY searches at the LHC in future. Only a small part of the SUSY parameter space has been skimmed, and the exclusions are highly model dependent. Thus it is essential that we probe signatures in all possible situations and improvements have to be made to access kinematically challenging regions of the parameter space.

II.9 List of Publications

1. Title : *Event-shape selection cuts for supersymmetry searches at the LHC with 7 TeV energy.*
   Co-authors: M. Guchait.
   Published: Phys.Rev. D84 (2011) 055010, arXiv:1102.4785[hep-ph].

2. Title : *Probing a Mixed Neutralino Dark Matter Model at the 7 TeV LHC.*
   Co-authors : M. Guchait, D.P. Roy.
   Published : Phys.Rev. D85 (2012) 035024,arXiv:1109.6529[hep-ph].

3. Title : *Higgs Signal in Chargino-Neutralino Production at the LHC.*
   Co-authors : D. Ghosh, M. Guchait.
   Published : Eur.Phys.J. C72 (2012) 2141, arXiv:1202.4937[hep-ph].

4. Title : *How Constrained is the cMSSM?*
   Co-authors : D. Ghosh,M. Guchait, S. Raychaudhuri.
   Published : Phys.Rev. D86 (2012) 055007,arXiv: 1205.2283[hep-ph].

5. Title: *Probing Supersymmetry using Event Shape variables at 8 TeV LHC.*
   Co-authors: R.M. Chatterjee, M. Guchait.
   Published : Phys.Rev. D86 (2012) 075014, arXiv:1206.5770[hep-ph].

6. Title : *Searching the sbottom in the four lepton channel at the LHC.*
   Co-authors : D. Ghosh.
   Published : Eur.Phys.J. C73 (2013) 2342, arXiv:1209.4310[hep-ph].

7. Title : *Looking for an Invisible Higgs Signal at the LHC.*
   Co-authors : D. Ghosh, R. Godbole, M. Guchait, K. Mohan.
   Published : Physics Letters B 725 (2013),arXiv:1211.7015[hep-ph].

8. Title : *Stop and sbottom search using dileptonic MT2 variable and boosted top technique at the LHC.*
   Co-authors : A. Chakroborty, D.K. Ghosh, D. Ghosh.
   Published : arXiv:1303.5776[hep-ph] (Accepted for publication at JHEP).

9. Title : *Probing the flavor violating scalar top quark signal at the LHC.*
   Co-authors : G. Belanger,D. Ghosh, R. Godbole, M. Guchait.
   Pre-print : arXiv:1308.6484[hep-ph] (In communication with PRD).

10. Conference Proceedings:
    Title : *Event shape variables in supersymmetry searches at 7-TeV LHC.*
    Published: Pramana 79 (2012) 1313-1315 . Conference proceedings for Lepton-Photon 2011.

Chapter 1

Introduction

The Standard Model (SM) of particle physics began to take shape from the late 1960's and was a resounding triumph in explaining the known force and matter content of the universe (with the exception of gravity). It provided a framework of gauge theories which was experimentally tested to remarkable precision at the LEP, Tevatron and now at the LHC. The first vindications of the SM came with the discovery of the neutral current interactions in the 1970's and was formally established with the discovery of the W and the Z boson in the 1980's. The final frontier has been conquered recently, with the discovery of the Higgs boson at 125 GeV. The success of the SM in explaining physics at the electroweak scale not withstanding, several deficiencies prompt us to look beyond. The hierarchy problem, the issue of neutrino masses, the absence of a dark matter candidate are some the concerns that needs to be addressed in this context. Hence a wide range of theories that attempted to resolve some of these issues began emerging as early as the late 1970's, and more propositions are pouring in even today. Some of the robust attempts have been supersymmetry, extra dimensional models and little Higgs models.

The emergence of the proposition that nature is likely to be supersymmetric, was borne out of the need to address the deficiencies of the Standard Model (SM) and embed it within a structure that that can be extended up to the grand unified scale. While the historic development followed from a series of observations in string theory, QCD and later a mathematical construction leading to a loophole in the Coleman Mandula theorem in the 1960's, the realization that a phenomenological model of supersymmetry (SUSY) was viable as an extension of SM was realized only in the 1980's. Over the last two decades this has served as the springboard to study SUSY in all its glory. What started as a purely mathematical and theoretical construction has lingered on as the biggest hope in the attempts to find signatures of new physics at colliders in the effort to find an unified theory.

The last two decades have seen the emergence of SUSY as the most attractive model of a beyond Standard Model (BSM) theory. The unification of gauge couplings, the resolution of the gauge hierarchy problem, the presence of a viable dark matter candidate all pointed to SUSY as the theory that could be a natural extension of the SM.

A phenomenologically viable model of SUSY required the theory to be broken at some scale. As the breaking mechanism is not well established, a variety of conditions and mechanisms of SUSY breaking lead to a plethora of low energy spectrums at the electroweak scale.

The investigation of SUSY signals began alongside the Higgs searches at the LEP collider in the late 1980's. The searches at LEP provided limits on charginos and sleptons, and some of them still serve as model independent limits in this regard. The search for a SUSY signal continued through the era of the Tevatron and produced limits on strongly interacting sparticles (gluinos and squarks).

With the ushering of the LHC era the search for sparticles gathered momentum; and while the early searches were conducted in the model context of the minimal supergravity(mSUGRA)/ constrained minimal supersymmetric standard model(CMSSM), it was later expanded to encompass a whole class of supersymmetric models.

An enormous amount of effort and work have been conducted to unearth the SUSY signal from the humongous rubble of the SM background. The SM background is gargantuan in terms of cross section as compared to SUSY processes, and thus discerning a signal out of this debris amounts to looking for a needle in the haystack. At a hadron collider like the Large Hadron Collider(LHC), the ambient background from quantum chromodynamic(QCD), as well as electroweak processes are huge, and therefore specialized techniques are required to be devised in order to suppress this huge mess. To this end various strategies have been formulated to achieve this objective. Some of these schemes have been fairly general, and have attempted to optimize the sensitivity of the signal with the aim of covering a wide range of SUSY signatures and catering to different regions of the SUSY parameter space in the context of various models. These strategies generally rely on the use of a large missing energy, a robust signature of SUSY in a class of models termed as "R-parity conserving". There are other designs, which attempt to look at specific properties of the SUSY signal like end point characteristics of a kinematical distribution, end points in mass distributions, and the topology of the SUSY signature. Some of these methods have been extremely successful in attempting to suppress the SM background in order to look for a SUSY signal. It is therefore an important task to hatch strategies that attempt to cover more ground in the quest for a SUSY signal in collider experiments.

The dawn of the LHC era has ushered in a whole new regime in the search for BSM physics including SUSY. The early LHC data for 7 and 8 TeV center of mass energy have been used to probe SUSY signatures. However no hints of a SUSY signature has been observed till date. This should not be a concern, as we have only skimmed the surface of the vast SUSY parameter space. After all if SUSY does exist, it will correspond to one particular point in this huge parameter space, and thus negative searches will only narrow this real estate. It is therefore imperative to analyze the constraints arising from existing data in order to get an indication of the kind of parameter space one should be investigating in order to look for a SUSY signal. Low energy flavor constraints like the branching ratios of the decays $B_s \to \mu^+\mu^-$, $B \to X_s\gamma$, the anomalous magnetic moment of the muon also constrain the SUSY parameter space. These constraints evolve as more data is analyzed, such that experimental uncertainties in these numbers reduce, and therefore it is necessary that a study of these constraints is conducted to delineate the regions of parameter space that survive these bounds. We perform such a study in the framework of CMSSM by taking into account the LHC search results on SUSY, the flavor and dark mark matter constraints.

With the discovery of the Higgs boson at 125 GeV, the triumph of the SM is now almost well established. However the discovery of the Higgs boson has a significant impact on the SUSY parameter space. The Higgs mass which was only required to satisfy the LEP lower bound of 114 GeV, is a much stricter contsraint for all SUSY spectrums now. However, as we argued earlier, this should be taken as a boon, as it allows us to narrow down the parameter space in which to look for a SUSY signal. Additionally, the Higgs boson can be used as a signal of SUSY, as one can obtain the lightest Higgs boson in decays of heavier sparticles. Moreover the Higgs can invisibly to a pair of sparticles, thus leading to an invisible decay width. We address both these issues in a couple of studies in this thesis.

The aim of this thesis is to explore signatures of SUSY at the LHC, and to devise search strategies that are efficient to quash the SM backgrounds. The endeavour is to improve the current

schemes in use at the LHC and various phenomenological works to access kinematically challenging regions of the SUSY parameter space. As we shall present in this thesis, it is indeed possible to achieve this goal by a judicious choice of kinematic variables to dig out the signal out of the debris of the background. In this thesis we will introduce the use of event shape variables in SUSY searches for the first time and demonstrate that such a search strategy is capable of achieving a better sensitivity than the existing search programmes in a wide region of the SUSY parameter space. It will be demonstrated that these variables are fairly simple, easy to implement and are potentially prone to less systematic errors by construction.

The early SUSY searches at the LHC primarily looked for the gluino and the squarks of the first two generations in the model framework of CMSSM. However the negative searches have pushed the gluino and the squarks of the first two generations above 1 TeV. The focus therefore has shifted to the third generation squarks as the primary sparticles of interest. This is well motivated from the point of view of naturalness, as the third generation squarks are crucial for a natural SUSY theory. Moreover, the connection of the third generation squarks with the mass of the light Higgs boson has also aided to its emergence as the focal point of SUSY searches and phenomenology. In this thesis we will present a couple of studies on the signatures of third generation squarks.

This thesis is organized as follows; In Chapter 2 a brief description of the SM, along with the discovery of the Higgs boson, the constraints on the SM and a motivation to SUSY is provided. In Chapter 3, a brief account of minimally supersymmetric standard model (MSSM) is provided. This is by no means an exhaustive account; the attempt here is to merely make a connection between theoretical ideas and experimental searches. The constraints on SUSY parameter space from flavor, dark matter and collider searches is discussed in Chapter 4. An analysis of the CMSSM parameter space, taking these constraints into account is provided in Chapter 5. A brief overview of the Large Hadron Collider (LHC), the kinematics, jets and monte carlo tools required for the works is described in Chapter 6. In Chapter 7, we introduce event shape variables for SUSY searches for 7 and 8 TeV LHC energy. In Chapter 8, we investigate Higgs signatures in the context of MSSM. Here we study a Higgs signal in neutralino decays using jet substructure methods. Secondly, we also probe the invisible decay of the Higgs at the LHC in vector boson fusion (VBF), and associated production of Higgs with a Z boson. In Chapter 9, we investigate signatures of third generation SUSY (the lighter stop and sbottoms). Finally we conclude in Chapter 10.

Chapter 2

The Standard Model

This chapter briefly describes the Standard Model (SM) of particle physics . A brief summary of the particle and force content along with the SM Lagrangian is introduced, followed by the Higgs mechanism [1]. We also discuss the theoretical and experimental constraints on the SM Higgs boson, followed by a brief description of the discovery of the Higgs boson and the shortcomings of the SM. Finally, we introduce supersymmetry.

2.1 The Standard Model Lagrangian

The SM [50–53] is built on the three pillars of gauge theory. The first is quantum electrodynamics (QED) described by the gauge group $U(1)_{em}$. QED describes the interaction of electrically charged particles with its gauge boson, namely the photon. [2]. The second building block is the theory of weak interactions expressed by the gauge group $\mathrm{SU}(2)$. This block describes the weak gauge bosons $(\mathrm{W}^1_\mu, \mathrm{W}^2_\mu, \mathrm{W}^3_\mu)$ and its interaction with the matter particles charged under the $\mathrm{SU}(2)$ gauge group. The final block is the theory of strong interactions, namely Quantum Chromodynamics(QCD) [54, 55], described by the $\mathrm{SU}(3)_\mathrm{c}$ gauge group with the gauge bosons termed as gluons $(\mathrm{G}^\mathrm{a}_\mu)$. The strong sector describes the interactions of quarks with gluons.

The synthesis of the three gauge groups is described by the Standard Model(SM). The electroweak part, proposed by Sheldon Glashow, Abdus Salam and Steven Weinberg [50–53] requires the theory to be invariant under the gauge group $SU(2)_L \times U(1)_Y$.

The entire structure provides a framework describing the known particle and the force content of nature (with the exception of gravity).

The particle content of the theory, charged under various gauge groups is given by the following clusters :

Weak Iso–doublet of leptons : $\mathrm{L_i} = \begin{pmatrix} \nu_i \\ e_i^- \end{pmatrix}_\mathrm{L} \sim (\mathbf{2}, \mathbf{1^c});\ (\mathbf{i} = \mathbf{e}, \mu, \tau).$

Weak Iso–singlet of leptons : $\bar{\mathrm{e}}_\mathrm{iL} = \mathrm{e}^-_\mathrm{iR} \sim (\mathbf{1}, \mathbf{1^c});\ (\mathbf{i} = \mathbf{e}, \mu, \tau).$

Weak Iso–doublet of quarks :$\mathrm{Q_i} = \begin{pmatrix} u_i \\ d_i \end{pmatrix}_\mathrm{L} \sim (\mathbf{2}, \mathbf{3^c});\ (\mathbf{u_i} = \mathbf{u}, \mathbf{c}, \mathbf{t}),\ (\mathbf{d_i} = \mathbf{d}, \mathbf{s}, \mathbf{b}).$

Weak Iso–singlet of quarks : $\bar{\mathrm{u}}_\mathrm{iL} = \mathrm{u}^-_\mathrm{iR} \sim (\mathbf{1}, \bar{\mathbf{3}}^\mathbf{c});\ (\mathbf{u_i} = \mathbf{u}, \mathbf{c}, \mathbf{t}).$

[1] We use the notations followed by [3]. Some of the Feynman diagrams are also used from [3]

[2] The gauge field of QED is termed A_μ by convention while the particle is called γ. The gauge field of the U(1) group in the unbroken $SU(2)_L \times U(1)_Y$ phase is termed as B_μ, which after electroweak symmetry breaking is reduced to $U(1)_{em}$, as explained later.

Weak Iso–singlet of quarks : $\bar{d}_{iL} = d^{-}_{iR} \sim (\mathbf{1}, \bar{\mathbf{3}}^{\mathbf{c}})$; $(\mathbf{u_i} = \mathbf{d}, \mathbf{s}, \mathbf{b})$,

where the quantities in the parenthesis describe the isospin and the color assignments of the respective particles.

The fermion hypercharge Y is related to the electric charge Q and the weak isospin T_3 via $Q = T_3 + Y/2$. Thus in terms of the unit charge +e the hypercharge assignments are given by,

$$Y_{L_i} = -1,\ Y_{e_{R_i}} = -2,\ Y_{Q_i} = \frac{1}{3},\ Y_{u_{R_i}} = \frac{4}{3},\ Y_{d_{R_i}} = -\frac{2}{3}.$$

Note that $\sum Y_f = \sum Q_f = 0$, ensuring the cancellation of chiral anomalies [56] and thus preserving the renormalizability of the theory. The gauge invariant field strengths for the gluons represented by the field strengths $G_\mu^{1,\cdots,8}$, the weak gauge bosons $W_\mu^{1,2,3}$ and the U(1) gauge boson described by B_μ, are given by,

$$\begin{aligned} G^a_{\mu\nu} &= \partial_\mu G^a_\nu - \partial_\nu G^a_\mu + g_3\, f^{abc} G^b_\mu G^c_\nu,\ a,b,c = 1,...,8 \\ W^a_{\mu\nu} &= \partial_\mu W^a_\nu - \partial_\nu W^a_\mu + g_2\, \varepsilon^{abc} W^b_\mu W^c_\nu,\ a,b,c = 1,..,3 \\ B_{\mu\nu} &= \partial_\mu B_\nu - \partial_\nu B_\mu, \end{aligned}$$

where g_3, g_2 and g_1 are the coupling constants corresponding to the gauge groups $SU(3)_C$, $SU(2)_L$ and $U(1)_Y$ respectively. The quantities $f^{abc}, \varepsilon^{abc}$, are the structure constants of the non-abelian groups $SU(3)_c$ and $SU(2)_L$ respectively, described by the Lie algebra,

$$[T^a, T^b] = 2i f^{abc} T^c,\ [\tau^a, \tau^b] = 2i\varepsilon^{abc}\tau^c, \tag{2.1.1}$$

where T^a and τ^a are the generators of the respective gauge groups. The non–abelian nature of the SU(2) and SU(3) groups leads to self–interactions between their gauge fields, $V_\mu \equiv W_\mu$ or G_μ, leading to the tripple gauge boson couplings $ig_i \mathrm{Tr}(\partial_\nu V_\mu - \partial_\mu V_\nu)[V_\mu, V_\nu]$ and quartic gauge boson couplings $\frac{1}{2} g_i^2 \mathrm{Tr}[V_\mu, V_\nu]^2$.

The SM Lagrangian can then be expressed in terms of the matter and the force content as,

$$\begin{aligned} \mathscr{L}_{SM} &= -\frac{1}{4} G^a_{\mu\nu} G^{\mu\nu}_a - \frac{1}{4} W^a_{\mu\nu} W^{\mu\nu}_a - \frac{1}{4} B_{\mu\nu} B^{\mu\nu} \\ &\quad + \bar{L}_i\, iD_\mu \gamma^\mu\, L_i + \bar{e}_{Ri}\, iD_\mu \gamma^\mu\, e_{R_i} + \bar{Q}_i\, iD_\mu \gamma^\mu\, Q_i + \bar{u}_{Ri}\, iD_\mu \gamma^\mu\, u_{R_i} + \bar{d}_{Ri}\, iD_\mu \gamma^\mu\, d_{R_i}, \end{aligned} \tag{2.1.2}$$

where the first line of Eq. 2.1.2 describes the force content, captured in the kinetic terms of the gauge fields, and the second line describes the fermionic kinetic terms and the interaction of matter fields with the gauge fields, charged under the respective gauge groups, encoded in the covariant derivatives. The self interactions of the gauge bosons are encoded in the gauge kinetic terms providing the three point and four point functions of the weak gauge bosons and the gluons.

The covariant derivative, that couples matter fields ψ to gauge fields is given by (for left handed quarks),

$$D_\mu \psi = \left(\partial_\mu - i g_3 T_a G^a_\mu - i g_2 \tau_a W^a_\mu - i g_1 \frac{Y_q}{2} B_\mu \right) \psi, \tag{2.1.3}$$

leading to unique couplings between the fermion and gauge fields V_μ $(V = B_\mu, W^i_\mu, G^a_\mu)$ of the form $-g_i \overline{\psi} V_\mu \gamma^\mu \psi$. Analogous terms can be written for the other fermions with the covariant derivative containing the fields charged under the corresponding gauge groups.

The left handed and the right handed sectors of the electroweak part of the SM, along with the gauge fields transform under gauge transformations in the following way,

$$L_i(x) \to L_i'(x) = e^{i\alpha_a(x)\tau^a + i\beta(x)Y} L_i(x) \ , \ R_i(x) \to R_i'(x) = e^{i\beta(x)Y} R_i(x)$$
$$\vec{W}_\mu^a(x) \to \vec{W}_\mu{}^a(x) - \frac{1}{g_2}\partial_\mu \vec{\alpha}(x) - \vec{\alpha}(x) \times \vec{W}_\mu^a(x) \ , \ B_\mu(x) \to B_\mu(x) - \frac{1}{g_1}\partial_\mu \beta(x). \qquad (2.1.4)$$

2.2 The Higgs boson in the Standard Model

2.2.1 Requirement of a Higgs scalar in the theory

Note that there are no explicit mass terms for gauge bosons and fermions in the above Lagrangian. The legacy of the SM electroweak gauge symmetry ensures that one cannot write down mass terms of the form $\frac{1}{2}M_V^2 W_\mu W^\mu$, without explicitly violating it. Similarly the electroweak gauge symmetry ensures that fermionic mass terms of the form $m\bar{\psi}\psi$ are forbidden as $\bar{\psi}\psi = \bar{\psi}_L \psi_R$, and hence is not invariant under $SU(2)_L \times U(1)_Y$. However experimental observations contradict this as we have observed massive electroweak gauge bosons and fermions. A SU(2) doublet scalar field comes to the rescue here, generating mass terms for the SM particles, as explained in the next section.

Along with the above problem it was also known that the amplitude of the gauge boson scattering process $W^\pm W^\mp \to W^\pm W^\mp$ diverges at high energies. At high energy the longitudinal component of the W boson dominates the amplitude. With only the Z boson and the photon exchange diagrams in the s and the t channels, the amplitude grows with the energy E as $\sim g_2^2 E^2/M_W^2$, resulting in a loss of unitarity at high energies. With the introduction of a scalar Φ in the exchange of $W^\pm W^\mp$ scattering, the $\sim E^2$ behaviour is eliminated, with the resulting amplitude now proportional to the mass of the scalar itself, $\sim g^2 M_\Phi^2/M_W^2$. Thus a new scalar regulates the E^2 growth of the amplitude, thus preserving unitarity.

2.2.2 The Higgs mechanism and its interactions

The mechanism of generation of mass to gauge bosons and fermions in the SM was proposed in a series of works by Higgs–Brout–Englert–Guralnik–Hagen–Kibble, which we know as the Higgs mechanism [57–62] in the literature today. Instead of going into the full glory of the mechanism, a brief description is provided here.

As a preamble we quote the Goldstone theorem [63, 64] without an explicit proof : In a theory where a continuous symmetry is spontaneously broken, the remnant of the broken symmetry consists of massless scalars called Goldstone bosons. The number of such massless scalars equals the number of broken generators of the gauge group.

As an example if we consider a theory with O(N) symmetry broken to O(N-1), the $\frac{1}{2}N(N-1)$ generators reduce to $\frac{1}{2}(N-1)(N-2)$, leaving behind (N-1) massless Goldstones bosons.

In the SM spontaneous symmetry breaking (SSB) generates mass terms for the weak bosons while leaving the U(1) gauge boson, namely the photon massless after the electroweak symmetry is broken (EWSB) via the Higgs mechanism, as explained below. In the process the $SU(2)_L \times U(1)_Y$ gauge group is broken to $U(1)_{em}$.

The electroweak part of the SM Lagrangian, as noted earlier is given by ,

$$\mathscr{L}_{SM} = -\frac{1}{4}W_{\mu\nu}^a W_a^{\mu\nu} - \frac{1}{4}B_{\mu\nu}B^{\mu\nu} + \overline{L}_i\, iD_\mu \gamma^\mu L_i + \overline{e}_{Ri}\, iD_\mu \gamma^\mu e_{Ri} + \cdots . \qquad (2.2.1)$$

To this we add the scalar potential,depicted in Fig. 2.1. The Lagrangian containing the kinetic and the potential term is given by,

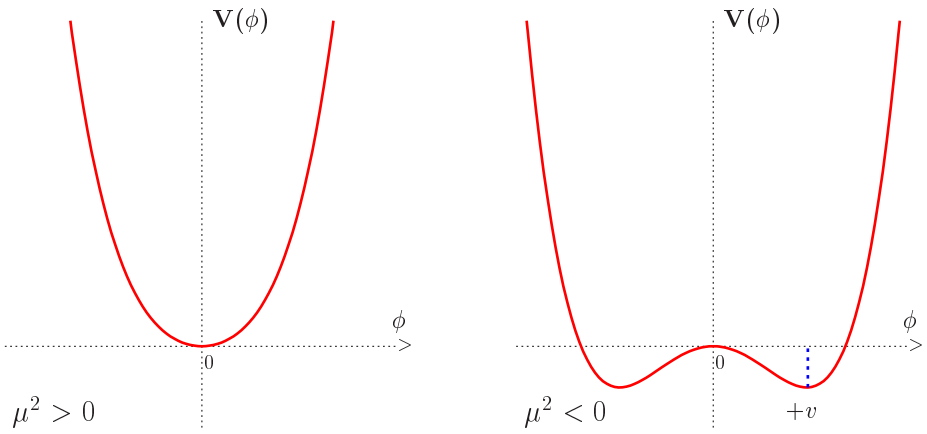

Figure 2.1: *The potential V of the scalar field ϕ in the case $\mu^2 > 0$ (left) and $\mu^2 < 0$ (right).*

$$\mathscr{L}_S = (D^\mu \Phi)^\dagger (D_\mu \Phi) - \mu^2 \Phi^\dagger \Phi - \lambda (\Phi^\dagger \Phi)^2. \tag{2.2.2}$$

where Φ a complex doublet scalar of SU(2),

$$\Phi = \begin{pmatrix} \phi^+ \\ \phi^0 \end{pmatrix}, \quad Y_\phi = +1. \tag{2.2.3}$$

The scalar potential is given by,

$$V(\Phi) = \mu^2 \Phi^\dagger \Phi + \lambda (\Phi^\dagger \Phi)^2. \tag{2.2.4}$$

Clearly from Fig. 2.1, it is evident that $\mu^2 > 0$ leads to the trivial minima at the origin, and does not facilitate the necessary breaking of the symmetry. Also note that λ has to be positive to ensure that the potential is stable. With $\lambda > 0$ and $\mu^2 < 0$, the neutral component of the scalar potential gets a vacuum expectation value (VEV) after the minimization of the potential. The choice of a particular direction in the configuration space hence breaks the symmetry, with,

$$\langle \Phi \rangle_0 \equiv \langle 0 | \Phi | 0 \rangle = \begin{pmatrix} 0 \\ \frac{\mathrm{v}}{\sqrt{2}} \end{pmatrix} \text{ with } \mathrm{v} = \left(-\frac{\mu^2}{\lambda} \right)^{1/2}. \tag{2.2.5}$$

We expand the scalar potential around the vacuum in terms of four fields $\theta_{1,2,3}(x)$ and $h(x)$,

$$\Phi(\mathrm{x}) = \begin{pmatrix} \theta_2 + i\theta_1 \\ \frac{1}{\sqrt{2}}(\mathrm{v} + \mathrm{h}(\mathrm{x})) - \mathrm{i}\theta_3 \end{pmatrix} = \mathrm{e}^{\mathrm{i}\theta_\mathrm{a}(\mathrm{x})\tau^\mathrm{a}(\mathrm{x})/\mathrm{v}} \begin{pmatrix} 0 \\ \frac{1}{\sqrt{2}}(\mathrm{v} + \mathrm{h}(\mathrm{x})) \end{pmatrix}, \tag{2.2.6}$$

where τ^a are pauli spin matrices.

To remove unphysical degrees of freedom, the unitary gauge is used (also known as Kibble parametrization), to rotate them away,

$$\Phi(\mathrm{x}) \to \mathrm{e}^{-\mathrm{i}\theta_\mathrm{a}(\mathrm{x})\tau^\mathrm{a}(\mathrm{x})} \Phi(\mathrm{x}) = \frac{1}{\sqrt{2}} \begin{pmatrix} 0 \\ \mathrm{v} + \mathrm{h}(\mathrm{x}) \end{pmatrix}. \tag{2.2.7}$$

Note that the fields $\theta_{1,2,3}(\mathrm{x})$ and $\mathrm{h}(\mathrm{x})$, vanish at the vacuum. We also understand that under gauge transformations along the three broken directions, the fields $\theta_{1,2,3}(\mathrm{x})$ transform inhomogeneously but linearly. However, the field $\mathrm{h}(\mathrm{x})$ remains gauge invariant. We also observe the Goldstone theorem in action. The Higgs potential had an O(4) symmetry broken down to O(3) by the choice of the VEV. The 6 generators of O(4) are reduced to 3, leaving behind three Goldstone bosons.

The kinetic term of the scalar potential by an explicit expansion of the term $\mathscr{L}_S$ gives:

$$\begin{aligned}
|\mathrm{D}_\mu\Phi)|^2 &= \left|\left(\partial_\mu - \mathrm{i}g_2\frac{\tau_\mathrm{a}}{2}\mathrm{W}^\mathrm{a}_\mu - \mathrm{i}g_1\frac{1}{2}\mathrm{B}_\mu\right)\Phi\right|^2 \\
&= \frac{1}{2}\left|\begin{pmatrix} \partial_\mu - \frac{i}{2}(g_2W^3_\mu + g_1B_\mu) & -\frac{ig_2}{2}(W^1_\mu - iW^2_\mu) \\ -\frac{ig_2}{2}(W^1_\mu + iW^2_\mu) & \partial_\mu + \frac{i}{2}(g_2W^3_\mu - g_1B_\mu) \end{pmatrix}\begin{pmatrix} 0 \\ \mathrm{v}+\mathrm{h} \end{pmatrix}\right|^2 \\
&= \frac{1}{2}(\partial_\mu \mathrm{h})^2 + \frac{1}{8}g_2^2(\mathrm{v}+\mathrm{h})^2|\mathrm{W}^1_\mu + \mathrm{i}\mathrm{W}^2_\mu|^2 + \frac{1}{8}(\mathrm{v}+\mathrm{h})^2|g_2\mathrm{W}^3_\mu - g_1\mathrm{B}_\mu|^2.
\end{aligned}$$

We make the following field redefinitions, so as to express the weak eigen states ($\mathrm{W}^\mathrm{i}_\mu$) in terms of the mass eigen states as,

$$W^\pm_\mu = \frac{1}{\sqrt{2}}(W^1_\mu \mp iW^2_\mu)\ ,\ Z_\mu = \frac{g_2W^3_\mu - g_1B_\mu}{\sqrt{g_2^2+g_1^2}}\ ,\ A_\mu = \frac{g_2W^3_\mu + g_1B_\mu}{\sqrt{g_2^2+g_1^2}}. \tag{2.2.8}$$

The mass terms for $W^\pm$, and Z boson are now given by, $\mathrm{M}^2_\mathrm{W}\mathrm{W}^+_\mu\mathrm{W}^{-\mu} + \frac{1}{2}\mathrm{M}^2_\mathrm{Z}\mathrm{Z}_\mu\mathrm{Z}^\mu + \frac{1}{2}\mathrm{M}^2_\gamma\mathrm{A}_\mu\mathrm{A}^\mu$, with,

$$\mathrm{M_W} = \frac{1}{2}\mathrm{v}g_2\ ,\ \mathrm{M_Z} = \frac{1}{2}\mathrm{v}\sqrt{g_2^2+g_1^2}\ ,\ \mathrm{M}_\gamma = 0. \tag{2.2.9}$$

The value of the vacuum expectation value v is fixed in terms of the mass of W boson or the Fermi constant G_μ,

$$\mathrm{M_W} = \frac{1}{2}g_2\mathrm{v} = \left(\frac{\sqrt{2}g_2^2}{8\mathrm{G}_\mu}\right)^{1/2} \Rightarrow \mathrm{v} = \frac{1}{(\sqrt{2}\mathrm{G}_\mu)^{1/2}} \simeq 246\ \mathrm{GeV}. \tag{2.2.10}$$

The mass of M_W is measured to be 80.399 ± 0.023 GeV, while the mass of M_Z is measured to be $M_Z = 91.1875 \pm 0.0021$ GeV [65]. In acquiring masses, the longitudinal degrees of freedom of the W and the Z boson have eaten away the Goldstone bosons. The gauge symmetry $\mathrm{SU(3)_c} \times \mathrm{SU(2)_L} \times \mathrm{U(1)_Y}$, is broken down to $\mathrm{SU(3)_c} \times \mathrm{U(1)_{em}}$. The unbroken part of the EW Lagrangian, namely the $\mathrm{U(1)_{em}}$, ensures that the photon is massless.

The Weinberg angle is defined as,

$$\cos\theta_\mathrm{W} = \frac{g_2}{\sqrt{g_1^2+g_2^2}},\ \ \frac{\mathrm{M}^2_\mathrm{W}}{\mathrm{M}^2_\mathrm{Z}} = \cos^2\theta_\mathrm{W},$$

with the global fitted value $\sin^2\theta_W = 0.2312 \pm 0.00015$ [65]. The electric charge is given by,

$$e = \frac{g_1g_2}{\sqrt{g_1^2+g_2^2}},$$

such that,

$$\sqrt{g_1^2+g_2^2}=\frac{e}{cos\theta_W sin\theta_W}.$$

The parameter ρ, which is a measure of the relative strengths of charged and neutral currents is defined as,

$$\rho=\frac{M_W^2}{cos^2\theta_W M_Z^2},$$

and is equal to 1 in the SM at the tree level.

Thus far a mechanism is introduced to generate the mass terms for gauge bosons by adding a Higgs field. We can generate mass terms for charged fermions using the same field by introduction of Yukawa terms to supplement the SM Lagrangian. To these end we introduce the $SU(2)_L\times U(1)_Y$ invariant Yukawa Lagrangian,

$$\mathscr{L}_{\rm Yu}=-{\rm y_{e_i}}\,\bar{\rm L_i}\,\Phi\,{\rm e_{R_i}}-{\rm y_d}\,\bar{\rm Q_i}\,\Phi\,{\rm d_{R_i}}-{\rm y_u}\,\bar{\rm Q_i}\,\tilde{\Phi}\,{\rm u_{R_i}}\;+\;{\rm h.c.},\tag{2.2.11}$$

where $\tilde{\Phi}=i\tau^2\Phi$, and is required to give masses to up type quarks.

After electroweak symmetry is broken we have (choosing the Yukawa couplings to be real),

$$\begin{aligned}\mathscr{L}_{\rm Yu} &= -\frac{1}{\sqrt{2}}y_{e_i}(\bar{\nu}_{e_i}\bar{e}_{L_i})\begin{pmatrix}0\\ {\rm v+h}\end{pmatrix}e_{R_i}\;+\cdots\\ &= -\frac{1}{\sqrt{2}}\lambda_{e_i}\,({\rm v+h})\,\bar{\rm e}_{\rm L_i}{\rm e_{R_i}}\;+\cdots,\end{aligned}\tag{2.2.12}$$

We thus have the fermion masses as,

$${\rm m_e}=\frac{{\rm y_e\,v}}{\sqrt{2}}\;\;,\;{\rm m_u}=\frac{{\rm y_u\,v}}{\sqrt{2}}\;\;,\;{\rm m_d}=\frac{{\rm y_d\,v}}{\sqrt{2}}.$$

Note that the upper component of the lepton doublet namely the neutrinos have no mass. The original leptonic kinetic terms had a $U(3)\times U(3)$ global symmetry, which is broken to three global vectorial transformations, corresponding to three lepton numbers, ${\rm L_i}\to{\rm e}^{\alpha_{\rm i}}{\rm L_i},\;\bar{\rm e_i}\to{\rm e}^{-{\rm i}\alpha_{\rm i}}\bar{\rm e_i}$.

We now turn our attention to the Higgs part of the Lagrangian itself. We note that after EWSB, the scalar potential can be written as,

$${\rm V}\;=\;\frac{\mu^2}{2}(0,\,{\rm v+H})\begin{pmatrix}0\\ {\rm v+h}\end{pmatrix}+\frac{\lambda}{4}\left[(0,\,{\rm v+h})\begin{pmatrix}0\\ {\rm v+h}\end{pmatrix}\right]^2.$$

Thus the self interaction and kinetic terms read;

$$\begin{aligned}\mathscr{L}_{\rm h} &= \frac{1}{2}(\partial_\mu h)(\partial^\mu h)-V\\ &= \frac{1}{2}(\partial^\mu{\rm h})^2-\lambda{\rm v}^2{\rm h}^2-\lambda{\rm v}{\rm h}^3-\frac{\lambda}{4}{\rm h}^4.\end{aligned}\tag{2.2.13}$$

The mass of the Higgs boson is given by ${\rm m_h^2}=2\lambda{\rm v}^2=-2\mu^2$, with the interaction vertices,

$${\rm g_{h^3}}=(3!){\rm i}\lambda{\rm v}=3{\rm i}\,\frac{{\rm m_h^2}}{\rm v}\;\;,\;{\rm g_{h^4}}=(4!){\rm i}\frac{\lambda}{4}=3{\rm i}\frac{{\rm m_h^2}}{\rm v^2}.$$

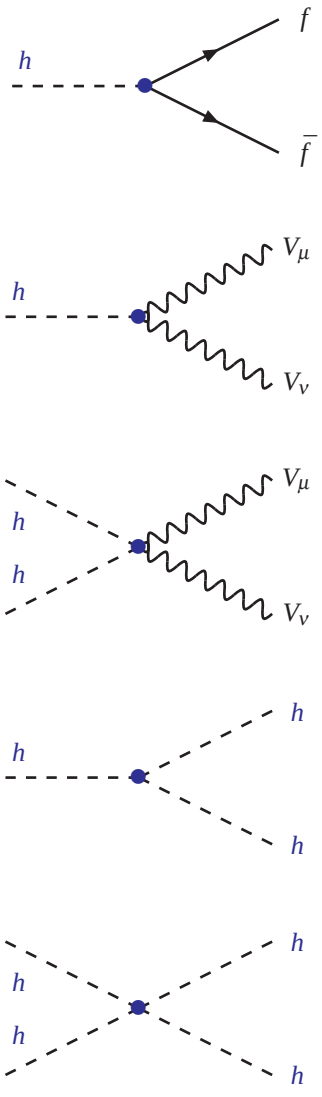

$$g_{hff} = m_f/\mathrm{v} = (\sqrt{2}\mathrm{G}_\mu)^{1/2}\,\mathrm{m_f} \qquad \times (i)$$

$$g_{hVV} = 2M_V^2/v = 2(\sqrt{2}G_\mu)^{1/2} M_V^2 \qquad \times (-ig_{\mu\nu})$$

$$g_{hhVV} = 2M_V^2/v^2 = 2\sqrt{2}G_\mu M_V^2 \qquad \times (-ig_{\mu\nu})$$

$$g_{hhh} = 3m_h^2/v = 3(\sqrt{2}G_\mu)^{1/2} m_h^2 \qquad \times (i)$$

$$g_{hhhh} = 3m_h^2/v^2 = 3\sqrt{2}G_\mu m_h^2 \qquad \times (i)$$

Figure 2.2: The interactions of the Higgs boson to fermions and gauge bosons and the Higgs self–couplings in the SM, along with relevant Feynman rules. Figure used from [3].

Note that the mass of the Higgs boson cannot be predicted in this theory and has to be determined experimentally. The couplings to gauge bosons and fermions are given by (Fig. 2.2),

$$g_{hff} = i\frac{m_f}{v} \ , \ g_{hVV} = -2i\frac{M_V^2}{v} \ , \ g_{hhVV} = -2i\frac{M_V^2}{v^2}.$$

2.3 Global symmetries and the Yukawa sector of the Standard Model.

As mentioned earlier the fermionic part of the Lagrangian is invariant under the global $U(3)_L \times U(3)_R \times U(3)_R$ symmetry for the quarks and global $U(3)_L \times U(3)_R$ symmetry for the leptons.

These are explicitly broken by Yukawa interactions. In general the Yukawa matrices are neither hermitian nor real.

For the left handed fermions,the following rotations can be made,

$$L_L^{'i} \to \sum_{j=1}^{3} U_{e,L}^{ij} L_L^{'j}, \ \ Q_L^{'i} \to \sum_{j=1}^{3} U_{u,L}^{ij} Q_L^{'j},$$

while for right handed fields,

$$e_R^{'i} \to \sum_{j=1}^{3} U_{e,R}^{ij} e_R^{'j}, \ \ u_R^{'i} \to \sum_{j=1}^{3} U_{u,R}^{ij} u_R^{'j}, \ \ d_R^{'i} \to \sum_{j=1}^{3} U_{d,R}^{ij} d_R^{'j},$$

where U are the unitary matrices that diagonalize the Yukawa matrices for the respective gauge group. As a consequence the Yukawa matrices transform as,

$$y_e = U_{e,L} y_e^{'} U_{e,R}^{\dagger}, \ \ y_u = U_{u,L} y_u^{'} U_{u,R}^{\dagger} \ \ y_d = U_{d,L} y_d^{'} U_{d,R}^{\dagger}.$$

These relations imply that it is possible to simultaneously diagonalize either $y_e^{'}$,$y_u^{'}$, or $y_e^{'}$,$y_d^{'}$ by a suitable choice of chiral transformations. Assuming that the first of these possibilities is realized, the transform of $y_d^{'}$ is neither real nor diagonal. Instead we can write,

$$VD_d = U_{u,L} y_d^{'} U_{d,R}^{\dagger},$$

where $D_d = U_{u,L} y_d^{'} U_{d,R}^{\dagger}$ and,

$$V = U_{u,L} U_{d,L}^{\dagger},$$

is the Cabibo-Kobayashi-Maskawa (CKM) mixing matrix. In the process of rephrasing the fermionic fields, we may diagonalize the Yukawa couplings by choosing a new basis leptons and quarks. This is the physical basis , since it is the basis in which mass matrices are diagonalized. This 3×3 unitary matrix has 4 independent parameters, 3 of which are mixing angles (θ_{ij}), and the other being an overall phase (δ_{13}). This phase is the CP violating complex phase. The currently known values for these parameters are [66],

$$\theta_{12} = 13.04 \pm 0.05^{\circ}, \ \theta_{13} = 0.021 \pm 0.011^{\circ}, \ \theta_{23} = 2.38 \pm 0.06^{\circ}, \ \delta_{13} = 1.20 \pm 0.08 \text{ rad}.$$

An analogous mixing pattern also occurs in the neutrino sector, with the mixing matrix known as Pontecorvo-Maki-Nakagawa-Sakata (PMNS) matrix.

2.4 Theoretical constraints on the Higgs boson

The requirement of the SM to be valid in the perturbative regime restricts the mass range in which the Higgs boson is likely to be present. Arguments of constraints from unitarity of scattering amplitudes and perturbativity of Higgs self coupling set upper limits on the mass of the Higgs boson. The first problem is related to the growth of the longitudinal components W_L and Z_L at high energies leading to a violation of unitarity at some scale in the W^+W^- scattering. A partial wave decomposition of the amplitude and the use of optical theorem leads to the following result,

$$a_0 \xrightarrow{s \gg m_h^2} -\frac{m_h^2}{8\pi v^2} \text{ for the j} = 0 \text{ state},$$

where a_j are the partial waves for the orbital angular momentum state j. Preservation of unitarity from the above relationship leads to $m_h^2 < 870$ GeV [67–70].

The second type of constraint, namely perturbativity arises from decay of the Higgs boson to gauge bosons. The partial decay width of the Higgs decay to a pair of Z bosons is given by the expression, $\Gamma(h \to ZZ) \sim \frac{m_h^3}{32\pi v^2}$. Higher order loop corrections to the Born term is significantly large. For a large Higgs mass (~ 1 TeV), two loop contributions to this term becomes as significant as the one loop term [71, 72]. One would therefore expect the Higgs boson to be below the TeV scale for perturbation theory to be valid. Additionally, as the partial decay width is proportional to the cube of the Higgs mass itself, for large Higgs masses the decay width becomes comparable to the Higgs mass itself (~ 1.3 TeV). Thus the Higgs mass is said to be 'obese' and cannot be treated as a true resonance.

The recently observed 125 GeV Higgs boson certainly passes these upper limits, and the attention turns to the lower end, where we shall encounter some cause for concern.

Constraints from vacuum stability

The quantum corrections to the running of the quartic coupling λ includes contributions from fermions and gauge boson loops. For the fermions, the top quark with the largest mass makes the most significant contribution.

For quartic couplings much smaller with respect to the top Yukawa and the gauge boson couplings, $\lambda << \lambda_t, g_1, g_2$, the RGE is approximated by [73–79],

$$\frac{d\lambda}{d\log Q^2} \simeq \frac{1}{16\pi^2}\left[-12\frac{m_t^4}{v^4} + \frac{3}{16}\left(2g_2^4 + (g_2^2+g_1^2)^2\right)\right], \tag{2.4.1}$$

leading to,

$$\lambda(Q^2) = \lambda(v^2) + \frac{1}{16\pi^2}\left[-12\frac{m_t^4}{v^4} + \frac{3}{16}\left(2g_2^4 + (g_2^2+g_1^2)^2\right)\right]\log\frac{Q^2}{v^2}. \tag{2.4.2}$$

If the quartic coupling is small, the top quark can drive the quartic coupling to negative values ($\lambda(Q^2) < 0$), leading to an unstable vacuum. Since the Higgs mass is given by $m_h^2 = 2\lambda v^2$, to keep the vacuum stable the Higgs mass should satisfy [80–85],

$$m_h^2 > \frac{v^2}{8\pi^2}\left[-12\frac{m_t^4}{v^4} + \frac{3}{16}\left(2g_2^4 + (g_2^2+g_1^2)^2\right)\right]\log\frac{Q^2}{v^2}. \tag{2.4.3}$$

Assuming that the SM is valid upto a grand unification scale $\Lambda_{GUT} \simeq 10^{16}$ GeV, the lower bound on the Higgs mass from Eq. 2.4.3 turns out to be ~ 130 GeV.

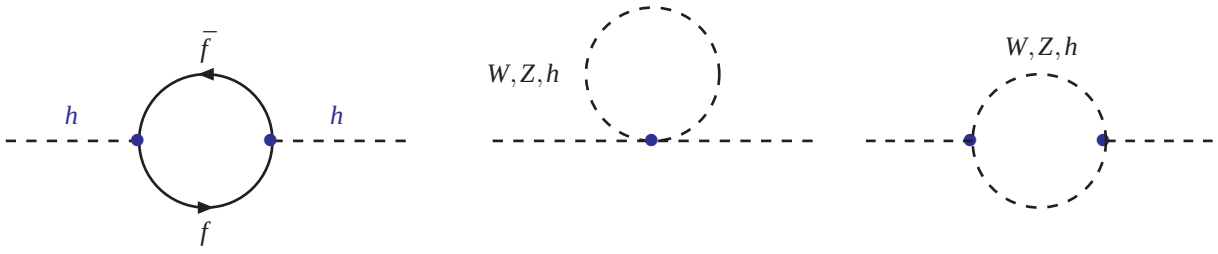

Figure 2.3: Feynman diagrams for the one–loop corrections to the SM Higgs boson mass.

It should also be noted that the SM effective potential can have a true minimum which is deeper than the electroweak minimum. The latter can have a lifetime greater than that of the universe. Thus it is possible to have a situation where the universe falls in the false vacuum in its early hot phase and is stuck there as the universe cools off. This results in the metastability bound [85–88].

Recently the two loop calculation has been performed and sets the limit on the Higgs mass to be [89],

$$m_h \geq 129.2 + 1.8 \times \left(\frac{m_t^{\text{pole}} - 173.2\ \text{GeV}}{0.9\ \text{GeV}} \right) - 0.5 \times \left(\frac{\alpha_s(M_Z) - 0.1184}{0.0007} \right) \pm 1.0\ \ \text{GeV}. \quad (2.4.4)$$

The top mass of 173.2 ± 0.9 GeV is measured at Tevatron by the collaborations CDF and D0. The error $\pm$ 1 GeV reflects the theoretical uncertainties in the Higgs mass bound which takes into account the differences in computation of results from NLO to NNLO.

The vacuum stability of the Higgs potential thus crucially depends how precisely one can measure the top mass.

We thus find that if we expect the SM to be the theory that can be extrapolated to a high scale, the vacuum stability bounds pose serious constraints for a 125 GeV Higgs.

However if there is some new physics that takes over at a lower energy scale, this bound is relaxed significantly. For example if we take the scale of the new physics to be 10^3 GeV, the vacuum stability arguments requires the mass of the Higgs boson to be $m_h > 70$ GeV [3].

The hierarchy problem

The fine tuning argument has often been one of the principal reasoning for the demand of physics beyond SM.

The problem arises because of self energy corrections to the Higgs mass. The most important corrections originate from gauge bosons and fermion loops (Fig 2.3). The fermionic loop contribution is dominated by the top quark with the following loop integral,

$$\begin{aligned}
\Pi^t_{hh}(0) &= (-1) \int \frac{d^4k}{2\pi^4}\, \text{Tr}\left(\frac{-iy_t}{\sqrt{2}}\right) \frac{i}{\not{k} - m_t} \left(\frac{-iy_t}{\sqrt{2}}\right) \frac{i}{\not{k} - m_t} \\
&= -2y_t^2 \int \frac{d^4k}{2\pi^4} \frac{k^2 + m_t^2}{(k^2 - m_t^2)^2} \\
&= -2y_t^2 \int \frac{d^4k}{2\pi^4} \left[\frac{1}{k^2 - m_t^2} + \frac{2m_t^2}{(k^2 - m_t^2)^2} \right], \qquad (2.4.5)
\end{aligned}$$

where y_t is the top quark Yukawa coupling. The first term in Eq. 2.4.5 is quadratically divergent. If we demand the SM to be an effective theory upto the Planck scale $\Lambda = 10^{18}$ GeV, the one loop correction is about 30 orders of magnitude more than the bare mass. Since this loop correction is independent of the Higgs mass, setting it to zero does not increase the symmetry of the theory. Thus there is no symmetry that protects the Higgs mass. Adding the contribution of the gauge bosons the one loop contribution to the Higgs mass is given by,

$$m_h^2 = (\mathrm{m_h^0})^2 + \frac{3\Lambda^2}{8\pi^2 \mathrm{v}^2}\left[\mathrm{m_h^2} + 2\mathrm{M_W^2} + \mathrm{M_Z^2} - 4\mathrm{m_t^2}\right], \tag{2.4.6}$$

where the reference scale is set to the electroweak minimum v. It is interesting to note that there can be an accidental cancellation provided,

$$m_h^2 = 4m_t^2 - 2M_W^2 - M_Z^2 \sim (320\ \mathrm{GeV})^2. \tag{2.4.7}$$

This cancellation, called the Veltman cancellation [90] also serves as a prediction for the Higgs mass. However this is only a one loop result, and higher loops complicate this result significantly.

One could cancel divergences in Eq.2.4.5 consistently in quantum field theory by adding suitable counter terms. However one would have to arrange for a very precise cancellation (1 part in 10^{26}) between the bare mass squared and the renormalized mass to keep the Higgs mass to the electroweak scale. One can define a measure of this fine tuning by [91],

$$\Delta_{\mathrm{FT}} = \left|\frac{\Delta m_h^2(\Lambda)}{m_h^2}\right|. \tag{2.4.8}$$

Therefore the weak scale is fine tuned to one part in Δ_{FT}, with no fine tuning for $\Delta_{FT} \leq 1$.

2.5 Standard Model at LEP and Tevatron

The electroweak theory has been tested to remarkable precision at the Large Electron Positron(LEP) collider and later at the Tevatron [65]. The first vindications of the electroweak theory came with the discovery of the neutral current interactions in 1973 in bubble chamber experiments, which photographed electrons suddenly starting to move, seemingly of their own accord. This was interpreted as a neutrino interacting with the electron by the exchange of an unseen Z boson. The formal discovery of the W and the Z bosons were observed in the experiments UA1 (lead by Carlo Rubia) and UA2 (lead by Peter Jennni) [92,93]. The W and Z bosons were copiously produced at the LEP collider. Along with LEP, Tevatron (which ended its operation in 2011), also produced an enormous amount of W and Z boson. The obtained masses and decay widths from these experiments for the Z boson is found to be [65],

$$M_Z = 91.1875 \pm 0.0021\ \mathrm{GeV},\ \Gamma_Z = 2.4952\ \pm 0.0023\ \mathrm{GeV},$$

while for the W boson it is [65],

$$M_W = 80.399 \pm 0.023\ \mathrm{GeV},\ \Gamma_W = 2.085\ \pm 0.042\ \mathrm{GeV}.$$

The top quark discovered at the Tevatron in 1995 [94,95]. The measured mass of the top quark, was to be $173.18 \pm 0.56(\mathrm{stat}) \pm 0.75(\mathrm{sys})$ [65]. The mass of the top quark is an extremely important ingredient to the electroweak precision fits.

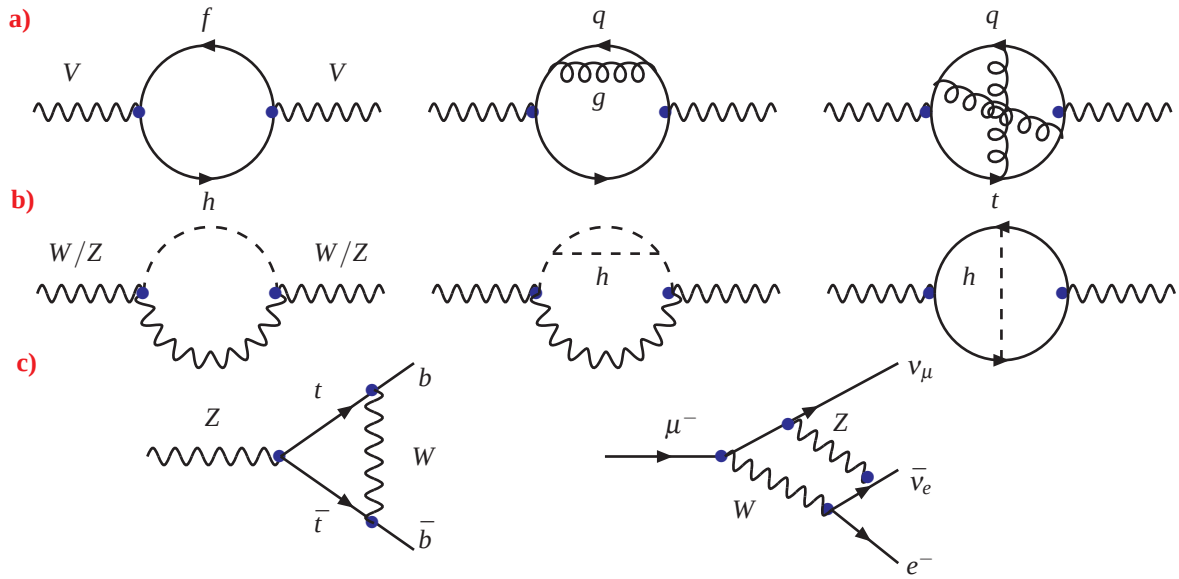

Figure 2.4: The Feynman diagrams for electroweak radiative corrections. a) (Top row) The fermionic contributions to the self energy corrections $V = W/Z$ bosons, b)(Middle row) The Higgs contributions to the self energy corrections and c) (bottom row) The vertex and box diagrams. Feynman diagrams from [3].

The masses of the fermions and gauge bosons obtained in LEP and Tevatron allows us to calculate any observable in the framework of SM. While the tree level approximations serve the purpose to a large extent, radiative corrections are required for comparison with accurate high precision experimental measurements. The sensitivity of LEP and Tevatron to these quantum measurements also serve as stringent tests of SM. Along with α_s,G_μ and M_Z, the following electroweak observables have been measured with a high degree of accuracy [65]:

- Lineshape measurements of Z: The total (Γ_Z) and partial decay widths ($Z \to l^{\pm}l^{\mp}, c\bar{c}..$) of Z boson.
- The forward backward(A_{fb}^f) and the τ polarization asymmetry A_{pol}^{τ}, which provide a determination of $sin^2\theta_W$.
- The longitudinal polarization asymmetry $A_{L,R}^f$ providing the best measured value of $sin^2\theta_W$ at 0.2312 ± 0.00015 .
- The mass(M_W) and the width Γ_W of the W boson.
- The effective mixing angle and the ρ parameter, with the two loop QCD correction $\Delta\rho^{QCD} = -\frac{2}{3}\frac{\alpha_s}{\pi}\left(\frac{\pi^2}{3}+1\right) - 14.59\left(\frac{\alpha_s}{\pi}\right)^2$ [3], where α_s is the strong coupling constant. Note that the two loop QCD correction is essentially a QCD correction on top of a electroweak correction.
- In addition there are top quark mass measurements, the measurement of the fine structure constant α, and the value of the quantum corrections $\Delta\alpha$ due to leptonic and hadronic contributions.

Overall it has been seen that these measurements vindicate the case for the $SU(2)_L \times U(1)_Y$ gauge theory. The electroweak couplings of leptons and quarks to gauge bosons, the trilinear

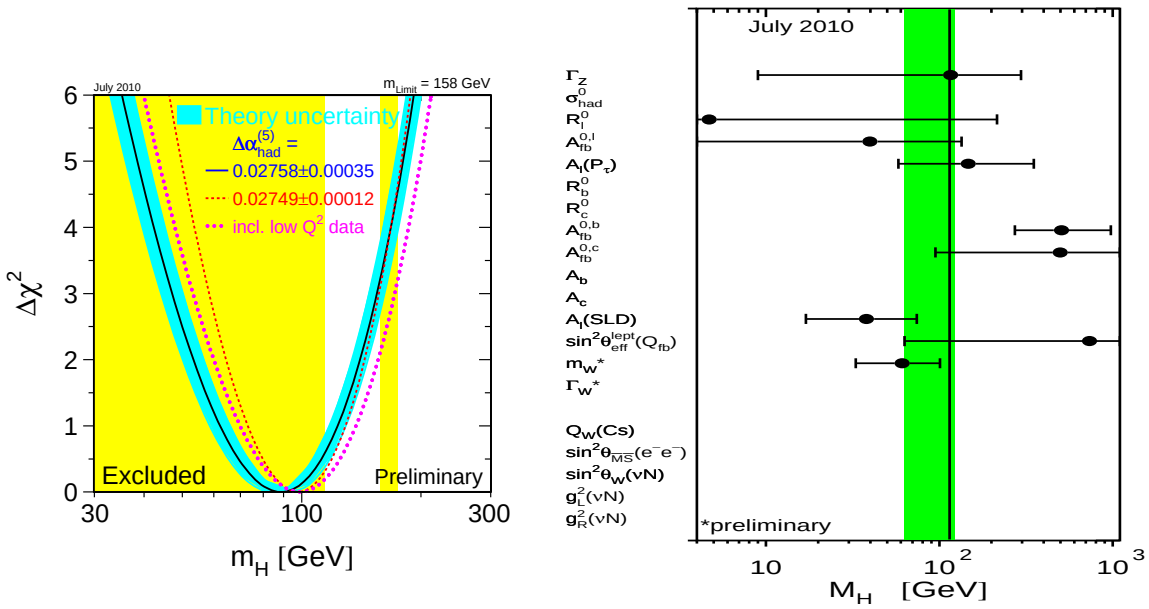

Figure 2.5: Left Panel : The $\Delta\chi^2$ of the fit to the electroweak precision data as a function of m_h. Right Panel :Constraints on the mass of the Higgs boson from electroweak precision data from [65].

couplings of gauge bosons have been measured and is in tune with the principle of gauge symmetry. In addition the strong coupling constant α_s, and other features of strong interactions have also been fairly well measured and is in agreement with the theory of strong interactions [31].

Although the Higgs boson was not observed at LEP, constraints from electroweak observables narrowed the parameter space to a large extent. The Higgs contributes to radiative corrections of electroweak precision observables providing indirect constraints on its mass (Fig. 2.4). Combining the W mass measurements, measurements on the weak mixing angle, measurements of forward backward asymmetries and combined fits to these measurements, one can obtain the likely mass range in which the Higgs boson is expected to be observed. The likely range of the Higgs boson mass, taking the electroweak precision observations into account is presented in the right panel of Fig. 2.5.

The $\Delta\chi^2$ fit to all precision measurements, taking into account the uncertainties on $\alpha_s(M_Z), \alpha, m_t$ and M_Z is presented in the left hand panel of Fig. 2.5. The projected upper limit turns out to be $m_h < 158\ GeV$ at 95 % confidence level [65].

As far as direct searches are concerned, the lower limit on the Higgs boson mass was obtained from the negative searches at LEP-II with center of mass(c.m) energy of 209 GeV. At LEP the dominant production mechanism for the Higgs was the Higgs-strahlung process, namely, $e^+e^- \rightarrow Z^* \rightarrow Zh$. The Higgs searches were conducted in the channel $e^+e^- \rightarrow Z(\rightarrow \nu\bar{\nu})h(\rightarrow b\bar{b})$, $e^+e^- \rightarrow Z(\rightarrow l\bar{l})h(\rightarrow b\bar{b})$, $e^+e^- \rightarrow Z(\rightarrow l\bar{l})h(\rightarrow \tau\bar{\tau})$ and $e^+e^- \rightarrow Z(\rightarrow \tau\bar{\tau})h(\rightarrow b\bar{b})$. The four experiments in LEP did not observe any excess over the background, and the lower limit was set to 114.4 GeV. The Tevatron searched for Higgs boson, both for the high mass and low mass. At the end of its run, it collected about 10 fb^{-1} data, and reported an excess of events with 3σ local significance for $m_h = 125$ GeV [96].

2.6 The discovery of the Higgs boson at the LHC

The search for the Higgs boson continued through the era of the Tevatron, ruling out a wide swath of parameter space in various channels, specially in the high and intermediate mass region. However it was widely speculated that the Higgs boson was likely to be light. This was mainly driven by the theoretical considerations and from the indirect hints of electroweak precision measurements. The search for the light Higgs boson gathered pace with the 7 TeV run of the Large Hadron Collider(LHC). The early hints of a resonance in the $h \to \gamma\gamma$, channel at 125 GeV was observed at the end of 7 TeV run with 5 fb^{-1} data [97, 98]. The observation of a new particle was announced on July 4th 2012, by combining data worth 5 fb^{-1} luminosity at 7 TeV and 5 fb^{-1} luminosity for 8 TeV LHC energy. The persistence of the resonance across various channels [1, 2] was observed. The reported resonance was claimed to be a Higgs like boson rather than the Higgs itself, as measurements of coupling and spin is expected to finally confirm whether the discovered particle is indeed the SM Higgs.

At the LHC the production cross section of the Higgs boson is dominated by the gluon fusion(ggF) process followed by the vector boson fusion process(VBF), with the Zh and $t\bar{t}h$ being the sub-dominant processes [45, 99–137]. The Feynman diagrams for the processes are presented in Fig. 2.6. The left panel of Fig. 2.7 shows the Higgs cross sections at 8 TeV. The branching ratios for the Higgs decay to various channels are shown in the right panel of Fig 2.7.

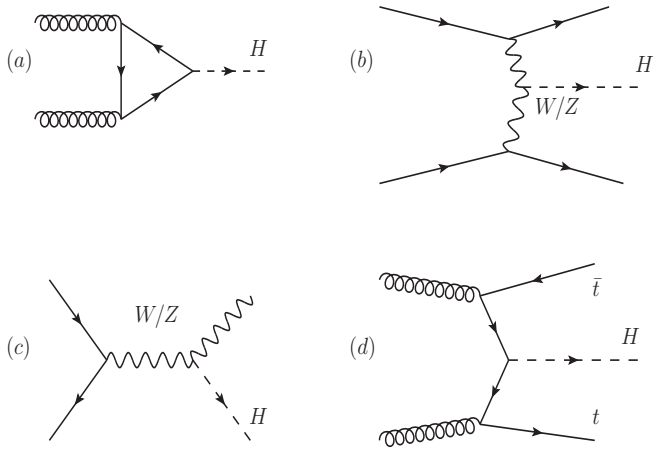

Figure 2.6: Feynman diagrams for Higgs production at the LHC, a)Gluon fusion, b) VBF fusion, c) associated production and d) $t\bar{t}h$ process respectively.

The primary decay mode of the Higgs at 125 GeV is via a pair of b quarks [138]. However this channel is plagued by $t\bar{t}$,QCD and other backgrounds. One of the primary channels for an observation of the 125 GeV Higgs turns out to be $h \to \gamma\gamma$. With the completion of the 8 TeV LHC run, the results for the 20 fb^{-1} luminosity data were obtained. The Higgs resonance for the di-photon channel as measured by the ATLAS collaboration [139] is presented in the left panel of Fig. 2.8.

The combined fit of the measurements in various channels is estimated to be $125.5 \pm 0.2\ ^{+0.6}_{-0.5}$, with a combined signal strength, defined as $\mu = \frac{\sigma \times BR}{(\sigma \times BR)_{SM}}$, of 1.43 ± 0.16(stat) $\pm$ 0.14(sys) [139]. The CMS collaboration reports the combined best fit mass value to be 125.7 ± 0.3(stat) $\pm$ 0.3(sys) corresponding to the channels $\gamma\gamma, ZZ, WW, b\bar{b}, \tau\bar{\tau}$. The reported signal strength is quoted to be

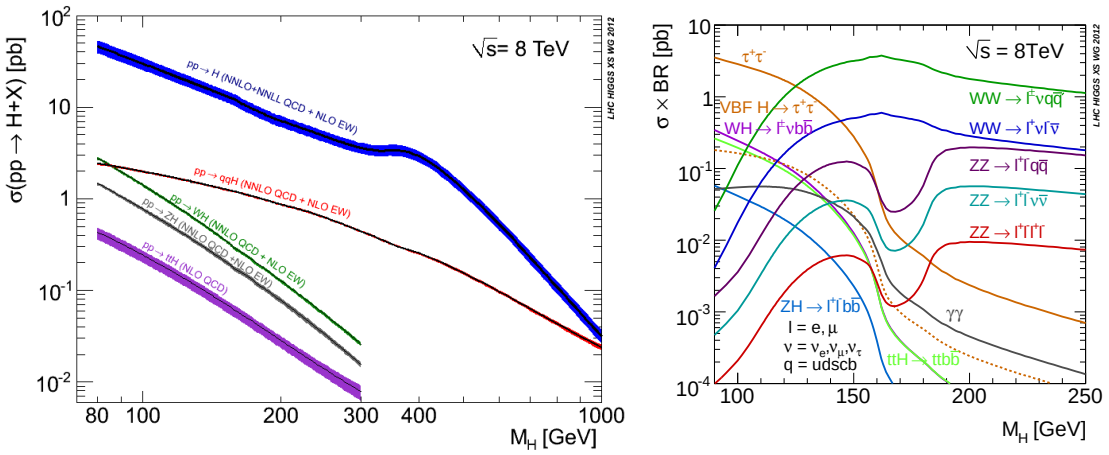

Figure 2.7: *The Higgs cross section(left panel) and cross section times branching ratios(right panel) [103] at 8 TeV LHC energy.*

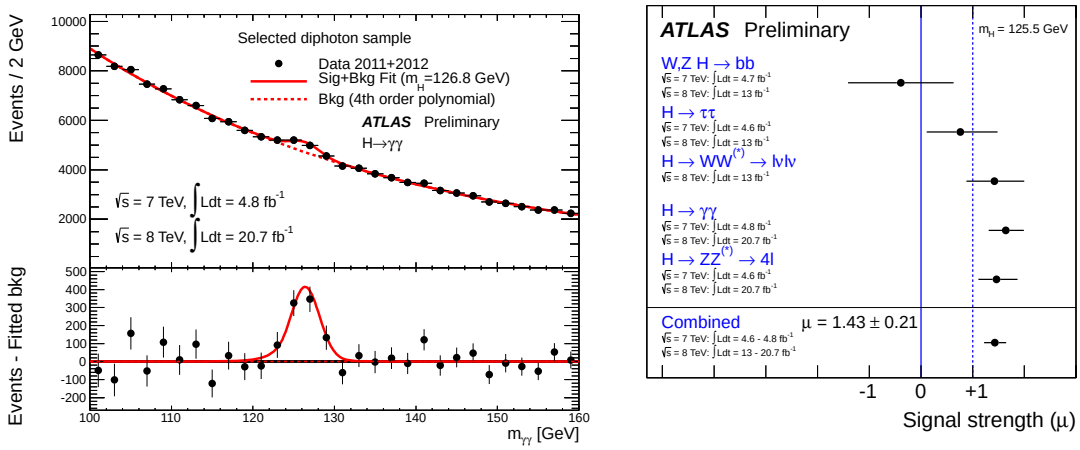

Figure 2.8: *The Higgs mass discovery plot for ATLAS (left panel) in the* h → *γγ, and the signal strength for various channels [139].*

0.8±0.14 [140].

2.7 Beyond Standard Model and supersymmetry

2.7.1 Shortcomings of the Standard Model

In spite of the success of the electroweak theory several deficiencies prompt us to look beyond. Some of the key problems are raised below,

- The hierarchy problem : As observed earlier, the one loop self energy corrections lead to an unnaturally large value of the Higgs boson mass, if SM is extrapolated till the Planck scale. To achieve the correct Higgs mass at the electroweak scale one needs a fine cancellation between the bare Lagrangian and the renormalized Lagrangian, thus leading to a fine tuning of the theory.

- It is now well known that the universe contains a significant proportion of dark matter and dark energy. SM does not offer any candidate particle to explain such a large amount of dark matter.
- An aesthetic wish is that the gauge couplings of SM should unify at some high scale at which a hitherto unknown theory would take over. In SM the gauge couplings do not unify at any scale.
- The SM does not explain the observed asymmetry of matter anti-matter in the universe.
- The SM does not explain the masses of neutrinos.

Due to the above deficiencies of the SM one would like a theory which explains these issues. There are several examples of BSM theories that have attracted attention over the last few decades, each with its pros and contras. Some of the most widely studied BSM scenarios are listed below.

- **Supersymmetry**: This possibility attempts to solve the fine tuning problem by introduction of new particles which differ by spin half from their SM counterparts. SUSY advocates gauge coupling unification at a scale of 10^{16} GeV, as well as provides a dark matter candidate in a wide class of models.
- **Extra Dimensions**: These come in various varieties. The first of these is the Arkani-Hamed-Dimopoulous-Dvali(ADD) model [141], which advocates that the SM fields are confined to four dimensions, while gravity propagates in additional spatial dimensions that are large compared to the Planck scale. The second of these is the Randall-Sundrum model [142], which assumes that the universe is part of a 5 dimensional anti-desitter brane in which SM fields live in the (3+1) dimension, while the graviton propagates in the "warped" 5'th dimension. These models bring the scale of the new physics to a lower value.
- **Little Higgs Models** : This is based on the idea that the Higgs boson is a pseudo Nambu-Goldstone boson that arises from the breaking of a global symmetry at the TeV scale [143–145].

The most popular of these, in terms of simplicity and the ability to explain a wide range phenomenological consequences is supersymmetry. The minimal version, termed as the minimally supersymmetric standard model(MSSM), has been widely studied and is the one of the most sought after BSM model at the LHC. In this thesis we will work entirely in the framework of MSSM.

2.7.2 Motivation for supersymmetry

As the first motivation we revisit the fine tuning problem again. We add a pair of complex scalar field to the Higgs potential such that that the quadratic part relevant Lagrangian can now be written as,

$$\mathscr{L} = \lambda_f |h|^2 (|\phi_l|^2 + ... \tag{2.7.1}$$

Schematically this can be represented by Fig. 2.9. The contribution from these loops can be summarized as,

$$\Pi^{\phi}_{hh}(0) \;=\; \lambda_\phi \int \frac{d^4k}{2\pi^4} \left[\frac{1}{k^2 - m^2_{\phi_l}} + \frac{1}{(k^2 - m^2_{\phi_r})} \right] + \ldots \;. \tag{2.7.2}$$

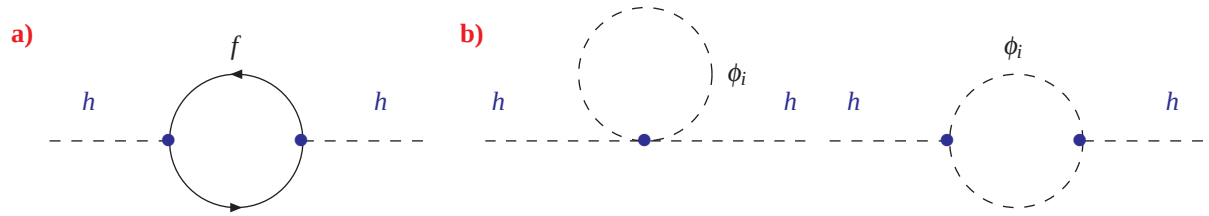

Figure 2.9: Diagrams for the contributions of a)fermions and b)scalars to the self energy corrections of the Higgs boson.

The first term, which is quadratically divergent can be cancelled with the SM fermionic contribution i.e $\Pi^{f}_{hh}(0)+\Pi^{\phi}_{hh}(0)$=0, if the coupling constants $\lambda_\phi = -\lambda_f^2$.

The remaining part of the divergence includes logarithmic terms. Requiring $m_{\phi_l} = m_{\phi_r}$, the one loop contribution can be written as,

$$\begin{aligned}\Pi^{f}_{hh}(0)+\Pi^{\phi}_{hh}(0) &= -\mathrm{i}\frac{\lambda_\mathrm{f}^2}{16\pi^2}\left[-2\mathrm{m}_\mathrm{f}^2\left(1-\ln\frac{\mathrm{m}_\mathrm{f}^2}{\mu^2}\right)+4\mathrm{m}_\mathrm{f}^2\ln\frac{\mathrm{m}_\mathrm{f}^2}{\mu^2}\right.\\ &\left.+2\mathrm{m}_\phi^2\left(1-\ln\frac{\mathrm{m}_\phi^2}{\mu^2}\right)-4\mathrm{m}_\phi^2\ln\frac{\mathrm{m}_\phi^2}{\mu^2}\right],\end{aligned}$$

which vanishes if $m_f = m_\phi$. If we have scalar counterparts to fermions, with fermion Yukawa couplings equal to the quartic couplings to these scalars, the one loop quadratic divergence vanishes exactly. Thus the fine tuning problem in standard model is cured or in the worst case if SUSY is badly broken, the level of fine tuning is modest. The essence of this exercise, is to introduce supersymmetry(SUSY), the details of which are described in Chapter 3.

Chapter 3

The Minimally Supersymmetric Standard Model

3.1 Formal Aspects

Historically the first attempts to construct a theory with a symmetry relating bosons to fermions were studied in [146–148]. The algebraic aspects were developed in [148, 149]. The first supersymmetric field theories were developed by Wess and Zumino [150] along with Salam and Stratdhee [151]. The mathematical construction leading to the violation of the Coleman-Mandula theorem [152] was provided by Haag, Lopuzanski and Sohnius [153]. The formulation of the Minimally Supersymmetric Standard Model(MSSM) was first studied in [154]. The successful resolution of problem of gauge hierarchy was addressed in [155–157]. The subject of SUSY has found its way into the textbooks [158–161] and is too rich a subject to be covered in this thesis in detail. The attempt here is to follow the theoretical development to a phenomenological approach and finally make a connection with the experimental searches. In the following section a brief description some of these formal aspects is discussed. Since the amount of literature in the subject is enormously large to be covered here, we refer to [158–161] and references therein with due apologies.

The free Wess–Zumino model and Superspace

We start by analyzing the free Wess–Zumino model consisting of a complex scalar and one fermion. In all our subsequent discussion, the two component notation shall be used. The Lagrangian for the Wess–Zumino model can be written as,

$$\mathscr{L} = (\partial_\mu \phi)(\partial_\mu \phi)^* + i\xi\sigma^\mu \partial_\mu \xi^\dagger - m^2\phi^*\phi - \frac{m}{2}(\xi\xi + \xi^\dagger\xi^\dagger). \tag{3.1.1}$$

In the above equation spinorial indices have been suppressed with the contractions defined as $\psi\chi = \psi^a\chi_a$ and $\psi^\dagger\chi^\dagger = \psi^\dagger_{\dot{a}}\chi^{\dagger\dot{a}}$. The Lagrangian in Eq.3.1.1 is invariant under the SUSY transformations,

$$\delta\phi = \varepsilon\xi,\ \delta\xi = -i\sigma^\mu\partial_\mu\varepsilon^\dagger - m\phi^*\varepsilon, \tag{3.1.2}$$

where ε is a constant two component spinor [1]. Since ϕ and ξ have mass dimensions of 1 and 3/2 respectively, the spinor ε has a mass dimension of -1/2. These transformations imply that these

[1] The two component ε is defined as $\varepsilon^{ab} = \begin{pmatrix} 0 & 1 \\ -1 & 0 \end{pmatrix}$, $\varepsilon_{ab} = \begin{pmatrix} 0 & -1 \\ 1 & 0 \end{pmatrix}$.

fields acquire infinitesimal components in each others direction, thus providing a framework of "superspace" with fermions and scalars [2]. To find the algebra of SUSY, we construct the commutator $[\delta_{\varepsilon_1}, \delta_{\varepsilon_2}]\phi$. This can be worked out using the SUSY transformations in Eq.3.1.2 to obtain,

$$[\delta_{\varepsilon_1}, \delta_{\varepsilon_2}]\phi = i\alpha^\mu P_\mu \phi, \tag{3.1.3}$$

where $\alpha^\mu = i(\varepsilon_1\sigma^\mu\varepsilon_2^\dagger - \varepsilon_2\sigma^\mu\varepsilon_1^\dagger)$. This is reminiscent of the ordinary space time translation with the infinitesimal parameter given by α_μ. Noting that α_μ is real, one could extend the notion of ordinary spacetime to superspace to include "fermionic dimensions" as $(x^\mu, \theta_a, \theta_{\dot{a}}^\dagger)$, where θ is the spinorial dimension of the superspace. They obey $\theta_1\theta_2 = \theta_2\theta_1$, and $\theta_1^2 = 0$. As a consequence no function of fields expanded in terms of these Grassmann valued quantities can have more than four θ. The superspace transformations are implemented by demanding,

$$\begin{aligned} x^\mu &\rightarrow x^\mu - i\theta\sigma^\mu\varepsilon^\dagger + i\varepsilon\sigma^\mu\theta^\dagger, \\ \theta_a &\rightarrow \theta_a + \varepsilon_a, \\ \theta_{\dot{a}}^\dagger &\rightarrow \theta_{\dot{a}}^\dagger + \varepsilon_{\dot{a}}^\dagger. \end{aligned} \tag{3.1.4}$$

The commutator of two translations can now be written as,

$$[\delta_{\varepsilon_1}, \delta_{\varepsilon_2}]x^\mu = 2i(\varepsilon_2\sigma^\mu\varepsilon_1^\dagger - \varepsilon_1\sigma^\mu\varepsilon_2^\dagger). \tag{3.1.5}$$

The above equation is the geometrical realization of the superspace with the co-ordinates $(x^\mu, \theta_a, \theta_{\dot{a}}^\dagger)$. Note that $[\delta_{\varepsilon_1}, \delta_{\varepsilon_2}]\theta = 0$, implying that the translation is only in the bosonic part of the theory. The charges that generate SUSY are defined as,

$$Q_a = -i(\partial_a + i\sigma^\mu_{a\dot{b}}\theta^{\dagger\dot{b}}\partial_\mu),\ Q_{\dot{a}}^\dagger = i(\partial_{\dot{a}} - i\theta^{\dot{b}}\sigma^\mu_{\dot{b}a}\partial_\mu),$$

with the algebra,

$$\{Q_a, Q_{\dot{b}}^\dagger\} = 2i\sigma^\mu_{a\dot{b}}\partial_\mu. \tag{3.1.6}$$

A generic SUSY transformation can therefore be denoted by,

$$Q|Fermion\rangle = |Boson\rangle,\ \ Q|Boson\rangle = |fermion\rangle. \tag{3.1.7}$$

Superfields

The consequence that a general function cannot have more than four anti-commuting θ s, leads to the fact that the Taylor expansion is finite. We can therefore expand a general "superfield" as,

$$\begin{aligned} \mathscr{F}(x,\theta,\theta^\dagger) &= \phi(x)|_{\theta=\theta^\dagger=0} + \sqrt{2}\theta\xi(x) + \sqrt{2}\theta^\dagger\chi^\dagger(x) + \theta\theta M(x) + \theta^\dagger\theta^\dagger N(x) \\ &\quad + \theta\sigma^\mu\theta^\dagger A_\mu(x) + \theta\theta\theta^\dagger\lambda^\dagger(x) + \theta^\dagger\theta^\dagger\theta\eta(x) + \frac{1}{2}\theta\theta\theta^\dagger\theta^\dagger D(x). \end{aligned} \tag{3.1.8}$$

One would also like to define analytic superfields to truncate the above general expression by demanding that $\mathscr{F}$ is independent of $\theta^\dagger$(or equivalently θ), i.e , $\frac{\partial}{\partial\theta_{\dot{a}}^\dagger}\mathscr{F} = 0$. Under this constraint,

$$\mathscr{F} = \phi(x) + \sqrt{2}\theta\xi(x) + \theta\theta F(x). \tag{3.1.9}$$

[2] The bilinear $\sigma^{\mu\nu} = \frac{1}{4}[\sigma^\mu, \sigma^\nu]$.

Note however that in this case, the constraint operator $\frac{\partial}{\partial\theta^\dagger}$ fails to commute with the charges $Q, Q^\dagger$. Thus the operator cannot be deemed to be supercovariant. Defining the "supercovariant" derivative as,

$$\mathscr{D}_a = \frac{\partial}{\partial\theta^a} - i(\sigma^\mu\theta^\dagger)_a\partial_\mu,\ \ \mathscr{D}^\dagger_{\dot{a}} = -\frac{\partial}{\partial\theta^{\dot{a}\dagger}} + i(\theta\sigma^\mu)_{\dot{a}}\partial_\mu,$$

the following relations are obtained,

$$\{\mathscr{D}, Q\} = \{\mathscr{D}, Q^\dagger\} = \{\mathscr{D}^\dagger, Q\} = \{\mathscr{D}^\dagger, Q^\dagger\} = 0, \{\mathscr{D}_a,\ \mathscr{D}^\dagger_{\dot{b}}\} = 2i\sigma^\mu_{a\dot{b}}\partial_\mu. \tag{3.1.10}$$

Thus $\mathscr{D}^\dagger_{\dot{a}}\Phi = 0$ is a supercovariant constraint. Thus a superfield Φ is deemed to be chiral if it satisfies $\mathscr{D}^\dagger_{\dot{a}}\Phi = 0$, and antichiral if it satisfies $\mathscr{D}_a\Phi^\dagger = 0$. We can also shift co-ordinates from x^μ to $y^\mu = x^\mu - i\theta\sigma^\mu\theta^\dagger$, to observe that $\mathscr{D}_a y^{\mu\dagger} = \mathscr{D}^\dagger_{\dot{a}} y^\mu = 0$.

The chiral superfield $\Phi(y,\theta)$ can be expanded as,

$$\Phi(y,\theta) = \phi(y) + \sqrt{2}\theta\xi(y) + \theta\theta F(y), \tag{3.1.11}$$

where F is an auxiliary field.

Sueprspace action

The ordinary space-time action is written as $S = \int d^4x\,\mathscr{L}$. In superspace the action is given by,

$$S_D = \int d^4x\, d^2\theta\, d^2\theta^\dagger\, \mathscr{L}(\Phi, \Phi^\dagger). \tag{3.1.12}$$

The integral over $\theta, \theta^\dagger$ can be performed by the rules of Grassmann (Berezin) integration [3]. The action for chiral or antichiral fields can be summarized as,

$$S_F = \int d^4x\, d^2\theta \mathscr{L}(\Phi) + c.c. \tag{3.1.13}$$

For the free theory a suitable kinetic term is the quadratic expression $\Phi\Phi^\dagger$. Note that this is a general superfield. The action for this quadratic can be written as ,

$$S = \int d^4x\, d^2\theta\, d^2\theta^\dagger\, [\Phi\Phi^\dagger]_D. \tag{3.1.14}$$

as only the D term in the expansion of $\Phi\Phi^\dagger$ remains after integration. Also note that the since the $d\theta$ has mass dimensions of +1/2, the whole expression is dimensionless without a coefficient. The mass term originates from the F term action,

$$S_F = \int d^4x\, m^2[d^2\theta\ \Phi^2 + d^2\theta^\dagger\Phi^{\dagger 2}]. \tag{3.1.15}$$

Note that the fields F and D are auxiliary and have no dynamics in them. It should therefore be integrated out using the equations of motion. It is necessary to maintain the on-shell and off-shell

[3] To integrate a general function $\mathscr{F}(t,\theta) = f(t) + \theta g(t)$,

$$\begin{aligned}\int \mathscr{F}(t,\theta) &= \int d\theta(f(t) + \theta g(t)) \\ &= f(t)\int d\theta.1 + g(t)\int d\theta\theta.\end{aligned}$$

$\int d\theta\theta = \int d(\theta+\varepsilon)(\theta+\varepsilon) \Rightarrow \int d\theta.1 = 0$. Normalization gives $\int d\theta\theta = 1$

degrees of freedom in a superfield. It can be observed that on-shell, the complex scalar field, which has two degrees of freedom matches the two spin polarized state of the fermion. However an off-shell Weyl fermion is a two component object with four real degrees of freedom. Therefore the F and the D terms are required to close the SUSY algebra.

For interacting theories involving $\Phi, \Phi^\dagger$, the D term action can be written as,

$$\int d^4x\, d^2\theta\, d^2\theta^\dagger \mathscr{K}(\Phi_i, \Phi_i^\dagger).$$

The function $\mathscr{K}(\Phi_i, \Phi_i^\dagger)$, is a real function of the superfields termed as the Kahler potential. Similarly the most general F term is a holomorphic function and can be written as $\int d^4x d^2\theta \mathscr{W}(\Phi) + c.c$. The free theory is given by,

$$\mathscr{K}(\Phi_i, \Phi_i^\dagger) = \Phi^\dagger \Phi.$$

Additionally the function $\mathscr{W}(\Phi) = \frac{1}{2}\Phi^2$ contains mass terms and auxiliary fields. The functions $\mathscr{K}, \mathscr{W}$ should have a sensible expansion in Φ in an interacting theory. Written in terms of ordinary fields, a Taylor expansion yields,

$$\int d^2\theta d^2\theta^\dagger \mathscr{K}(\Phi_i, \Phi_i^\dagger) = \mathscr{K}_{,ij}(\phi, \phi^*)\partial_\mu \phi^i \partial^\mu \phi^{*i} + ...,$$

where the notation $\mathscr{K}_{,ij}(\phi, \phi^*)$ implies a double differential with respect to the fields ϕ.

Vector Superfield

One can define a vector superfield by demanding the condition of reality from Eq.3.1.8, $\mathscr{F} = \mathscr{F}^\dagger = V(x, \theta, \theta^\dagger)$. Therefore,

$$\begin{aligned} V(x,\theta,\theta^\dagger) &= C(x) + \sqrt{2}(\theta\xi + \theta^\dagger\xi^\dagger) + [\theta\theta M(x) + \theta^\dagger\theta^\dagger M^*(x)] \\ &\quad + \theta\sigma^\mu\theta^\dagger A_\mu(x) + [\theta\theta\theta^\dagger\lambda^\dagger(x) + \theta^\dagger\theta^\dagger\theta(x)\lambda(x)] + \frac{1}{2}\theta\theta\theta^\dagger\theta^\dagger D(x) \end{aligned} \quad (3.1.16)$$

Observe that if Φ is a chiral superfield $\Phi + \Phi^\dagger$ is a vector superfield. Expanding $\Phi(y^\mu, \theta)$ and adding its complex conjugate we obtain,

$$\begin{aligned} \Phi + \Phi^\dagger &= 2Re(\alpha) + \sqrt{2}(\theta\chi + c.c) + (\theta\theta F + c.c) - 2\theta\sigma^\mu\theta^\dagger\partial_\mu(Im(\alpha)) - \\ &\quad \frac{i}{\sqrt{2}}(\theta\theta\sigma^\mu\theta^\dagger\partial_\mu\chi + c.c) - \frac{1}{2}\Box\, Re(\alpha). \end{aligned} \quad (3.1.17)$$

To investigate a possible gauge invariance on the superfield, consider, $V \to V + \Phi + \Phi^\dagger$. One can make the following transformations,

$$\begin{aligned} C \to C + 2Re(\alpha),\ \ \xi \to \xi + \chi, \\ M \to M + F,\ \ A_\mu \to A_\mu - 2\partial_\mu(Im(\alpha)), \\ D \to D - \Box Re(\alpha),\ \ \lambda \to \lambda - \frac{i}{\sqrt{2}}\sigma^\mu\partial_\mu\chi^\dagger. \end{aligned} \quad (3.1.18)$$

Therefore the fields C, ξ, M can be gauged away by an opportune choice of $Re(\alpha)$, χ, F. This gauge is known as Wess-Zumino gauge. However it is not possible to gauge away A_μ with one

parameter α. We realize that C,ξ, M are not physical degrees of freedom and hence can be gauged away. One can also realize that A_μ is a U(1) gauge field. Redefining $\beta(x) = -2Im(\alpha)$, one has the gauge transformation, $A_\mu \to A_\mu + \partial_\mu \beta$. Finally defining,

$$\lambda \to \lambda + \frac{i}{\sqrt{2}}\sigma^\mu \partial_\mu \xi^\dagger,\ D \to D + \Box C,$$

it can be realized λ, D are gauge invariant fields. Thus the fields $Re(\alpha)$, χ, F can be used to fix the Wess–Zumino gauge. We can perform U(1) gauge transformation in Wess–Zumino gauge using $\Phi + \Phi^\dagger$, with $Re(\alpha)$, χ, $F = 0$. Thus after the redefinition we can chose the fields such that $A_\mu \to A_\mu + \partial_\mu \beta$ while $\lambda \to \lambda$, $D \to D$ remain unchanged. The gauge part of the vector superfield is,

$$V = ... + \theta\sigma^\mu\theta^\dagger A_\mu + ... + \theta\theta\theta^\dagger\lambda^\dagger. \tag{3.1.19}$$

The kinetic term for V can be written as,

$$\frac{1}{8}\int d^2\theta \int d^2\theta^\dagger \mathscr{D}\mathscr{D}V\mathscr{D}^\dagger\mathscr{D}^\dagger V.$$

Plugging V in component fields it can be shown that the kinetic term can be reduced to,

$$\frac{1}{2}D^2 - \frac{1}{4}F_{\mu\nu}F^{\mu\nu} + \frac{i}{2}\lambda\sigma^\mu \overset{\leftrightarrow}{\partial}_\mu \lambda.$$

It is easy to see that V is an invariant of the superspace action under the transformation $V \to V + i(\Lambda - \Lambda^\dagger)$, where $\Lambda(\Lambda^\dagger)$ is a chiral (antichiral) superfield.

The kinetic term can be expressed in a slightly asymmetric fashion as,

$$\frac{1}{16}\int d^2\theta d^2\theta^\dagger(\mathscr{D}^\dagger\mathscr{D}^\dagger\mathscr{D}_a V\mathscr{D}_a V + c.c)_D,$$

where integration over the Grassmann co-ordinates leaves only the D term of the above expression.

Defining $W_a = -\frac{1}{4}\mathscr{D}^\dagger\mathscr{D}^\dagger\mathscr{D}_a V$, and the corresponding conjugate, the kinetic term is,

$$-\frac{1}{4}\int d^2\theta d^2\theta(W^a\mathscr{D}_a V + c.c).$$

W_a thus has mass dimensions of 3/2. We immediately recognize W_a ($W_a^\dagger$) as a chiral (antichiral) superfield as $\mathscr{D}^{\dagger a}W_a = \mathscr{D}_b W^{\dagger b} = 0$. W_a can be expanded as a chiral superfield with a spinor index in the following way,

$$W_a(y,\theta) = \lambda_a(y) + D(y)\theta_a - (\sigma^\mu\theta)_a F_{\mu\nu} + i\theta\theta(\sigma^\mu\partial_\mu\lambda^\dagger)_a. \tag{3.1.20}$$

Thus it can be observed that the D term has appeared as the co-efficient of θ, while the gauge field A_μ appears as its curl, namely $F_{\mu\nu}$. Therefore W_a is itself gauge invariant, with,

$$V \to V + i(\Lambda - \Lambda^\dagger),\ \ W_a \to W_a - \frac{i}{4}\mathscr{D}^\dagger\mathscr{D}^\dagger\mathscr{D}_a(\Lambda - \Lambda^\dagger).$$

Hence W_a and its conjugate play the role of gauge invariant field strengths. In abelian gauge theories this mimics A_μ, where the gauge potential just shifts by a derivative. It can be checked by expanding W_a in component fields that the F term of the following is given by,

$$\frac{1}{4}[W^a W_a + c.c]_F = \frac{1}{2}D^2 - \frac{1}{4}F_{\mu\nu}F^{\mu\nu} + \frac{i}{2}\lambda\sigma^\mu \overset{\leftrightarrow}{\partial}_\mu \lambda. \tag{3.1.21}$$

Therefore modulo surface terms the following identity holds between the F and D terms,

$$\int d^4x[W^aW_a+c.c]_F=\int d^4x(W^a\mathscr{D}_aV+c.c)_D. \tag{3.1.22}$$

Notice that there is no mass term for the abelian gauge field.

Construction of the interacting SUSY Lagrangian

We know that ordinary matter fields transform under U(1) by a phase, $\phi_i \rightarrow e^{igt_i\,\beta(x)}\,\phi_i(x)$, where g is the coupling constant, t_i are the charges of the fields ϕ_i and $\beta(x)$ is the infinitesimal parameter of local gauge transformation. In superfield formalism, the transformation can be written as,

$$\Phi_i\rightarrow e^{-2igt_i\,\Lambda(y,\theta)}\Phi(y,\theta),\;\;\Phi_i^\dagger\rightarrow e^{+2igt_i\,\Lambda^\dagger(y^\dagger,\theta^\dagger)}\Phi(y^\dagger,\theta^\dagger),$$

where both Φ ($\Phi^\dagger$) and Λ ($\Lambda^\dagger$) are chiral(anti-chiral) superfields. Since Φ ($\Phi^\dagger$) is chiral (antichiral) superfield, after a gauge transformation it has to remain a chiral (antichiral) superfield and hence Λ ($\Lambda^\dagger$) has to be a chiral (antichiral) superfield. The phase is thus superfield valued. Observe that the combination $\Phi_i^\dagger\Phi_i$ is not supergauge invariant as $\Phi_i^\dagger\Phi_i\rightarrow e^{2igt_i(\Lambda^\dagger-\Lambda)}\Phi_i^\dagger\Phi_i$. We are thus obliged to put an exponential coupling in V to express the gauge invariant kinetic term as,

$$\Phi_i^\dagger e^{2gt_iV}\Phi_i,$$

and hence the kinetic term is invariant under the gauge transformations $V\rightarrow V+i(\Lambda-\Lambda^\dagger)$, while Φ and $\Phi^\dagger$ transforms as noted above. The full action for an abelian interacting theory can be written,

$$S_{abelian}=\int d^4x\Bigg[\int d^2\theta d^2\theta^\dagger(\Phi_i^\dagger e^{2gt_iV}\Phi_i)+\frac{1}{4}\Bigg(\int d^2\theta W^aW_a+c.c\Bigg)+\Bigg(\int d^2\theta\mathscr{W}(\Phi_i\Bigg)+c.c\}+\eta[\int d^2\theta d^2\theta^\dagger V] \tag{3.1.23}$$

where the last term is known as the Fayet Illiopoulous D term. Expanding in component fields and integrating over the Grassmann co-ordinates yields the Lagrangian density,

$$\begin{aligned}\mathscr{L} &= \frac{1}{2}D^2-\frac{1}{4}F_{\mu\nu}F^{\mu\nu}+\frac{i}{2}\lambda\sigma^\mu\overset{\leftrightarrow}{\partial}_\mu\lambda+\eta D+i\xi_i\sigma^\mu(\partial_\mu-igt_iA_\mu)\xi_i+|(\partial_\mu+igt_iA_\mu)\phi_i|^2+\\ &\quad F_iF_i^*+(\mathscr{W}F_i+c.c)-(\frac{1}{2}\xi_i\xi_j\mathscr{W}_{,ij}+c.c)+\sqrt{2}gt_i(\lambda^\dagger\xi_i^\dagger\phi_i+c.c)+gt_i|\phi_i|^2D.\end{aligned} \tag{3.1.24}$$

Thus ξ is conventional fermion , λ is the gaugino and ϕ is the sfermion. If ϕ_i gets a vaccuum expectation value(VEV), the Yukawa term would generate a mass term with generic mixing between gauginos and matter fermions. The other mass terms originate from superpotential derivatives coupling to ξ. The auxiliary fields can be integrated to yield,

$$F_i^*=-\mathscr{W}_{,i};\;\;D=-gt_i|\phi_i|^2-\eta.$$

Substituting back in the Lagrangian (Eq 3.1.24), the scalar potential can be written as,

$$V(\phi,\phi^*)=F_iF^i+D^2=|\mathscr{W}_{,i}(\phi)|^2+\frac{1}{2}(\eta+gt_i|\phi_i|^2)^2. \tag{3.1.25}$$

The first term in the Eq. 3.1.25 is generated from the F term contribution while the second from the D term. Clearly the scalar potential is positive definite.

The non-abelian gauge fields can be constructed in analogy with the Yang-Mills theory, i.e, $A_\mu \to A^a_\mu$, where a runs over the adjoint of the group in question.

The vector superfield for the non abelian case is an extension of the abelian one, with, $V^a(x,\theta,\theta^\dagger)$, where a =1,... dim(G), where dim(G) is the dimensionality of the gauge group. The generators satisfy $[\mathrm{T^a},\mathrm{T^b}] = \mathrm{f^{abc}T^c}$, with normalization $Tr(T^aT^b) = T(\mathscr{R})\delta^{ab}$ in the representation $\mathscr{R}$. Therefore the matrix valued superfield V is defined as as $\vec{V} = 2g\sum V^aT^a$. The non abelian gauge transformation $e^{i\beta^a(x)T^a}$ in ordinary space is extended to the superspace by replacing the former with $e^{2ig\Lambda^aT^a}$. Defining $\Lambda = 2ig\Lambda^aT^a$, it can be observed that the group element is $e^{i\vec{\Lambda}}$. The vector superfield V thus transforms as,

$$e^{\vec{V}} \to e^{-i\Lambda^\dagger}e^{\vec{V}}e^{i\Lambda}.$$

The non abelian field strength is given by,

$$\vec{W}_a = \frac{1}{4}\mathscr{D}^\dagger\mathscr{D}^\dagger e^{-V}\mathscr{D}_A e^V.$$

Noting that V transforms as $e^{\vec{V}} \to e^{-i\Lambda^\dagger}e^{\vec{V}}e^{i\Lambda^\dagger}$, $\vec{W}_a$ transforms as,

$$\vec{W}_a \to e^{-i\vec{\Lambda}}\vec{W}_a e^{i\Lambda}.$$

Thus the choice of $\vec{W}_a$ preserves the chirality of $\vec{W}_a$. In the Wess Zumino gauge $\vec{W}_a$ is given by,

$$\vec{W}_a = \vec{\lambda}_a(y) + \vec{D}(y)\theta_a - (\sigma^{\mu\nu}\theta\vec{F}_{\mu\nu}(y) + i\theta\theta(\sigma^\mu D_\mu\lambda^\dagger(y))_a,$$

where $\vec{F}_{\mu\nu}$ is the non abelian field strength and,

$$D_\mu\lambda^\dagger = \partial_\mu\lambda^\dagger + ig[A_\mu, A_\nu],$$

where λ is in the adjoint representation of the gauge group.

The gauge invariant action for the non-abelian gauge theory can be expressed as,

$$\frac{1}{16T(\mathscr{R})}\int(d^2\theta Tr(\vec{W}^{Ia}\vec{W}^I_a + c.c) + \int d^2\theta d^2\theta^\dagger\Phi^{I\dagger}_i(e^V)_{ij}\Phi^I_j, \tag{3.1.26}$$

where the index I runs over any number of copies of non-abelian gauge groups. For SM fermions this index runs over 3 generations of fermions while i is the spinor index.

Note that for an SU(N) gauge theory $\mathrm{Tr(T^a)}$=0, and hence the trace over the Fayet Illipoulous D term of the vector superfield $Tr(\vec{D}) = Tr(T^aD_a) = 0$.

3.2 The Minimally Supersymmetric Standard Model(MSSM)

3.2.1 Field and particle content

To build the MSSM the following superfields are introduced to incorporate particles and "sparticles". Note however that for sfermions, which are scalars, the term chirality is a misnomer and only denotes that they are superpartners of the corresponding chiral fermion. In the next few sections, spinor indices will be ruthlessly suppressed unless explicitly required.

The following prescription for the fields is followed,

- **Chiral Superfields** : For the left handed doublet sleptons,

$$L_e = \tilde{e}_L + \sqrt{2}\theta e_L + \theta\theta F,$$

where the superfield L_e has an index that makes it the lower component of the left handed doublet. The left handed positron superfield is similarly called $\bar{E_1}$, which means antiparticle but not complex conjugation. Similarly for the left handed doublet squarks we have the following superfield

$$Q_u = \tilde{u} + \sqrt{2}\theta\tilde{u}_L + \theta\theta F$$

along with the left handed $\bar{U_1}$.

- **Gauge Superfields** : These fields transform in the adjoint representation of the respective gauge group. The first of these is the $U(1)_Y$ gauge superfield, i.e (B_μ) and the Bino($\tilde{B}$). The electroweak $SU(2)_L$ sector contains the SM gauge bosons W^a_μ and the corresponding Wino($\tilde{W}^a$). Finally the SU(3) sector contains gluons (g^a_μ) and the gluinos ($\tilde{g}^a$). These fields are embedded in the vector superfields $V^y, V^a(2), V^a(3)$ respectively.
- Finally the Higgs sector of the theory, which has two doublet superfields as compared to 1 doublet field in the SM. The Higgs sector is explained below.

In contrast to SM where there is a single Higgs doublet field, MSSM requires at least two Higgs doublets. To realize this necessity, notice that in SM the Yukawa couplings for quarks can be written as,

$$-(f^d(\bar{q})_L\phi^c\bar{d_L} + f^{*(d)}(\bar{q})_R\phi\bar{d_R}) - (f^u\bar{q_L}\phi\bar{u_L} + f^{*(u)}(\bar{q})_R\phi^{(c)}\bar{u_R}),$$

for the down type and the up type quarks respectively. To find the corresponding SUSY analogue, note that q_L is contained in Q_1, while $\bar{d_L}$, $\bar{u_L}$ is contained in $\bar{D_1}$ and in $\bar{U_1}$ respectively. Yukawa interactions in SUSY originate from chiral superfields and thus if ϕ^c is in a chiral superfield, ϕ must be a part of an antichiral superfield, and the two are clearly mutually incompatible. Thus the only way to reconcile the two is to put them in separate chiral superfields H_1 and H_2 such that the Yukawa couplings can be written as,

$$-f^d\int d^2\theta\ Q_1H_1\bar{D}_1 + c.c - f^{*u}\int d^2\theta\ Q_1H_2\bar{U}_1 + c.c,$$

where $\mathrm{H}_2 = \begin{pmatrix} h_2^+ \\ h_2^0 \end{pmatrix}$ and $\mathrm{H}_1 = \begin{pmatrix} h_1^0 \\ h_1^- \end{pmatrix}$.

The second reason as to why two Higgs doublets are required is from considerations of anomaly cancellation. With one Higgs doublet and its counterpart higgsino fields the anomaly, proportional to the cube of the hypercharges ($\sum_{\tilde{h}} Y^3_{\tilde{h}}$), is non vanishing. Note that the superfields contain the two scalar Higgs doublets and its SUSY counterparts, namely the higgsinos which are chiral fermions with opposite hypercharge assignments, hence ensuring cancellation of the anomalies. Note however that the gauginos do not contribute to the anomaly as they are in the adjoint representation of the gauge group and hence are real like the corresponding gauge partners. The particle content is summarized in Table 3.1.

Therefore assuming no SUSY breaking the MSSM Lagrangian can be written as (extending Eq.3.1.26),

$$\mathscr{L}_{gauge} = \frac{1}{4}\int d^2\theta\ (W^{(y)}W^{(y)} + Tr(\vec{W}^2\vec{W}^2) + Tr(\vec{W}^3\vec{W}^3)), \tag{3.2.1}$$

	Superfield	Particle	Spin	Superpartner	Spin
Matter Fields	Q	$(u,d)_L$	$\frac{1}{2}$	$(\tilde{u}_L, \tilde{d}_L)$	0
	U^c	$\bar{u}_R$	$\frac{1}{2}$	$\tilde{u}^*_R$	0
	D^c	$\bar{d}_R$	$\frac{1}{2}$	$\tilde{d}^*_R$	0
	L	$(\nu, e)_L$	$\frac{1}{2}$	$(\tilde{\nu}_L, \tilde{e}_L)$	0
	E^c	$\bar{e}_R$	$\frac{1}{2}$	$\tilde{e}^*_R$	0
Gauge Fields	V^y	B_μ	1	$\tilde{B}$	$\frac{1}{2}$
	$V^a(2)$	W^i_μ	1	$\tilde{W}^i$	$\frac{1}{2}$
	$V^a(3)$	G^a_μ	1	$\tilde{g}^a$	$\frac{1}{2}$
Higgs Fields	H_1	(H^0_1, H^-_1)	0	$(\tilde{H}^0_1, \tilde{H}^-_1)$	$\frac{1}{2}$
	H_2	(H^+_2, H^0_2)	0	$(\tilde{H}^+_2, \tilde{H}^0_2)$	$\frac{1}{2}$

Table 3.1: Field content of the MSSM.

$$\mathscr{L}_{matter} = \frac{1}{4}\int d^2\theta d^2\theta^\dagger \; (L^\dagger e^{(g_1 V^y y + \vec{V}^2)} L^i) + \bar{E}^\dagger_i e^{\;(g_1 V_y y)}\; E_i + Q^\dagger_i e^{(g_1 V_y + \vec{V}^2 + \vec{V}^3)} Q_i + \ldots, \quad (3.2.2)$$

$$\mathscr{L}_{Higgs} = \int d^2\theta \; d^2\theta^\dagger \sum_{i=1}^{2} H^\dagger_i e^{(g_1 V_y y + \vec{V}_2)} H_i. \quad (3.2.3)$$

Eq. 3.2.1 contains the gauge kinetic terms for the U(1), SU(2) and SU(3) part of the theory.

The matter sector in Eq, 3.2.2 contains the kinetic terms for lepton doublet(L_i), invariant under the $\mathrm{SU(2)_L \times U(1)_Y}$ part, while the corresponding kinetic part involving $\bar{E_i}$ in Eq. 3.2.2 is invariant only under the $\mathrm{U(1)_Y}$ part. The quark-squark follows the similar pattern analogous to SM. The Higgs sector in Eq. 3.2.3 runs over the two Higgs doublet superfields H_1, H_2.

Finally the Yukawa and the interaction terms in the Higgs doublet is written with the following superpotential term,

$$\mathscr{L}_{superpotential} = -\int d^2\theta(-\mu H_1.H_2 - f^{(2)}_{ij} L_i H_1 \bar{E_i} - f^{(d)}_{ij} Q_i.H_2 \bar{D}_j - f^{(u)} Q_i H_2 \bar{U}_j) + c.c, \quad (3.2.4)$$

where $H_1.H_2 = \varepsilon_{ab} H^a_1 H^b_2$. Note that the Yukawa structure necessarily implies that the quarks and squarks within the same superfield obtain the same masses. Also the $H_1.H_2$ term is hypercharge neutral as the two chiral superfields have opposite hypercharges. Notice that objects like $H_1.H_1$, $H_2.H_2$ vanish once indices are contracted.

In the SUSY Lagrangian we have ignored certain types of interactions. These are terms like $L_i.H_2$, $L_i.L_j\bar{E_k}$, $\bar{U_i}\bar{D_j}\bar{D_k}$ or $L_i.Q_j\bar{D_k}$ which respect SUSY gauge invariance and have no analogous SM counterpart.

We would however like to suppress these interactions in the minimal version of SUSY as they do not appear in the SM. These terms also lead to rapid proton decay. The suppression is achieved by a discrete Z_2 symmetry known as R parity under which $\bar{L_i}, \bar{E_i}, Q_i, \bar{D_i}$ are odd and H_1, H_2 are even.

The idea is to realize that since superspace contains complex fermionic co-ordinates θ, it's natural to consider phase transformations,

$$\theta_a \to e^{i\alpha}\theta_a, \;\; \theta^\dagger_{\dot{a}} \to e^{-i\alpha}\theta^\dagger_{\dot{a}}.$$

This is a spacetime symmetry in superspace, and an internal symmetry in ordinary space as the co-ordinates θ lie entirely in superspace. Therefore we can implement a global U(1) symmetry termed as R symmetry by the following,

$$\Phi(x,\theta,\theta^\dagger) \to \Phi'(x,\theta,\theta^\dagger) = e^{(i\alpha R_\phi)}\Phi(x,e^{i\alpha}\theta,e^{-i\alpha}\theta^\dagger),$$

where $\Phi = \phi + \sqrt{2}\theta\xi + \theta\theta F$.

Thus to implement the above symmetry, the component fields must satisfy,

$$\phi \to e^{i\alpha R_\Phi}\phi, \;\; \xi \to e^{i\alpha(R_\Phi - 1)}\xi, \;\; F \to e^{i\alpha(R_\Phi - 2)}F \tag{3.2.5}$$

with the transformation of the measure being $d^2\theta \to e^{-2i\alpha}d^2\theta$.

As an example, the interaction, $m\int d^2\theta\Phi^2$ is invariant under R symmetry with the assignment, $R_\Phi = 1$. The component fields therefore transform as,

$$\phi \to e^{i\alpha}\phi, \;\; \xi \to \xi, \;\; F \to e^{-i\alpha}F.$$

After removal of the auxiliary field this reduces to,

$$(m^2\phi^*\phi + m\xi\xi + c.c),$$

which is clearly invariant under the phase rotation and is non anomalous as the phase rotation does not act on ξ.

However the following problems are integral to imposing an R symmetry,

- R-symmetry is generically anomalous once we have gauge fields.
- Vector multiplets are neutral, implying that gaugino transforms with a phase $\lambda \to e^{i\alpha}\lambda$. This forbids Majorana mass terms like $\lambda\lambda$ for gauginos once SUSY is broken.

Hence R symmetry as an U(1) global symmetry is constrained. However the Z_2 subgroup, termed as R-parity is non anomalous and can be imposed as a symmetry. In MSSM R parity is implemented as $R = (-1)^{(3B-L+2s)}$ where B is the baryon number, L the lepton number and s the spin of the particle.

Quantities like $L_i, \bar{E}_j, ..$ are odd under R-parity while H_1, H_2 are even. Hence it forbids unwanted couplings like $L_iQ_jE_k$. We thus assert that MSSM preserves R-parity [4]. As a consequence the lepton doublet superfield L_e, which is odd under R parity has the scalar component, namely the selectron as odd and the SM fermion even. Thus SM particles are even under R parity while the corresponding sparticles are odd. Since the Higgs superfield is even under R parity, the scalar component is even while the higgsino is odd. Under R-parity, the vector superfield transforms $A_\mu \to A_\mu$, while the corresponding gaugino transforms as $\lambda \to -\lambda$. The consequence of this is that superpartners must be produced in pairs and hence the lightest superparticle must be stable as it is the lightest R-odd state.

[4] Note that R-parity is imposed by hand, and does not follow from any deep underlying principle. R-parity violating MSSM models have also been widely studied in the literature.

3.3 SUSY breaking

Notice that the formalism of MSSM thus developed predicts that the chiral multiplets that occur in the same superfield must necessarily have the same mass. This is in clear contradiction with experiments and thus SUSY must be broken. SUSY breaking comes under two broad classes; firstly classical, which implies that the SUSY is broken spontaneously by the minimization of the classical potential analogous to the SM. The second option is to achieve it dynamically by quantum corrections.

However if neither of the above turn out to be the correct way of breaking SUSY, the other option is explicit breaking by adding terms in the SUSY Lagrangian which are manifestly non supersymmetric due to some unknown mechanism in the underlying theory.

3.3.1 General aspects of SUSY breaking

Note that the SUSY algebra can be written as [158], $P_\mu = \frac{1}{4} 2\sigma_\mu^{\dot{b}a\dagger}\{Q_a, Q_{\dot{b}}^\dagger\}$. The Hamiltonian can be expressed as,

$$H = P_0 = \frac{1}{4}\{Q_1, Q_{\dot{1}}^\dagger\} + \frac{1}{4}\{Q_2, Q_{\dot{2}}^\dagger\}.$$

Thus for any state $|\alpha\rangle$ the expectation value of the Hamiltonian can be written as,

$$\langle\alpha|H|\alpha\rangle = \frac{1}{4}\sum_{a=1}^{2}\sum_{n}(|\langle\alpha|Q_a|n\rangle|^2 + |\langle\alpha|Q_{\dot{a}}^\dagger|n\rangle|^2).$$

The total energy is thus positive definite and invertible as long as SUSY algebra is intact. The SUSY vacuum state can be defined as $|\Omega\rangle$, with the condition that it remains invariant under SUSY transformations namely under the infinitesimal transformation,

$$\delta|\Omega\rangle = i(\varepsilon^a Q_a + \varepsilon_{\dot{a}}^\dagger Q^{\dagger\dot{a}})|\Omega\rangle = 0,$$

implying $Q_a|\Omega\rangle = Q_{\dot{a}}|\Omega\rangle = 0$. Therefore the SUSY vacuum must have vanishing total energy. The scalar sector of the theory which is described by a complex scalar field has a physical vacuum configuration corresponding to a minimum of the effective potential $V(\phi)$, including quantum corrections. We thus assert that SUSY breaking corresponds to a global minima of $V(\phi)$ such that, SUSY is broken either when,

$$\mathrm{Q_a}|\Omega\rangle \neq 0 \text{ or } \mathrm{Q_{\dot{a}}^\dagger}|\Omega\rangle \neq 0$$

.

As a digression we mention a toy SUSY breaking scenario. Consider the chiral superfield $\Phi = \phi + \sqrt{2}\theta\xi + \theta\theta F$, and the SUSY transformations that leave it invariant $\delta\phi \sim \varepsilon\xi$, $\delta\xi \sim \varepsilon^\dagger\sigma^\mu\partial_\mu\phi + \varepsilon F$ and $\delta F \sim \varepsilon^\dagger\sigma^\mu\partial_\mu\xi$.

It is obvious that to break SUSY one of the terms in the chiral superfield must have a VEV, such that the variation of Φ does not leave it invariant. ξ cannot get a VEV as it destroys Lorentz invariance,

while if ϕ gets a VEV it has to be a constant VEV and hence $\partial_\mu\phi = 0$. Hence the only quantity left is F which develops a VEV to break SUSY. We note therefore that for a chiral superfield, the only term that can get a VEV is the F term, and thus the configuration $|\langle\Omega|F|\Omega\rangle > | = \Lambda_s^2 \neq 0$, leads to SSB in SUSY. Since F has mass dimensions of 2, Λ_s can be identified by a mass scale. For the vector multiplet, we must have $|\langle\Omega|D|\Omega\rangle > | = \Lambda_s^2 \neq 0$.

To construct a superpotential with a set of interacting superfields Φ_i, note that any superpotential of the form $\mathscr{W} = \frac{1}{2}m_{ij}\Phi_i\Phi_j + \frac{1}{6}f_{ijk}\Phi_i\Phi_j\Phi_k$ without a linear term in Φ fails to produce a suitable F term required for SUSY breaking. In such a case $F_i^* = -\frac{\partial \mathscr{W}}{\partial \Phi_i}$, can be made 0 with the choice of all expectation values $\langle \Phi_i \rangle = 0$.

A widely studied SUSY breaking scenario is the O'Raifeartaigh's model [162]. This is given by the superpotential,

$$\mathscr{W}(\Phi_1, \Phi_2, \Phi_3) = m\Phi_2\Phi_3 + \lambda\Phi_1(\Phi_3^2 - \mu^2).$$

For simplicity m, λ, μ are assumed to be real. The equations of constraint are given by,

$$F_1^* = -\lambda(\phi_3^2 - \mu^2), \;\; F_2^* = -m\phi_3, \;\; F_3^* = -m\phi_2 - 2\lambda\phi_1\phi_3.$$

It can be observed that there is no consistent set of solutions which can make all the F's vanish simultaneously. Thus F is always non zero everywhere in the ϕ space including the minima of $V(\phi)$, thus breaking SUSY. The scalar potential in O'Raifeartaigh's model is given by

$$V(\phi_1, \phi_2, \phi_3) = |\lambda(\phi_3^2 - \mu^2)|^2 + m^2\phi_3^2 + |m\phi_2 + 2\lambda\phi_1\phi_3|^2.$$

In this model however model the supertrace, defined as $STr(\underset{\sim}{m}^2) = \sum_{J=0}^{1/2}(-1)^{2J}(2J+1)m_J^2$, (where J is the spin and the sum runs over all the fields in the chiral multiplet) vanishes. It will be later shown explicitly that the vanishing of the supertrace leads to phenomenologically inconsistent results, and in order for SUSY to be broken the supertrace must be non zero.

SUSY breaking can also be triggered by the D term in a vector superfield or a combination of F and D term with coupled chiral and vector superfield. We take this up in the next section with the connection to the supertrace formula.

3.3.2 The general mass sum rule

We remind ourselves that the scalar potential can be written as,

$$\begin{aligned} V &= \sum_i |\mathscr{W}_{,i}|^2 + \frac{1}{2}\sum(\eta + \phi^\dagger T^a \phi)^2 \\ &= \sum |F_i|^2 + \frac{1}{2}\sum D^a D^a. \end{aligned} \tag{3.3.1}$$

A minimization of the scalar potential leads to mass terms for the fermions and scalars (both left handed and right handed sectors). The squared mass matrix have components consisting of superpotential derivatives and derivatives of D terms. Summing up the contributions from the scalar fermion and the vectors the supertrace formula can be written as,

$$\begin{aligned} S\,Tr(\tilde{m}^2) &= Tr(m^2)_s - Tr(m_f^\dagger m_f + c.c) + 3Tr(m_v^2) \\ &= -2Tr\; T^a \langle D^a \rangle. \end{aligned}$$

However it turns out that even this violation of the sum rule is not enough to realize MSSM with spontaneous SUSY breaking.

In MSSM this sum rule amounts to taking the trace over the gauge groups of $\mathrm{SU(2)_L}$ and $\mathrm{U(1)_Y}$. Thus,

$$S\,Tr(\tilde{m}^2) = -2(g_2 T_3 \langle D^3 \rangle + g_1 \frac{Y}{2}\langle D^y \rangle).$$

Summing over the hypercharges and isospin of the lepton and the neutrino superfields and similarly quark superfields,

$$\begin{aligned} STr(M_e^2) &= g_2\langle D^3\rangle + g_1\langle D^y\rangle - 2g^y\langle D^y\rangle \\ &= g_2\langle D^3\rangle - g_1\langle D^y\rangle, \\ STr(M_v^2) &= -g_2\langle D^3\rangle + g_1\langle D^y\rangle, \\ STr(M_u^2) &= -g_2\langle D^3\rangle + g_1\langle D^y\rangle, \\ STr(M_d^2) &= g_2\langle D^3\rangle - g_1\langle D^y\rangle. \end{aligned}$$

Therefore the supertrace over the lepton and the quark superfield reads,

$$\begin{aligned} STr(M_e^2) + STr(M_v^2) = m_e^2 - m_{\tilde{e}}^2 + m_v^2 - m_{\tilde{v}}^2 &= 0, \\ STr(M_u^2) + STr(M_d^2) = m_e^2 - m_{\tilde{u}}^2 + m_d^2 - m_{\tilde{d}}^2 &= 0. \end{aligned}$$

The above statement is true even after D term SUSY breaking. Thus, although asserting that this was the most general D term breaking and in spite of the fact that the D term breaking did split the individual multiplet, the supertrace over the full multiplet vanishes. Thus in every generation some squark/slepton is lighter than the corresponding quarks and leptons and contradicts experimental observations.

3.3.3 Soft SUSY breaking

The only remaining option therefore is to add SUSY breaking terms in the Lagrangian by construction. These terms are not manifestly supersymmetric but are chosen specifically so that they don't destroy the high energy properties of SUSY, in particular that it does not bring back the quadratic divergences which we struggled to eliminate.

The general idea is to assume that there is a hidden sector of fields in some high scale unbroken theory which are singlets under the SM gauge group. SUSY can be spontaneously broken there at a scale Λ_s. SUSY breaking is then transmitted to the visible sector(SM) by a set of fields called "messengers". Thus instead of abandoning the SSB altogether it is passed on to a higher scale theory. It is generally true that the scale of the messenger fields must be at least two orders of magnitude higher than the SM scale. Hence if we integrate out the hidden sector fields from the gravity mediated interactions what remains of the theory contains the MSSM Lagrangian with the addition of soft SUSY breaking terms. As it turns out the term soft refers to the fact that the Lagrangian should only consist of terms with mass dimensions less than or equal to 3 so that we do not introduce terms that bring back quadratic divergences into play. With these the most general soft SUSY breaking terms can be written as,

$$\begin{aligned} \mathscr{L}_{soft} &= \phi^* m_{ij}^2 \phi_j + (c_i\phi_i - \frac{1}{2}B_{ij}\phi_i\phi_j + \frac{1}{3!}f_{ijk}\phi_i\phi_j\phi_k) + c.c \\ &\quad -\frac{1}{2}(M\lambda^a\lambda^a + c.c). \end{aligned} \tag{3.3.2}$$

The first line in Eq. 3.3.2 involves mass term for scalars and interactions of scalars while the second line has Majorana mass terms for gauginos. Note that there are no mass terms for ordinary

fermions. A bilinear like $\xi_i\xi_j + c.c$ can be obtained from the scalar bilinear and a bilinear involving chiral superfields. It can be shown that if chiral gauge superfields are present the mass terms for chiral fermions no longer happen to be soft. Note also that there are no terms of the form $\phi^*\phi\phi$ as they tend to generate quadratic divergences from tadpole diagrams.

In component form the content of $\mathscr{L}_{soft}$ in MSSM has contributions from the squark/slepton mass terms in the sfermion sector along with the gaugino and the Higgs mass terms. In addition there are trilinear terms involving the Higgs and the sfermions. Note that there are no single scalar terms of the form $C_i\phi_i$ as there are no such gauge invariant terms in the SM. The content of $\mathscr{L}_{soft}$ can be written as,

$$\begin{aligned} -\mathscr{L}_{soft} &= \tilde{q}^*_{iL}(\mathscr{M}^2_{\tilde{q}})_{ij}\tilde{q}_{jL} + \tilde{u_{iR}}^*(\mathscr{M}^2_{\tilde{u}})_{ij}\tilde{u}_{jR} + \tilde{d_{iR}}^*(\mathscr{M}^2_{\tilde{d}})_{ij}\tilde{d}_{jR} + \tilde{l_{iL}}^*(\mathscr{M}^2_{\tilde{l}})_{ij}\tilde{l}_{jL} \\ &+ \tilde{e_{iR}}^*(\mathscr{M}^2_{\tilde{e}})_{ij}\tilde{e}_{jR} + [h_1.\tilde{l}_{iL}(f^eA^e)_{ij}\tilde{e^*}_{jR} + h_1.\tilde{q}_{iL}(f^dA^d_{ij}\tilde{d^*}_{jR} \\ &+ \tilde{q}_{iL}.h_2(f^uA^u)_{ij}\tilde{u^*}_{jR} + h.c] + m_1^2|h_1|^2 + m_2^2|h_2|^2 + (B\mu h_1.h_2 + h.c) \\ &+ \frac{1}{2}(M_1\tilde{B}\tilde{B} + M_2\tilde{W}^a\tilde{W}^a + M_3\tilde{g}^a\tilde{g}^a) \end{aligned} \tag{3.3.3}$$

The unfortunate consequence of the above Lagrangian is in the vast number of free parameters that emerge out of these soft terms. Adding up the masses, trilinear terms and the phases the total number turns out to be 105. With the contribution of the SM parameters, this amounts to over 120 undetermined quantities. Simplifying assumptions like flavor diagonal mass matrices and no extra sources of CP violating phases beyond SM reduces the number significantly. This model is termed as the phenomenological MSSM(pMSSM).

3.4 Hidden Sector models

A number of hidden sector SUSY breaking scenarios are present in the literature each with its pros and contras. We list the three most widely studied models of hidden sector SUSY breaking.

- Gravity Mediation : SUSY is broken in the hidden sector of fields by higher dimensional operators. In terms of economy and simplicity, this is the most widely studied model. Throughout this thesis we will be working in the framework of this model.
- Gauge mediation (GMSB): SUSY is broken in the hidden sector by a set of gauge fields. The lightest SUSY particle in this case turns out to be the gravitino.
- Anomaly mediation (AMSB): SUSY is broken in the hidden sector by Super Weyl anomalies. The LSP in this case can either be χ^0_1, which is almost degenerate with the next to leading SUSY particle, or the sneutrino ($\tilde{\nu}_L$).

3.4.1 Minimal Supergravity(mSUGRA)/Constrained MSSM(CMSSM)

In terms of economy and simplicity, the most widely utilized model of hidden sector SUSY breaking is the gravity mediated breaking, namely the minimal supergravity model [163–168]. So far we have considered N=1 SUSY under invariant under a global symmetry. Elevating the infinitesimal parameters of transformation to being local functions of spacetime coordinates requires to treat the spacetime metric as a dynamical object. The simplest theory which achieves this is Einstein's theory of General Relativity.

The supergravity multiplet for N=1, D=4 consists of the spin 2 quantized particle of gravity, namely the graviton , and a vector-spinor of spin 3/2 denoted by ψ_μ^α known as the gravitino. The problem of constructing locally supersymmetric Lagrangians for the supergravity multiplet can be tackled in two stages, namely to construct the globally supersymmetric Lagrangian and then use the Noether procedure to turn the global symmetry into a local one.

A detailed derivation is beyond the scope of this thesis [5], and merely the salient features are sketched. The supergravity multiplet is constructed out of the Einstein-Hilbert action for the graviton and the Rarita-Schwinger action for the gravitino written in terms of the affine connections and vielbein quantities defined in terms of the spin connection [6] . The interactions involving chiral (matter) and vector (gauge) superfields are written in terms of the Kahler potential $\mathscr{G}$, a gauge singlet function of complex scalar fields and the gauge kinetic function f_{ab}, where the gauge group indices a and b transform as the symmetric product of two adjoint representations. The second derivatives of $\mathscr{G}$ determine the form of kinetic energy for chiral superfields while f_{ab} determines terms for the gauge superfields. Canonical kinetic energy terms correspond to $\mathscr{G}_i^j = \delta_i^j$ and $f_{ab} = \delta_{ab}$. In general the supergravity Lagrangian is not a renormlizable one.

A SSB in these locally supersymmetric models take place if the F term of the superfield develops a non zero VEV. This results in a massless fermion, the goldstino which is subsequently eaten by the gravitino to acquire a mass given by $m_{3/2} = M_{pl} e^{-\langle \mathscr{G} \rangle/(2M_{Pl}^2)}$, thus increasing the degrees of freedom of the gravitino from two to four. The masses for the scalar and the fermion sectors can then be computed, by treating low energy supergravity in the limit of $M_{Pl} \to \infty$ holding $m_{3/2}$ fixed. Thus one can follow the following ansatz for the minimal supergravity model. The first of these assume universal SUSY breaking parameters for the scalar sector derived from the Kahler metric, namely,

$$m_{ij}^2 = m_0^2 \delta_{ij},\ A_{ijk} = A_0,\ \ B_{ij} = B_0 \tag{3.4.1}$$

Since RGE of the soft parameters evolve differently, the above relations do not hold at all scales once quantum corrections are taken into account. The above relations therefore should be interpreted as boundary conditions at scales just below M_{Pl}. For the gaugino masses, since gauge couplings unify at a scale close to $M_{GUT} \sim 10^{16}\ GeV$, it is reasonable to assume that the gauge kinetic function f_{ab} at this scale is proportional to δ_{ab}. This implies that all gaugino masses can be assumed to acquire an universal value of $M_\alpha(M_{GUT}) = m_{1/2}$. Therefore these universal boundary conditions when evolved with RGE equations yield the low energy spectrum. In general spectrum calculators like SUSPECT use a two loop RGE to evolve a generic high scale SUSY breaking model down to the electroweak scale.

A characteristic relationship in mSUGRA is the following relationship at the electroweak scale,

$$M_1(100GeV) \simeq 0.41 m_{1/2},\ \ M_2(100GeV) \simeq 0.82 m_{1/2}\ \ M_3(500GeV) \simeq 2.6 m_{1/2}. \tag{3.4.2}$$

The gaugino masses therefore follow the relationship (for $\mu \gg M_1, M_2$),

$$m_{\chi_1^0} \simeq \frac{1}{2}\, m_{\chi_2^0, \chi_1^\pm} \simeq \frac{1}{6} m_{\tilde{g}}. \tag{3.4.3}$$

[5] For a detailed discussion consult [163–168] and [169–171]

[6] The Lagrangian for the mSUGRA multiplet can be written as $L_0 = L_{EH} + L_{RS}$, where L_{EH}, L_{RS} are the Einstein Hilbert and the Rarita Schwinger contribution respectively. Written in terms of the vielbeins quantities this reads,

$$L_0 = -\frac{1}{4}|e| e_a^\mu e_b^\nu R_{\mu\nu}^{ab}[\omega] + \frac{1}{2}\varepsilon^{\mu\nu\rho\lambda}\, \bar{\psi_\nu}\gamma_5\gamma_\mu D_\rho \psi_\lambda$$

.

The gluino mass is approximately 2.5-2.8 times $m_{1/2}$, depending on the choice of scale. The gluino pole mass receives corrections from the squark sector and is roughly given by [158],

$$m_{\tilde{g}}^{pole} \simeq M_3(M_3)\left[1+\frac{\alpha_3(M_3)}{4\pi}\left(15+\sum_{\tilde{q}}\frac{m_{\tilde{q}}}{M_3}\right)\right]. \tag{3.4.4}$$

On the other hand slepton and the squark masses receive significant corrections from the gaugino sector. As an example, the selectron and squark masses are given by [158],

$$\mathrm{m}^2_{\tilde{\mathrm{e}}_\mathrm{R}}(100\mathrm{GeV}) = m_0^2+0.15m_{1/2}^2 + D\,terms \tag{3.4.5}$$

$$\mathrm{m}^2_{\tilde{\mathrm{e}}_\mathrm{L}}(100\mathrm{GeV}) = m_0^2+0.53m_{1/2}^2 + D\,terms \tag{3.4.6}$$

$$\mathrm{m}^2_{\tilde{\mathrm{q}}_\mathrm{L}}(500\mathrm{GeV}) = m_0^2+5.6m_{1/2}^2 + D\,terms \tag{3.4.7}$$

$$\mathrm{m}^2_{\tilde{\mathrm{q}}_\mathrm{R}}(500\mathrm{GeV}) = m_0^2+5.2m_{1/2}^2 + D\,terms \tag{3.4.8}$$

The D term contributions are not significantly large. In the large $m_{1/2}$ region, the squarks and the gluino are almost degenerate to each other. This has important consequences in collider phenomenology, as we shall explore in Chapter 7. Note that although the Yukawa couplings of the first two generations of squarks can be neglected, the third generation Yukawas are significant and play a role in radiative electroweak symmetry breaking. The large hierarchy between the unification scale and the electroweak scale ($\ln \frac{\mathrm{M_U}}{\mathrm{M_Z}} = 33$), also make it easy to obtain values of a negative eigen value in the Higgs mass matrix (see 3.6.1) by RGE running, required for EWSB. Generally the soft parameter B_0 is traded for $tan\beta$ and thus the set of parameters that completely determine mSUGRA/CMSSM are $m_0, m_{1/2}, A_0, tan\beta, sgn(\mu)$. The EWSB conditions can be expressed as,

$$\frac{1}{2}M_Z^2 = \frac{m_1^2 - m_2^2 tan^2\beta}{tan^2\beta} - |\mu|^2. \tag{3.4.9}$$

In terms of the mSUGRA parameters this is given by,

$$\frac{1}{2}M_Z^2 = c_0 m_0^2 + c_1 m_{1/2}^2 + c_2 A_0^2 + c_3 m_{1/2} A_0 - |\mu|^2, \tag{3.4.10}$$

where c_0, c_1, c_2, c_3 are numerical coefficients. Thus given the high scale values of $m_0, m_{1/2}, A_0$, the higgsino mass parameter μ^2 is determined from the EWSB condition at the electroweak scale. The sign of μ however has to be fixed by hand. Low energy constraints like the anomalous magnetic moment of the muon ($(g-2)_\mu$) favor the sign to be positive. Observe that the electroweak symmetry breaking condition also has a quadratic dependence on the parameter A_0. This is particularly important, since the third generation trilinear coupling A_t derived from RGE running of A_0 controls the loop corrections to the Higgs mass. Typically a large negative value of A_t is required to achieve the correct Higgs mass of 125 GeV. This however forces A_0 to take up large negative values thus reintroducing some amount of fine tuning in the theory.

Apart from the economy of the model, (which also results in a large predictive power of the model) the mSUGRA/CMSSM also is a favorable model for the suppression of large FCNC contributions. Along with this it also predicts a viable dark matter compatible regions in certain parts of the parameter space as we shall explore in Chapter 5.

The perturbativity of the Yukawa couplings require $\tan\beta < \frac{\mathrm{m_t(Q_0)}}{\mathrm{m_b(Q_0)}} \simeq 60$. The bound $A_0 > -4m_0$ follows from the fact that scalar potential should not have a minimum that breaks electromagnetic charge ($\mathrm{U(1)_{em}}$) or color charge $\mathrm{SU(3)_c}$. Since the scalar potential contains soft terms

of the form $f_t A_t \tilde{t}_L \tilde{t}_R h_2^0$, a choice of phases can be made such that these terms are negative. One generally expects only the neutral Higgs to acquire a non-zero VEV at the minima. However it is possible that for large values of $|A_t|$ the left and right stop states can acquire non-zero VEVs.

3.5 Masses and mixing in MSSM

3.5.1 Gaugino-higgsino-mixing

The mass terms in the MSSM Lagrangian come from two sources, namely the D terms and the soft terms. The key term responsible in the MSSM Lagrangian are terms like $\tilde{W}\tilde{h}h^*$ from the D term in $H^\dagger e^{2g_2 V} H$(Eq.3.2.3) and from the soft mass term (Eq.3.3.3). After EWSB the gauginos and higgsinos charged under U(1) mix with the relevant Lagrangian given by,

$$\mathscr{L}_{chargino} = -\frac{g_2}{\sqrt{2}}(v_1 \tilde{W}^+ \tilde{H}_1^- + v_2 \tilde{W}^- \tilde{H}_2^\dagger) - (M_2 \tilde{W}^+ \tilde{W}^- + c.c) + (\mu \tilde{H}_1^+ \tilde{H}_2^- + c.c).$$

[7] The weak eigen states ψ are given by ,

$$\psi = \begin{pmatrix} \tilde{W}^+ \\ \tilde{H}^+ \end{pmatrix}^{[8]}. \tag{3.5.1}$$

In terms of the mass of the W boson and the weak mixing angle θ_W, the mass matrix can be read off from Eq.3.5.1,

$$M^c = \begin{pmatrix} M_2 & \sqrt{2} M_W \sin\beta \\ \sqrt{2} M_W \cos\beta & \mu \end{pmatrix}. \tag{3.5.2}$$

Note that in general both M_2 and μ are not real. For complex M_2 and μ the relative phases between M_2 and μ and between M_2 and M_1 may be important. However in the subsequent discussions, we shall assume the relative phases to be zero. Since the two basis $(\tilde{W}^+ \; \tilde{H}^+)$ and its complex conjugate are different, two different unitary transformations on the two matrices are required to diagonalize the mass matrix. This bi-unitary transformation can be used to diagonalize the hermitian matrix $M^{c\dagger} M^c$. Thus,

$$\mathscr{U} M \mathscr{V}^{-1} = M_c^D,$$

where $\mathscr{U}, \mathscr{V}$ are the unitary matrices that diagonalize the chargino mass matrix.

The eigen states conventionally known as charginos $(\chi_{1,2}^\pm)$,

$$|\chi^+\rangle = \mathscr{V}_{km} \psi_m^+, \;\; |\chi^-\rangle = \mathscr{U}_{km} \psi_m^-.$$

The matrix $M^{c\dagger} M^c$ can be written as,

$$M^{c\dagger} M^c = \begin{pmatrix} |M_2|^2 + 2M_W^2 cos^2\beta & \sqrt{2} M_W (M_2^* \sin\beta - \mu \cos\beta) \\ \sqrt{2} M_W (M_2 \sin\beta - \mu^* \cos\beta) & |\mu|^2 + 2M_W^2 sin^2\beta \end{pmatrix}. \tag{3.5.3}$$

The eigen values of the above equation are given by,

$$M_{1,2}^2 = \frac{1}{2}\left[M_2^2 + \mu^2 + 2M_W^2 \mp \sqrt{(M_2^2 - \mu^2)^2 + 4M_W^4 \cos^2 2\beta + 4M_W^2 (M_2^2 + \mu^2 + 2M_2 \mu \sin 2\beta)} \right]. \tag{3.5.4}$$

[7] Note of course that the Majorana gluinos($\lambda_a, a = 1,2,\ldots,8$) being part of SU(3) don't mix.

[8] We adopt the following convention, following [158]. $\tilde{H}^+ = \begin{pmatrix} \tilde{h}_2^1 \\ \bar{\tilde{h}}_1^{2T} \end{pmatrix}$, $\tilde{W}^+ = \begin{pmatrix} \lambda^+ \\ \bar{\lambda}^{-T} \end{pmatrix}$.

It is interesting to look at limits of Eq. 3.5.4, In the limit $|\mu| \gg M_2, M_W$, with $\varepsilon_\mu = \frac{\mu}{|\mu|}$ being the sign of μ,

$$m_{\chi_1^\pm} \simeq M_2 - \frac{M_W^2}{\mu^2}(M_2 + \mu \sin 2\beta) \quad , \quad m_{\chi_2^\pm} \simeq |\mu| + \frac{M_W^2}{\mu^2}\varepsilon_\mu (M_2 \sin 2\beta - \mu)$$

such that for large μ, the lighter chargino is gaugino like, while the heavier chargino is higgsino like. In the opposite limit, i.e for $|\mu| \ll M_2, M_W$, the above pattern is reversed.

The Lagrangian for the neutral gauginos and the higgsinos come from the soft mass terms for the gauginos (Eq.3.3.3), from the superpotential term $\mu H_1.H_2$, and finally from the Higgs part of the Lagrangian (Eq.3.2.3) with matter-gauge-Higgs couplings. Schematically the Lagrangian for the neutral gaugino sector can be written as,

$$\mathscr{L}_{Gaugino-higgsino} = -\frac{1}{2} M_3 \tilde{g}_a \tilde{g}_a - \frac{1}{2}\bar{\chi} M^{(0)} \chi. \tag{3.5.5}$$

The matrix χ is given by,

$$\chi = \begin{pmatrix} \tilde{B}^0 \\ \tilde{W}^3 \\ \tilde{H}_1^0 \\ \tilde{H}_2^0 \end{pmatrix}. \tag{3.5.6}$$

The neutralino mass matrix is,

$$M^{(0)} = \begin{pmatrix} M_1 & 0 & -M_Z \cos\beta \sin\theta_W & M_Z \sin\beta \sin\theta_W \\ 0 & M_2 & M_Z \cos\beta \cos\theta_W & -M_Z \sin\beta \cos\theta_W \\ -M_Z \cos\beta \sin\theta_W & M_Z \cos\beta \cos\theta_W & 0 & -\mu \\ M_Z \sin\beta \sin\theta_W & -M_Z \sin\beta \cos\theta_W & -\mu & 0 \end{pmatrix}.$$

The mass eigen states χ_i^0, termed neutralinos are obtained by diagonalization as,

$$|\chi_l^0\rangle = Z_{ln}\psi_n^0, \;\; Z^* M^n Z^{-1} = M_n^D.$$

In general the entries of the matrix Z can be purely real or purely imaginary. For real Z, the eigen values of the neutralino matrix can sometimes be negative. These have to be then redefined by chiral rotations to make them positive.

In the limit $|\mu| \gg |M_{1,2}| >> M_W, M_Z$ the mass eigen states are given by,

$$\begin{aligned}
m_{\chi_1^0} &\simeq M_1 - \frac{M_Z^2}{\mu^2}(M_1 + \mu \sin 2\beta)\sin^2\theta_W \\
m_{\chi_2^0} &\simeq M_2 - \frac{M_Z^2}{\mu^2}(M_2 + \mu \sin 2\beta)\cos^2\theta_W \\
m_{\chi_3^0} &\simeq |\mu| + \frac{1}{2}\frac{M_Z^2}{\mu^2}\varepsilon_\mu (1 - \sin 2\beta)\left(\mu + M_2 \sin^2\theta_W + M_1 \cos^2\theta_W\right) \\
m_{\chi_4^0} &\simeq |\mu| + \frac{1}{2}\frac{M_Z^2}{\mu^2}\varepsilon_\mu (1 + \sin 2\beta)\left(\mu - M_2 \sin^2\theta_W - M_1 \cos^2\theta_W\right),
\end{aligned}$$

such that for large μ, the two lightest neutralinos are gaugino like, while the heavier neutralinos are higgsino like.

In the opposite limit $|M_1| \gg |\mu| \gg M_W, M_Z$, the lightest chargino and the two lighter neutralinos are higgsino like while the heavier ones are gaugino like.

3.5.2 Sfermion mixings

Fo the sleptons, the relevant contributions come from the F and D terms of $-\mu H_1.H_2 - f^e_{ij} L_i.H_1 \bar{E}_j$, the slepton mass term $\tilde{l_{iL}}^* (\mathscr{M}^2_{\tilde{l}})_{ij} \tilde{l}_{jL} + \tilde{e_{iR}}^* (\mathscr{M}^2_{\tilde{e}})_{ij} \tilde{e}_{jR}$ and the term $h_1.\tilde{l}_{iL}(f^e A^e)_{ij} \tilde{e^*}_{jR}$ in the soft Lagrangian. These terms contribute to the sfermion mass matrix after the Higgs field have acquired a VEV. The analogous terms can be written for squark mixings as well.

The general six component sfermion vector can be written as,

$$\tilde{f} = \begin{pmatrix} \tilde{f}_L \\ \tilde{f}_R \end{pmatrix} \tag{3.5.7}$$

where $\tilde{f}_L$ and $\tilde{f}_R$ are three component vectors in the generation space with $\tilde{f}_{iL}$ and $\tilde{f}_{iR}$ as the superpartner of the quark or the lepton field.

The squared mass matrices can be written as,

$$M^2_{\tilde{f}} = \begin{pmatrix} M^2_{\tilde{f}_{LL}} & M^2_{\tilde{f}_{LR}} \\ M^2_{\tilde{f}_{RL}} & M^2_{\tilde{f}_{RR}} \end{pmatrix}. \tag{3.5.8}$$

It is instructive to consider to limits to this above general mixing structure. In the limit of no L–R mixing the mass matrices are diagonal, and the unitary matrix diagonalizing the mass matrix can be brought into a chiral block diagonal form.

The second limit to consider is the limit of no flavor mixing, but general L-R mixing. In this situation the 6×6 mixing matrix couples the left and right states of a given flavor.

We consider the special case of third generation where it is reasonable to take them as decoupled from the first two generations. However due to large Yukawa couplings there can be a significant L–R mixing.

The third generation mass matrices can be summarized by the following,

$$\begin{pmatrix} \tilde{m}^2_{tL} & m_t(A_t - \mu \cot\beta) \\ m_t(A_t - \mu \cot\beta) & \tilde{m}^2_{tR} \end{pmatrix}, \tag{3.5.9}$$

$$\begin{pmatrix} \tilde{m}^2_{bL} & m_b(A_b - \mu \tan\beta) \\ m_b(A_b - \mu \tan\beta) & \tilde{m}^2_{bR} \end{pmatrix}, \tag{3.5.10}$$

$$\begin{pmatrix} \tilde{m}^2_{\tau L} & m_\tau(A_\tau - \mu \tan\beta) \\ m_\tau(A_\tau - \mu \tan\beta) & \tilde{m}^2_{\tau R} \end{pmatrix} \tag{3.5.11}$$

with,

$$\begin{aligned}
\tilde{m}^2_{tL} &= \tilde{m}^2_Q + m^2_t + \tfrac{1}{6}(4M^2_W - M^2_Z)\cos 2\beta, \\
\tilde{m}^2_{tR} &= \tilde{m}^2_U + m^2_t - \tfrac{2}{3}(M^2_W - M^2_Z)\cos 2\beta, \\
\tilde{m}^2_{bL} &= \tilde{m}^2_Q + m^2_b - \tfrac{1}{6}(2M^2_W + M^2_Z)\cos 2\beta, \\
\tilde{m}^2_{bR} &= \tilde{m}^2_D + m^2_b + \tfrac{1}{3}(M^2_W - M^2_Z)\cos 2\beta, \\
\tilde{m}^2_{\tau L} &= \tilde{m}^2_L + m^2_\tau - \tfrac{1}{2}(2M^2_W - M^2_Z)\cos 2\beta, \\
\tilde{m}^2_{\tau R} &= \tilde{m}^2_E + m^2_\tau + (M^2_W - M^2_Z)\cos 2\beta.
\end{aligned}$$

The eigen values for the stop sector are given by,

$$(m_{\tilde{t}_1,\tilde{t}_2})^2 = \frac{1}{2}\{m^2_{\tilde{t}_L} + m_{\tilde{t}^2_R} \pm \sqrt{[(m^2_{\tilde{t}_L} - m^2_{\tilde{t}_R})^2 + 4X_t{}^2 m^2_t]}\} \tag{3.5.12}$$

where $X_t = A_t - \mu \cot\beta$.

3.6 The Higgs sector of MSSM

3.6.1 The potential and stability

Recall that MSSM was constructed to have two Higgs doublets, whose scalar parts are given by,

$$h_1^D = \begin{pmatrix} h_1^0 \\ h_1^- \end{pmatrix}, \; h_2^D = \begin{pmatrix} h_2^+ \\ h_2^0 \end{pmatrix} \tag{3.6.1}$$

The hypercharge assignments for h_1^D and h_2^D are Y=-1,1 respectively thus fixing the isospin assignments of the doublet. Note that the first doublet (h_1^D) provides masses to the down type quarks while the second doublet (h_2^D) gives masses to the up type quarks.

After the Higgs mechanism, the neutral parts of the scalar components is assigned a VEV,

$$< h_2 >= \frac{1}{\sqrt{2}} \begin{pmatrix} 0 \\ \mathrm{v}_2 \end{pmatrix}; < h_1 >= \frac{1}{\sqrt{2}} \begin{pmatrix} \mathrm{v}_1 \\ 0 \end{pmatrix}.$$

The doublets are complex and hence in components adds up to 8 real fields. 3 of these fields are expected to be used up to generate masses for the W and the Z bosons leaving behind 5 physical Higgs bosons. Out of these, 3 are neutral from the neutral components of the doublet while we have 1 charged Higgs field and its complex conjugate counterpart.

The contribution to the Higgs potential comes from 3 sources, the F term, originating from the superpotential with $\mathrm{F}_\mathrm{k}^* = -\frac{\partial \mathscr{W}_{\mathrm{MSSM}}}{\partial \Phi_\mathrm{k}^\dagger}$, the D term from the kinetic term in the MSSM Lagrangian, and finally from the soft term. The F, D and the soft term contributions are summarized as,

$$\begin{aligned} V_F &= |\mu|^2(|h_1|^2+|h_2|^2), \\ V_D &= \frac{g_1^2+g_2^2}{8}(|h_1|^2-|h_2|^2)^2+\frac{g_2^2}{2}|h_1^\dagger h_2|^2, \\ V_{soft} &= m_1^2|h_1|^2+m_2^2|h_2|^2-(m_3^2 h_1.h_2+h.c), \end{aligned}$$

where the coefficients m_1^2, m_2^2 and $m_3^2 = -B\mu$ have dimensions of mass squared.

Observe that the D term contribution is reminiscent of the quartic coupling λ in the SM Lagrangian. However unlike the SM where λ was a free parameter the quartic term is totally determined by the value of the gauge couplings which are fixed experimentally. It can also be observed that all the quartic dependence only appear in the D term and nowhere else.

Thus the tree level scalar potential can be written down as,

$$V_{tree} = m_1^2|h_1|^2+m_2^2|h_2|^2-m_3^2(h_1.h_2+h.c.)+\frac{g_2^2+g_1^2}{8}(|h_1|^2-|h_2|^2)^2+\frac{g_2^2}{2}|h_1^\dagger h_2|^2+|\mu|^2(|h_1|^2+|h_2|^2). \tag{3.6.2}$$

To minimize Eq. 3.6.2, we differentiate with respect to h_1^0,h_2^0 and set the VEV of the neutral components of the two Higgs doublets to v_1 and v_2. The resulting equations of constraint are given by,

$$-2B\mu = 2m_3^2 = (m_1^2-m_2^2)\tan 2\beta + M_Z^2 \sin 2\beta, \tag{3.6.3}$$

$$|\mu|^2 = \frac{1}{\cos 2\beta}(m_2^2 sin^2\beta - m_1^2 cos^2\beta) - \frac{1}{2}M_Z^2, \tag{3.6.4}$$

with,

$$\langle h_1 \rangle \equiv \mathrm{v}_1 = \mathrm{v}\cos\beta, \quad \langle \mathrm{h}_2 \rangle \equiv \mathrm{v}_2 = \mathrm{v}\sin\beta,$$

$$v^2 = v_1^2 + v_2^2, \quad \tan\beta \equiv \frac{v_2}{v_1},$$

such that,

$$M_W^2 = \frac{g_2^2}{2} v^2, \quad M_Z^2 = \frac{g_1^2 + g_2^2}{2} v^2.$$

Finally the tree level potential in the component form for the neutral Higgs can be written as,

$$\begin{aligned} V &= (m_1^2 + |\mu|^2)|h_1^0|^2 + (m_2^2 + |\mu|^2)|h_2^0|^2 - \\ &\quad B\mu(h_1^0 h_2^0 + \frac{g_2^2 + g_1^2}{8} \bar{h}_1^0 \bar{h}_2^0)(|h_1^0|^2 - |h_2^0|^2)^2. \end{aligned} \tag{3.6.5}$$

Setting $h_1^0 = \pm h_2^0$, the tree level potential can be written as,

$$V \sim [(m_1^2 + m_2^2 + 2|\mu|^2 \pm B\mu)]|h_1^0|^2. \tag{3.6.6}$$

The positivity of the potential thus requires,

$$m_1^2 + m_2^2 + 2|\mu|^2 > 2B|\mu|. \tag{3.6.7}$$

On the other hand quadratic part of the tree level potential can be put in matrix form to obtain,

$$\begin{pmatrix} m_1^2 + |\mu|^2 & -B\mu \\ -B\mu & m_2^2 + |\mu|^2 \end{pmatrix}. \tag{3.6.8}$$

in the h_1, h_2 space and is to be worked out before the Higgs mechanism. Clearly the trace is positive, and hence for non zero VEV's to develop (i.e , for EWSB), one eigen value must be negative, implying that the determinant must be negative. Therefore,

$$(m_1^2 + |\mu|^2)(m_2^2 + |\mu|^2) < (B\mu)^2. \tag{3.6.9}$$

In the limit where $m_1^2 = m_2^2 = \mu$, the simultaneous requirement of the positivity of the potential (Eq. 3.6.7) and the negative determinant (Eq. 3.6.9) are in contradiction to each other. These equations are therefore mutually incompatible at the GUT scale and at tree level leads to the conclusion that spontaneous breaking of SU(2) gauge symmetry, a necessity in SM does not happen in MSSM. This is potentially bad news; however note that this is only a tree level result and is valid only at the GUT scale with universal soft parameters. As we run down in RGE these relations indeed change as the parameters get renormalized, and the large hierarchy between the EW scale and the GUT scale is sufficient to drive one of the eigen values (Eq . 3.6.9) to be negative.

3.6.2 Masses for the Higgs sector

The charged Higgses acquire masses from the usual suspects, namely, the F term in the superpotential, the D term from the kinetic term, and finally from the soft terms. In the basis of $(h_1^+ \; h_2^+)$ and its complex conjugate the charged Higgs mass matrix can be expressed as (noting that $\frac{v_2}{v_1} = \tan\beta$),

$$M_{H^\pm}^2 = \left\{ B\mu \frac{v_2}{v_1} + \frac{g_2^2 v_2^2}{4} \right\} \begin{pmatrix} tan\beta & 1 \\ 1 & cot\beta \end{pmatrix}. \tag{3.6.10}$$

Clearly there is a zero eigen vector which corresponds to the charged Goldstone bosons which will finally be eaten up to give masses to the $W^{\pm}$ bosons. The eigen values and eigen vectors of the matrix are thus,

$$H^{\pm} = \sin\beta \mathrm{h}_1^{\pm} + \cos\beta \mathrm{h}_2^{\pm},\ \mathrm{m}^2_{\mathrm{H}^{\pm}} = (\mathrm{B}\mu\frac{\mathrm{v}_2}{\mathrm{v}_1} + \frac{\mathrm{g}_2^2\mathrm{v}_2^2}{4})(2\mathrm{cosec}\,2\beta):\ \mathrm{G}^{\pm} = -\cos\beta \mathrm{h}_1^{\pm} + \sin\beta \mathrm{h}_2^{\pm},\ \mathrm{m}^2_{\mathrm{G}^{\pm}} = 0. \tag{3.6.11}$$

We next turn our attention to the neutral Higgs bosons. The imaginary parts of the neutral Higgs bosons $\mathscr{I}m\, h_1^0, h_2^0$ mix, thus generating the massless Goldstone boson (which finally gets eaten up to provide mass to the Z boson after EWSB), and the CP odd (being a linear combination of the imaginary parts of the neutral Higgs fields) Higgs A. The mass matrix can be expressed as,

$$M^2_{\mathscr{I}m\, h^0} = (\mathrm{B}\mu\frac{\mathrm{v}_2}{\mathrm{v}_1}) \begin{pmatrix} \tan\beta & 1 \\ 1 & \cot\beta \end{pmatrix}. \tag{3.6.12}$$

with eigen values $\mathrm{m}^2_{\mathrm{G}^0} = 0$, and $\mathrm{m}^2_{\mathrm{A}} = |\mathrm{B}\mu|\mathrm{cosec}\,2\beta$. The corresponding eigen vectors are given by,

$$\frac{G^0}{\sqrt{2}} = \sin\beta\, \mathscr{I}m\, h_1^0 + \cos\beta\, \mathscr{I}m\, h_2^0,\ \ \frac{A}{\sqrt{2}} = -\cos\beta\, \mathscr{I}m\, h_1^0 + \sin\beta\, \mathscr{I}m\, h_2^0.$$

Finally the $\mathscr{R}e\, h_1^0, h_2^0$ mix to give the neutral CP even Higgs bosons. In the above basis the mass matrix can be expressed as,

$$M^2_{\mathscr{R}e\, h^0} = \begin{pmatrix} m_A^2\sin^2\beta + M_Z^2\cos^2\beta & -(m_A^2+M_Z^2)\sin\beta\cos\beta \\ -(m_A^2+M_Z^2)\sin\beta\cos\beta & m_A^2\cos^2\beta + M_Z^2\sin^2\beta \end{pmatrix}. \tag{3.6.13}$$

The eigen values are given by,

$$m^2_{H,h} = \frac{1}{2}\left[m_A^2 + M_Z^2 \pm \sqrt{(m_A^2+M_Z^2)^2 - 4m_A^2M_Z^2\cos^2 2\beta}\right], \tag{3.6.14}$$

with H being the heavier Higgs boson by convention. As usual the eigen vectors are given by,

$$\frac{H}{\sqrt{2}} = (\mathscr{R}\mathrm{e}\,\mathrm{h}_1^0 - \frac{\mathrm{v}_1}{\sqrt{2}})\cos\alpha + (\mathscr{R}\mathrm{e}\,\mathrm{h}_2^0 - \frac{\mathrm{v}_2}{\sqrt{2}})\sin\alpha,\ \ \frac{\mathrm{h}}{\sqrt{2}} = -(\mathscr{R}\mathrm{e}\,\mathrm{h}_1^0 - \frac{\mathrm{v}_1}{\sqrt{2}})\sin\alpha + (\mathscr{R}\mathrm{e}\,\mathrm{h}_2^0 - \frac{\mathrm{v}_2}{\sqrt{2}})\cos\alpha.$$

The mixing angle α in the neutral Higgs sector can be read off from the mass matrix and is given by,

$$sin2\alpha = -\frac{m_H^2 + m_h^2}{m_H^2 - m_h^2}\sin 2\beta. \tag{3.6.15}$$

Note $0 \leq \beta \leq \frac{\pi}{2}$ thus restricting α to the interval $-\frac{-\pi}{2} \leq \alpha \leq 0$.

The following tree level relations that emerge out of the above discussion,

$$\begin{aligned}
m^2_{H^{\pm}} &= m_A^2 + M_W^2 > max(M_W^2, m_A^2), && (3.6.16)\\
m_h^2 + m_H^2 &= m_A^2 + M_Z^2. && (3.6.17)\\
m_h &< min(M_A, M_Z)|\cos 2\beta| < min(M_A, M_Z), && (3.6.18)\\
m_H &> max(M_A, M_Z) \\
\cos^2(\beta-\alpha) &= \frac{m_h^2(M_Z^2 - m_h^2)}{m_A^2(m_H^2 - m_h^2)}. && (3.6.19)
\end{aligned}$$

As passing comments we note that as $m_A \to 0$, $m_h \to 0$. In the other extreme limit, $m_A \to \infty$ (the decoupling limit) [9], the mass of the lightest Higgs boson $m_h \to M_Z \cos 2\beta$. In this limit thus we have $m_A \sim m_H \sim m_{H^\pm}$ while $\cos(\beta - \alpha) = 0$. The lightest Higgs boson is thus bounded by the mass of the Z boson while the rest are uniformly heavy. Thus in this limit the MSSM decouples from the SM and it can be shown that the couplings of the lightest higgs to SM fermions are not different between SM and MSSM.

The radiative correction to the lightest Higgs mass can be significantly large. The one loop correction can be summarized by,

$$\delta m_h^2 = \frac{3G_F}{\sqrt{2}\pi^2} m_t^4 \left[log \frac{M_{SUSY}^2}{m_t^2} + \left\{ \frac{X_t^2}{M_{SUSY}^2} \left(1 - \frac{X_t^2}{12 M_{SUSY}^2} \right) \right\} \right], \tag{3.6.20}$$

where $X_t = A_t - \mu cot\beta$, the mixing in the stop mass matrix and $M_{SUSY} = \sqrt{\tilde{t}_1 \tilde{t}_2}$. The expression is maximized when $X_t = \sqrt{6} M_{SUSY}$, and the Higgs mass can be as large as ~ 135 GeV. Note that the Higgs like particle discovered at LHC has a mass of 125 GeV and thus can be easily incorporated in this scenario. We thus observe that the stop sector has important consequences for the Higgs sector.

3.7 Interactions in MSSM

The MSSM Lagrangian , Eq. 3.2.1-3.2.3, and the soft SUSY breaking terms, once deconstructed reveal the interactions between various sparticles and the SM counterparts. Some of the main interactions are summarized below,

- Strong interactions: These are interactions between the gluino, gluon along with the squarks and quarks, following the laws of QCD characterized by the strong coupling constant g_3.

  Some of the principal strong interaction vertices are listed below,

  1. $\mathscr{L}_{g\tilde{g}\tilde{g}} = -\frac{1}{2} g_3 \tilde{g}_a \tilde{g}_c f^{abc} \gamma_\mu g_b$,
  2. $\mathscr{L}_{g\tilde{q}_{L,R}\tilde{q}_{L,R}} = -\, g_3 g_a \tilde{q}_{L,R} T^a \partial_\mu \bar{\tilde{q}}_{L,R} + \text{h.c}$,
  3. $\mathscr{L}_{\tilde{g}\tilde{q}_{L,R}q} = -\sqrt{2} g_3 \bar{q} T^a P_L \tilde{g}_a \tilde{q} + \sqrt{2} g_3 \bar{q} T^a P_R \tilde{g}_a \tilde{q} + \text{h.c.}$

     In terms of the quark/squark flavor rotation matrices U,W the above can be expressed as,

     $$\mathscr{L}_{\tilde{g}\tilde{q}_{L,R}q} = \sqrt{2} g_3 \sum_{q=u,d} \bar{q} [U_{ji}^{q_R} W_{j+3\ s}^{\tilde{q}} P_L - U_{ji}^{q_R} W_{j\ s} P_R] T^a \tilde{g}_a \tilde{q}_s + \text{h.c},$$

     where the subscript on the squark denotes the mass eigen state and the squark fields are written in the vector color space. In Fig. 3.1 the production of the gluino pair and the squark gluino is presented illustrating the relevant Feynman rules.

- Weak interactions between sfermions and gauginos: Written in terms of the two component spinors $\xi_{Q_i}^{1(2)}$ and $\xi_{L_i}^{1(2)}$ for left handed quarks(Q_i) and leptons(L_i) respectively, the following

[9] Although $m_A \to \infty$ is the definition of the decoupling limit, for all practical purposes $m_A > 250$ GeV can be taken as the decoupling limit.

terms emerge,

$$\begin{aligned}\mathscr{L}_{f\tilde{f}'^{*}\chi^{\pm}} &= -g_2(\tilde{\lambda}^{-}\xi^{1}_{Q_i}\tilde{d}^{*}_{iL}+\tilde{\lambda}^{+}\xi^{2}_{Q_i}\tilde{u}^{*}_{iL}+\tilde{\lambda}^{-}\xi^{1}_{L_i}\tilde{e}^{*}_{iL}+\tilde{\lambda}^{+}\xi^{2}_{L_i}\tilde{\nu}^{*}_{iL})\\ &+\frac{g_2(m^{*}_{u})_{ij}}{\sqrt{2}M_W\sin\beta}(\tilde{h}^{1}_{2}\xi^{2}_{Q_i}\tilde{u}^{*}_{jR}+\tilde{h}^{1}_{2}\xi_{\bar{U}_j}\tilde{d}_{iL})\\ &+\frac{g_2(m^{*}_{d})_{ij}}{\sqrt{2}M_W\cos\beta}(\tilde{h}^{2}_{2}\xi^{2}_{Q_i}\tilde{d}^{*}_{jR}+\tilde{h}^{2}_{2}\xi_{\bar{D}_j}\tilde{u}_{iL})\\ &+\frac{g_2(m^{*}_{e})_{ij}}{\sqrt{2}M_W\cos\beta}(\tilde{h}^{2}_{2}\xi^{2}_{L_i}\tilde{e}^{*}_{jR}+\tilde{h}^{2}_{2}\xi_{\bar{E}_j}\tilde{\nu}_{iL})+h.c.\end{aligned} \tag{3.7.1}$$

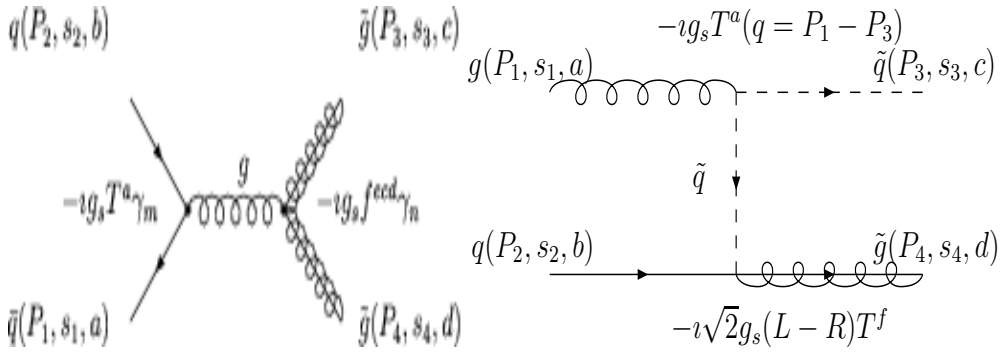

Figure 3.1: *The gluino production (left panel) and the squark gluino production (right) panel with Feynman rules*

In the above expression the first line describe the the gaugino-fermion-sfermion interactions, while the last three lines describe the higgsino-fermion-sfermion interaction. It can be observed that the higgsino interactions are proportional to the masses, so that in the limit of massless fermions the higgsinos decouple from the matter sector. In terms of the physical basis of chargino mass eigen states, and a sum over all fermions f_{u_i}, f_{d_i} (quarks/squarks and leptons/sleptons with generation indices i and j), the above equation can be written as,

$$\begin{aligned}\mathscr{L}_{f\tilde{f}'^{*}\chi^{\pm}} &= -g_2[\mathscr{U}_{k1}\bar{f}_{u_i}P_R\chi^{\pm}_{k}\tilde{f}_{d_iL}+\mathscr{V}_{k1}\bar{f}_{d_i}P_R(\chi^{\pm}_{k})^{C}\tilde{f}_{u_iL}]\\ &+\frac{g_2(m_{f_d})_{ij}}{\sqrt{2}M_W\cos\beta}\mathscr{U}_{k2}[\bar{f}_{u_i}P_R\chi^{\pm}_{k}\bar{f}_{d_jR}+\tilde{f}^{*}_{u_iL}\overline{(\chi^{\pm}_{k})^{C}}P_Rf_{d_j}]\\ &+\frac{g_2(m_{f_u})_{ij}}{\sqrt{2}M_W\sin\beta}\mathscr{V}_{k2}[\bar{f}_{d_i}P_R(\chi^{\pm}_{k})^{C}\bar{f}_{u_jR}+\tilde{f}^{*}_{u_iL}\overline{(\chi^{\pm}_{k})}P_Rf_{u_j}]+h.c.\end{aligned} \tag{3.7.2}$$

- The sfermion-fermion-neutralino interactions : In the physical basis of neutralino eigen states, the relevant Lagrangian can be written as,

$$\begin{aligned}\mathscr{L}_{f\tilde{f}'^{*}\chi^{0}} &= \sum_{f=u,d,e,\nu}\overline{\chi^{0}_{l}}(G^{f_L}_{l}\tilde{f}^{*}_{iL}P_L+G^{f_L}_{l}\tilde{f}^{*}_{iL}P_R)f_i\\ &-\frac{g_2}{\sqrt{2}M_W\sin\beta}[(m^{*}_{u})_{ij}Z^{*}_{l4}\tilde{u}^{\dagger}_{jR}\overline{\chi}^{0}_{l}P_Lu_i+(m_u)_{ij}Z_{l4}\tilde{u}^{\dagger}_{iL}\overline{\chi}^{0}_{l}P_Ru_j]\\ &-\frac{g_2}{\sqrt{2}M_W\cos\beta}[(m^{*}_{d})_{ij}Z^{*}_{l3}\tilde{d}^{\dagger}_{jR}\overline{\chi}^{0}_{l}P_Ld_i+(m_d)_{ij}Z_{l3}\tilde{d}^{\dagger}_{iL}\overline{\chi}^{0}_{l}P_Rd_j]\\ &-\frac{g_2}{\sqrt{2}M_W\cos\beta}[(m^{*}_{e})_{ij}Z^{*}_{l3}\tilde{e}^{\dagger}_{jR}\overline{\chi}^{0}_{l}P_Le_i+(m_e)_{ij}Z_{l3}\tilde{e}^{\dagger}_{iL}\overline{\chi}^{0}_{l}P_Re_j]+h.c,\end{aligned} \tag{3.7.3}$$

where the coupling strengths $G_l^{f_L}, G_l^{f_R}$ is given by,

$$\begin{aligned} G_l^{f_L} &= -\sqrt{2}g_2[T_{3L}^f Z_{l2}^* + \tan\theta_W (Q_f - T_{3L}^f) Z_{l1}^*] \\ G_l^{f_R} &= \sqrt{2}g_2 \tan\theta_W Q_f Z_{l1}. \end{aligned} \tag{3.7.4}$$

Chapter 4

Direct and indirect constraints on the SUSY parameter space

SUSY parameter spaces are constrained from a variety of sources. The constraints on the SUSY parameter spaces can be divided in three categories. The first category are theoretical constraints, and some of them are listed as follows

1. As described in Chapter 3, the SUSY vacuum must be stable even after quantum corrections.
2. Secondly the RGE must be convergent at all scales while evolution from a high scale theory.
3. The SUSY vacuum must not break $U(1)_{em}$ or $SU(3)_c$(color charge breaking).

The second type of constraints are purely experimental, and can be divided in two parts.

1. Firstly constraints from direct searches of supersymmetric particles in colliders. This is by far the most robust direct experimental constraint on SUSY. The experimental searches at LEP and Tevatron, along with LHC have looked for SUSY signatures, and in the absence of any signal have put limits on the sparticles which have been translated into constraints on the SUSY parameter space in the framework of certain specific models.
2. Secondly, where SUSY particles appear in loops in low energy processes, in particular flavor processes. The sources of flavor violation in SUSY occur mainly from the soft SUSY breaking terms. This leads to the fact that squarks and slepton mass matrices are not diagonal. The size of these off diagonal contributions can be significantly large thus leading to sizeable enhancement or suppression of branching ratios of rare decays. The size of these off diagonal terms are strongly restricted by experimental data. An usual simplifying assumption is that these matrices are diagonal, although there is no compelling theoretical reasoning behind this. In general the indirect constraints point to the region of parameter space that one should probe in order to look for SUSY signatures.

The third type, which should be taken as a pointer rather than an explicit constraint is from dark matter. The SUSY parameter space satisfying the dark matter relic density constraint is limited, and depends crucially on the interplay of various parameters. The assertion that the observed dark matter in the universe only consists of one candidate is also a simplified one. It should therefore be taken as wishful requirement rather than a hard constraint.

A detailed description of these constraints is beyond the scope of this thesis. A brief outline of various constraints is described below. A detailed analysis of the constraints on the CMSSM parameter space is provided in Chapter 5.

4.1 Constraints from flavor physics

The origin of the flavor problem in MSSM is in the occurrence large FCNC amplitudes due to sizable mixings in the sfermion mass matrices.

An example of the flavor problem in MSSM is the $K^0 - \bar{K}^0$ mixing, with the mass eigen states given by K_L and K_S. In standard model the $K^0 - \bar{K}^0$ occurs via the diagram in the Fig. 4.1.

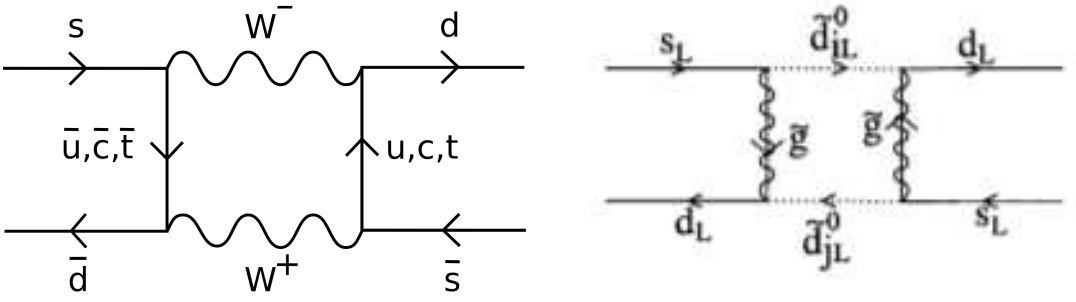

Figure 4.1: *Diagrams for $K^0 - \bar{K}^0$ mixing for SM contribution (Left panel) and MSSM contribution (right panel).*

The experimental value for the difference in the masses of $m_{K_L} - m_{K_S} = 3.5 \times 10^{-6}$ eV [31], which is close to the SM expectation. In MSSM the extra contribution originates from the right panel diagram in Fig. 4.1. The contribution is summarized by the amplitude,

$$\frac{g_3^4}{\tilde{m}^6} |\sum U_{1i}^{\tilde{d}_L} U_{i2}^{\tilde{d}_L^\dagger} \Delta\, m_{\tilde{d}_i}^2|^2, \tag{4.1.1}$$

where g_3 is the strong coupling constant, U the unitary matrices that diagonalize the sfermion mass matrices while $\tilde{m} = \max(m_{\tilde{q}}, m_{\tilde{g}})$. If the difference in the squark masses are $\mathcal{O}(100)$ GeV, this contribution yields a value 3 orders of magnitude larger than the SM contribution.

To suppress the unwanted large FCNC contribution in MSSM, the first choice is to make $\tilde{m}^6$ large, i.e to make the first two generations of squarks fairly heavy. The second solution is to align the sfermion mixing matrix to make it proportional to the fermion mixing matrix, such that the fermion and sfermion mass matrix can be diagonalized in the same basis leading to $U_{1i} U_{i2}^\dagger = 0$. The last option is to make all the sfermions degenerate such that $\Delta m_{\tilde{d}_i}^2 = 0$.

Thus any measurement of a low-energy process which (*a*) gets contributions from these sparticles, and (*b*) is measured with sufficient accuracy to access these usually small effects, will impose a constraint on the MSSM. Based on these two criteria, we can now discern *three* distinct types of low-energy constraints.

1. The first type is where the low-energy effect is observed and the measurement is consistent with the SM prediction. In this case, any contributions from the MSSM will have to be small enough to fit into the small leeway allowed by the error bars. Such constraints have a tendency to get tighter and tighter as more data are collected in an experiment and the error bars shrink.The relevant example of this is the radiative B decay $B \to X_s\gamma$, where the measured value of the branching ratio $\mathrm{BR}(B \to X_s\gamma)$ is $(3.55 \pm 0.24 \pm 0.09) \times 10^{-4}$ [26] against an SM prediction of $(3.15 \pm 0.23) \times 10^{-4}$ [27, 172–175].

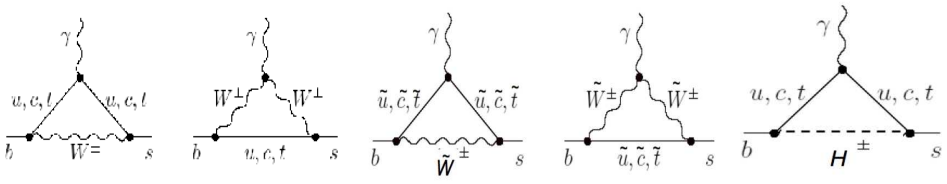

Figure 4.2: *The SM and MSSM diagrams for the transition $B \to X_s\gamma$. The first two diagrams represent the SM contribution while the last three includes the MSSM contribution.*

The SM contribution, which comes from the first two diagrams in Fig. 4.2 is proportional to,

$$Br(B \to X_s\gamma) \propto \left|\frac{V_{ts}^* V_{tb}}{V_{cb}}\right|^2 . \tag{4.1.2}$$

The MSSM contribution comes from the last three diagrams shown in Fig. 4.2. The corrections are enhanced by $\tan\beta$ and are dominated by the diagrams with the chargino and charged Higgs contributions. The $\tan\beta$-enhanced chargino contributions to $BR_{MSSM}(B \to X_s\gamma)$ can be expressed as [176, 177],

$$BR_{MSSM}(B \to X_s\gamma)\Big|_{\chi^\pm} \propto \mu A_t \tan\beta\, f(m_{\tilde{t}_1}^2, \tilde{m}_{\tilde{t}_2}^2, m_{\chi^\pm}) \frac{m_b}{v(1+\delta m_b)}, \tag{4.1.3}$$

Here all dominant higher-order contributions are included through δm_b, and f is the integral appearing in the one-loop diagram. The charged-Higgs contributions to $\mathrm{BR_{MSSM}(B \to X_s\gamma)}$, which is enhanced for large $\tan\beta$ is [176, 177] ,

$$BR_{MSSM}(B \to X_s\gamma)\Big|_{H^\pm} \propto \frac{m_b(y_t\cos\beta - \delta y_t \sin\beta)}{v\cos\beta(1+\delta m_b)} g(m_{H^\pm}, m_t), \tag{4.1.4}$$

where g is the loop integral appearing in the diagram.

2. The second type is where the SM effect is not consistent with the existing experimental upper bound, which leaves room for reasonably significant contributions from the MSSM. Even more than the previous case, these constraints get tighter as the experimental bounds are tightened, but often, even with improvements in experimental techniques, this bound remains significantly above the SM prediction, so that there is always some room for a MSSM contribution. A good example of this was the decay $B_s \to \mu^+\mu^-$, where the experimental upper bound on $\mathrm{BR}(B_s \to \mu^+\mu^-)$ has been recently improved to 4.5×10^{-9} [28] against a SM prediction of $(3.2 \pm 0.2) \times 10^{-9}$ [29].[1] Thus, the MSSM contribution must satisfy,

$$\mathrm{BR_{MSSM}}(B_s \to \mu^+\mu^-) \leq 1.8 \times 10^{-9} .$$

In MSSM the largest contribution with an enhancement of $\tan^6\beta$ comes from the diagram on the extreme right panel of Fig. 4.2.

[1] At the time of writing this thesis the evidence for the decay $B_s \to \mu^+\mu^-$ has been reported by LHCb [178] and CMS [179]. The branching ratio obtained by CMS is $(3.0^{+1.0}_{-0.9}) \times 10^{-9}$ while the LHCb reported is $(2.9^{+1.1}_{-1.0}) \times 10^{-9}$.

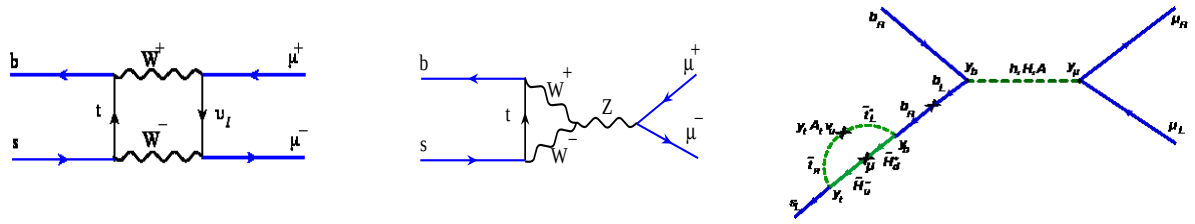

Figure 4.3: *The SM and MSSM diagrams for the transition $B_s \to \mu^+\mu^-$. The first two diagrams represent the SM contribution, while the last diagram includes the MSSM contribution.*

The MSSM contribution to the branching ratio for $B_s \to \mu^+\mu^-$ has been calculated in [180, 181],

$$BR_{MSSM}(B_s \to \mu^+\mu^-) = \frac{2\tau_B M_B^5}{64\pi} f_{B_s}^2 \sqrt{1-\frac{4m_l^2}{M_B^2}} \times \left[\left(1-\frac{4m_l^2}{M_B^2}\right) \left| \frac{(C_S - C_S')}{(m_b+m_s)} \right|^2 + \left| \frac{(C_P - C_P')}{(m_b+m_s)} + 2\frac{m_\mu}{M_{B_s}^2}(C_A - C_A') \right|^2 \right], \tag{4.1.5}$$

where f_{B_s} is the B_s decay constant, M_B is the B-meson mass, τ_B is the mean life time and m_l is the mass of the lepton. The quantities C_S, C_S', C_P, C_P' represent the SUSY loop contributions due to the diagrams involving stop, chargino, sneutrino, Higgs. The dominant contribution to C_S is given approximately by [180, 181],

$$C_S \simeq \frac{G_F \alpha}{\sqrt{2}\pi} V_{tb} V_{ts}^* \left(\frac{\tan^3\beta}{4\sin^2\theta_W}\right) \left(\frac{m_b m_\mu m_t \mu}{M_W^2 M_A^2}\right) \frac{\sin 2\theta_{\tilde{t}}}{2} \left(\frac{m_{\tilde{t}_1}^2 \log\left(m_{\tilde{t}_1}^2/\mu^2\right)}{\mu^2 - m_{\tilde{t}_1}^2} - \frac{m_{\tilde{t}_2}^2 \log\left(m_{\tilde{t}_2}^2/\mu^2\right)}{\mu^2 - m_{\tilde{t}_2}^2} \right), \tag{4.1.6}$$

where $\theta_{\tilde{t}}$ is the mixing angle in the stop mass matrix. Evidently the amplitude grows as $\tan^6\beta$. Thus if the experimental value is consistent with the SM expected result, the large $\tan\beta$ scenario in MSSM will be constrained. It can be observed, however, that the $\tan\beta$ dependence can be suppressed if the stop masses become equal.

3. There exists a third – and rare – type of low-energy process where the experimental result is not consistent with the SM prediction at some level between 1–2σ. The experience of the past few decades has generally been that a more accurate measurement of the process, or a more sophisticated computation of the SM prediction generally brings the two into perfect consistency, but there are results which have till date defied this comfortable precedent. An example of this is the anomalous magnetic moment of the muon($a_\mu = (g-2)_\mu/2$).

   A review on the theoretical value of $(g-2)_\mu$ can be found in [182], which is in agreement with the latest values from [183]. The measurement of the anomalous magnetic moment of the muon indicates a small deviation from the SM of the order of 3 σ [184]:

$$\begin{aligned} a_\mu^{exp} &= 11\,659\,2080(63) \times 10^{-11}, \\ a_\mu^{SM} &= 11\,659\,1790(64) \times 10^{-11}, \\ \Delta a_\mu &= a_\mu^{exp} - a_\mu^{theor} = (290 \pm 90) \times 10^{-11}, \end{aligned}$$

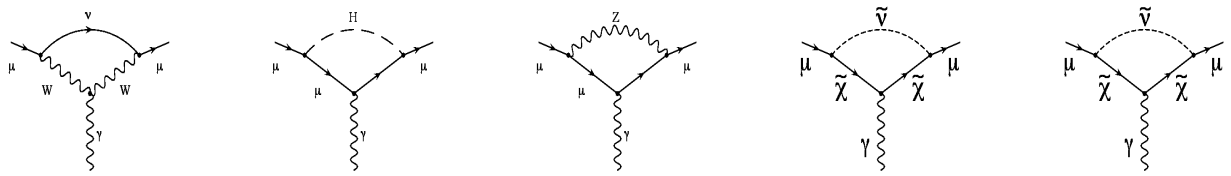

Figure 4.4: *The diagrams contributing to a_μ in the SM and in the MSSM.*

where the SM contributions can be summarized as,

$$a_\mu^{QED} = 11\,658\,4718.1\ (0.2) \times 10^{-11},$$
$$a_\mu^{weak} = 153.2\ (1.8) \times 10^{-11},$$
$$a_\mu^{hadron} = 6918.7\ (65) \times 10^{-11}.$$

The accuracy of the experiment is close to the QED contribution predicted by theoretical calculation. The SM diagrams contributing to $(g-2)_\mu/2$ are presented in in Fig. 4.4.This apparent discrepancy can be reconciled by the SUSY contributions arising from the last two diagrams of Fig. 4.4.

The MSSM contribution to a_μ from Fig. 4.4 has been calculated in [185]. The dominant contribution originates from chargino induced diagrams and is enhanced by $\tan\beta$ [186]. The MSSM contribution favors the sign of μ to be positive [187]. It must be noted that in order to reconcile the experimental and theoretical values, the MSSM spectrum is expected to be light.

4.2 Dark matter relic density constraints

It is now a well established fact that only about 4% of the total energy budget of the universe is composed of baryonic matter. The relic density (Ω) values for the matter content of the universe can be summarized as [32],

$$\Omega_{total} = 1.02 \pm 0.02,$$
$$\Omega_{vacuum} = 0.73 \pm 0.04,$$
$$\Omega_{matter} = 0.23 \pm 0.04,$$
$$\Omega_{baryon} = 0.044 \pm 0.004.$$

The evidence of dark matter is manifested in rotation curves of galaxies, as well as gravitational lensing studies in Bullet clusters, and large scale structure formation. Since the dark matter candidate acts only via gravity and weak interaction it is incapable of producing compact objects. In terms of the thermal evolution of the early universe a situation can arise when some species of particles decouple from the thermal bath of the others. We asserted that MSSM with exact R-parity with the lightest neutralino as the LSP was a potential dark matter candidate [188].

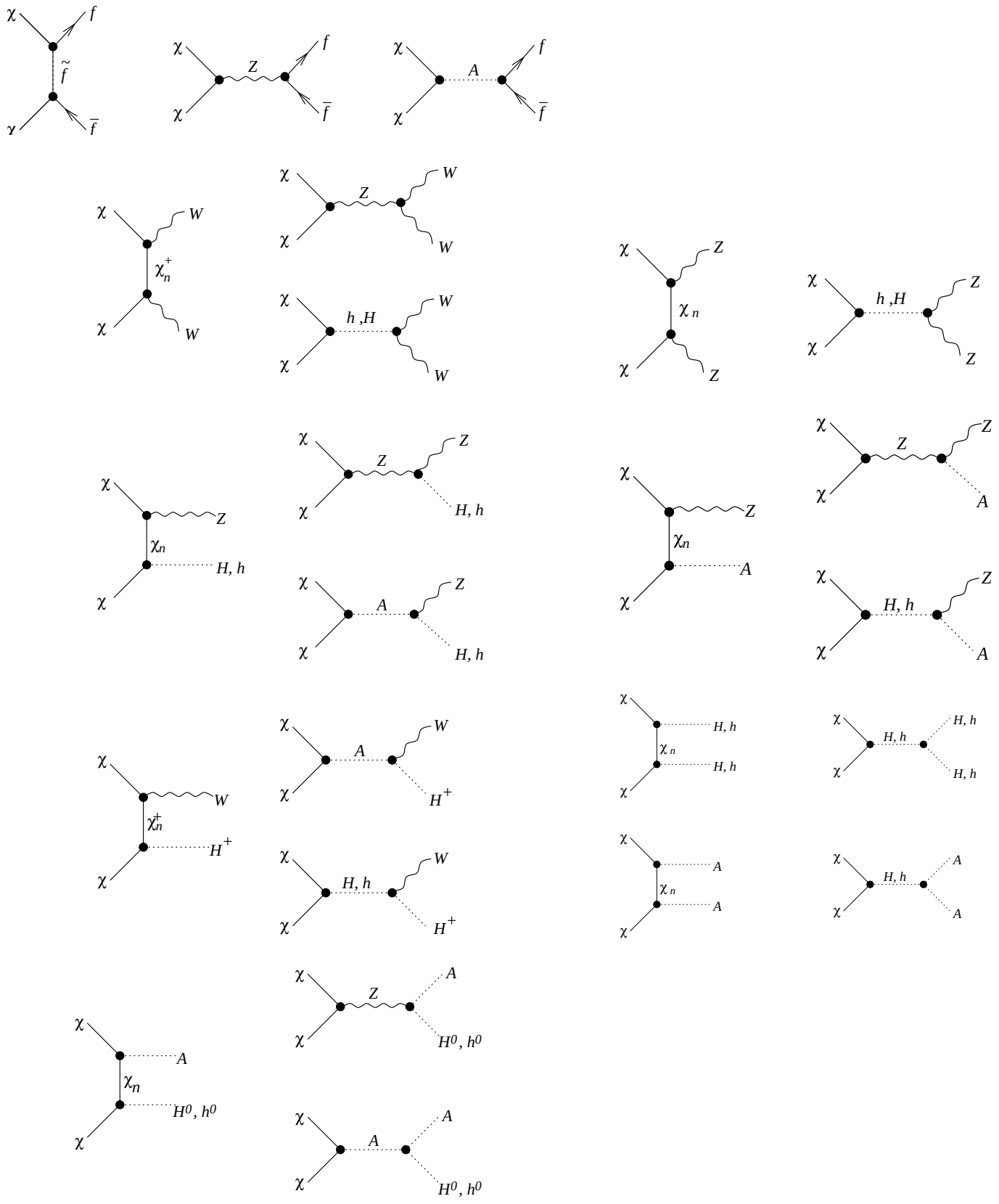

Figure 4.5: Some of the most important Feynman diagrams for neutralino annihilation.

The dark matter relic density is calculated using the Boltzmann equation [189],

$$\frac{dn_\chi}{dt} + 3Hn_\chi = -\langle\sigma v\rangle(n_\chi^2 - n_{\chi,eq}^2), \tag{4.2.1}$$

where $H = \dot{R}/R$ is the Hubble parameter, $n_{\chi,eq}$ the equilibrium concentration of the LSP, $\langle\sigma v\rangle$ the thermally averaged annihilation cross section over the velocity v. In early universe, when the temperature was much higher than the mass of the LSP (m_χ), the creation and annihilation of the LSP occurred at equal rates. With the Hubble expansion of the universe, and the depletion of χ particles by annihilation, the number density of χ particles became sufficiently small such that they ceased to interact with each other, and hence surviving till the present day. The relic abundance is expressed in terms of n_χ as [189],

$$\Omega_\chi h^2 = \frac{m_\chi n_\chi}{\rho_c} \approx \frac{2\cdot 10^{-27}\ \mathrm{cm}^3\ \mathrm{sec}^{-1}}{\langle\sigma v\rangle}, \tag{4.2.2}$$

The above cross section is in the ball park of the electroweak cross section. This leads to the speculation that the dark matter candidate is a weakly interacting massive particle (WIMP). The above calculation however does not take into account the effect of co-annihilations. In these cases, particles other than the WIMP itself can play an important role in the freeze-out process. Such a situation can arise when a particle is quasi-degenerate with the WIMP and hence can co-annihilate with it.

The WIMP candidate must be electrically neutral and stable for it to satisfy all the known facts about the known dark matter relic abundance in the universe. SUSY as advocated earlier offers the lightest neutralino as the candidate for dark matter. The lightest neutralino χ_1^0 is a combination of (Eq. 3.5.7),

$$|\tilde{\chi}_1^0\rangle = N_1|\tilde{B}_0\rangle + N_2|\tilde{W}_0^3\rangle + N_3|\tilde{H}_1\rangle + N_4|\tilde{H}_2\rangle.$$

Over much or most of the supersymmetric parameter space, the relic abundance of neutralinos is predicted to be in excess of the observed dark matter density and hence we are forced to constrain ourselves to specific regions of parameter space. The following scenarios emerge in this context.

- Bulk region : The lightest neutralino has a higgsino or wino fraction: In this case the couplings can be fairly large and, as a result, annihilate very efficiently.
- Funnel Region : Resonance with the CP-odd Higgs A. If the mass of the lightest neutralino is near this resonance, then with small couplings it can annihilate efficiently.
- $\tilde{\tau}$ co-annihilation region, where the light $\tilde{\tau}$ is nearly degenerate with the LSP.

In Fig. 4.5 some of the most important diagrams for neutralino annihilation are presented.

4.3 Constraints from collider experiments

The quest for SUSY signatures in colliders began at the UA1, UA2 experiments and followed by the LEP experiment. Te LEP collider being an e^+e^- collider, the production proceeds through electroweak interactions. Hence the primary sparticles of interest were charginos and sleptons.

In addition the signatures of lightest stop and the sbottom was also studied. In absence of any signal the following limits were imposed on the sparticle masses from LEP II [31],

$$m_{\tilde{e}} \geq 105 \text{ GeV}, \; m_{\tilde{t}} \geq 90 \text{ GeV}$$
$$m_{\chi_1^{\pm}} \geq 100 \text{ GeV}, \; m_{\tilde{\mu}} \geq 100 \text{ GeV}, \; m_{\tilde{b}} \geq 80 \text{ GeV}, \; m_{\tilde{\tau}} \geq 80 \text{ GeV}.$$

An extensive detail of SUSY signatures at LHC and recent results on various channels is discussed in Chapter 7. Here we only summarize the results from the Tevatron run II on squark and gluino which stands at $m_{\tilde{q}} \geq 300$ GeV, $m_{\tilde{g}} \geq 195$ GeV [190]. At the LHC, the current limits on the squarks of the first two generations and the gluino in the framework of CMSSM stand at $m_{\tilde{g}} \gtrsim 1.5$ TeV for almost degenerate gluino and squarks and $m_{\tilde{q}} > 1.4$ TeV for very high squark masses, [191, 192].

An analysis of the CMSSM parameter space is discussed in Chapter 5 taking flavor, dark matter and direct collider search constraints into account with the 7 TeV LHC data.

We conclude this chapter with few comments. Apart from the direct searches in colliders, most of the constraints on the MSSM parameter space are subject to various assumptions on the parameter spaces and the model in question, which when relaxed can lead to significantly different interpretations. Some of the constraints like $(g-2)_\mu$ are subject to uncertainties in theoretical calculations and hence the interpretations should be treated with caution. Flavor constraints like $B \to \tau\nu$ are also important in this regard and constraints on MSSM parameter space have been studied in the literature [193].

Chapter 5

Constraining the CMSSM parameter space with LHC data

As discussed in detail in Chapter 4 the SUSY parameter space is constrained by theoretical and low energy constraints from flavor physics, collider search bounds and from the dark matter relic density. In this work we constrain the CMSSM parameter space at the end of the 7 TeV run at the LHC as well as results from recent flavor physics data [25]. It has to be noted of course that as more data was collected and analyzed some of these constraints are updated. As noted earlier the evidence of the decay $B_s \to \mu^+\mu^-$ has been observed by the CMS and the LHCb collaborations [178, 179]. Moreover, the Higgs boson which was not observed during the time of this work has been discovered. These facts have been taken into account in a wide range of works post this study [33, 194–219].

5.1 Constraints on the model

Till some time ago, the mSUGRA/CMSSM was often dubbed as the 'standard model' of physics beyond the Standard Model (SM), but perhaps because of the string of negative results obtained so far, there has lately arisen a tendency to disparage the CMSSM as a model which makes too many arbitrary assumptions and hence is — not-surprisingly — on the verge of getting ruled out by the LHC data [220, 221]. Such views, are however, less than fair to the CMSSM, for, in many ways, the CMSSM may be regarded as the most simple and economical model of supersymmetry, and the one which would most obviously suggest itself in the absence of contradictory experimental evidence. In fact, if one thinks about it, we should rather regard the multifarious alternatives to the CMSSM which appear in the literature as the ones where extra assumptions are introduced. Moreover, the mere fact that the CMSSM parameter space is getting reduced by experimental searches should not be regarded as a setback for the model, for, after all, Nature corresponds to but a single point in the parameter space. The example of the top quark (and maybe the Higgs boson) serves to clearly illustrate this kind of shrinkage of the parameter space to the actual value. Note however, the Higgs boson was still undiscovered during the time of this work.

The purpose of this work was not, however, to pontificate in defence of the CMSSM, but rather to investigate the status of different experimental constraints on this model. Among others, we take up the recent measurement of the process $B_s \to \mu^+\mu^-$ by the LHCb Collaboration [28] and study its impact on the CMSSM parameter space in conjunction with other low energy constraints. Since the precision of this particular measurement has increased considerably, one would expect it

to rule out a wide swath of the parameter space. We quantify this expectation and find, that while the last statement is certainly true at large values of $\tan\beta$, the constraint weakens and disappears as $\tan\beta$ is lowered. We shall demonstrate that even in the large $\tan\beta$ region, the CMSSM is still a possible explanation of not just the hierarchy problem, but also of the dark matter problem.

To analyze the impact of the constraints on the CMSSM parameter space we impose the following criteria:

1. The ranges of the CMSSM parameters are:

   $$0 \leq m_0 \leq 4 \text{ TeV} \qquad 0 \leq m_{1/2} \leq 1 \text{ TeV} \qquad -1 \text{ TeV} \leq A_0 \leq +1 \text{ TeV} \qquad 1 \leq \tan\beta \leq 60$$

   with $\mu > 0$, since $\mu < 0$ is strongly disfavoured not only by $(g-2)_\mu/2$ but also by $B \to X_s\gamma$.

   As noted in section 3.4.1, note that except for rather loose naturalness considerations, there are no *a priori* theoretical guidelines for the choice at the GUT scale of values of m_0, $m_{1/2}$ and A_0, or the sign of μ. For $\tan\beta$, however, we note that the Yukawa couplings of the top and bottom quarks remain comfortably perturbative so long as $1.2 \lesssim \tan\beta \lesssim 65$ [222].

   Very small values of m_0 and $m_{1/2}$ ($\sim$ few GeV) are not viable in the CMSSM, for then the RGE would drive the electroweak symmetry-breaking to happen rather close to the GUT scale, and this would imply a much lower GUT scale than appears to be indicated by the measured running of the gauge coupling constants. For larger values of m_0 and $m_{1/2}$, there arise two kinds of *a posteriori* constraints which act collectively on the parameters m_0, $m_{1/2}$ and A_0 when the CMSSM spectrum is run down from the GUT scale to the electroweak scale. One is the requirement that the scalar potential in the theory remain bounded from below – this is referred to as the *vacuum stability* constraint [223]. The other is the requirement that the lightest SUSY particle (LSP) be a neutral particle – which is demanded if it is to be the major component of dark matter. This is found to rule out a region of the parameter space where the RGE evolution makes the lighter stau $\widetilde{\tau}_1$ the LSP.

   Another consideration, which is not a constraint but may be regarded as some sort of wishful thinking, is a requirement that the parameters m_0, $m_{1/2}$ and A_0 not be much more than a few TeV. This is because higher values of these parameters – especially the first two – tend to drive the masses of all the SUSY particles outside the kinematic range of the LHC (and even its foreseeable successors), while the lightest Higgs boson mass gets pushed close to a value around 120 GeV. [1] In this, so-called *decoupling limit* the CMSSM Higgs boson would be indistinguishable, for all practical purposes, from its SM counterpart. Such a scenario, though by no means impossible, would be a great disappointment for seekers of new physics, as it would leave the existence of SUSY as a wide open question without a hope of solution in the near future. Of course, requiring the m_0, $m_{1/2}$ and A_0 to be in this convenient range is essentially dogma, but it is what renders studies of the present kind worth carrying out.

2. The entire set of constraints from the CERN LEP-2 collider data is imposed. The most restrictive among these are the requirements that

   - the mass of the lighter chargino must satisfy $m_(\widetilde{\chi}_1^\pm) \geq 94.0$ GeV [66], and
   - the mass of the lightest Higgs boson $m_h \geq 93.0$ GeV for $\tan\beta \gtrsim 6$, and $m_h \geq 114.0$ GeV [66] for $\tan\beta \lesssim 6$, with a range of intermediate values in the neighbourhood of $\tan\beta \simeq 6$.

[1] At the time of this work as emphasized, the Higgs boson was not discovered.

Constraints arising from other considerations (such as, for example, the mass of the lighter stop and the lighter stau) are generally subsumed in the disallowed parameter space due to these two major constraints, but we impose them nevertheless. Like the previous case, these constraints have been in place for some time now, ever since the final data analyses from the LEP Electroweak Working Group became available.

3. The area of parameter space disallowed by direct searches at the LHC is taken over from the ATLAS and CMS Collaborations [220, 221]. These are obtained by combining the negative results of searches in many channels, but the most important of these is the search in the jets + MET channel.

4. Constraints on the CMSSM from the rare decay $B \to X_s\gamma$ [26] are imposed. The specific requirement is that the CMSSM contribution to the decay width should satisfy

$$-0.55 \times 10^{-4} \leq \mathrm{BR}_{\mathrm{CMSSM}}(B \to X_s\gamma) \leq 1.35 \times 10^{-4} \,,$$

at 95% C.L..

5. Constraints on the CMSSM from the recently-measured upper bound on the rare decay $B_s \to \mu^+\mu^-$ [28] are imposed. This measurement has recently been substantially improved by the LHCb experiment and their updated result has been used in this work.The specific requirement is that the CMSSM contribution to the decay width should satisfy

$$\mathrm{BR}_{\mathrm{CMSSM}}(B_s \to \mu^+\mu^-) \leq 1.8 \times 10^{-9} \,,$$

at 95% C.L..

6. Finally, we have mapped the part of the CMSSM parameter space which is compatible with the requirement that the observed dark matter component of the Universe be purely a relic density of LSPs $\widetilde{\chi}_1^0$. The specific requirement is that

$$0.1053 \leq \Omega_d h^2 \leq 0.1193$$

at 95% C.L. [32] and the stable value of $\Omega_d h^2$ is calculated by solving the relevant Boltzmann equation for the time evolution of the relic density. We do not treat this as a constraint, but merely show the allowed region alongside that permitted by all other considerations.

Apart from the requirement that $\mu > 0$, we have not imposed any specific constraint from the data on $(g-2)_\mu/2$, and we have chosen not to consider low-energy constraints arising from $B^+ \to \tau^+\nu_\tau$. This last has not been taken into account because we feel that the situation vis-a-vis the SM has not yet stabilised and it may be premature to use this to constrain new physics. But all this is not to say that other constraints on the CMSSM parameter space from low-energy data do not exist — in fact, every measurement which is compatible with the SM prediction and has a CMSSM contribution will impose a constraint. However, we find that, except for $(g-2)_\mu/2$ and $B^+ \to \tau^+\nu_\tau$, none of these are as restrictive on the CMSSM parameter space as the set of constraints listed above: the range of parameter space affected by these is always a subset of that ruled out by the combination of those from the above-listed set.

At this juncture, we note that several papers [224–228] have appeared in which the constraints on the CMSSM from the decays $B \to X_s\gamma$ and $B_s \to \mu^+\mu^-$ have been studied, both independently, and in conjunction with the LHC constraints from direct searches. Some of these have been used to predict the most likely values of the CMSSM parameters. We have chosen the more conservative

approach of mapping out the parts of the parameter space which are disallowed, and assuming equal *a priori* probability for the rest. Our presentation of the constraints is, therefore, very close to the way in which direct constraints from the experimental data are available.

5.2 Update on the CMSSM parameter space

Once we have fixed the sign of μ to be positive, as explained above, the CMSSM parameter space is a four-dimensional space, with the parameters being m_0, $m_{1/2}$, A_0 and $\tan\beta$, as described above. Since one can plot only two of them at a time, it is traditional to pick two of these parameters and keep the others either fixed, or floating. The most common plots are made in the $m_{1/2}$–m_0 plane, with A_0 and $\tan\beta$ fixed. This is because the masses of the superparticles depend most directly on these two parameters m_0 and $m_{1/2}$, with the other two contributing mostly through mixing that occurs between pure superparticle states when the electroweak symmetry is broken. For our first plot, therefore, we choose the $m_{1/2}$–m_0 plane, for three separate values of $A_0 = 0$ and ± 1 TeV, with $\tan\beta = 10$, the last choice being influenced by the latest plots available from the ATLAS and CMS Collaborations. We shall later have occasion to vary A_0 and $\tan\beta$, so this particular choice may be regarded merely as an opening gambit. We generate the CMSSM spectrum using SUSPECT [14] and calculate the low-energy observables (including the dark matter relic density) using SUPERISO [16]. Our results are shown in Fig. 5.1. It may be noted that these plots correspond to a top quark mass of 172.9 GeV [66].

The three panels in Fig. 5.1 correspond, from left to right, to choices of $A_0 = +1$ TeV, 0 and -1 TeV respectively. In each panel, we have plotted $m_{1/2}$ in the range $0-1$ TeV, and m_0 in the range $0-4$ TeV, keeping $\tan\beta = 10$ as mentioned above. It is worth recalling, at this juncture, that the superparticle masses tend to grow with both m_0 and $m_{1/2}$. Thus increased energy of the machine will increase the discovery reach of these plots, and this is what is, in fact seen.

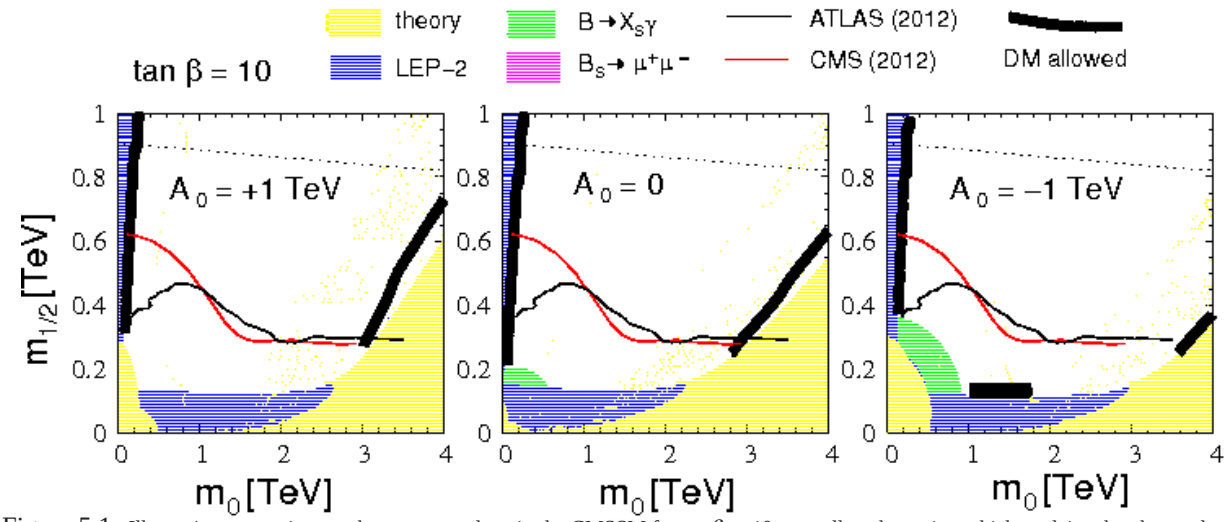

Figure 5.1: Illustrating constraints on the m_0–$m_{1/2}$ plane in the CMSSM for $\tan\beta = 10$, as well as the region which explains the observed relic density of dark matter. The details are marked on the different panels or in the key above. The dotted line is the contour for a gluino mass of 2 TeV. Note that $\mu > 0$ for all the plots. The ATLAS and CMS exclusion curves correspond to $A_0 = 0$ but are not very sensitive to A_0 or even $\tan\beta$.

In each plot, the region shaded yellow is ruled out by 'theory constraints'. Of these, the requirement of vacuum stability is the dominant constraint in the region close to the abscissa and the stau-LSP is the dominant contribution in the region close to the ordinate. For large values of

m_0 some of the points are disallowed simply because the renormalisation group equations (RGE) used to calculate the CMSSM spectrum at the electroweak scale have no real solutions. Shapes vary somewhat between the three panels, illustrating the influence of the parameter A_0 on the RGE running of the CMSSM parameters, but the basic features are common, with small values of m_0 and $m_{1/2}$ being ruled out in every case. The regions shaded blue in the three panels of Fig. 5.1 correspond to constraints arising from LEP-2 data. These are generally stronger than the theoretical constraints, except for extreme values of $m_{1/2}$. Most of the LEP-2 disallowed region arises from the chargino mass constraint. The small sliver of space ruled out by LEP-2 for very low values of m_0 at relatively large values of $m_{1/2}$ corresponds to negative searches for light stau states at LEP-2.

In Fig. 5.1, constraints arising from the non-discovery of CMSSM signals in 4.7 fb^{-1} of data at the ATLAS (CMS) detector are shown by the solid black (red) line, with the region *below* the curve getting ruled out. The ATLAS exclusion curve arises from a combination of all processes, whereas the CMS exclusion plot arises only from searches for the 0 lepton + jets + MET final states made using 'razor variables' [21]. These published analyses both choose $A_0 = 0$. Strictly speaking, therefore, this constraint should appear only in the central panel. However, the constraints from a jets + MET search are not very sensitive to the choice of A_0, and hence, we have made bold to use the same curve for all the three cases. Differences, if any, will be marginal, and should not make any qualitative impact on our discussions regarding these plots. The most important qualitative feature of these constraints is that, unless A_0 is strongly negative, they represent significant improvements over the LEP-2 bounds. As more data is collected and analysed, one may expect the LHC constraints to become stronger, and eventually cover most of the parameter space marked in the panels of Fig. 5.1. It may be noted that though we have not marked any projected reach of the LHC on these plots, a ballpark estimate may be formed from the contour of gluino mass 2 TeV, which is shown by the dotted line near the top of each panel. Therefore, we may conclude that eventually the LHC will be able to explore 80–90% of the parameter space shown in Fig. 5.1, barring the uppermost regions of each panel. Of this, roughly one half is already ruled out, but this is equivalent to saying that roughly one half is still allowed.

The constraints from low-energy data are marked on the graph in green for $B \to X_s\gamma$ and pink for $B_s \to \mu^+\mu^-$. What immediately strikes the eye is the fact that these are rather weak – at least, in the three panels of Fig. 5.1 — where the strongly $\tan\beta$ dependent $B_s \to \mu^+\mu^-$ constraint (see below) makes no appearance at all, while the $B \to X_s\gamma$ data adds on a little to the LEP-2 constraint for $A_0 = -1$ TeV. Even this is totally subsumed in the LHC constraints. One may be tempted to conclude that low-energy measurements are not competitive with the direct searches in constraining the CMSSM parameter space, but we must remember that the plots of Fig. 5.1 are for a fixed value of $\tan\beta$. The situation changes, quite dramatically, when we go to larger values of $\tan\beta$.

Before we go on to discuss high $\tan\beta$ results, however, let us note that the regions in Fig. 5.1 which are consistent with the dark matter (DM) relic density are marked by narrow black bands on all the three plots. This allowed band appears only as the so-called 'stau co-annihilation region', i.e. very close to the region disallowed by the stau-LSP constraint, and again for large values of m_0, in the so-called 'focus point region'. Nevertheless, it is heartening to see that there is always a region of the parameter space which can be the explanation of the dark matter phenomenon in the CMSSM. This model has not, therefore, lost its most attractive phenomenological feature, and the continuation of at least one small portion of the black bands into the regions inaccessible to the LHC tells us that even if the LHC completes its run without finding any signatures of the CMSSM, we will still be able to argue that the neutralino (albeit a heavier one than we now think) is the main

component of the dark matter.

To sum up this part of the discussion, then, *for low values of* $\tan\beta$, for which the value $\tan\beta = 10$ serves as a benchmark, the CMSSM is under no serious threat (unless, as we have seen, constraints from $(g-2)_\mu/2$ and $B^+ \to \tau^+\nu_\tau$ are imposed [193]) from a combination of low-energy data and direct searches. Even if the next round of direct searches throws up a negative result, constraining the parameter space still further, it should not be regarded as the death-knell of the CMSSM, for all that may be happening is that we are in the process of eliminating a barren region in the parameter space as we approach the actual region of interest.

We have seen thus that for $\tan\beta = 10$, the only effect of including low-energy constraints is to marginally extend the LEP-2 bound [66], and that too, only for $A_0 = -1$ TeV. This feature continues to hold all the way up to for $\tan\beta = 35$, which covers a substantial fraction of the theoretically allowed range, (viz. up to 60). Around $\tan\beta = 40$, however, the low-energy constraints begin to become significant, and for $\tan\beta = 50$, they outstrip the direct searches and constrain a significant extra part of the parameter space. This is illustrated in Fig. 5.2.

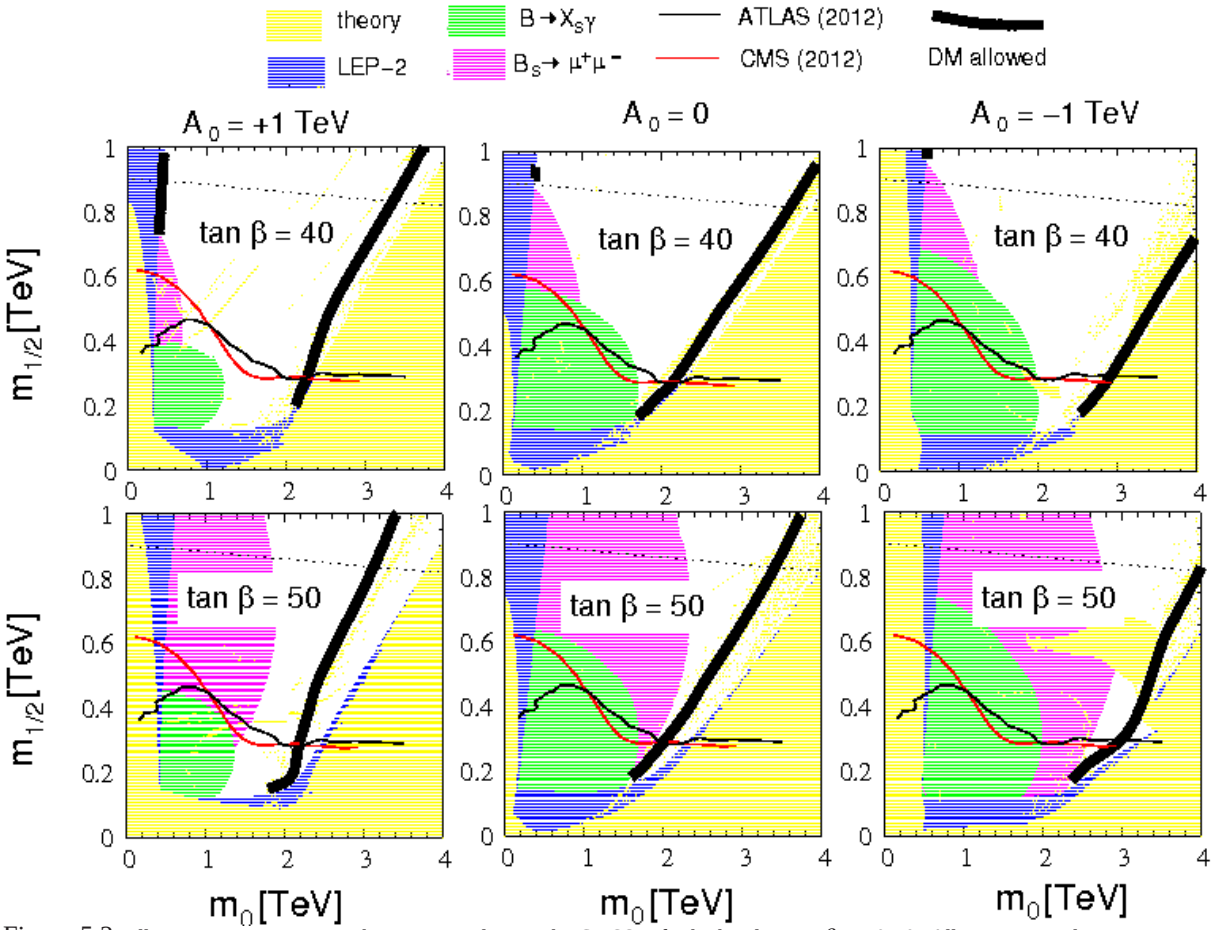

Figure 5.2: Illustrating constraints on the m_0–$m_{1/2}$ plane in the CMSSM for high values $\tan\beta = 40, 50$. All notations and conventions are the same as in Fig. 5.1. In these plots B-physics constraints become significant, especially for $A_0 \leq 0$. Note that the dark matter-compatible band always lies in the allowed region. Some of the (yellow) islands indicated as theory-disallowed for large values of m_0 represent numerical instabilities in the spectrum generator SUSPECT.

The conventions followed in Fig. 5.2 are exactly the same as those followed in Fig. 5.1, and are indicated, as in Fig. 5.2, by the little key on the top. The three panels in the first row correspond to $\tan\beta = 40$, while the three panels in the second row correspond to $\tan\beta = 50$. In each row, the

three panels correspond to choices of $A_0 = +1$ TeV, 0 and -1 TeV (from left to right). Regions shaded yellow (blue) correspond to constraints from theory (LEP-2), and solid lines marked in black (red) correspond to the exclusion plot of the ATLAS (CMS) Collaboration[2]. The black strips correspond to regions which are consistent with the neutralino interpretation of dark matter, and the dotted line near the top of each panel corresponds to the contour of $M(\tilde{g}) = 2$ TeV. For large values of m_0, some of the yellow islands indicating theory-disallowed regions, especially in the bottom right panel, represent numerical instabilities in the spectrum generator SUSPECT, and would be allowed if a different spectrum generator had been used.

Let us begin by discussing the situation for $\tan\beta = 40$, i.e. the upper row of panels in Fig. 5.2. The first thing that strikes the eye is that the theoretically constrained area is larger than in the case of $\tan\beta = 10$, not only in the region which is identified as due to a stau LSP, but over a very large region for higher values of m_0. The first part is easy to understand, since the off-diagonal terms in the mass matrix for staus $\widetilde{\tau}_1$, $\widetilde{\tau}_2$ are proportional to $\tan\beta$. Larger values of $\tan\beta$ can be interpreted as causing a larger splitting between the mass of the heavier and lighter stau, thus pushing the mass of the lighter stau $\widetilde{\tau}_1$ downwards, below the mass of the neutralino $\widetilde{\chi}_1^0$. This last is not much changed by increasing $\tan\beta$ — a statement which is generically true for all gauginos, including the lighter chargino $\widetilde{\chi}_1^\pm$, as a result of which the constrained region from the LEP-2 data remains much the same as before. For large values of m_0, the RGE evolution is simply not enough to drive one of the scalar mass parameters to negative values, and this manifests as non-convergence of the RGE when we demand such negative values. Alternatively we can simply say that for such parameter choices the electroweak symmetry remains unbroken. Even more than the theoretical constraints, however, for large values of $\tan\beta$ the constraints from low-energy measurements become much more significant. For example, the constraints from $B \to X_s\gamma$, which made such a modest appearance in the case of $\tan\beta = 10$, now begin to outstrip the LHC exclusion boundaries, especially for $A_0 \leq 0$. Even more dramatic than the growth of the $B \to X_s\gamma$ constrained region is the appearance of a significant (pink-shaded) region which is now disallowed by the $B_s \to \mu^+\mu^-$ constraint. For $\tan\beta = 40$, this is still a smallish appendage to the region already disallowed by other constraints, but if we now look at the lower set of three panels in Fig. 5.2, where $\tan\beta = 50$, it is clear that this new constraint affects large parts of the parameter space which are allowed by all other constraints. This growth in importance of the $B_s \to \mu^+\mu^-$ constraint can be readily understood in terms of an enhanced CMSSM contribution from the lighter stop $\widetilde{t}_1$. Indeed, for large $\tan\beta$, the CMSSM contribution is known [225] to scale as $\tan^6\beta/(M_A)^4$.

If we take a quick glance at the lower three panels in Fig. 5.2, one might be tempted to say that a value of $\tan\beta$ as large as 50 seems to be disfavoured because the low-energy constraints combine with the existing ones from theory and direct searches to choke off most of the parameter space accessible to the LHC. However, large $\tan\beta$ values are interesting as they led to distinctive sparticle decay signatures, especially those involving tau final states. It is apparent from the very same figure that the black bands, denoting consistency with the dark matter relic density, go right through the allowed 'focus point region' in every panel, showing that a high $\tan\beta$ solution of the dark matter problem is very much a viable one.

Fig. 5.3 illustrates the constraints in the upper three panels of Fig. 5.2 (i.e. $\tan\beta = 40$), when translated into the squark-gluino mass plane. Once again, we use the conventions and notations of Fig. 5.1. The most important feature of this graph is the large yellow area ruled out by theory considerations. This arises because the squarks (except in the third generation) are generally heav-

[2]We reproduce the exclusion plots already exhibited in Fig. 5.1, which, strictly speaking, are valid only for $\tan\beta = 10$ GeV. However, as we have taken the combined exclusion plot from ATLAS and the purely hadronic exclusion plot from CMS, the larger values of $\tan\beta$ in these plots will not make a significant difference.

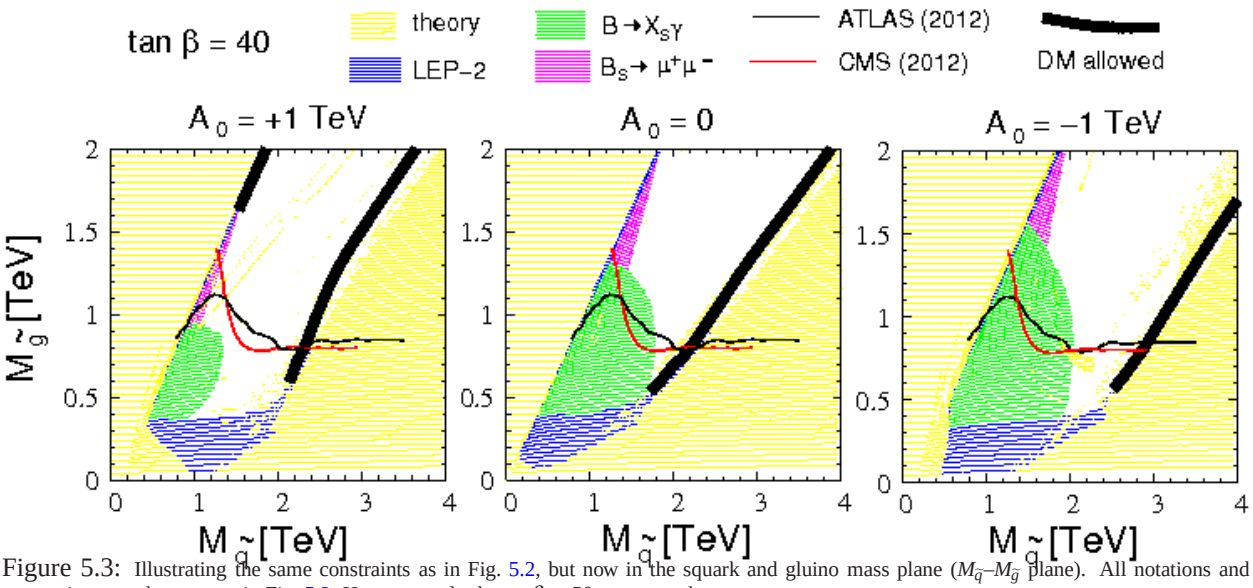

Figure 5.3: Illustrating the same constraints as in Fig. 5.2, but now in the squark and gluino mass plane ($M_{\tilde{q}}$–$M_{\tilde{g}}$ plane). All notations and conventions are the same as in Fig. 5.2. However, only the $\tan\beta = 50$ cases are shown.

ier than the gluino in scenarios where the lighter stau is heavier than the lightest neutralino. Light gluinos up to a couple of hundred GeV appear to be ruled out by the requirement of vacuum stability. Higher values of the squark mass cannot break the electroweak symmetry unless the gluino is also comparably heavy. There is, then, for all values of A_0, a funnel-shaped region which is allowed by theoretical considerations. Note that theoretically the gluino can be substantially lighter for $A_0 \leq 0$ than it is for the $A_0 = +1$ TeV case.

As in the previous two figures, we have shown bounds arising from the LEP-2 data by blue shading. As we have seen, this arises principally from the non-observation of chargino pairs, and this bound on the lighter chargino mass translates more-or-less to a constant bound on the gluino mass in the ballpark of $300 - 400$ GeV. However, the LHC bounds, shown by solid black (ATLAS) and red (CMS) lines as before, are much stronger, and they push both the squark and the gluino mass to values around a TeV or more. The effect of the low-energy constraints (the green and pink-shaded regions) is to marginally constrain some of the remaining parameter space. No extra constraint is obtained for $A_0 = +1$ TeV, but modest constraints appear for $A_0 \leq 0$, where the squark mass is pushed up to at least 1.5 TeV. However, if we consider $\tan\beta = 50$ (not shown) most of the allowed region is shut off, and for even higher values of $\tan\beta$, nothing is left of it.

The lesson which is learned from the above studies is that while direct searches for squarks and gluinos at the LHC produce the same kind of constraints for both low and high values of $\tan\beta$ and A_0, the situation is different for the indirect constraints from low-energy measurements, which are generally stronger as $\tan\beta$ increases and A_0 is driven more strongly negative. To illustrate the full extent of this constraint, in Fig. 5.4, we have plotted the disallowed regions in the plane of $\tan\beta$ and M_A, where M_A is the mass of the physical pseudoscalar A^0. In this figure, as in the earlier ones, we show three panels for $A_0 = +1, 0$ and -1 TeV respectively (from left to right) and set $\mu > 0$ throughout. The values of m_0 and $m_{1/2}$ are allowed to range from $0 - 4$ TeV and $0 - 2$ TeV as before. Of course, for a given value of A_0 and $\tan\beta$, these cannot vary independently. In fact, as the variation of M_A is more directly related to that of m_0, one can imagine $m_{1/2}$ as the floating variable. Thus, if a point in the $\tan\beta$–M_A plane is marked as disallowed, that means that it is

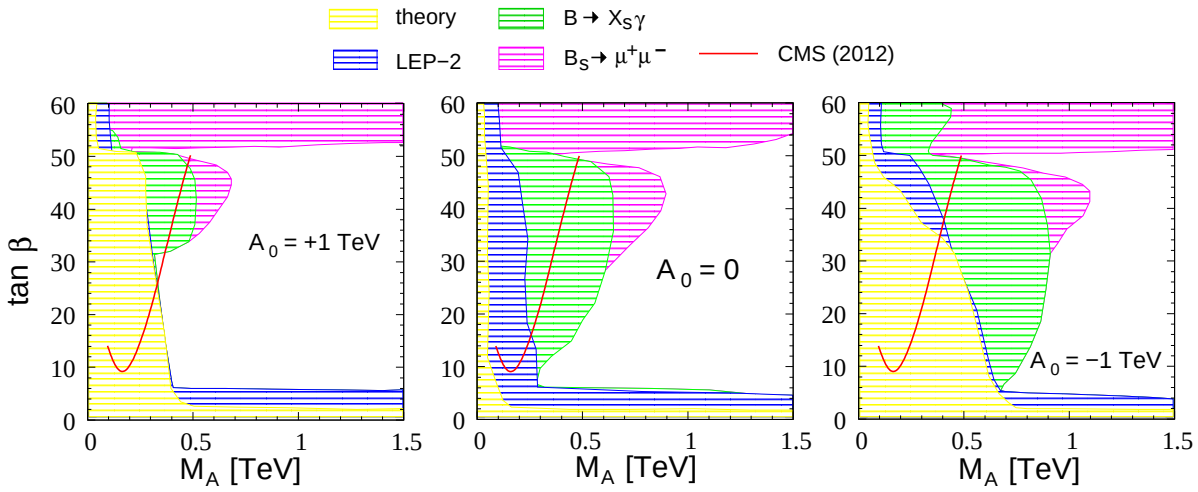

Figure 5.4: Illustrating the same constraints as before, but now in the $\tan\beta$–M_A plane. All notations and conventions are the same as in Figure 5.2, except that m_0 and $m_{1/2}$ are allowed to float in the same ranges as shown in Figure 5.2. In each panel, regions above and to the left of the red line are disallowed by direct LHC searches by the CMS Collaboration.

disallowed for *all* values of m_0 and $m_{1/2}$ in the box $m_0 = 0 - 4$ TeV and $m_{1/2} = 0 - 2$ TeV.

In Fig. 5.4, as before, the region shaded yellow indicates that it is ruled out by theoretical considerations, or is not accessible for the given ranges of m_0 and $m_{1/2}$. It is interesting that the disallowed region is very small when $A_0 = 0$, but is significantly larger when $A_0 \neq 0$. This may be traced, as earlier, to a larger mixing among the stau gauge eigenstates, leading to a stau LSP. The LEP-2 constraints do not change much from panel to panel, which is expected, since we have seen that their dependence on m_0 is somewhat weak. What is of greatest interest in Fig. 5.4, however, is the regions ruled out by the low-energy constraints. In each case, it is clear that for $\tan\beta \geq 50$, the constraint from $B_s \to \mu^+\mu^-$ is highly restrictive, effectively pushing the A^0 mass to the decoupling limit in the Higgs sector. However, this constraint becomes ineffective when the value of $\tan\beta$ is lowered, as we have already seen. In this case, however, the constraint from $B \to X_s\gamma$ comes into play unless A_0 is large, and this has the effect of driving the mass of M_A to larger values for intermediate values of $\tan\beta$ around 20 – 45. For low values of $\tan\beta$, the low-energy constraints disappear, as we have seen in Fig. 5.1, and we fall back to the LEP-2 constraints. Finally, there is a sort of wedge around $\tan\beta = 50$ where M_A as low as 500 GeV is allowed by all the constraints. Direct searches for the A^0 and the charged Higgs bosons $H^\pm$ at the LHC [229] lead to the exclusion of points above and to the left of the solid red curve — this is, however, less restrictive than the indirect constraints[3]. If we consider all the diagrams together, we have an absolute minimum of around 300 GeV for the A^0. This means that the charged Higgs boson, which is easier to detect, is of mass around 310 GeV. In fact, all the heavy scalar states in the CMSSM will now have masses of 300 GeV or above, which already makes them difficult to detect. In this sector, if not in the sector for SUSY particles, the CMSSM is fast approaching the limit where detection at the LHC will no longer be possible.

What about the light scalar state? Obviously, if the heavier scalars start approaching their decoupling limit, the lightest scalar h will also approach its decoupling limit, viz. around 119 – 120 GeV. The exact situation is illustrated in Fig. 5.5, where we plot m_h instead of M_A, keeping m_0

[3]It is also relevant to note that these constraints were derived in the so-called m_h-max scenario, which is more restrictive than the CMSSM.

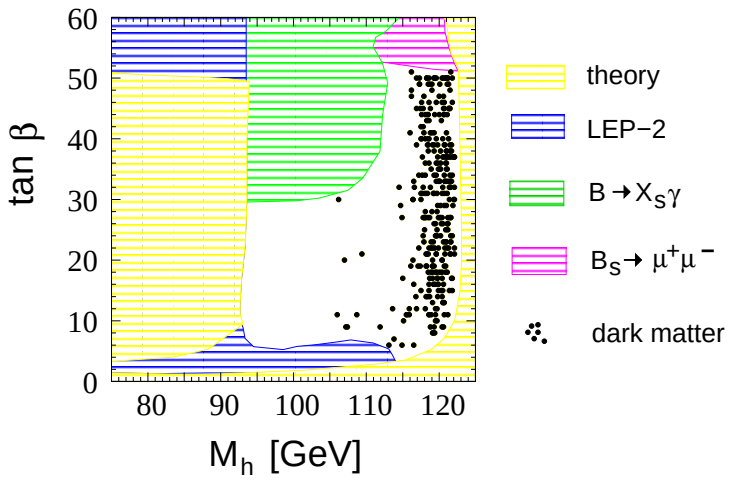

Figure 5.5: Illustrating the same constraints as before, but now in the $\tan\beta$–m_h plane. All notations and conventions are the same as before, except that A_0 floats as well as m_0 and $m_{1/2}$. Note that this region is unaffected by the limits from WW^* searches at the LHC.

and $m_{1/2}$ floating as before. For this plot, we allow A_0 also to float over all values from -1 TeV to $+1$ TeV. As before, a point is marked as disallowed if this is valid for all values of m_0, $m_{1/2}$ and A_0 in the given ranges (only two of these are independent, for reasons explained before).

In Fig. 5.5, as in the others, the region shaded yellow corresponds to the region which is theoretically inaccessible in the CMSSM. Of these, the yellow region on the left of the figure arises because of the requirement of vacuum stability and convergence of RGE's, whereas the yellow region on the right is simply not accessible for the parameter range chosen for our study. After all, we must recall that $m_h \leq M_Z$ at the tree-level, and hence much of the region shown in this plot corresponds to radiative corrections to m_h. We shall come back to this issue presently. Of the remaining theoretically-accessible region in Fig. 5.5, a small portion is ruled out by the LEP-2 searches, and comparatively larger regions by the low-energy constraints, especially for large values of $\tan\beta$. However, for $\tan\beta$ in the range $6-30$, these constraints allow for m_h anywhere in the region between 93 GeV to about 123 GeV. The lower range in $\tan\beta$ is essentially shut off by a combination of theoretical constraints and LEP-2 bounds.

Much of the above is already well known. The most interesting feature of Fig. 5.5, however, is the cluster of black dots, which indicates the regions compatible with the dark matter requirement. Obviously, these favour a Higgs boson mass in the neighbourhood of $120-122$ GeV, and strongly disfavour the lighter end of the permitted region. Interestingly, the favoured region is also close to the decoupling regime for the sparticles, and hence, we seem to be looking at a strong hint that the sparticles, if found, will turn out to have masses well in the ballpark of a few TeV.

To conclude this section, let us highlight the main results of our analysis of the CMSSM parameter space. The main features are

- The CMSSM is still viable in large parts of the parameter space. This is especially so for $\tan\beta$ in the range from 10 - 35 and $A_0 > 0$, though there are patches which are allowed even outside these ranges. There is no imperative reason, therefore, to write off the CMSSM and invoke one or other of its variants.

- The constraints from low-energy processes such as $B \to X_s\gamma$ and $B_s \to \mu^+\mu^-$ are marginal for large positive A_0 and only become really effective for large negative A_0 and large $\tan\beta$. Other low-energy processes yield even weaker constraints. The two exceptions are the muon

anomalous magnetic moment and the rare decay $B^+ \to \tau^+ \nu_\tau$, which together rule out practically all of the CMSSM parameter space, except a small region which would be accessible to the next set of LHC data analyses.

- Even when all the constraints are imposed, there are enough allowed regions where the CMSSM is compatible with the observed dark matter relic density. This will remain true even if the LHC completes its run without finding signatures of superparticles. However, if the LHC fails to find a light Higgs boson the CMSSM — as indeed the SM and most other supersymmetric models — will be ruled out.
- The heavy scalars of the CMSSM are likely to be too heavy to be seen at the LHC, at least in the early runs. The light scalar should have a mass less than 123 GeV if the SUSY particles are light enough to be seen at the LHC. A light scalar h with mass around 125 GeV is consistent with the CMSSM only in some corners of the parameter space, where the superparticles may well turn out to the too heavy to be seen at the the LHC. In this case, the CMSSM will still be a possibility, and will still constitute and explanation for dark matter, but we will have to await a new machine to furnish the experimental proof.

Chapter 6

The Large Hadron Collider: Kinematics and Jets

6.1 The Large Hadron Collider

The Large Hadron Collider (LHC) [230] is a proton proton collider located at CERN, Geneva. A circular tunnel contains the collider, with a circumference of 27 km, at a depth ranging from 50 m to 175 m. The tunnel was originally commissioned for LEP and then recommissioned for the LHC after the LEP-II run ended. Two adjacent parallel beam lines are contained in the tunnel, intersecting at four points, each containing a proton beam travelling in opposite directions. There are 1232 dipole magnets that keep the beams on their circular path while there are 392 quadrupole magnets that focus the beam. Over 1600 superconducting magnets were installed with about 96 tonnes of liquid helium required to keep the magnets at their operating temperature of 1.9K(-271.25°C). The design energy of the LHC is 14 TeV; although the early runs were conducted at 7 (April 2010–December 2011) and 8 TeV (April 2012–December 2012) center of mass energy. It is now in a phase of upgradation for the design energy run of 14 TeV. Although the LHC programme is mainly focused on p p collision, there is a slot for heavy ion collision with lead ions at 2.76 TeV per nucleon.

There are 7 detectors that have been constructed at LHC; two of them ATLAS [231] and CMS [232] are general purpose detectors while LHCb [233] and ALICE [234] are dedicated to heavy ion collisions. The smaller detectors meant for specialized purposes include TOTEM,MoEDAL and LHCf.

The primary physics goal of the LHC is to probe the nature of electroweak symmetry breaking, in particular the search for the SM Higgs boson. The other major goal is to look for signatures of physics beyond the standard model. A major LHC programme in this regard is the search for SUSY signatures at LHC. These general searches are conducted mainly from the data gathered from the general purpose detectors ATLAS and CMS. Additionally the detectors LHCb and ALICE are designed for flavor physics studies and the study of quark gluon plasma respectively.

6.2 Kinematics at LHC

The LHC is a proton proton collider and hence the primary interactions are governed by the laws of QCD. In particular we use the notions of perturbative QCD (pQCD) [18] to describe the hard interaction, while models of non perturbative QCD are used to describe the hadronization of the

partons into subsequent hadrons (baryons and mesons) which are the final observable particles. At high enough energies we are essentially probing the nucleon structure. The reference frame in this case is chosen such that the Z axis is taken to be the beam axis. The lab frame is described by the co-ordinates (E,P(p_x, p_y, p_z)), while the center of momentum frame moves along the Z direction with some boost described by (E′,$\tilde{P}'$(p'_x, p'_y, p'_z)). Therefore it is convenient to describe the picture in terms of boost invariant quantities. Note that although the phase space element $d\Gamma = \frac{d^3p}{E} = \frac{dp_x dp_y dp_z}{E}$ is Lorentz invariant, but is not boost invariant. Since the beam axis is along the Z direction, the quantities E and p_z (and hence $\frac{dp_z}{E}$) are not boost invariant while the transverse components p_x, p_y are indeed boost invariant. Therefore for convenience co-ordinates can be defined such that they are boost invariant. Hence one can choose the transverse momenta p_T, and the azimuthal angle ϕ as the boost "invariant" transverse components. The other component is chosen as rapidity (y) or the pseudorapidity (η) defined as,

$$\begin{aligned} y &= \frac{1}{2} ln\left\{\frac{E+p_z}{E-p_z}\right\}, \\ \eta &= \frac{1}{2} ln\left\{\frac{|\vec{p}|+p_z}{|\vec{p}|-p_z}\right\}. \end{aligned} \tag{6.2.1}$$

Note that the pseudorapidity can also be written as $\eta = -\ln(\tan\theta/2)$, where θ is the angle between a particle with momentum $\vec{p}$ and the beam axis. The rapidity as a function of pseudorapidity is given by,

$$y = \ln \frac{\sqrt{m^2 + p_T^2 \cosh^2\eta} + p_T \sinh\eta}{\sqrt{m^2 + p_T^2}}. \tag{6.2.2}$$

Note that for a massless particle $y = \eta$. For a boost β along the Z axis the rapidity transforms as an additive quantity given by $y' = y + y_b$ where $y_b = \ln\{\gamma(1+\beta)\}$, with $\gamma = 1/\sqrt{1-\beta^2}$ being the Lorentz factor. Thus the difference of rapidity Δy is a boost invariant quantity. The Lorentz invariant phase space element can also be written as,

$$d\Gamma = \frac{d^3\tilde{p}}{E} = \frac{1}{2} dp_T^2 d\phi dy.$$

For two partons with four momenta q_1 and q_2, with momentum fraction x_1, x_2 respectively from the two protons the four vectors can be written as (aligning the beam axis to be the Z axis),

$$\begin{aligned} q_1 &= \frac{1}{2}\sqrt{s}(x_1, 0, 0, x_1), \\ q_2 &= \frac{1}{2}\sqrt{s}(x_2, 0, 0, -x_2), \end{aligned} \tag{6.2.3}$$

where $E = \sqrt{s}$ is the center of mass energy. The rapidity of the system $q_1 + q_2$ is thus,

$$y = \frac{1}{2}\ln\left\{\frac{E+p_z}{E-p_z}\right\} = \frac{1}{2}\ln\frac{x_1}{x_2}. \tag{6.2.4}$$

Hence $x_1 = x_2\, e^{2y}$. If the partonic center of mass is denoted as $\hat{s} = M^2 = x_1 x_2 s$, then $x_1 = (M/\sqrt{s})e^y$, $x_2 = (M/\sqrt{s})e^{-y}$. Therefore different values of M and y probe different values of x_1, x_2.

In terms of the angle θ defined earlier, the rapidity can be expressed as,

$$\mathrm{y} = \frac{1}{2}\ln\frac{(1+\beta\cos\theta)}{(1-\beta\cos\theta)}.$$

Simple algebra shows that $\beta\cos\theta = \tanh\mathrm{y}$, and hence,

$$\begin{aligned} \mathrm{p_z} &= |\vec{p}|cos\theta = E\ \tanh y \\ \mathrm{E_T^2} &= m_T^2 = p_T^2 + m^2 = E^2 - p_z^2 = E^2[1-(\tanh y)^2] = E^2/(\cosh y)^2, \end{aligned} \tag{6.2.5}$$

where $p_T^2 = p_x^2 + p_y^2$. Hence $\mathrm{E} = \mathrm{E_T}\cosh\mathrm{y} = \mathrm{m_T}\cosh\mathrm{y}$, where $\mathrm{E_T^2} = \mathrm{m^2} + \mathrm{p_T^2}$ while $\mathrm{p_z} = \mathrm{m_T}\sinh\mathrm{y}$.

In the lab frame therefore, the four momenta of the final state partons are,

$$\begin{aligned} \mathrm{q_1} &= (\mathrm{m_T}\cosh\mathrm{y_1}, \mathrm{p_T}\cos\phi, \mathrm{p_T}\sin\phi, \mathrm{m_T}\sinh\mathrm{y_1}), \\ \mathrm{q_2} &= (\mathrm{m_T}\cosh\mathrm{y_2}, -\mathrm{p_T}\cos\phi, -\mathrm{p_T}\sin\phi, \mathrm{m_T}\sinh\mathrm{y_2}). \end{aligned} \tag{6.2.6}$$

In the center of mass frame of the two partons a boost in the Z direction is effectively a translation in the rapidity axis, with the rapidities of the two partons being $\pm y$ with $\mathrm{y} = \mathrm{y_2} - \mathrm{y_1}$. Thus in the center of mass frame,

$$\begin{aligned} \mathrm{q_1^{'}} &= (\mathrm{m_T}\cosh\mathrm{y}, \mathrm{p_T}\cos\phi, \mathrm{p_T}\sin\phi, \mathrm{m_T}\sinh\mathrm{y}), \\ \mathrm{q_2^{'}} &= (\mathrm{m_T}\cosh\mathrm{y}, -\mathrm{p_T}\cos\phi, -\mathrm{p_T}\sin\phi, -\mathrm{m_T}\sinh\mathrm{y}). \end{aligned} \tag{6.2.7}$$

This discussion on the kinematics thus provides the geometrical picture of the collider environment against the backdrop of which our studies will be based. Since the net momentum transverse to the direction of the beam axis is zero, it is convenient to describe the picture in the transverse plane.

Having described the collider environment, the next important issue in a hadron collider is the estimation of the hard scattering cross section.

The cross section of the hard scattering process at a hadron collider between two partons (say a,b ; e.g gluons) to produce final state particles A and B is given by,

$$\sigma(P(a)P(b) \to A\,B) = \sum_{a,b}\int dx_a \int dx_b\, f_{a/P}(x_a,\mu_f^2)\, f_{b/P}(x_b,\mu_f^2)\hat{\sigma}(\alpha_{s'}(\mu_R))(ab \to A\,B). \tag{6.2.8}$$

The functions $f_{a/P}(x_a,\mu_f^2)$, $f_{b/P}(x_b,\mu_f^2)$, known as the parton density functions (PDF), represent the probability of finding a parton "i" a inside the proton target with momentum fraction x_i at a scale μ_f. Here μ_R, μ_f are the renormalization and factorization scales respectively. The PDF is constrained from the deep inelastic scattering process, and its evolution is governed by the solutions of Dokshitzer-Gribov-Lipatov-Altarelli-Parisi(DGLAP) equation or commonly known as the Altarelli-Parisi equations. The above equation for the cross section is a result of the factorization theorem in QCD, the essence of which is to separate the short distance hard scattering process described by pQCD and the long distance non-perturbative interaction. Once parton densities and the value of the strong coupling constant is known from experiments, the cross section can be calculated without much ambiguity.

The hard scattering process is followed by showering to include QCD and QED radiation. The final components in a generic proton proton collision includes along with the hard scattering process, soft QCD and QED radiation, beam remnants. Thus the overall picture is quite noisy. The underlying event can be defined as all the activity of a single proton proton collision superimposed on

the hard scattering. This includes initial and final state radiations(ISR/FSR), beam remnants, and multi parton interactions. It is therefore extremely important to model such effects and compare them with experiments, to get a picture of the physics. Monte carlo generators like PYTHIA [6] and Herwig [235] provide an efficient description of some of the above mentioned effects.

The process of showering is followed by the process of hadronization. It is well known that QCD below energy scales of Λ_{QCD} ($\sim$ 200 MeV), is a confining theory, and hence quark and gluons finally form color singlet objects like baryons and mesons. The process of hadronization is non-perturbative and models of hadronization are used to this end. For example the process of hadronization is done by the method of string fragmentation in PYTHIA, which relies on the assumption of linear confinement, pictured as color flux tubes between partons(e.g $q\bar{q}$ from e^+e^-) as they move away from each other.

6.3 Jets

As discussed in the previous section, quarks and gluons finally hadronize to form color singlet objects like baryons and mesons. In a collider experiment, the hadrons are collected in detectors and clustered to form jets. The definition of jets depends on the algorithm. A "good" algorithm must be experimentally easy to use and must be theoretically stable and robust. In terms of the snowmass accord [236] the following criteria of jets should be met:

- It should be simple to implement in an experimental analysis.
- It should also be simple to implement in a theoretical calculation.
- The definition should be valid to all orders of perturbation theory.
- It should yield finite cross sections at any order of perturbation theory.
- The cross section should be insensitive to the process of hadronization.

Historically the first jet algorithms were constructed at the e^+e^- colliders, by Sterman and Weinberg [237], along with Ellis [238]. In Sterman Weinberg jets, an event was classified as having two jets if at least a fraction $1-\varepsilon$ of the total energy was contained in two cones with a half opening angle δ. These algorithms are known as cone algorithms. The widely used cone algorithms are iterative cones, where a particle i is taken as a seed, and all particles j within a cone of radius R are clustered such that,

$$\Delta R_{ij}^2 = (y_i - y_j)^2 + (\phi_i - \phi_j)^2 < R^2.$$

This process is repeated with the above resultant as a seed, till the direction of the resultant is stabilized. The problem with cone algorithms are however in the fact that they are not infrared or collinear (IRC) safe. The infrared and colinear safety can be summarized by the following criteria:

- Colinear splittings, soft particle emission in QCD are a part of any hadronic interaction. In a tree level fixed order perturbative calculation these processes are reflected as soft and co-linear singularities. These singularities are however cancelled by corresponding loop level diagrams. In an IRC unsafe algorithms, tree level and loop level splittings may lead to different sets of jets, breaking the cancellation. A jet algorithm should thus be free of these IRC problems and should be insensitive to all these effects.

- Since the experimental detectors have non-zero momentum resolution they provide some regularization of infrared and colinear safety but this depends on the electronics of the detector. IRC unsafe algorithms can be ambiguous in providing a correct picture of the above.

It turns out that iterative cone algorithms are IRC unsafe, and IRC unsafety impacts observables in question.

Modern day algorithms use sequential recombination algorithms, which has its roots in e^+e^- colliders. The first of these algorithms was known as the JADE algorithm used by the Jade collaboration in the 1980's [239, 240]. Here we describe the three major algorithms currently in use at the LHC. The first of these is termed as k_t algorithm [241]. The procedure is summarized as,

- Define the distance measures between particles i,j (d_{ij}) and the beam B (d_{iB}).

$$d_{ij} = \min(p_{ti}^2, p_{tj}^2)\frac{\Delta R_{ij}^2}{R^2}, \qquad \Delta R_{ij}^2 = (y_i - y_j)^2 + (\phi_i - \phi_j)^2, \qquad d_{iB} = p_{ti}^2,$$

  where R is the cone size of the jet.

- Calculate all the d_{ij} and d_{iB}, and find the minimum.
- If the minimum is d_{ij}, recombine i and j and return to step 1.
- If the minimum is d_{iB}, declare i to be a jet, and remove it from the particle list.
- Stop when no particles remain.

Hence all the stable particles are included in final state jets, there is no concept of a beam jet.

The second set is known as the anti-k_t [7] algorithm, where the distance measure is defined as,

$$d_{ij} = \min(p_{ti}^{-2}, p_{tj}^{-2})\frac{\Delta R_{ij}^2}{R^2}, \qquad \Delta R_{ij}^2 = (y_i - y_j)^2 + (\phi_i - \phi_j)^2, \qquad d_{iB} = p_{ti}^{-2}. \quad (6.3.1)$$

The anti-k_t algorithm clusters the hardest particle as the seed and grows around this seed. It must be noted however that since collinear splittings get clustered at the very beginning the algorithm is collinear safe. The advantage of anti-k_t is in the fact that this algorithm gives circular jets and hence is preferred by experimental collaborations.

The final algorithm of interest is the Cambridge/Aachen (C/A) [242] algorithm, originally introduced as the Cambridge algorithm for the e^+e^- collider. This introduces the distance measures defined in Eq. 6.3.1 and the angular measure $v_{ij} = (1 - \cos\theta)$. Along with this it introduces the measure $y_{ij} = \frac{2E_iE_j(1-\cos\theta)}{Q^2}$ where Q is the total energy of the system and follows the following steps :

- If only one particle is left deem it as a jet.
- If not, calculate the measure v_{ij}, and find the smallest pair.
- If the corresponding y_{ij} is smaller than some predefined y_{cut}, replace i,j with the recombined one and go back to step 1.
- Else call the less energetic of i and j to be a jet, remove it from the particle list and go back to step 1.

The motivation of this algorithm was to obtain angular ordered jets in combination with the k_t measure. The improved version of the Cambridge algorithm, designed for hadron colliders is the Cambridge/Aachen algorithm which replaces the y_{ij} cut by the smallest ΔR_{ij} measure and repeating the k_t algorithm procedure.

Finally we proceed to discuss some aspects of jet substructure methods. For a highly boosted particle, the resulting decayed partons are highly collimated, and thus in the process of jet formation, it is possible that these particles are clustered as part of the same jet instead of two separate ones. The method of jet substructure attempts to resolve this "fat-jet" containing two subjets. The first of these is the method to resolve the subjets for a boosted Higgs decaying to a pair of b quarks. This was first introduced in [35], and subsequently improvements have been made. Here the salient features of this technique is discussed. For a highly boosted Higgs decaying to a pair of b-quarks, the decay products are extremely collimated and may not result in two separate b-jets. The angular resolution is p_T dependent and is roughly given by,

$$\mathrm{R_{b\bar{b}}} \simeq \frac{1}{\sqrt{\mathrm{x(1-x)}}}\frac{\mathrm{m_h}}{\mathrm{p_T}}. \tag{6.3.2}$$

where x, (1-x) are the momentum fractions carried by the two b quarks. Along with the resolution of the b jets, any gluon emission should be captured, while the contamination from underlying events has to be rejected. To look for subjets a jet algorithm is required that captures the angular resolution and clusters the hardest particles at the last stage of jet formation. The anti-k_t algorithm is not suitable for this purpose as it clusters the hardest jets first. The best suited algorithm for this process is the Cambridge-Aachen (C/A) which produces angular ordered jets. The jet substructure algorithm for boosted Higgs scenario is described below following [35]:

- A jet j clustered with C/A algorithm is declustered into two jets $\mathrm{j_1}, \mathrm{j_2}$ with masses m_{j_1}, m_{j_2}, by undoing the last stage of clustering.
- With a pre-defined quantity μ, check if there was a significant mass drop in the system $m_{j_1} < \mu m_j$. Along with the above also check the asymmetry criteria, i.e, $\mathrm{y} = \frac{\min(\mathrm{p^2_{Tj_1}}, \mathrm{p^2_{Tj_2}})}{\mathrm{m^2_j}} \Delta \mathrm{R^2_{j_1,j_2}} > \mathrm{y_{cut}}$, where $\mathrm{y_{cut}}$ is a predefined value. If the above two criteria are met, then deem j to be the heavy particle neighbourhood and exit.
- If the above criteria is not satisfied replace j by j_1 and repeat.

If the final jet has two subjets with b -tags, then it can be considered as a Higgs candidate within a pre-defined Higgs mass window. If there is a gluon radiation then the effective size of the jet j is just sufficient to capture it. For the values of μ, it is noted that if $\mu \geq 1/\sqrt{3}$, and the Higgs decays producing a mercedes-benz configuration of jets consisting of a pair of b quarks along with the gluon radiation, the mass drop criteria is triggered. The $\mathrm{y_{cut}}$ is used to reject fake jets satisfying the mass drop criteria. It is observed that a $\mathrm{y_{cut}}$ of 0.15 is optimal to improve the signal to background ratio. The mass peak is then obtained by demanding that the mass window is within a predecided value (typically within 10 GeV of the central value of the Higgs mass).

The mass peak is however subject to degradation from underlying events. This is reduced by the process of filtering the Higgs neighbourhood, in which the parameter $\mathrm{R_{filt}} < \mathrm{R_{b\bar{b}}}$ is chosen such that only the dominant $\mathcal{O}(\alpha_S)$ radiation is captured while rejecting the underlying events. A value of $\mathrm{R_{filt}} < \min(0.3, \mathrm{R_{b\bar{b}}}/2)$ was found to be effective by [35].

It was observed that in general the k_t algorithm has a better background rejection than the C/A algorithm, but suffers from a poorer mass resolution [35].

The second substructure algorithm is to tag boosted tops. The boosted top regime occurs in a variety of beyond standard model processes, and thus is extremely well motivated. The algorithm proceeds with a similar philosophy as that of the boosted Higgs algorithm. In this case however, 3 subjets (the b-jet and the two jets from the W decay) are required to be tagged. At the first step of iteration the C/A jet is declustered by undoing the last step, and rejecting the softer jet if the transverse momentum divided by the transverse momenta of the parent jet is less than a predetermined value of δ_p [243]. The value of δ_p is p_T dependent, and the typical values found to be efficient in [243] are $\delta_{\rm p} = 0.1, 0.05, 0.05$ for $\rm p_T = 1000, 1600, 2000$ GeV respectively. This procedure is repeated till 3 subjets are found in the original jet. The resultant subjets then must have 1 b-tagged jet and two non b-tagged jet with the invariant mass of the non b-tagged jet within the W mass corridor (65-95 GeV) while the invariant mass of the 3 subjet system to be within the top quark mass corridor (145-205 GeV).

6.4 Monte carlo, jet finding and matrix element generator tools

Monte carlo tools are an essential necessity for a realistic simulation of the experimental conditions at a collider. In earlier days, parton level monte carlo modules were used, that estimated only the hard scattering process and made a crude assessment of a hadron collider environment. However this is not the correct picture in most scenarios. The process of QCD and QED radiation, which become exceedingly complex at each order of perturbation theory, and finally the process of fragmentation and hadronization which follow extremely complicated non-perturbative dynamics make the hadron collider environment extremely noisy. Thus the simple kinematics of the two body partonic hard scattering process ends up with a large number of final state partons. Event generators that simulate this entire sequence come to the rescue here, by dividing the entire process into components, where the output of the first process is used as the input of the next. The event generator gives a realistic feeling of the kind of events that one can expect in an experimental process and the rates at which they occur.

The two popular event generators in wide use are PYTHIA [6] and Herwig [235]. In all the subsequent work described in this thesis, PYTHIA is used for generating events. The origin of PYTHIA have the foundations in the LUND string model [244] which provided the earliest framework of hadronization and string fragmentation.

The main steps of event generation from the initial state radiation to the final stage of hadronization in PYTHIA is summarized below,

- **The initial state radiation**(ISR): The incoming beam particles are composed of partons which take part in the hard scattering process. Before the hard scattering process, the incoming partons may shower and initiate a sequence of branchings which build up the ISR.
- **The hard scattering process** : Two partons from the two beams enter the hard process and produce two partons in the final state. As discussed earlier this is done by convoluting the PDF with hard scattering cross section [1]. Note that PYTHIA only calculates leading order matrix elements. If the final particles are resonances like Z/W or a heavy quark like top or short lived BSM particles, they decay to normal particles with decay widths taken into account.

[1] Note that the total proton proton collision cross section at 7 TeV center of mass energy is about 110 millibarns [245]. Out of this the inelastic cross section is about 60 millibarn, the single diffractive cross section is about 12 millibarn, while the elastic scattering is about 40 millibarn. The hard scattering process is dominated by the QCD cross section, which is about 10^7 pb at 7 TeV center of mass energy.

- **The final state showers**(FSR) are built by branching the final state partons from the hard interaction. Along with the hard interactions there are also semihard interactions.
- **The beam remnant**: is composed of everything that is left behind once the hard interaction process is removed.
- **The process of hadronization** takes place at this stage producing color neutral hadrons. Some of these hadrons are unstable and may decay further to give stable hadrons. At the end of the process stable hadrons, leptons and photons are left as final state stable particles.

As was earlier discussed, the final state hadrons are clustered in detector to form jets. Although PYTHIA has built in cone algorithms for this purpose, cone algorithms suffer from inherent issues of soft and colinear divergences. Instead, recombination algorithms like k_t [241], anti-k_t [7] and C/A [242] are used as IRC safe algorithms. The most widely used jet finding package is FASTJET [8] and this is used with an interface to PYTHIA in works described in this thesis. The general algorithm used is anti-k_t with a size parameter R=0.5, while for boosted objects C/A algorithm is used.

We noted earlier that PYTHIA only computes leading order matrix elements. The real corrections of higher order effects are taken care to some extent by parton showering in the final state. While this may suffice for some processes, specially for processes with low cross sections at the leading order, it may give unreliable prediction for a variety of processes with large cross sections like QCD, W/Z+jets. In these cases parton showering to include higher order effects may not be the realistic estimate of the actual matrix element hard scattering process. Hence generating matrix elements for these processes becomes an absolute necessity. Some of these processes can be quite complex as the number of diagrams one has to calculate with every order of perturbation theory grows quite fast.

In this thesis we use the software packages ALPGEN [9] or Madgraph [10], to compute multi-parton final state processes like $t\bar{t}+$jets, W/Z +jets processes wherever required.

This is then passed to PYTHIA for showering and hadronization. The additional complication arises because of double counting of events. Note that the matrix element method works best for large momentum regions of the phase space while low momenta region is best described by parton shower methods which takes into account soft and colinear emissions. Hence it is useful to merge the two to get a correct feeling for the entire region of phase space. A given configuration of (N+1) jet event in a process can be obtained either by the collinear/soft parton evolution of a (N+1) parton state, or by a large angle emission of a hard jet from a N parton system. Therefore a scheme is required which decides , on an event by even basis which of the two is to be followed. Furthermore parton showering may mimic an actual matrix element generated configuration in certain regions of phase space. Therefore a double counting of events occur in the process of merging matrix elements with parton showers. This therefore must be avoided by a judicious procedure of merging such that parton shower and matrix element events represent the relevant regions of phase space. This is done by the procedure of MLM matching [11]. The partons from the matrix element level calculation is defined with a minimum p_T^{min} and a separation $\Delta R_{ij} > R_{min}$. After showering a jet defined within a cone R_{min}, with a threshold of p_T^{min}, is applied to the final state partons. The partons are then matched with the closest jet in the (η, ϕ) plane, and if the distance less than R_{min}, the jet and parton is said to be matched, with the matched jet removed from the jet list. These procedure is repeated for all partons. The double counting is removed by demanding that there is exactly one parton that matches with a particular jet. For configurations in which there are two partons that satisfy the matching criteria, the event is removed. Any event below the transverse

momenta threshold is considered a part of the parton shower process, while the ones above are described by matrix element process. The final matched sample thus contains events where the low momentum end of the phase space are described by parton shower process, while the high momenta regime is described by matrix element generated events.

Chapter 7

Probing generic SUSY signals at the LHC

In this chapter we describe the generic SUSY signals at LHC and the ways to probe such signals by an effective selection of certain kinematic variables. We introduce SUSY searches based on event shape variables for the first time. Indeed, it is shown that such a strategy can be more efficient than existing search strategies, employed by both phenomenological studies as well as by the experimental collaborations.

7.1 Signatures of SUSY at the LHC

If one assumes R-parity conservation, the signatures of SUSY follows that of SM, but two of the particles at each vertex are replaced by superpartners. The LHC is essentially a hadronic machine, where the gluon flux can be large and hence the sparticle production at LHC is dominated by strong production processes governed by QCD. The SUSY electroweak interactions initiated by quarks at the initial state mediated by W/Z and the photon are sub dominant. However for low masses the cross sections for chargino and neutralino can still be significant. Fig. 7.1 presents some of the Feynman diagrams for sparticle production. The first row in the Fig. 7.1, presents the gluino production from s and t channel gluon initiated process, and the s and t channel quark initiated process. The second and third rows display the squark pair and the squark gluino pair production processes, and finally the last row presents the electroweak gaugino pair productions.

The parton level gluino pair production cross section ($\hat{\sigma}$) from gluon initiated process at leading order (LO) is given by [246, 247],

$$\begin{aligned}\frac{d\hat{\sigma}(g(p_1)g(p_2)\to\tilde{g}(p_3)\tilde{g}(p_4))}{dt} &= \frac{9\pi\alpha_s^2}{4s^2}\left[\frac{2(M^2-t)(M^2-u)}{s^2}+\frac{(M^2-t)(M^2-u)-2M^2(2M^2+t)}{(M^2-t)^2}\right.\\ &+\frac{(M^2-t)(M^2-u)-2M^2(2M^2+u)}{(M^2-u)^2}+\frac{M^2(s-4M^2)}{(M^2-t)(M^2-u)}-\\ &\left.\frac{(M^2-t)(M^2-u)+M^2(u-t)}{s(M^2-t)}-\frac{(M^2-t)(M^2-u)+M^2(t-u)}{s(M^2-u)}\right],\end{aligned}$$

where s,t and u are the Mandelstam variables defined as $s=(p_1+p_2)^2=(p_3+p_4)^2$, $t=(p_1-p_3)^2=(p_2-p_4)^2$, $u=(p_1-p_4)^2=(p_2-p_3)^2$. α_s is the strong coupling constant and M is the mass of the gluino.

The total cross section (σ) is obtained by convoluting Eq. 7.1.1 with the parton density function,

$$\sigma(PP \to \tilde{g}\tilde{g}) = \int dt \int dx_1 \int dx_2 f_{g/P}(x_1,\mu_f^2) f_{g/P}(x_2,\mu_f^2) \frac{d\hat{\sigma}}{dt}(gg \to \tilde{g}\tilde{g}), \tag{7.1.1}$$

where only the gluon dominated process is presented in Eq. 7.1.1.

The functions $f_{g/P}(x_1,\mu_f^2)$, $f_{g/P}(x_2,\mu_f^2)$, known as the parton density functions (PDF), represent the probability of finding a parton a inside the nucleon target with momentum fraction x at a scale μ_f. Here μ_f is the factorization scale respectively and in general set to the hard scattering scale Q, where $Q = \sqrt{\hat{s}}$ is the center of mass energy in the parton frame.

The next to leading order(NLO) cross sections can be quite large as compared to the LO cross sections. The NLO cross sections have been calculated in the literature in a wide range of works [248–251]. The SUSY QCD corrections generally consists of two parts; QCD corrections due to the real correction of gluon and quark radiation and the virtual correction due to gluon loops, and secondly the virtual corrections due to the squark and the gluino loops. The virtual SUSY corrections are sub dominant at large squark and gluino masses. In general cross section calculators like Prospino [17] make the assumption of degenerate left and right squarks for the first five flavors. In addition, electroweak corrections have also been calculated in the literature [252, 253].

The inclusive cross section is dominated by the strong production processes and varies from as much as 50 pb for gluino and squark masses of 400 GeV to $\mathcal{O} \sim 1$ fb for gluino and squark masses of 1 TeV at 7 TeV center of mass energy. The cross section for various supersymmetric processes is presented in Fig. 7.2, where the gluino and squark masses are assumed to be degenerate. It can be observed that the largest contribution to the cross section comes from the squark gluino process, while the sub dominant strong sparticle productions are the squark pair, and the gluino pair production. Notice that the fall of the cross section is rapid with increasing mass, with the net strong particle production falling to about ~ 1 fb at about 1 TeV squark and gluino masses.

Once produced the squarks and gluinos cascade decays immediately to lighter states and finally to the lightest neutralino. The decay widths of the gluino and the squarks depend on the masses of the parent and the decaying particle and the nature of the coupling. As an example the decay width for the gluino decaying into a squark and a quark is given by [159],

$$\Gamma(\tilde{g} \to \tilde{q}_1 + q) = \frac{\alpha_s \lambda^{\frac{1}{2}}(m_{\tilde{q}_1}^2, m_{\tilde{g}}^2, m_q^2)}{m_{\tilde{g}}^3} \left(m_{\tilde{g}}^2 - m_{\tilde{q}_1}^2 + m_q^2 - 2\sin 2\theta_{\tilde{q}} m_{\tilde{g}} m_q\right), \tag{7.1.2}$$

$$\Gamma(\tilde{g} \to \tilde{q}_2 + q) = \frac{\alpha_s \lambda^{\frac{1}{2}}(m_{\tilde{q}_2}^2, m_{\tilde{g}}^2, m_q^2)}{m_{\tilde{g}}^3} \left(m_{\tilde{g}}^2 - m_{\tilde{q}_2}^2 + m_q^2 + 2\sin 2\theta_{\tilde{q}} m_{\tilde{g}} m_q\right), \tag{7.1.3}$$

where $\tilde{q}_{1,2}$ denote mass eigen states corresponding to the flavor eigen states $\tilde{q}_{L,R}$, $\theta_{\tilde{q}}$ is the mixing angle between the left and right squark states, and λ is the challan variable defined as $\lambda(x,y,z) = x^2 + y^2 + z^2 - 2xy - 2xz - 2yz$.

Similarly the squark decay widths are given by [159],

$$\Gamma(\tilde{q}_1 \to \tilde{g} + q) = \frac{2\alpha_s \lambda^{\frac{1}{2}}(m_{\tilde{q}_1}^2, m_{\tilde{g}}^2, m_q^2)}{3 m_{\tilde{q}_1}^3} \left(m_{\tilde{q}_1}^2 - m_{\tilde{g}}^2 - m_q^2 + 2\sin 2\theta_{\tilde{q}} m_{\tilde{g}} m_q\right), \tag{7.1.4}$$

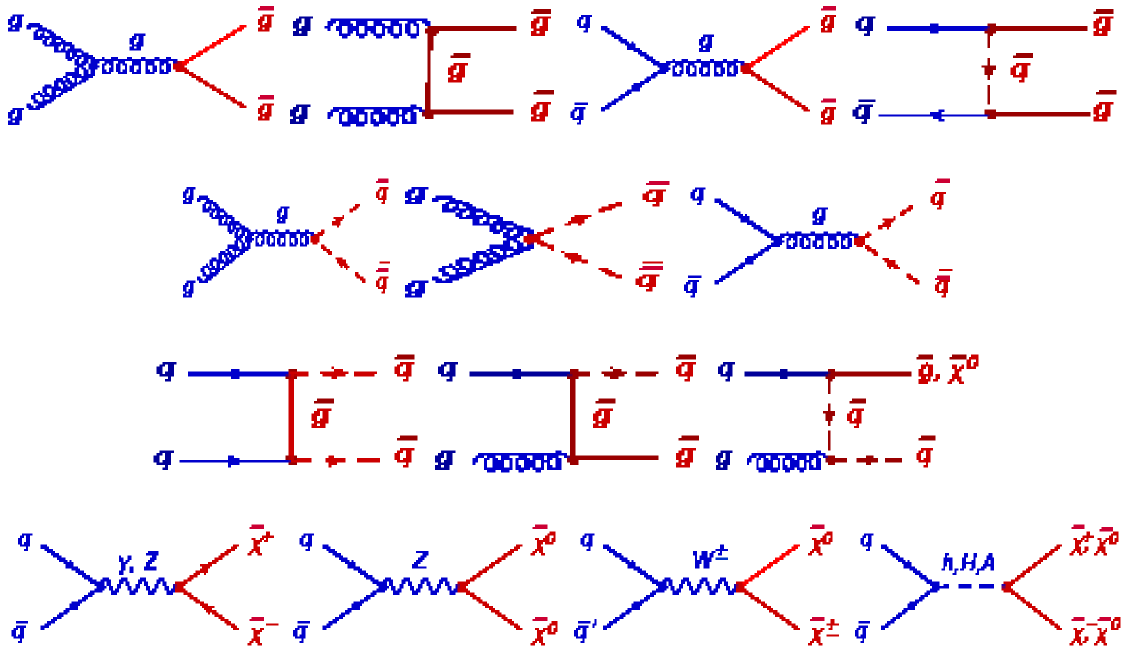

Figure 7.1: Examples of diagrams for the SUSY particle production via the strong interactions (top rows for $\tilde{g}\tilde{g}$, $\tilde{q}\bar{\tilde{q}}$ and $\tilde{g}\tilde{q}$, respectively) and the electroweak interactions (the lowest row).

$$\Gamma(\tilde{q}_2 \to \tilde{g} + q) \;=\; \frac{2\alpha_s \lambda^{\frac{1}{2}}(m^2_{\tilde{q}_2}, m^2_{\tilde{g}}, m^2_q)}{3 m^3_{\tilde{q}_2}} \left(m^2_{\tilde{q}_2} - m^2_{\tilde{g}} - m^2_q - 2\sin 2\theta_{\tilde{q}}\, m_{\tilde{g}} m_q\right). \tag{7.1.5}$$

If the mass hierarchy is $m_{\tilde{g}} > m_{\tilde{q}} > m_{\chi_1^\pm}, m_{\chi_2^0} > m_{\chi_1^0}$, the first step of the cascade decay initiated by the gluino is governed by QCD processes, which depend primarily on the masses of the initial and final state particles. In general a large mass gap between the parent and the daughter particles results in large boosts carried by the daughter particles. The second step of the cascade involves decays via weak interactions, to charginos and neutralinos. Contrary to the decay via strong processes, the decays via weak interaction depend on the exact nature of couplings and the composition of the charginos and neutralinos. These couplings dictate the branching ratios of various weak decays in SUSY. The decay of SU(2) doublet squarks to the chargino states contribute about $55-60\%$ of the total branching ratio, while the rest is via the decay to neutralinos. If the gluino is lighter than the squarks, the gluino decays off-shell as,

$$\tilde{g} \to qq'\chi_1^\pm,\; q\bar{q}\chi_2^0,$$

while the chargino and neutralino decays as,

$$\chi_1^\pm \to W\chi_1^0 \to ff'\chi_1^0,\;\; \chi_2^0 \to Z\chi_1^0 \to f\bar{f}\chi_1^0.$$

These decays however depends on the nature of the squarks and the charginos and neutralinos. An entirely right handed squark will decay to a quark and the lightest neutralino. Similarly if $\chi_1^\pm$ and χ_2^0 is gaugino like, the mass gap $\chi_1^\pm, \chi_2^0 - \chi_1^0$, is large, resulting in hard final state jets and leptons. In the other limit, when $\chi_1^\pm$ and χ_2^0 are higgsino like, $\chi_1^\pm$, χ_2^0 and χ_1^0 are almost degenerate

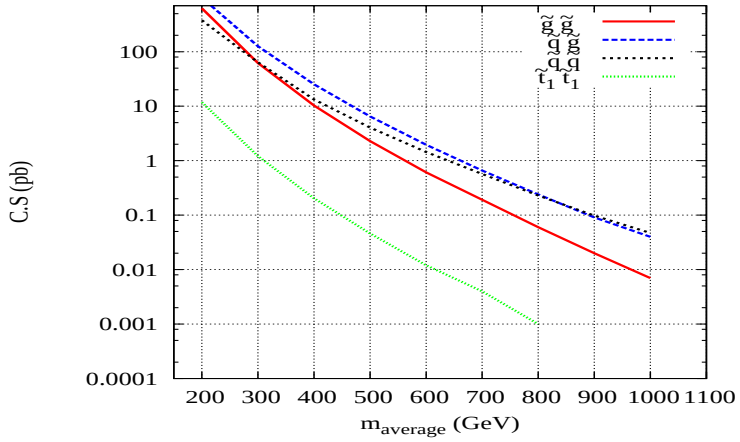

Figure 7.2: The cross sections for various supersymmteric processes by strong processes at 7 TeV LHC energy.

Production	Decay Modes	Signatures
• $\tilde{g}\tilde{g}, \tilde{q}\tilde{q}, \tilde{g}\tilde{q}$	$\tilde{g} \to q\bar{q}\tilde{\chi}^0_{1,2}$ $q\bar{q}'\tilde{\chi}^\pm_1$ $g\tilde{\chi}^0_1$ $\tilde{q} \to q\tilde{\chi}^0_i$ $\tilde{q} \to q'\tilde{\chi}^\pm_i$	$\not{p}_T$ + multijets (+leptons)
• $\tilde{\chi}^\pm_1\tilde{\chi}^0_2$	$\tilde{\chi}^\pm_1 \to \tilde{\chi}^0_1 l^\pm \nu$ $\tilde{\chi}^0_2 \to \tilde{\chi}^0_1 ll$	Trilepton + $\not{p}_T$
	$\tilde{\chi}^\pm_1 \to \tilde{\chi}^0_1 q\bar{q}'$ $\tilde{\chi}^0_2 \to \tilde{\chi}^0_1 ll$	Dilepton + jet + $\not{p}_T$

Table 7.1: Some of the production processes, decay modes and signatures of sparticles at a hadron collider like LHC.

and hence the final state objects are soft. At the end of the decay chain, a collection of leptons, quarks and missing transverse momentum ($\not{p}_T$) originating from the LSP is obtained. The $\not{p}_T$ in the system occurs from the fact that the lightest neutralino, being extremely weakly interacting, evades detection. The resultant imbalance in momentum shows up as $\not{p}_T$. Some of the SUSY signals initiated by strong/weak production processes are tabulated in Table 7.1,

Thus the generic SUSY signature, is often designated by,

$$m - leptons + n - jets + \not{p}_T \quad \mathrm{n,m} = 0,1,2... \ . \tag{7.1.6}$$

The task of extracting the SUSY signal at the LHC boils down to suppressing the enormous SM backgrounds. The SM background consists of two major components; the QCD background which is the largest background in terms of cross section and with no or insignificant $\not{p}_T$, and secondly the electroweak and the $t\bar{t}$ background which has large cross sections and associated $\not{p}_T$ from the neutrinos. Thus the principal backgrounds to a generic SUSY search can be summarized

as follows [254]:

- **QCD**: The QCD background, which includes copious productions of quarks and gluons in the final state is the largest SM background in terms of cross section of about $\sim \mathcal{O}\ 10^7$ pb at 7 TeV. The $\not{p}_T$ in the QCD background comes from semileptonic B meson decays, as well as non physics sources like detector effects. In the works described in this thesis, we do not take detector effects into account.
- $t\bar{t}+jets$: The $t\bar{t}$ production process can have semi-leptonic and fully hadronic final state. Since the cross section is significantly large ($\sim$ 160pb at 7 TeV) and there is a significant amount of missing energy from the neutrinos in case of semi-leptonic decays along with associated jets this too is a major background for SUSY searches.
- **Z+jets** :This electroweak process comprises of the irreducible part of the background in SUSY searches for fully hadronic final states when the Z boson decays to a pair of neutrinos. The cross section for this process is quite large ($\sim 10^4$ pb at 7 TeV) and hence this background is one of the most severe backgrounds to SUSY searches. This background also contributes significantly for dileptonic SUSY searches when the Z bosom decays to a pair of opposite sign leptons.
- **W+jets** : This electroweak background can be significantly large for leptonic and fully hadronic searches as the cross section is enormously large ($\sim 10^5$ pb at 7 TeV). For fully hadronic searches this is a major background in the situation when the lepton is not identified, or when the W decays hadronically via the tau lepton. This is also a significant background for single lepton searches for $W \to l\nu$.
- **WW/WZ/ZZ** : The SM electroweak processes, although low on cross sections as compared to the previous ones, can be serious backgrounds for a variety of SUSY searches, for both hadronic and leptonic final states.
- **tbW/tW/**$\nu\nu$qq$'$: These background processes can be significant for hadronic as well as leptonic SUSY searches.

The SUSY signal cross sections are thus miniscule ($\sim \mathcal{O}(1\ pb)$) as compared to the SM backgrounds and therefore the challenging task at hand is to extract the signal out of this haystack. The amount of suppression required is of the order of 1 part in 10^8, which is quite a daunting task.

The first works in probing SUSY signatures for the early LHC run with 7 TeV energy were conducted by [4, 5, 255]. In general these search strategies probed the following channels :

- jets + $\not{p}_T$.
- 1-lepton(1l) + jets + $\not{p}_T$.
- two opposite(OS)/same sign(SS) leptons + jets + $\not{p}_T$.
- three leptons + jets + $\not{p}_T$.

The general strategy employed in these searches relied on the use of a hard $\not{p}_T$ cut along with other standard cuts on the number of jets and hardness of the leading jets. This is well motivated since in a large region of the SUSY parameter space dominated by strong particle production, the leading jets and $\not{p}_T$ is expected to be hard. This provides an excellent handle to suppress the backgrounds. Using their strategy the authors in [4] found that they can probe up to 950 GeV in

gluino mass when the squark is degenerate with the gluino and 500 GeV when the gluino mass is much less than the squark mass.

In addition some specialized techniques like α_T [256], razor [257], M_{T2} [47] were also investigated in a wide range of the MSSM parameter space.

At the end of the 7 TeV and the 8 TeV runs at the LHC data worth 5 fb^{-1} and 20 fb^{-1} luminosity was acquired respectively. Most of the early searches in ATLAS and CMS were conducted in the model framework of CMSSM parameter space [21, 258]. The general strategy relied on the use of a high H_T and a high $\not{p}_T$ cut to suppress the backgrounds.

It was also observed that, these search strategies did not cover certain regions of parameter spaces with relatively low $\not{p}_T$. A typical example is the high m_0 and low $m_{1/2}$ region in CMSSM, where the squark masses are much higher than the gluino mass. In this case, although the $\not{p}_T$ is lower, this region is rich in jet activity, as the gluino undergoes a three body decay in the heavy flavor channel via off shell squarks. The multiplicity of jets in this case is expected to be high, as is the momentum of these jets. In this region the limits from ATLAS and CMS were observed to be weaker than the high $m_{1/2}$ region, where the gluino and the squark have almost degenerate masses. This region thus requires special treatment, and in the following section we take up the subject of event shape variables in supersymmetry searches [19,20] to show that such kinematically challenging regions can be probed more efficiently than the existing search strategies.

7.2 The event shape analysis for 7 TeV LHC energy

As was mentioned earlier the sparticle production at the LHC is dominated by the strong production process. The final states with the generic signature of jets, leptons and $\not{p}_T$ (Eq. 7.1.6) were studied in the following channels [19],

- a single lepton + jets(1ℓ) + $\not{p}_T$,
- di-leptons+ jets(2ℓ),
- jets + $\not{p}_T$.

It must be noted that the jets + $\not{p}_T$ channel offers the largest reach, as leptonic branching ratios in the cascade decay are much smaller.

The background processes consists of the entire set described in in the previous section. The most severe backgrounds consist of the $t\bar{t}+jets$ and the irreducible $Z(\rightarrow \nu\bar{\nu}+jets)$. Along with this, the single lepton and the jets + $\not{p}_T$ channel is plagued by the W($\rightarrow \ell\nu$) + jets and QCD due to its large cross section. In addition sub dominant backgrounds like WW/WZ/ZZ and tbW, $t\bar{t}$W also make a significant contribution to the final background.

The event generator PYTHIA6 [6] is used to generate signal events and background processes due to $t\bar{t}$, WW,WZ,ZZ and QCD. The $t\bar{t}$ and QCD backgrounds are generated by slicing the entire phase space in various $\hat{p}_T$ bins, where $\hat{p}_T$ stands for the transverse momentum of final state partons in the partonic center-of-mass frame. For $t\bar{t}$+ jets, W/Z+ jets , hard parton level events are generated using ALPGEN [9] and subsequently passed through PYTHIA6 for parton showering(PS). Jets are reconstructed using FastJet [8] with an anti $-$ K_T [7] algorithm using a size parameter R=0.5. Jets are selected with a cut of $p_T^j \geq 50$ GeV and $|\eta| \leq 3.0$. The total $\not{p}_T$ of the event is calculated out of the momentum of all visible particles present in the event. We pre-select events consisting jets and missing energy by imposing the following selection:

$$p_T^j > 50 \text{ GeV}, |\eta| < 3.0 \text{ and } \not{p}_T > 50 \text{ GeV}, \text{ n}_\text{j} > 1. \tag{7.2.1}$$

For the analysis with single and dilepton channels, leptons, both electron(e) and muon(μ) are selected with $p_T \geq$10 GeV and $|\eta| \leq$3. In the case of the single lepton final state, we apply $p_T \geq 20$GeV.

To analyze the signal and background we use the following strategy based on event shape variables with the selection variables as described below:

- **Transverse thrust** :The concept of event shape variables emerged with e^+e^- colliders, with the aim of defining the "shape" of an event, whether it is planar, spherical or pencil like, etc. These variables are defined to be infra-red safe against soft or colinear gluon emission and invariant under the branching $\vec{p}_i \rightarrow \vec{p}_j + \vec{p}_k$, whenever the momenta are parallel or one of them is small. Quantities made of linear sums of momenta always meet this criteria. The event shape variable we put to use is transverse thrust defined as [18],

$$T = max \frac{\sum_j |\vec{p}_T^{\,j}.\vec{n}_T|}{\sum_j |p_T^j|}, \tag{7.2.2}$$

  where $\vec{p}_T^{\,j}$ is the jet with momenta in the transverse direction, and $\vec{n}$ is an arbitrary unit vector in the transverse plane over which the maximization is performed. If the momenta $\vec{p}_T^{\,j}$ form colinear jets, the thrust axis after maximization lies parallel to the jet and hence the value of the T is equal to 1. For a di-jet event with jets in the back to back configuration the value of T is again equal to 1, as can be readily seen from Eq. 7.2.2. For an isotropically distributed configuration of jets, the value is close to $2/\pi$. The tail of the distribution is dominated by multi-jet events.

  We use this feature to good use for SUSY searches. We realize that SUSY processes where the heaviest particle (gluino or squark) cascades down to the lightest supersymmetric particle (LSP), the final state can have a large number of jets and leptons along with a significant amount of $\not{p}_T$ from the LSP. A typical region of interest which produce these kind of events in the framework of CMSSM is the region of moderate to high m_0 and relatively low $m_{1/2}$, leading to a low gluino mass and a high squark mass. In this case the gluino ($\tilde{g}$) decay mode proceeds as $\tilde{g} \rightarrow tb\chi_1^{\pm}, t\bar{t}\chi_2^0$ via off-shell squarks. The largest SM background namely QCD produces mostly di-jet events, and therefore the thrust distribution in this case lies close to 1. Thus putting a cut of $\tau > 0.1$ suppresses a huge amount of the QCD background leaving the signal mostly unaffected. The thrust distribution expressed in terms of $\tau = 1 - T$, subject to the cuts described in the figure is presented in Fig. 7.3. We can thus observe a clear distinction between signal and background processes [19] particularly QCD which lies close to 0.

- R_T: The remaining major background consists of the irreducible $Z(\rightarrow \nu\bar{\nu})$ + jets and the W+ jets background. Note that since the parent SUSY particle (gluino or squark) is fairly heavy the resulting jets are hard. Additionally the fact that the process consists of multi-jets motivates us to construct a ratio of the transverse momenta called R_T [19] and defined as,

$$R_T = \frac{\sum_1^{n_j^{min}} p_T^{j_i}}{H_T}, \tag{7.2.3}$$

  where the numerator runs over a minimum number of pre-selected jets (n_j^{min}) depending on the signal topology. The denominator H_T is the scalar sum of the transverse momenta of all

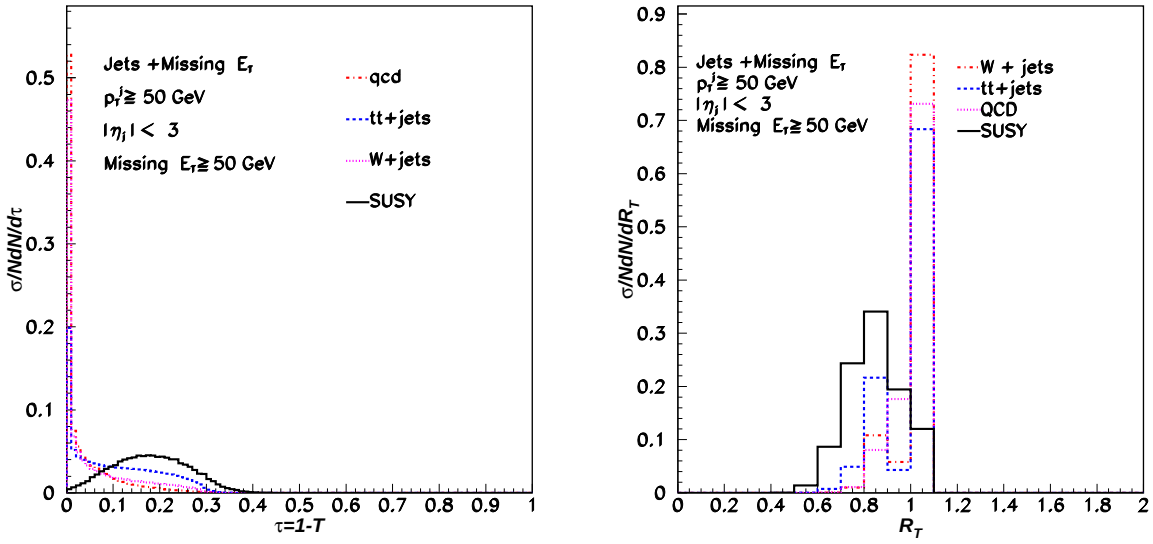

Figure 7.3: The $\tau = 1 - T$ distribution(left panel) and the R_T distribution(right panel). The benchmark signal point is in the CMSSM framework for $m_0 = 1500, m_{1/2} = 310, \tan\beta = 10, A_0 = 0, \mathrm{sgn}(\mu) > 0$ for 8 TeV LHC energy. The jet p_T threshold is chosen to be 50 GeV within $|\eta| < 3$. The figure is normalized to luminosity.

jets in a given event. For events which peak at 1, $n_j = n_j^{min}$, while values less than 1 are for events where the number of jets present in the event are greater than n_j^{min}. In our study we choose R_{T4}, implying $n_j^{min} = 4$. This is illustrated in the R_T distribution in the right hand panel of the Fig. 7.3, where the peak at 1, represents events with $n_j^{min} = n_j = 4$, while events at the tail of the distribution are corresponds to where $n_j \gg n_j^{min}$.

This is more than a naive implementation of a cut on the total number of jets, as this cut also utilizes the hardness of the final state objects. This variable is most effective in suppressing the $W(\to l\nu)$ + jets and the irreducible $Z(\to \nu\bar{\nu})$+jets background. For SM backgrounds the sub leading jets are expected to be much softer than the corresponding SUSY processes, where the jets originate from a fairly massive parent particle. Hence the tail of R_T distribution is expected to fall to much lower values for the signal process as compared to the background process.

Notice from Fig. 7.3, almost all the SM backgrounds, with $n_j > n_j^{min}$, falls close to 1, while the SUSY processes fall to values as low as 0.55. We put a cut $R_T < 0.85$ to optimize the signal to background ratio.

- M_T^{jj} : Finally the remaining background consists of $t\bar{t}$ + jets which can have a significantly high number of jets along with $\not{p}_T$. To suppress this we construct the variable with the leading two jets in the event as,

$$M_T^{jj} = \sqrt{2p_t^{j1} \times p_T^{j2}(1 - cos\phi)}, \tag{7.2.4}$$

where ϕ is the angle between the leading two jets in the transverse direction. We note certain facts about this variable which helps us to suppress the large $t\bar{t}$ + jets background. The $t\bar{t}$ process, after the R_T cut is always in the high H_T region implying that the top pairs are in the

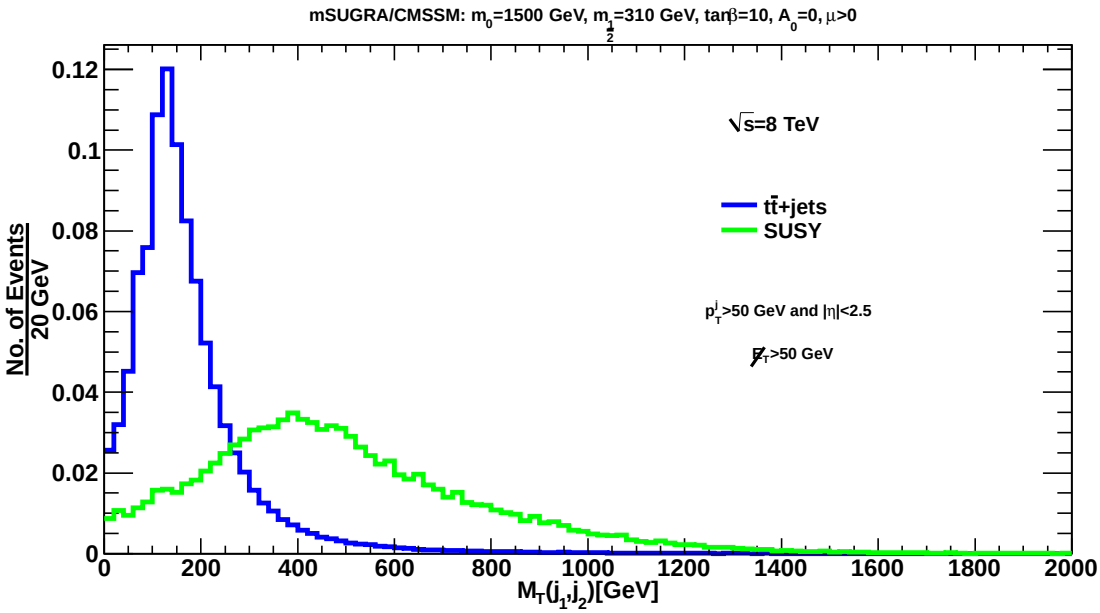

Figure 7.4: Comparison of M_T^{jj}) for $t\bar{t}$ and SUSY signal events subject to pre-selection cuts(Eq. 7.2.1) and with $\sqrt{S}$ =8 TeV. Parameter space P1 from Table 7.4 is used for SUSY.

boosted regime and hence the leading two jets are quite boosted and hard. Thus the opening angle ϕ between the two leading jets in this case is quite small, leading to a smaller value of M_T^{jj}. However in the SUSY signal, the leading jets are isotropically distributed, leading to a larger value of M_T^{jj} as the opening angle ϕ between the leading two jets are larger. This can be observed in Fig. 7.4 (subject to preselection cuts as described in the figure at 8 TeV), where we observe that the the distribution for the $t\bar{t}$ process peaks at 200 GeV, while the SUSY process peaks at 400 GeV and the tail extends to more than 1 TeV. There are other processes (not shown in the figure just for the sake of presentation), like the remaining fraction of W+ jets and Z+jets, which also suffer significantly To optimize the signal and the background where a cut of $M_T^{jj} > 450$ GeV can be applied at 8 TeV.

- H_T : In addition we also employ the H_T cut to reduce a certain fraction of the background.
- M_T : For the single lepton case, in all backgrounds, the lepton mainly comes from W decay, and hence the transverse mass between the lepton and $\not{p}_T$ is expected to be bounded by the W mass. Hence, events with a single lepton case is expected to suffer due to a cut on transverse mass [259],

$$M_T = \sqrt{2E_T^{\ell}\not{p}_T(1-\cos\phi(\ell,\not{p}_T))} \geq 60\ GeV,$$

  where ϕ is the azimuthal angle between the lepton and the $\not{p}_T$ direction.
- $m_{\ell^+\ell^-}$: For the dilepton case we use the additional cut on $m_{\ell^+\ell^-} \geq$10 GeV and $m_{\ell^+\ell^-} \neq$70-120 GeV to remove the $Z(\rightarrow l^+l^-)$ + jets background as the dilepton invariant mass is expected to give a peak at the Z boson mass. The cut $m_{\ell^+\ell^-} \geq$10 GeV is used to suppress dilepton mass peaks originating from a soft ISR photon splitting into dileptons.
- $\not{p}_T$: A $\not{p}_T > 150$ GeV is applied for all the search channels.

The left panel of Table 7.3 summarizes the cuts for various search channels.

As was the practice in the early analysis of SUSY search strategies at the LHC the model framework of CMSSM [4, 5, 255] was used to probe SUSY signatures.

As a recap we remind ourselves that the model is described by 4 parameters and a sign. These are $m_0, m_{1/2}$ an A_0, namely the universal scalar mass, the universal fermion mass and the universal trilinear coupling respectively, specified at the GUT scale. The remaining two parameters include $\tan\beta$, the ratio of the VEVs of two Higgs doublets and sgn(μ), where μ is the higgsino mass parameter, determined at the electroweak scale. The sparticle spectrum at the electroweak scale is determined by renormalization group evolution(RGE) from the GUT scale to the electroweak scale. The software package SUSPECT [14] is used to generate the sparticle spectrum. SUSPECT uses two loop RGE while evolving from a generic high scale SUSY breaking model to the electroweak scale, where all the masses and mixing angles are calculated. The subsequent branching ratios were computed using the interface SUSYHIT [15].

For the 7 TeV analysis where event shape variables were used for the first time in SUSY searches [19], the values of A_0, $\tan\beta$, sgn(μ) were fixed to 0, 45 and +1 respectively. Table 7.2 shows the benchmark points used for this analysis.

	P1	P2	P3	P4
m_0	500	1500	500	450
$m_{1/2}$	200	200	400	500
$m_{\tilde{g}}$	524	575	954	1161
$m_{\tilde{q}}$	660	1535	981	1133
$m_{\tilde{\chi}^{\pm}_{1,2}}$	142,296	126,241	308,515	391,623
$m_{\tilde{\chi}^{0}_{1,2}}$	78,143	76,130	164,309	207,392
$m_{\tilde{\chi}^{0}_{3,4}}$	274,295	196,240	499,514	610,623
μ	266	208	495	607
σ(pb)	2.5	0.32	0.08	0.018

Table 7.2: Masses(in GeV) of SUSY particles for four sets of $m_0, m_{1/2}$ and fixed values of A_0=0, $\tan\beta$=45, sign(μ)=+1. The leading order cross sections(σ) for SUSY particle production are in the last row. The mass of the top quark is set to 173.2 GeV

	1-lepton	di-lepton	jets+ $\not{p}'_T$
lepton	1	2	no-veto
T	< 0.9	<0.9	<0.9
R_T	<0.85	< 0.85	< 0.85
M_T^{jj}	-	-	450 GeV
$M_T^{l\nu}$	> 60 GeV	-	-
$m_{l^+l^-}$	-	70-110 GeV	-
H_T	900 GeV	900 GeV	1 TeV
$\not{p}'_T$	150 GeV	150 GeV	150 GeV

	Total Bg	P1	P2	P3	P4
$1\ell(\sigma_{0\not{p}'_T})$	101	179	20	7	2
$1\ell(\sigma_{\not{p}'_T})$	2.65	70.	8	5	1.3
$2\ell(\sigma_{0\not{p}'_T})$	5.43	56	7	2	0.5
$2\ell(\sigma_{\not{p}'_T})$	0.97	31	4	1.8	0.5
Jets$(\sigma_{\not{p}'_T})$	3.7	271	32.5	21.8	4.63

Table 7.3: The summary of cuts for 7 TeV event shape analysis(left hand side). Total signal(P1-P4) and background cross sections(fb) before and after $\not{p}'_T$ cut ($\sigma_{0\not{p}'_T}$,$\sigma_{\not{p}'_T}$ respectively) for the single lepton(1ℓ), di-lepton(2ℓ) and jets plus $\not{p}'_T$ case(right hand panel).

The event summary for the single lepton case can be found in [19]. In the right panel of Table 7.3, the final cross sections after all cuts for 7 TeV for all the channels is summarized. The con-

servative estimate predicts that in the single lepton channel and as well as the jets + $\not{p}_T$ channel, it is possible to achieve a reasonable signal-to-background ratio for $\tilde{g}$ and $\tilde{q}$ masses up to $\sim$ 1.1 TeV whereas the di-lepton channel alone is not very encouraging. It has to be noted that this conclusion is based on LO signal cross sections whereas in background evaluation the higher order effects are taken into account to a certain extent by considering hard emission of partons(jets), which is the real part of the NLO correction. Clearly, the discovery reach is signal rate limited rather than background limited, which is quite small after all cuts.

7.3 The updated event shape analysis at 7 TeV and 8 TeV LHC energy.

After scrutinizing the previous selection strategy and correlation of cuts [19] very closely, it was realized that the H_T cut was redundant and can be removed entirely. In addition, we also updated our study for 8 TeV LHC energy. In order to find the sensitivity of our search strategy we scan the entire region of CMSSM parameter space and predict the discovery reach of SUSY signal. Moreover, we also compare our results with the CMS and ATLAS results for 7 TeV with 5 fb^{-1} data .

In SUSY events the H_T distribution in signal is expected to be on the higher side as jets emerging from cascade decays of heavier particles are more energetic than their SM counterparts and hence, it is used as one of the background rejection tool. Following this observation, in our previous analysis we also adopted this H_T variable to eliminate SM backgrounds [19].

Therefore in the later work [20] where we probed SUSY signatures at 7 TeV with 5 fb^{-1} and 8 TeV with 5 and 20 fb^{-1} luminosity this issue was investigated further for the jets + $\not{p}_T$ channel. For this analysis , the following sets of cuts were imposed,

$$\tau > 0.1, \;\; R_T(4) < 0.85,$$
$$M_T^{jj} > 450 \text{ GeV}, \not{p}_T > 250 \text{ GeV}. \tag{7.3.1}$$

In Fig. 7.5, we present the interplay of cuts by making a two dimensional plot in $\not{p}_T - H_T$ plane imposing selection on τ and $R_T(4)$, as Eq. 7.3.1, requiring at least 4 jets in the event for both signal and all SM backgrounds. The signal benchmark point chosen in this case corresponds to P1 in Table 7.4. The $\not{p}_T - H_T$ distribution shown in Fig. 7.5 clearly reveals that signal events are located at the high H_T ($\gtrsim$ 750 GeV) region and in addition, requiring $\not{p}_T$ >250 GeV, it is possible to get rid of contamination due to the SM backgrounds. This exercise justifies the claim of dropping H_T cut from our selection strategy. These features are in stark contrast to almost all multijet search strategies which requires a large H_T cut in their analysis [260]. One of the most important background to SUSY searches is the irreducible $Z(\rightarrow \nu\bar{\nu})$+jets background with multijets and a large amount of $\not{p}_T$ [254]. Using $R_T(4)$ we have successfully managed to suppress this background

Model	μ	$A_{t,b,\tau}$	$\tilde{g}$	$\tilde{q}$	$\tilde{t}_1$	$\tilde{t}_2$	$\tilde{b}_1$	$\tilde{b}_2$	$\tilde{e}_l$	$\tilde{\tau}_1$	$\tilde{\chi}_1^0$	$\tilde{\chi}_2^0$	$\tilde{\chi}_1^+$	$\tilde{\chi}_2^+$
P1	408	541,803,184	825	1609	1004	1349	1155	1257	1507	1489	127	228	227	354
P2	645	909,1342, 308	1217	1238	916	1150	1120	1198	707	641	215	406	406	663

Table 7.4: Mass spectrum for benchmark point (P1) m_0 =1500 GeV, $m_{1/2}$=310 GeV tanβ=10.A_0=0, sgn(μ)$\geq$0, (P2)m_0 = 620 GeV, $m_{1/2}$ =520 GeV, tanβ=10. A_0=0, sgn(μ)$\geq$0 for the 8 TeV analysis. The top mass m_t is set to 173.2 GeV.

to a rather small level. It must also be emphasized that this variable being a dimensionless quantity is prone to less systematics, and is a fairly simple variable to implement in experiments.

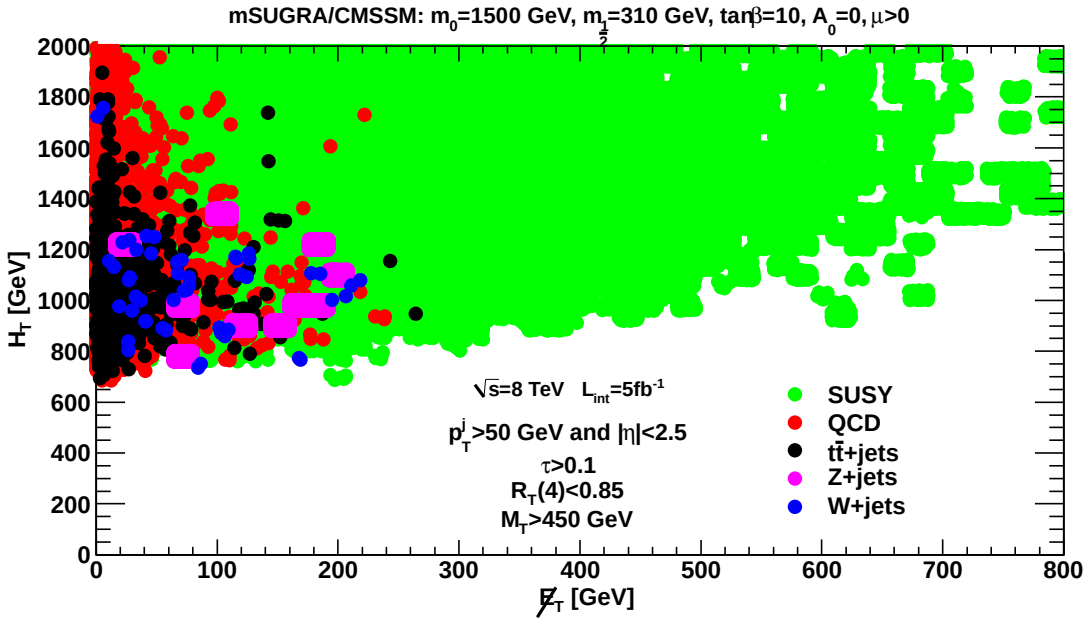

Figure 7.5: Distribution of signal and background events with $\tau > 0.1$, $R_T(4) < 0.85$, $M_T^{j_1,j_2} > 450$ GeV along with pre-selection cuts, Eq.7.2.1. Parameter space P1 in Table 7.4 is used for SUSY.

In order to understand the impact of our selection strategy as discussed in the previous section, we analyzed SUSY signal for two benchmark points shown in Table 7.4. One of the points(P1) corresponds to a lower gluino mass and a relatively higher squark mass in contrast to the other point(P2) where gluino and squark masses are almost equal. In Table 7.5, we summarize the cumulative effect of cuts for a center of mass energy 8 TeV. The production cross sections (CS) are presented in the second column of Table 7.5. It is to be noted that the signal cross sections are at the next-leading-order [17] level where as partially higher order corrections are taken into account by considering associated jets in the background processes. The 3rd column shows the number of events(N) generated and it is made sure that it corresponds to at least $5fb^{-1}$ integrated luminosity. From the 4th column onwards the number of events due to cumulative effect of cuts are presented. Finally, in the last column, the number of events selected after all cuts including matching efficiencies(Eq. 7.3.1) are shown normalized to cross section for $5fb^{-1}$ luminosity. In addition we also simulate signal and backgrounds with proper statistics for $20fb^{-1}$ luminosity for which only final results are presented.

The benchmark points(P1 and P2) are so chosen as to reveal the difference in the type of event distribution for the two points. The first point P1(Table 7.4) has a lower gluino mass and a comparatively higher squark mass which implies that the primary decay mode of gluino will be through $\tilde{g} \to tb\chi_1^{\pm}, t\bar{t}\chi_{1,2}^0$ via virtual top squarks. With top decaying in the hadronic mode for about 2/3, it yields a large number of jets. We find as expected that the suppression due to the thrust cut($\tau > 0.1$) for the signal is about 20% whereas for background it is the close to 90% for some cases, QCD in particular. The R_{T4} selection variable is effective for multijet backgrounds and is reflected in the 5th column of Table 2. Eventually, the M_T^{jj} cut as discussed previously is useful to get rid of the remaining top background. However, in case of parameter space P1 i.e for high m_0 and low

Process	C.S(pb)	N	τ > 0.1	R_{T4} $\leq .85$	M_T^{jj} ≥ 450 GeV	$\not{p}_T$ ≥ 250 GeV	# of Events $\mathscr{L} = 5fb^{-1}$
P1							
$\tilde{g}\tilde{g}$	0.087	20K	16809	9186	3840	1025	22.3
$\tilde{q}\tilde{g}$	0.023	20K	16474	9776	7363	3458	19
P2							
$\tilde{g}\tilde{g}$	0.002	20k	17781	13650	6227	3810	1.73
$\tilde{q}\tilde{g}$	0.015	20K	14895	5286	3490	2883	10.5
$\tilde{q}\tilde{q}$	0.02	20k	10713	1068	451	299	1.3
tt							
5-200	85	0.3M	147181	5738	133	0	0
200-500	10	0.1M	29490	4518	328	2	1
500-inf	0.13	20k	1986	248	147	9	0.3
$t\bar{t}+1j$	79.6	136083	68854	3354	20	0	0
$t\bar{t}+2j$	39.6	192983	11110	1180	14	0	0
$t\bar{t}+3j$	14.7	14993	9802	2239	110	0	0
$tt+4j$	4.5	12439	9192	3724	433	6	1.6
QCD							
300-500	1267	2M	263823	11765	4409	0	0
500-800	67	0.3M	32646	1720	1439	0	0
800-1500	3	0.1M	8110	412	394	0	0
1500-inf	0.01	10k	496	10	10	0	0
W+2j	1665	220879	122079	2	0	0	0
W+3 j	436.2	99616	43712	3	0	0	0
W+ 4j	105.3	68923	25324	342	36	0	0
Z+2j	1670	120199	67406	0	0	0	0
Z+3j	450	241202	106864	6	0	0	0
Z+4j	110	39203	17706	133	10	0	0

Table 7.5: Number of events after each set of cuts for signal and background for $\sqrt{S}$ =8 TeV. In the the last column, number of events are normalized for 5 fb^{-1} luminosity.

$m_{1/2}$, the mass differences among $\chi_1^{\pm}, \tilde{\chi}_2^0$ and χ_1^0 are comparatively small resulting in less available energy for final state particles leading to a softer spectrum including soft $\not{p}_T$. As a consequence, the effect of $\not{p}_T$(>250 GeV) cut is severe for signal in this case, as reflected in the penultimate column in Table 7.5. Hence, total acceptance efficiency turns out to be small yielding low signal sensitivity in this region.

The benchmark point P2 with m_0 and $m_{1/2}$ nearly equal, is different in the fact that the gluinos will preferentially decay to $\tilde{t}$ t with physical top squarks decaying further to $t\ \chi_{1,2}^0$. Hence the gluino decay will still yield a fair number of jets in the final states. The 1st two generation squarks will however decay predominantly to $q\chi_1^{\pm}$ with charginos decaying to $W\chi_1^0$. This channel therefore yields a less jet activity in most cases which is suppressed by the $R_T(4) < 0.85$, as can be seen from Table 7.5. In Table 7.6, we show the total number of background and signal events after all selection cuts for two parameters points P1 and P2 normalizing to cross section at $5fb^{-1}$ luminosity. We observe about 4(3) background events for integrated luminosity $5fb^{-1}$ at 7(8) TeV energy against a handful of signal events yielding $S/\sqrt{B}$ more than 5 for two selected representative signal parameters points P1 and P2. The suppression of background events indicate the robustness of our selection strategy.

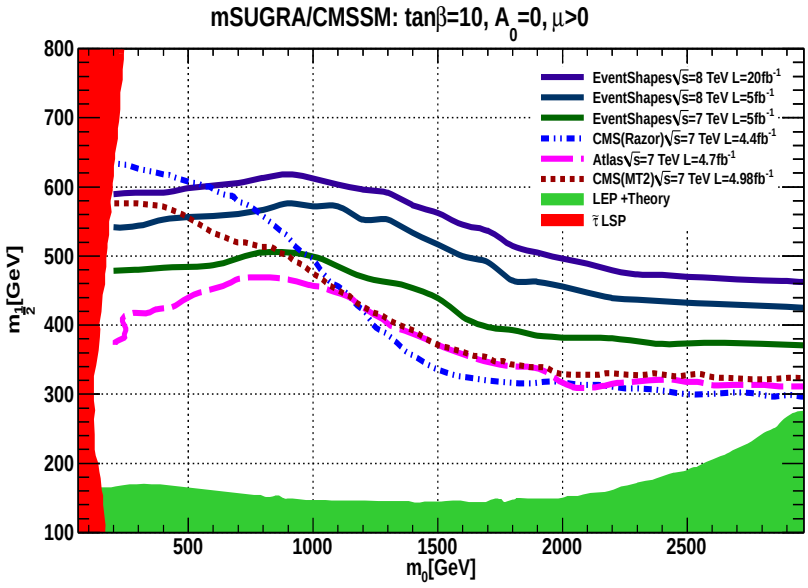

Figure 7.6: Discovery reach requiring $S/\sqrt{B} \geq 5$ for tanβ= 10, $A_0 = 0$, sign(μ)=+1. The two CMS(MT2 and Razor) [21, 258] and ATLAS [260] exclusion plots are at 95% C.L. The green shaded region is disallowed by theory and LEP constraints, red shaded region is forbidden by $\tilde{\tau}_1$ LSP condition.

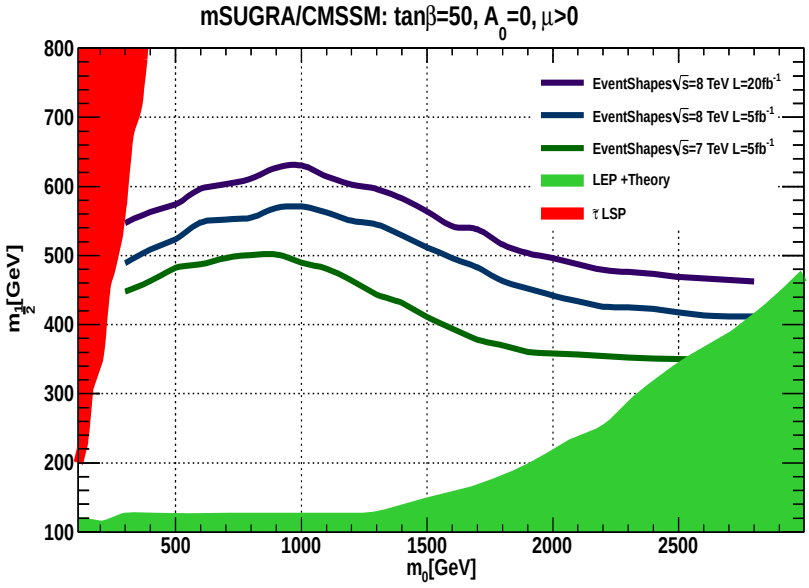

Figure 7.7: Same as Fig. 7.6, but for tanβ=50.

Armed with this selection strategy, we attempt to find the potential discovery region in the $m_0 - m_{1/2}$ plane. We scan the $m_0 - m_{1/2}$ parameter space setting A_0=0, sign(μ)=+1, tanβ=10, 50 and estimate the signal rates applying cuts, Eq. 7.2.1 and 7.3.1. We require $S/\sqrt{B} \geq 5$ to claim discovery of SUSY signal for each set of parameters points for a given energy and luminosity. In Fig. 7.6 and Fig. 7.7 we present the discovery reach in the $m_0 - m_{1/2}$ plane for $\tan\beta = 10$ and $\tan\beta = 50$ respectively. In both the figures the shaded area along the x-axis are mainly disallowed by no-EWSB breaking condition as well as the limit on chargino mass(>102 GeV) from LEP experiments [66]. On the other hand the shaded region along the y-axis are ruled out because $\tilde{\tau}_1$ appears to be LSP which is assumed to be forbidden because of offering LSP as a dark matter candidate which has to be neutral. We present our results for 7 TeV with 5 fb^{-1} luminosity and 8 TeV energy with $5 fb^{-1}$ and 20 fb^{-1} luminosity. The total background and signal cross sections are presented in Table 7.6. It is expected that the discovery reach for 8 TeV is higher and this enhancement occurs mainly due to the enhancement of sparticle production cross sections, approximately by a factor of 2. Notice that in the same plane we also delineate regions excluded at 95% C.L. by CMS and ATLAS at 7 TeV energy with $4.4 fb^{-1}$ and $4.7 fb^{-1}$ luminosity respectively. Note that for tanβ =50 case, exclusion plots are not available from both the experiments at this integrated luminosity. Notice that the two CMS exclusion plots are due to the two methods

$\sqrt{S}$ TeV	$\mathscr{L}(fb^{-1})$	$t\bar{t}$	W+jets	Z+jets	QCD	Total Bg	SUSY P1	SUSY P2
7	5	2.83	<1	1.32	< 1	4.15	20.7	5.24
8	5	2.9	<1	< 1	< 1	2.9	41.3	13.53
8	20	7.2	<1	< 1	< 1	7.2	165	54

Table 7.6: First two rows(last row) present the number of signal and background events for $5 fb^{-1}$(20 fb^{-1}) luminosity subject to all selection cuts, (Eq. 7.2.1,7.3.1) corresponding to center of mass energies as shown.

MT2 [258] and Razor [21] with almost same luminosity. The ATLAS exclusion plot is obtained by demanding the number of jets $\geq$6 to $\geq$9 along with $\not{p}_T$ in the final states [260], which is the similar type of final states where our search strategy is most sensitive.It is to be emphasized that in both CMS and ATLAS analysis, no isolated leptons, electrons or muons are required. It helps to suppress backgrounds, mainly due to $t\bar{t}$ and W+jets. However, in our analysis we do not require to veto any such events to suppress these backgrounds. It seems from these figures that our selection strategy works better for high m_0 values where as for low m_0 case it is comparable with other results. A naive comparison of our results with a recent paper of Ref. [4] which predicts the gluino mass up to ~800 GeV whereas our analysis claims it ~1 TeV for 7 TeV 5 fb^{-1} luminosity in the high m$_0$(>1500 GeV) region. It is to be noted that the signal rates in the paper [4] correspond to inclusive channel, but in our case it is due to the jets plus $\not{p}_T$ channel. It is true that at the high m_0, as discussed before, the $\not{p}_T$ in the events is softer and hence signal selection based on tight cut on $\not{p}_T$ suffers and sensitivity degrades very fast. However, in our case, instead of high $\not{p}_T$ cut, we exploit the multiplicity of jets in the events, which is on higher side in this high m_0 region due to the presence of heavy flavors(t,b quarks) in $\tilde{g},\tilde{q}$, cascade decay chains as discussed previously. As a consequence, selections based on our strategy achieves better significance than the others which are based on very hard cut on $\not{p}_T$ and H_T. On the other hand, towards the higher side of $m_{1/2}$ and comparatively low m_0 values, the masses of gluinos and squarks are close to each other,

multiplicity of jets is relatively lower and hence our strategy suffers to some extent.We observed that the difference in tanβ does not make a significant impact in the discovery reach, which is ex-

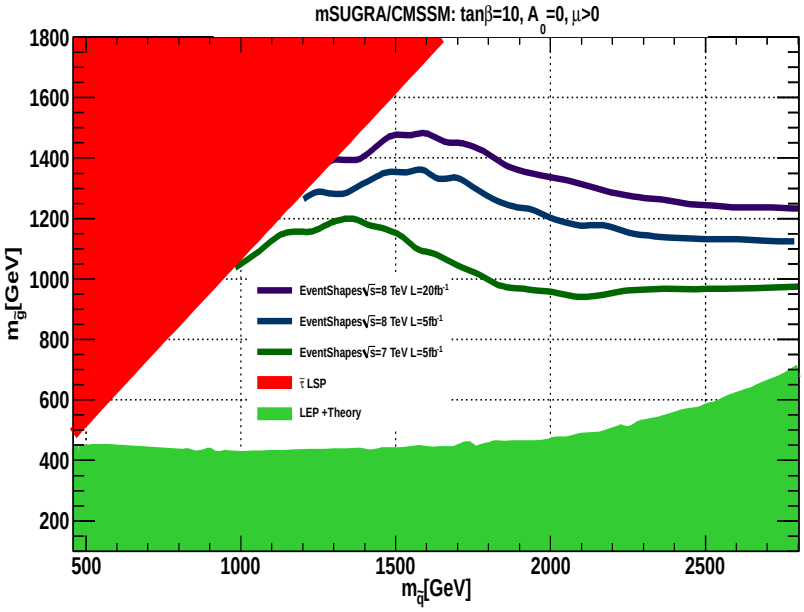

Figure 7.8: Discovery reach for tan β = 10,$A_0 = 0$, sign(μ=+1).

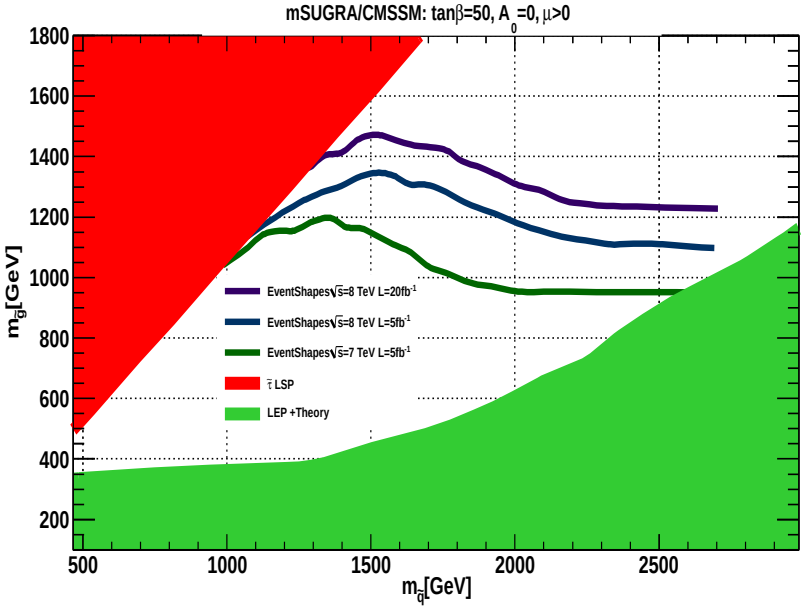

Figure 7.9: Same as Fig. 7.8, but for tan$\beta = 50$.

pected as rates in the hadronic channel is controlled by the cascade decays of the strong production process whereas tanβ affects the electroweak processes. However, the differences are subtle and appear only in parts of parameter space which has $\tilde{\tau}_1$ as the next to LSP due to large tan β and hence yield τ leptons in the final state. This yields a lesser number of jets in some parts of parameter space which in our search strategy translates to a lower reach in large tanβ region.

In order to understand the implication of this discovery region in $m_0 - m_{1/2}$ planes, we translate Figs. 7.6 and 7.7, to Figs. 7.8 and 7.9, which are in the physical $m_{\tilde{g}} - m_{\tilde{q}}$ mass planes (see 3.4.2 for mass relations between $m_0, m_{1/2}$ and $\tilde{g}, \tilde{q}$). Clearly, both the figures display the discovery reach of masses of $\tilde{g}$ for the corresponding $\tilde{q}$ masses and vice versa for a given set of SUSY parameter space. We find that for nearly degenerate case, $m_{\tilde{g}} \sim m_{\tilde{q}}$, it is possible to find SUSY signal for $m_{\tilde{g}}$ up to 1.2 TeV(1.35 TeV) for 7 TeV(8 TeV) energy with $5\,fb^{-1}$ luminosity where as for larger masses of $\tilde{q}$, this reach goes down to 1 TeV(1.1 TeV) for the same energy range. This conclusion remains true for high tanβ, case as well. For higher luminosity options, say $20\,fb^{-1}$ for 8 TeV energy this reach extends to $\sim$1.5 TeV. Note that our predictions are based purely from generator level analysis without taking care of any detector effects.

It is imperative to design search strategies that will access the edges of the SUSY parameter space. This will involve optimizing the signal to background ratio in large parts of the parameter space where the signal cross section is miniscule. In this study we have provided such a search strategy with its own merits of suppressing SM backgrounds to a rather small level. It must be emphasized that our strategy is not limited to CMSSM but expected to work also in other models which yield a large number of jets, for instance non-universal gaugino mass model [24] or the no scale F-SU(5) models which yield hard high multiplicity jets [261].

Chapter 8

Higgs signatures in MSSM

The observation of the Higgs boson is indeed the most important discovery in the MSSM framework in absence of any SUSY signal, as the lack of a Higgs boson would have ruled out MSSM. In section 3.6.2, it was shown that the tree level Higgs mass was bounded by the mass of the Z boson. However, it was also noted that loop corrections, dominated by top stop loops can significantly lift the mass of the lightest Higgs boson up to 135 GeV (Eq. 3.6.20). Therefore the 125 GeV Higgs boson can be accommodated in the framework of MSSM with certain choices of parameters.

The discovery of the Higgs boson puts a significant amount of restriction on the MSSM parameter space. Any spectrum of MSSM is required to have the correct Higgs mass, and hence this would rule out some of the available real estate in the MSSM landscape. The constraints on the MSSM parameter space post Higgs discovery has been carried out in a number of studies in various model contexts like CMSSM, non universal Higgs mass(NUHM), the next to MSSM(NMSSM), as well as in the framework of a general MSSM scenario [25, 33, 194–219].

While prima facie the large constraints imposed by the Higgs mass, and the inability to distinguish the lightest Higgs between SM and MSSM might seem a blow in its face, the discovery does indicate the region of parameter spaces,

(i.e regions with large scalar masses or light third generation squarks with maximal mixing scenarios) that one should be probing to find a SUSY signal.

On the practical side, the discovery of the Higgs boson allows us to study Higgs signatures in the framework of SUSY. Firstly, a Higgs signature in cascade decays of SUSY particles can be observed, increasing the production rate of the lightest Higgs boson. In this context we study the production of $\chi_1^\pm\chi_2^0$, and the subsequent decay of $\chi_2^0 \to \chi_1^0 h$, at 8 and 14 TeV LHC energy. Secondly, the decay of the lightest Higgs to a pair of SUSY particles can be a signal of MSSM. The prime example is the decay to a pair of LSP's which would evade the detector. This would result in an invisible branching ratio in the total Higgs decay width. In the following works we discuss both of the above possibilities.

8.1 Higgs signal from electroweak gaugino decays

In this section the prospects of a Higgs signal in sparticle decays is investigated. We study the production of chargino neutralino pairs and the subsequent decay of the neutralino to the lightest Higgs boson.

8.1.1 The production and decay of electroweak gauginos

Although the sparticle production at a hadron collider are dominated by strong interactions, the production of the electroweak gauginos can be significant for low masses($\lesssim$ 600 GeV). The production modes for these channels are schematically given by,

$$pp \rightarrow \chi_i \chi_j + X, \tag{8.1.1}$$

where i and j refer to chargino pairs, neutralino pairs or chargino-neutralino production processes. The production proceeds primarily through s channel quark annihilation and t channel squark exchange diagrams. The Feynman diagrams for the production modes are presented in Figure 8.1.

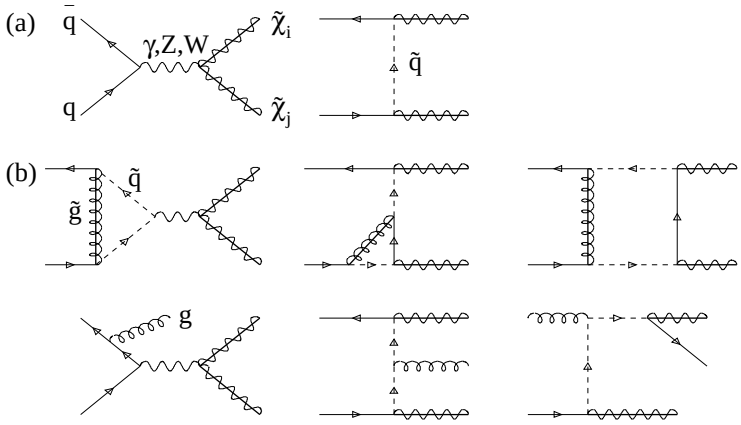

Figure 8.1: Feynman diagrams for the production of chargino/neutralino pairs at hadron colliders in quark-antiquark collisions; *a)* real diagrams, and *b)* NLO corrections.

The s channel process proceeds mainly through the coupling of the vector bosons to the gaugino($\tilde{W}$) and the higgsino($\tilde{H}$) components of the chargino and neutralino eigen states, while the squark exchange u and t channel diagrams are dominated by only the gaugino components. In terms of the unitary matrices $\mathscr{V}$,$\mathscr{U}$ and Z that diagonalize the chargino and the neutralino mass matrices, the eigen states can be written as (Eq. 3.5.1),

$$\begin{aligned}
\chi_i^+ &= \mathscr{V}_{ij}\,\psi_j^+, \qquad \text{basis:} \quad \psi_j^+ = \left(\tilde{W}^+, \tilde{H}_2^+\right), \\
\chi_i^- &= \mathscr{U}_{ij}\,\psi_j^-, \qquad \text{basis:} \quad \psi_j^- = \left(\tilde{W}^-, \tilde{H}_1^-\right), \\
\chi_i^0 &= Z_{ij}\,\psi_j^0, \qquad \text{basis:} \quad \psi_j^0 = \left(\tilde{B}^0, \tilde{W}^3, \tilde{H}_1^0, \tilde{H}_2^0\right).
\end{aligned} \tag{8.1.2}$$

The matrix element for the transition amplitudes are generally expressed in terms of bilinear charges defined in terms of the above unitary matrices after Fierze transformations. For the chargino neutralino pair production these are given by [262],

$$\begin{aligned}
Q_{LL} &= \frac{1}{\sqrt{2}\sin^2\theta_W}\left[\frac{Z_{j2}^*\mathscr{V}_{i1} - Z_{j4}^*\mathscr{V}_{i2}/\sqrt{2}}{s - M_W^2} + \frac{\mathscr{V}_{i1}}{cos\theta_W}\frac{Z_{j1}^*(e_{\tilde{q}} - I_{3\tilde{q}})\,sin\theta_W + Z_{j2}^* I_{3\tilde{q}}\,cos\theta_W}{u - m_{\tilde{q}}^2}\right], \\
Q_{LR} &= \frac{1}{\sqrt{2}\sin^2\theta_W}\left[\frac{Z_{j2}\mathscr{U}_{i1}^* + Z_{j3}\mathscr{U}_{i2}^*/\sqrt{2}}{s - M_W^2} - \frac{Z_{i1}^*}{cos\theta_W}\frac{Z_{j1}(e_{\tilde{q}'} - I_{3\tilde{q}'})\,sin\theta_W + Z_{j2} I_{3\tilde{q}'}\,cos\theta_W}{t - m_{\tilde{q}'}^2}\right] \\
Q_{RL} &= Q_{RR} = 0,
\end{aligned} \tag{8.1.3}$$

with $s=(p_q+p_{\bar{q}})^2$, $t=(p_q-p_{\tilde{\chi}_i})^2$ and $u=(p_q-p_{\tilde{\chi}_j})^2$.

The leading order parton level cross section is given by [262],

$$\frac{d\hat{\sigma}}{dt}[q\bar{q}^{(\prime)}\to\chi_i\chi_j]=\frac{\pi\alpha^2}{3s^2}\left[(|Q_{LL}|^2+|Q_{RR}|^2)\,u_iu_j+(|Q_{LR}|^2+|Q_{RL}|^2)\,t_it_j\right.$$
$$\left.+2\,\mathrm{Re}(Q^*_{LL}Q_{LR}+Q^*_{RR}Q_{RL})\,m_{\tilde{\chi}_i}m_{\tilde{\chi}_j}s\right], \tag{8.1.4}$$

where $t_{i,j}=t-m^2_{\tilde{\chi}_{i,j}}$ and $u_{i,j}=u-m^2_{\tilde{\chi}_{i,j}}$.

At the NLO level SUSY-QCD corrections, qqV and q$\tilde{\mathrm{t}}\chi$ vertex corrections enhance the leading order cross sections by K factors ranging from 1.2 to 1.35 [262]. The electroweak corrections are sub dominant and increase the Born cross section by about 5% [263]. At 14 TeV the NLO cross sections for the $\chi_1^\pm\chi_2^0$ pair production varies from as large 10 pb for masses of 100 GeV(assuming the masses of $\chi_1^\pm,\chi_2^0$ to be degenerate) to about 500 fb for 500 GeV.

The decay of charginos and neutralinos to gauge bosons and the Higgses are governed by the couplings of vertices, $\chi_i^0-\chi_j^+-W$, $\chi_i^0-\chi_j^0-\phi(\phi=Z/h/H/A)$.

• The relevant couplings for the decays of charginos and neutralinos to the weak gauge bosons $W^\pm,Z$ are expressed as [158]:

$$G^{L,R}_{\chi_i^0\chi_j^+W^+}=G^{L,R}_{ijW}\quad\text{with}\quad\begin{array}{l}G^L_{ijW}=\frac{1}{\sqrt{2}sin\theta_W}[-Z_{i4}\mathscr{V}_{j2}+\sqrt{2}Z_{i2}\mathscr{V}_{j1}]\\ G^R_{ijW}=\frac{1}{\sqrt{2}sin\theta_W}[Z_{i3}\mathscr{U}_{j2}+\sqrt{2}Z_{i2}\mathscr{U}_{j1}],\end{array} \tag{8.1.5}$$

$$G^{L,R}_{\chi_i^0\chi_j^0Z}=G^{L,R}_{ijZ}\quad\text{with}\quad\begin{array}{l}G^L_{ijZ}=-\frac{1}{2sin\theta_W cos\theta_W}[Z_{i3}Z_{j3}-Z_{i4}Z_{j4}]\\ G^R_{ijZ}=+\frac{1}{2sin\theta_W os\theta_W}[Z_{i3}Z_{j3}-Z_{i4}Z_{j4}].\end{array} \tag{8.1.6}$$

If $\chi_1^\pm$ is gaugino like (for $\mu\gg M_1,M_2$), the primary decay mode is $\chi_1^\pm\to W^\pm\chi_1^0$, via on or off shell W depending on the mass difference $\chi_1^\pm-\chi_1^0$. If there are squarks and sleptons that are lighter than $\chi_1^\pm$, the decay of charginos to sfermions are kinematically open, and hence the charginos decay as $\chi_1^\pm\to\tilde{f}f'\to ff'\chi_1^0$.

• The couplings of the neutralinos to the Higgs bosons:

$$G^{L,R}_{\chi_i^0\chi_j^0H_k}=G^{L,R}_{ijk}\quad\text{with}\quad\begin{array}{l}G^L_{ijk}=\frac{1}{2\sin\theta_W}\left(Z_{j2}-\tan\theta_WZ_{j1}\right)(e_kZ_{i3}+d_kZ_{i4})\;+\;i\leftrightarrow j\\ G^R_{ijk}=\frac{1}{2\sin\theta_W}\left(Z_{j2}-\tan\theta_WZ_{j1}\right)(e_kZ_{i3}+d_kZ_{i4})\,\varepsilon_k\;+\;i\leftrightarrow j,\end{array} \tag{8.1.7}$$

where $\varepsilon_{1,2}=-\varepsilon_3=1$ and the coefficients e_k and d_k are given by,

$$e_1/d_1=-tan\alpha\;,\;e_2/d_2=tan\alpha\;,\;e_3/d_3=-tan\beta, \tag{8.1.8}$$

where alpha is the mixing angle in the Higgs sector defined in Eq. 3.6.15, and tanβ is the usual ratio of the VEV s of the two Higgs doublets.

It should be noted that the W boson couples to both gaugino and higgsino components of the charginos. The Z boson on the other hand couples only to the Higgsino. We are interested in the decay mode $\chi_2^0\to\chi_1^0h$. The decay $\chi_2^0\to\chi_1^0h$ is kinematically allowed when the condition $M_2-M_1>m_h$ is satisfied. The decay mode that competes in this region of parameter space is the decay to the Z boson, namely $\chi_2^0\to\chi_1^0Z$. The coupling of the neutralinos to the Z boson depends crucially on the up type and the down type higgsino components and is given by Eq. 8.1.6,

$$Z_{i3}Z_{j3}-Z_{i4}Z_{j4}.$$

In this case, the decay $\chi_2^0 \to \chi_1^0 Z$ is strongly suppressed, as compared to $\chi_2^0 \to \chi_1^0 h$ in which the couplings depend on the product of gaugino and the higgsino components. In this region the decay $\chi_2^0 \to \chi_1^0 h$ can be as large as 95% [264] for 125 GeV.

8.1.2 Collider strategy and analysis of the signal

As mentioned in the previous section (8.1.1), we probe the decay channel [34],

$$pp \to \chi_1^+ \chi_2^0 \to W(\to l\nu)h(\to b\bar{b}) + 2\chi_1^0 \to \ell + b\bar{b} + \not{p}_T, \tag{8.1.9}$$

in the framework of CMSSM. To get a reasonable branching ratio for the decay, $\tilde{\chi}_2^0 \to \tilde{\chi}_1^0$h, $|\mu|$, the higgsino mass parameter is chosen to be large leading to the $\tilde{\chi}_1^\pm$, $\tilde{\chi}_2^0$ and $\tilde{\chi}_1^0$ states being gaugino like. Therefore, for very high values of $|\mu|$ (i.e., $|\mu| >> M_2, M_1$), $m_{\tilde{\chi}_1^\pm}$, $m_{\tilde{\chi}_2^0} \sim M_2 \sim M_{\tilde{g}}/3$ (see 3.5.1 and 3.4.1).

Hence, taking into account the limit on the $\tilde{g}$ mass, [1] $m_{\tilde{\chi}_1^\pm}$ and $m_{\tilde{\chi}_2^0}$ were expected to be around 250 GeV or more. For the sake of presentation of our results we select three benchmark points(P1-P3) corresponding to progressively higher values of gaugino masses which are presented in Table 8.1.

	$m_{1/2}$	μ	m_h	$m_{\tilde{g}}$	$m_{\tilde{q}}$	$m_{\tilde{t}_1}$	$m_{\tilde{\chi}_1^0}$	$m_{\tilde{\chi}_2^0}$	$m_{\tilde{\chi}_1^\pm}$
P1	300	1541	122.4	865	3000	1305	133	265	265
P2	380	1660	122.8	1046	3060	1335	168	332	332
P3	450	1653	123.2	1200	3096	1370	198	390	390

Table 8.1: Masses of some of the sparticles for three benchmark points. In all the cases $m_0 = 3000$, $\tan\beta$=30 and A_0=-4500. All mass units are in GeV.

We investigate the Higgs signal in SUSY cascade decay, given by Eq. 8.1.9, leading to a final state with a hard lepton(e, μ) from W decay and two b-jets from Higgs decay and a large $\not{p}_T$ due to the presence of $\tilde{\chi}_1^0$ and ν, but without any additional jet. The identical final state may also come from $t\bar{t}$, W$b\bar{b}$, Z$b\bar{b}$, WZ, Wh, Zh, tb, tbW processes. Recall that the $\tilde{\chi}_1^\pm \tilde{\chi}_2^0$ pair production cross sections(C.S.) for our considered parameter space are about 30-175 fb (LO) for 8 TeV in contrast to background cross sections which vary from few picobarn(pb) to more than 100 pb. Thus a huge suppression of background events is required to achieve a reasonable signal sensitivity, which is a challenging task. The added advantage is that the invariant mass constructed out of two b jets is expected to show a peak at the Higgs mass, which can be exploited to identify the signal region. Therefore, a good reconstruction of Higgs mass out of two b jets is one of the crucial issue to be studied in this analysis. In this analysis we report about the simulation of signal and backgrounds adopting two methods for Higgs reconstruction. In the first method(Method A) we identify two b-jets out of all jets in the events and obtain the Higgs mass by calculating their invariant mass. In the second method(Method B) reconstruction of Higgs mass is performed by using the jet substructures which will be discussed later. In this paper we present our results for both cases, method A and B.

In our simulation, events are generated using `PYTHIA` [6] for the signal and $t\bar{t}$, WZ, Wh, Zh backgrounds whereas `ALPGEN` [9] interfaced with `PYTHIA` has been used for the generation of tb, tbW, $Wb\bar{b}$ and $Zb\bar{b}$ backgrounds. We adopt MLM matching [11] to avoid double counting while performing parton showering after matrix element calculations in ALPGEN. We use `FastJet` for jet

[1] Corresponding to 8 TeV 5 fb^{-1} data

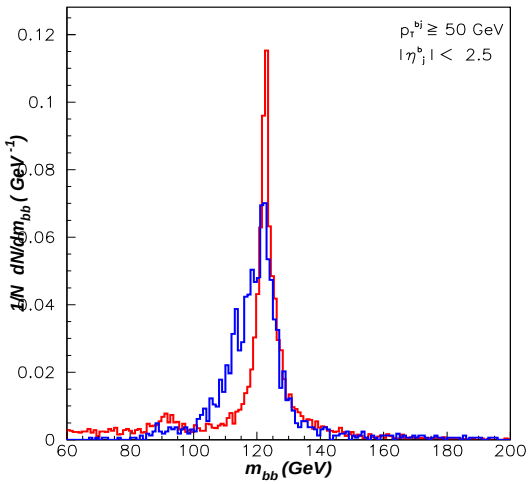

Figure 8.2: The reconstructed Higgs mass for method A (blue) and method B (red) for $\sqrt{s} = 8$ TeV. The y-axis is normalized to unity.

reconstruction using built-in anti-k_T algorithm [7] with ΔR=0.5 in method A, whereas Cambridge-Aachen [242] algorithm is used for method B. We use CTEQ6L parton distribution function while calculating cross sections [13]. `SuSpect` interfaced with `SUSYHIT` [15] is used to calculate SUSY mass spectrum and corresponding branching ratios.

We observe that use of Higgs mass reconstruction alone is not enough to eliminate backgrounds substantially. A certain set of selection cuts described below are necessary to reject backgrounds.
• Lepton : Leptons (e and μ) are selected with $p_T^{\ell} \geq 20$ GeV and $|\eta| \leq 2.5$. Isolation of leptons are ensured by estimating the total transverse energy $p_T^{AC} \lesssim$20% of p_T^{ℓ}, where p_T^{AC} is the scalar sum of transverse energies of jets close to leptons satisfying $\Delta R(\ell, j) \leq$0.2. We veto events if there exists a second lepton with a loose criteria of $p_T^{\ell} \geq 10$ GeV, primarily to suppress top background.
• Jets: Jets are selected using `FastJet` [8] with a $p_T \geq$50 GeV and $|\eta| \leq$3($|\eta| <$2.5 for method B).
• b-Jets: b like jets are identified by performing a matching of jets with b quarks assuming a matching cone $R(b, j) =$0.5. In addition, we require that the matched b jet transverse momentum should have at least 80% of the b quark transverse momentum. A proper method of b-tagging using displaced vertex is beyond the scope of this analysis. Finally, we multiply by a b-tagging efficiency(ε_b) of 70% [265] for each b-tagging i.e ε_b^2=0.5 for two b-tagged jets while estimating total event rates.
• $\not{p}_T$: Missing transverse momentum is calculated out of all visible stable particles. The $\not{p}_T$ in the signal arises due to the massive $\tilde{\chi}_1^0$ and ν as well, whereas in background events, it solely arises from ν in W decay. Nevertheless, the hardness of $\not{p}_T$ in signal is not significantly different than the large $t\bar{t}$ background making it very difficult to distinguish the signal from the background.
• $R_T^{b\bar{b}}$: We define a very robust variable which is extremely efficient in eliminating backgrounds by huge fraction as discussed in a previous analysis [19]. It is defined as,

$$R_T^{b\bar{b}} = \frac{p_T^{b_1} + p_T^{b_2}}{H_T},$$

where the numerator is the scalar sum of p_T of the two b-jets and H_T is the scalar sum of p_T

of all jets passing our pre-selection criteria. We define this variable keeping in mind that in the signal process no hard jets are expected except two b-jets from Higgs decay. Of course, few jets may arise from initial and final state radiations, but the number of such jets with $p_T \geq 50$ GeV is expected to be low. Hence $R_T^{b\bar{b}}$ turns out to be ~ 1 for signal. In backgrounds, particularly in top pair production there are additional hard jets arising due to the hadronic decay of W(since we are giving a veto on the second lepton) resulting in $R_T^{b\bar{b}} < 1$. Thus a judicious choice of a upper cut on $R_T^{b\bar{b}}$ suppresses backgrounds enormously without affecting the signal much.

• $\phi^{b\bar{b}}$: The azimuthal angle $\phi^{b\bar{b}}$ is defined as the angle between two b-jets in the transverse plane. In the signal process the angle is expected to be small, but in backgrounds, for example in top pair production they are in general widely separated. It has to be emphasized here that with the increase in $\tilde{\chi}_2^0$ mass, the $h \to b\bar{b}$ system gets more and more boosted and hence the b jets become more and more collinear which is an ideal situation for the jet substructure analysis described in the following section. We find that a reasonable cut on $\phi^{b\bar{b}}(\phi^{b\bar{b}} \leq 2)$ suppresses the backgrounds from $Wb\bar{b}$ and $t\bar{t}$ processes considerably.

• $M_T(\ell, \not{p}_T)$: The transverse mass is defined as $M_T = \sqrt{2p_T^{\ell} \not{p}_T (1 - \cos\phi(\ell, \not{p}_T))}$, where $\phi(\ell, \not{p}_T)$ is the azimuthal angle between the lepton and $\not{p}_T$ direction. The value of $M_T(\ell, \not{p}_T)$ is expected to be restricted by W mass if both leptons and $\not{p}_T$ originate from W decay, which is the case for backgrounds, particularly for $t\bar{t}$ and $Wb\bar{b}$ channels. Therefore, a reasonable cut on $M_T(\ell, \not{p}_T)$ is found to be extremely effective to reduce the background level.

• $m_{b\bar{b}}$: As mentioned above the invariant mass of two b-jets is very useful in isolating the signal region. In method A, this reconstruction is straight forward and is performed using two b-jets momenta obtained by matching b-jets with b-quarks. However, in method B, we use jet substructures to find b-jets inside a "fat-jet" from the Higgs decay. The use of jet substructure for the reconstruction of hadronic decays of boosted W, Z, Higgs boson and top quark has received considerable attention in recent years and the available literature is steadily increasing [266]. In our present study this method was motivated following the work of Ref. [35] where the authors reconstructed the Higgs mass using jet substructures to increase the signal sensitivity. The efficiency of jet substructure technique depends on the boost factor of the decayed object. A highly boosted system ensures that decay products are well collimated and appear as a "fat-jet". However, in the scenario of interest to us Higgs is moderately boosted as its p_T depends on $\Delta m = m_{\tilde{\chi}_2^0} - m_{\tilde{\chi}_1^0}$. In our analysis we first cluster all the stable final state particles into a “fat jets” using the C/A algorithm [242] with R =1.2 as implemented in Fastjet [8]. We select "fat jets" with $p_T \geq$100 GeV and $|\eta| <$2.5 and then perform jet substructure analysis. There are various methods of finding jet substructures [266]. We use the mass drop(MD) [2] method [35](built in the `FastJet` package [8]) in our analysis optimizing the two input parameters, $\mu = 0.4$ (the mass drop criteria) and $y_{\rm cut} = 0.1$(the asymmetry value). In the simulation we use PYTHIA event generator by setting Tune $Z2^*$ parameters described in Ref. [267] for underlying event modeling. In Figure.8.2, we show the reconstructed Higgs mass following method A(blue/light) and B(red/dark shaded) corresponding to parameters P2. This figure clearly demonstrates the usefulness of the jet substructure technique for Higgs mass reconstruction. In case of method A, some of the soft jets are incidentally passing the matching criteria resulting in a spread towards the lower side, whereas in the jet substructure method this type of contamination is avoided by the filtering procedure described in [35].

Method A:

In this section we discuss the simulation strategy of signal and backgrounds by reconstructing

[2] see discussion on MD method in 6.3

Process	σ(pb)	N_{EV}	1ℓ 2b-jets	$R_T^{b\bar{b}}$ $\geq$0.7	$m_{b\bar{b}}$ 110-130	$\not{p}'_T$ $\geq$175	ϕ_{bb} $\leq$2	c.s. (fb)
P1	0.175	0.1M	1392	1162	723	92	76	0.065
P2	0.065	0.1M	1767	1478	933	217	178	0.06
P3	0.03	0.1M	2142	1774	1122	424	391	0.055
Wh	0.58	50K	702	594	394	8	2	0.01
Zh	0.3	50K	210	162	51	1	1	0.003
$Wb\bar{b}$	3	619685	26841	24513	2269	8	3	0.014
$Zb\bar{b}$	5.1	378098	3863	2937	269	<1	<1	<1
$t\bar{t}$								
5-100	48.2	4M	207335	94337	10145	<1	<1	<1
100-200	36.3	2M	158450	50967	1205	8	1	0.01
200-500	9.5	1M	134238	22473	116	42	4	0.02

Table 8.2: Event summary for signal and backgrounds(method A) for 8 TeV after each set of cuts described in the text. The $t\bar{t}$ events are simulated for different $\hat{p}_T$ bins as shown. The energy units are in GeV.

Process	σ(pb)	N_{EV}	1ℓ 2b-jets	$R_T^{b\bar{b}}$ $\geq$0.7	$m_{b\bar{b}}$ 110-130	$\not{p}'_T$ $\geq$175	ϕ_{bb} $\leq$2	c.s. (fb)
P1	0.502	0.1M	3867	2500	1213	89	73	0.18
P2	0.202	0.1M	4391	2756	1381	273	229	0.23
P3	0.104	0.1M	4517	2824	1431	373	323	0.17
Wh	1.26	0.1M	3002	1639	750	21	15	0.09
Zh	0.69	0.1 M	799	280	85	1	1	0.004
$Wb\bar{b}$	4.5	362018	57764	47883	44160	3948	9	0.055
$Zb\bar{b}$	7.2	406110	442	380	322	<1	<1	<1
$t\bar{t}$								
5-100	188	10M	1163903	188856	16910	7	4	0.04
100-200	156	10M	1202319	82970	4367	70	32	0.25
200-500	48.5	1M	133840	2020	252	61	32	0.8

Table 8.3: Same as 8.2 but for 14 TeV. The same conventions as in Table 8.2 are used.

the Higgs mass out of two identified b-jets obtained by matching techniques as discussed above. In order to eliminate SM backgrounds additional cuts are applied with the following requirements:

- $R_T^{b\bar{b}} \geq 0.7$,
- $m_{b\bar{b}}$=110-130 GeV,
- $\not{p}'_T \geq 175$ GeV,
- $\phi_{b\bar{b}} \leq 2$.

In Table 8.2 we present event summaries of signal for three benchmark points shown in Table 8.1, along with backgrounds after applying these set of cuts. The second and third column present the raw leading order(LO) cross section and number of events N_{EV} simulated respectively. In the fourth column, we present the number of events requiring one single hard lepton along with two identified b-jets and veto the second lepton as well. Although we simulated all possible SM backgrounds including QCD, tb, tbW, but we present results only for non-negligible contributing channels. It clearly demonstrates that the $R_T^{b\bar{b}}$ cut is very effective in reducing backgrounds by an enormous amount, but except for channels, like $Wb\bar{b}$ and Wh. Selection of events in the Higgs mass window between 110-130 GeV is also useful to remove backgrounds keeping almost more than 50% of signal events. Finally, a very strong $\not{p}'_T$ cut is used to eliminate remaining backgrounds,

but at the cost of a sizable signal cross section; nevertheless we retain a good number of signal events. After all cuts, we find the total background cross section is about 0.057 fb with dominant contribution from $t\bar{t}$, whereas signal cross sections are in the range 0.065-0.055 fb. In both cases we use LO production cross sections. However, if we use NLO cross sections by multiplying K-factors which is $\sim$ 1.5 for signal [17] and about 1.6 for $t\bar{t}$ [268], then assuming a luminosity 100 fb^{-1}, one can expect S/$\sqrt{B}$ about 3.5 for these mass ranges of $\tilde{\chi}_1^{\pm}$ and $\tilde{\chi}_2^0$.

In Table 8.3, we present results for 14 TeV energy corresponding to the same set of benchmark points along with the SM background. We observe that the signal efficiency remains fairly the same as 8 TeV with the enhancement occurring only due to the increase in cross section. The top background however increases significantly due to a presence of a stronger missing momentum and more reconstruction of Higgs mass from the $b\bar{b}$ system. The total background cross section at 14 TeV turns out to be 1.23 fb as compared to the signal cross sections which are between 0.18 fb and 0.25 fb. As a consequence it becomes difficult to observe a signal with low luminosity options in this approach. However for an integrated luminosity of 1000fb^{-1} it may be possible to observe a signal in this method at a 5σ level.

Process	C.S. (pb)	N_{EV}	$m_{b\bar{b}}$	Lepton $\geq$20	$M_T(\ell, \not{p}_T)$ $\geq$ 90	$R_T^{b\bar{b}}$ $\geq$0.9	$\not{p}_T$ $\geq$ 125	C.S. (fb)
P1	0.175	25K	179	55	24	19	12	0.042
P2	0.065	10K	168	42	23	18	12	0.04
P3	0.03	10K	273	75	44	36	31	0.045
Wh	0.58	0.1M	871	239	12	11	<1	<1
Zh	0.3	0.2M	1698	37	<1	<1	<1	<1
$Wb\bar{b}$	3	619671	191	111	10	8	<1	<1
$Zb\bar{b}$	5.1	378086	81	13	<1	<1	<1	<1
$t\bar{t}$								
5-100	48.2	5M	1669	454	38	1	<1	<1
100-200	36.3	4M	1583	440	42	3	1	0.005
200-500	9.5	1M	315	98	9	2	<1	<1

Table 8.4: Event summary for signal and backgrounds(method B) for 8 TeV after each set of cuts described in the text. The same conventions as in Table 8.2 are used.

Method B: In this method we apply jet substructure technique in reconstructing mass of Higgs within the mass window between 117 - 128 GeV and with additional cuts as before to control background events,

- $M_T(\ell, \not{p}_T) \geq 90$ GeV [3],
- $R_T^{bb} \geq 0.9$,
- $\not{p}_T \geq 125$ GeV(150 GeV for 14 TeV).

After the Higgs mass reconstruction the remaining stable particles are used to find jets with C/A algorithm with $\Delta R = 0.5$, $p_T \geq 50$ GeV, $|\eta| \leq 2.5$. The Table 8.4 displays the robustness of $R_T^{b\bar{b}}$ cut along with $m_T(\ell, \not{p}_T)$ leading to a suppression of backgrounds to a negligible level without affecting signal significantly.

Notice that after cuts signal cross sections remain the same for all cases although production cross sections decrease with the increase of gaugino masses, which is compensated by the increase of acceptance efficiencies. The total background cross section turn out to be 0.007 fb, an order of

[3] Note that we have taken the finite width effects of W boson into account in our simulation. This results in a tail in the $m_T(\ell, \not{p}_T)$ distribution in processes like Wh and $t\bar{t}$. Thus forced us to opt for a higher value for $m_T(\ell, \not{p}_T)$ selection cut.

Process	C.S. (fb)	N_{EV}	$m_{b\bar{b}}$	Lepton $\geq$20	$M_T(\ell, \not{p}_T)$ $\geq$ 90	$R_T^{b\bar{b}}$ $\geq$0.9	$\not{p}_T$ $\geq$ 150	C.S. (fb)
P1	504	25K	242	55	23	16	5	0.05
P2	204	25K	461	113	55	43	26	0.1
P3	104	25K	713	197	116	67	46	0.095
Wh	1.3	0.1M	946	289	17	11	4	0.026
Zh	704	0.1M	866	13	1	<1	<1	<1
$W b\bar{b}$	5.5	431062	159	92	8	7	<1	<1
$Z b\bar{b}$	7.2	571166	150	<1	<1	<1	<1	<1
$t\bar{t}$								
5-100	190	10M	4178	1016	121	12	<1	<1
100-200	158	1M	4463	1181	137	11	2	0.01
200-500	49	0.25M	867	296	25	7	1	0.02

Table 8.5: Same as Table 8.4 but for for 14 TeV. The same conventions as in Table 8.2 are used.

magnitude less than the method A whereas signal cross sections are of the same level. Assuming 100 fb^{-1} luminosity, one can expect signal to background ratio S/$\sqrt{B} \sim 7$ using NLO cross sections as before. It implies that probing the Higgs signal in this channel is promising with 8 TeV LHC energy and high luminosity options. In both cases signal sensitivity is low because of the tiny production cross section in comparison with the backgrounds.

	P1 $m_{\chi_2^0}, m_{\chi_1^0}$(GeV)	P2 265,133	P3 332,168	390,198
Method A	8 TeV	2.7	2.5	2.3
	14 TeV	1.6	2.1	1.6
Method B	8 TeV	6	6	6.1
	14 TeV	2.1	4.2	4

Table 8.6: The signal sensitivities $S/\sqrt{B}$ with 100 fb^{-1} luminosity for 8 and 14 TeV energies for method A(top row) and method B(bottom row) for the three benchmark points described in Table 8.1. The cross section after all cuts are normalized to NLO cross sections, for signal and $t\bar{t}$.

For 14 TeV energy, as presented in Table 8.5, we find that the results are not significantly different for method B. Comparing Table 8.4 and Table 8.5 we observe a better reconstruction of the Higgs mass because of the enhanced boost of the $b\bar{b}$ system at 14 TeV energy. However this gain is diluted due to an increase in $\not{p}_T$ cut compared to 8 TeV to suppress the backgrounds. It has to be noted that at 14 TeV we receive a finite background contribution from Wh process due to an increase in $\not{p}_T$. We find that after all cuts the total background cross section is 0.05 fb while the signal cross sections vary between 0.05 fb to 0.1 fb. It is therefore possible to discover a signal for this type of parameter space at the $\sim 5\,\sigma$ level at 100 fb^{-1} luminosity. The signal sensitivities for 8 and 14 TeV LHC energies for both methods is presented in Table 8.6.

8.2 Probing signatures of an invisible Higgs decay

The current measurements of the Higgs decay widths by the LHC are compatible with SM predictions within experimental errors. However this does not rule out the presence of any non standard decay mode of Higgs. A large number of such models allow for a significant branching frac-

tion for the decay of the Higgs to a stable weakly interacting particle providing a channel where the Higgs decay is "invisible" to the detector. In the SM the Higgs can decay invisibly through $H \to ZZ^* \to 4\nu$, which can only contribute to roughly 0.1% of the branching ratio [269]. Therefore, the observation of a sizable invisible branching ratio ($\mathrm{Br_{inv}}$) of the Higgs will be a strong indication for BSM physics. Strong cosmological evidence supporting the existence of Dark Matter (DM) means that almost all extensions of SM must include in their spectra a candidate for it which is supposed to be neutral and weakly interacting. There exist several examples of BSM physics models where the Higgs can have an invisible decay, such as, the decay of the Higgs to the lightest supersymmetric particle (LSP) [270], decay to graviscalars in extra-dimensional models [271,272] in gauge extensions of the SM [273, 274] and in models for neutrino masses [275–277]. It has been noticed in various analysis [278–281] that if this resonance is interpreted as a Higgs boson, the currently available information on its properties can allow non trivial values of $\mathrm{Br_{inv}}$. In fact a recent analysis by the CMS collaboration performing a global fit to the LHC data, suggests that an invisible branching ratio of the Higgs of mass $\sim$125 GeV in non SM channel as large as 62% at 95% confidence level is still allowed [36] [4]. In fact detailed analysis of LEP data showed no evidence for an invisibly decaying Higgs of mass less than 112.1 GeV [283].

The feasibility of finding an invisible branching fraction of the Higgs for $\sqrt{s} = 7$ TeV,8 TeV and 14 TeV at the LHC has been studied in various production modes of the Higgs [37, 39, 284–292].

We look at the production of Higgs in association with a electroweak gauge boson as well as through Vector Boson Fusion (VBF) in detail. In earlier studies, the leptonic decay of the Z boson was used to identify the invisible decay of a Higgs produced in association with a Z boson [39]. In the present study we update the analysis in the leptonic channel and also probe the possibility of detecting an invisible decay of the Higgs by identifying the associated Z boson through b-tagged jets both for 8 TeV and as well as 14 TeV LHC. We also apply the jet-substructure algorithm [35] for b-tagged final states which marginally help in improving signal acceptance efficiencies. In addition, we study how the invisible decay channel can be probed in the production of the Higgs via vector boson fusion for both 8 TeV and 14 TeV LHC energy.

8.2.1 The invisible decay width of the Higgs in MSSM

As noted above invisible Higgs decay is viable in a vast range of BSM models, including Graviscalars, Higgs portal models, extra dimensional theories among others. Each of these models have an LSP to which the Higgs boson can decay. In this section however we will only discuss the case of the lighest stable neutralino in R-parity conserving SUSY models, although the discussion can easily be extended to other models. The Higgs decay to neutralinos has been widely studied in the literature. If kinematically allowed, the branching ratio for this decay can be quite large. In the simplest assumption, one assumes that the production cross section of the Higgs boson is SM like, i.e the gluino, the sfermions and the charged Higgs are sufficiently heavy such that they do not contribute to the Higgs production cross section in loops. This is likely to be true given the current limits on the gluino and the squarks of the first two generations. The Higgs decay width to the lighest neutralino is given by [293],

$$\Gamma(h \to \chi_1^0 \chi_1^0) = \frac{G_F M_W^2 m_h}{2\sqrt{2}\pi} \left(1 - 4m_{\chi_1^0}^2/m_h^2\right)^{3/2} \left|N_{h\chi_1^0\chi_1^0}\right|^2 , \tag{8.2.1}$$

[4] Similarly ATLAS also obtained a upper bound of 84% at 95 % confidence level on the invisible branching ratio of the Higgs without any assumption on the total decay width [282].

where the quantity $N_{h\chi_1^0\chi_1^0}$ is given by,

$$N_{h\chi_1^0\chi_1^0} = \left(Z_{12} - \tan\theta_W\, Z_{11}\right)\left(\sin\beta\, Z_{14} - \cos\beta\, Z_{13}\right), \tag{8.2.2}$$

where Z is the usual matrix that diagonalizes the neutralino mass matrix. The constraint to the above scenario comes from the invisible decay of the Z boson, which has been measured to the precision of $\Gamma^Z_{\rm inv} = \mathcal{O}(1)$MeV. However, since this is comparable to the total Higgs decay width, $\mathcal{O}(1)$ invisible decay of Higgs is comparable to the Z pole data. For completion, we note that the decay width of $Z \to \chi_1^0\chi_1^0$ with the LEP constraint (95% C.L) is given by [294],

$$\Gamma(Z \to \chi_1^0\chi_1^0) = \frac{\alpha}{3} M_Z \left(1 - 4m^2_{\chi_1^0}/M_Z^2\right)^{3/2} \left|N_{Z\chi_1^0\chi_1^0}\right|^2 < 3 \text{ MeV}, \tag{8.2.3}$$

where,

$$N_{Z\chi_1^0\chi_1^0} = \frac{1}{2\cos\theta_W\, \sin\theta_W}\left(Z_{14}^2 - Z_{13}^2\right). \tag{8.2.4}$$

From the above equations it is obvious that the invisible decay widths of both vanish in the pure bino limit. For a typical value, $tan\beta = 10$, the Higgs decay is dominated by the higgsino component Z_{14}, while the Z boson decay is a democratic combination of Z_{14} and Z_{13}. With an increase in M_1(increase in bino mass), the Z_{13} component remains significantly large while Z_{14} decreases, thus making the LEP constraint even more relevant. Above the kinematic boundary of $Z \to \chi_1^0\chi_1^0$, the invisible Higgs width can be comparable to the SM Higgs width without violating the LEP bound [295].

8.2.2 Signatures of an invisibly decaying Higgs

There are four main production mechanisms of the Higgs boson in a hadron collider. The most dominant one is gluon-gluon fusion via a top quark loop (ggF) $(gg \to H)$ followed by VBF $(q\bar{q} \to q\bar{q}H)$, then Higgs production in association with vector bosons (VH) $(q\bar{q} \to ZH/WH)$ and finally in association with top quark pairs (ttH) $(gg/q\bar{q} \to t\bar{t}H)$ with the lowest cross section [45,99–137]. The various production channels are shown in Fig. 2.6. Needless to say that the signatures of the Higgs particle are characterized by the pattern of the Higgs decay channels [3]. Recall that the BR of the Higgs decay in the invisible channel in the framework of SM is too low to be observed, therefore, any observation of invisible decay channel of the Higgs will shed some light about BSM physics. On the other hand the production cross section of the Higgs can vary in various models due to the presence of new particles inside loops and modified couplings of Higgs with gauge bosons and fermions. For example, supersymmteric (SUSY) particles may alter the loop contribution in ggF channel [223, 296–312]. Consequently signal in the invisible decay channel will be a combined effect due to the modified Higgs production cross section and its branching ratio in the invisible channel. Hence this makes it difficult to constrain only the invisible decay branching ratio of the Higgs $\text{BR}_{\text{inv}}(\text{H} \to \text{inv})$. Instead what can be constrained is in fact

$$R_{inv} \equiv \sigma_H^{BSM} BR(H \to inv)/\sigma_H^{SM} \tag{8.2.5}$$

where σ_H^{BSM} and σ_H^{SM} stand for the Higgs production cross sections in the framework of corresponding BSM and SM respectively. At leading order, the Higgs produced through ggF and decaying invisibly would be hard to detect because of soft missing transverse momentum ($\not{p}_T$). However, at higher orders in QCD for ggF, the Higgs can be produced in association with a single jet and one can then look for a considerably large missing transverse momentum along with

a jet. Interestingly, such final states with a mono-jet have been analyzed with 1 fb^{-1} of data at $\sqrt{s} = 7$ TeV for both CMS [313] and ATLAS [314]. Using those results, R_{inv} in eq. 8.2.5 can be constrained and is found to be more than 10 at 95% CL with 1fb^{-1} data [290]. Moreover, the mono-jet search has also been analyzed by including a second hard jet [313] thus also including events from VBF and VH processes in the signal. It has been argued recently that at 4.7 fb^{-1} data at $\sqrt{s} = 7$ TeV, this can be reduced to $R_{inv} < 2$ and for 15 fb^{-1} of data at 8 TeV this can be further reduced to $R_{inv} < 0.9$ [291]. One should note here that even though the production cross-section is large the mono-jet searches are plagued by large V+jets ($V = W, Z$) background (Bg).

The most promising channel for the detection of an invisibly decaying Higgs is VBF since it has a relatively large cross section and has an unique event topology that can be used to effectively remove backgrounds [286, 288, 292]. The signal consists of jets moving in opposite directions with large rapidity gaps. A recent study has shown that R_{inv} as low as 0.21 can be probed with 30 fb^{-1} data at $\sqrt{s} = 14$ TeV and for $\sqrt{s} = 7$ TeV with 20 fb^{-1} it can be probed to as low as 0.4 with 95% CL [37].

We revisit this analysis for 8 TeV and 14 TeV energies [38]. In our current analysis we employ a different set of kinematic selection cut values to that used in Ref [37]. Moreover, in this analysis a precise method of jet reconstruction with anti $-$ k$_t$ [7] algorithm built in the FastJet [8] package is implemented. It has to be noted that in our analysis we consider the additional W/Z+3 jets backgrounds which were not considered in earlier works [37, 315]. These additional modes do contribute a sizable fraction to the total background cross section, in particular Z+3 jets channel. As a consequence, our conclusion appears to be different than previous works [37, 315] which is discussed in Sec.3. However, the main drawback of VBF channels is that it has large systematic uncertainties and it is difficult to estimate the QCD background [288, 292].

The $t\bar{t}H$ channel has been studied in detail [316] for $\sqrt{s} = 14$ TeV LHC in both the semileptonic, $t\bar{t} \to WbWb \to l\nu bq\bar{q}b$, and as well as in the hadronic mode $\to q\bar{q}bq\bar{q}b$. The complex final state and the combinatorial background requires a very sophisticated analysis.

The cleanest channel by far is the associated production channel $VH(V = W, Z)$. Incidentally, the couplings between gauge boson and Higgs are not expected to deviate from the SM significantly because of the unitarity of the theory and restrictions from electroweak precision tests. As a consequence, in any BSM model, the parton level cross sections for VBF and ZH channels turn out to be very close to SM values. Under the assumption that the Higgs gauge couplings do not deviate from standard model couplings, these channels therefore give a direct probe of the invisible branching ratios, unlike ggF. However, the WH channel is diluted by the inclusive W background which makes it difficult to use for detecting an invisible Higgs decay [317] where as the ZH channel is more promising because of the presence of two leptons from the Z boson decay. We study here the efficacy of this channel in detecting invisible branching ratio at $\sqrt{s} = 8$ TeV and $\sqrt{s} = 14$ TeV energies. Like earlier studies of this channel [37, 39, 317] for 14 TeV energy, we use the leptonic decay to identify the Z boson. In addition to revisiting this channel for 14 TeV energy, we analyze it for 8 TeV energy which are the new results for this channel. Moreover, we consider the hadronic decay mode, specifically decay to b quarks and investigate the viability of use of jet substructure and clustering methods for detection of b jets in reducing backgrounds.

8.2.3 Invisible Higgs signal via VBF

In this section we study the feasibility of finding the invisible Higgs signal through the VBF process which is the sub dominant process for the Higgs production in hadron colliders. This channel has

been studied previously for 14 TeV LHC [286, 288, 291, 317] and very recently for 7 TeV and 8 TeV [37]. We also revisit this analysis for 8 TeV and 14 TeV LHC energy for the Higgs mass of 125 GeV using a different set of selection cut values. In this channel, the Higgs is produced through vector boson fusion, where vector bosons originate by radiating off two initial quarks along with two jets,

$$\mathbf{pp \to qqh \to 2jets + \not{p}'_T}. \tag{8.2.6}$$

The final state consists of two jets in the forward and backward directions with a wide separation in rapidity and a reasonably large $\not{p}'_{\rm T}$ due to the presence of non-interacting particles from Higgs decay. In addition to this pure VBF processes, there are some non VBF processes which also provide the same final state consisting of 2 jets and $\not{p}'_{\rm T}$. For instance, higher order QCD effects in ggF process can give rise to two jets in the final states because of a hard emission of partons from the initial states with a non negligible cross section. The dominant SM background processes for this signal are due to ($W \to \ell\nu$)+jets, ($Z \to \nu\bar{\nu}$)+jets, $t\bar{t}$ (tbW) and QCD. For W+jets, a significant background can arise if the lepton is not detected. Note that the background cross sections mimicking the signal are significantly large, and hence a sizable reduction is required to achieve a reasonable signal sensitivity. The signal and background processes are simulated using `MadGraph/Madevent` [10] and subsequently passed through `PYTHIA6` [6] for parton showering. In this study for all numerical calculations we use CTEQ6L [318] for parton distribution functions. In the process of showering, we adopt MLM matching [11] using default values set by the `MadGraph/MadEvent` suite to avoid double counting of jets. Jets are reconstructed using `FastJet` [8] with anti-K$_{\rm T}$ [7] algorithm using size parameter $R = 0.5$ and applying a jet p_T threshold of 40 GeV and $|\eta| < 4.5$. Notice that the signal is completely free from leptonic activities whereas background channels may contain leptons in the final state. Therefore, a leptonic veto might help to eliminate certain fraction of backgrounds. Leptons are selected with p_T^{ℓ} >10 GeV, $|\eta_\ell|$ <2.5. We compute missing transverse energy from the momenta of all visible particles. The following set of cuts are used in the simulation :

1. VBF selections: The leading jets in Higgs production through the VBF process are produced in the forward and backward direction and hence is expected to have a large rapidity gap. Therefore, we select events where the absolute rapidity difference between the two leading jets is $|\eta_{j1} - \eta_{j2}| = |\Delta\eta|$ >4. To ensure that the two jets are in the opposite direction, the product of rapidity of two jets are required to be, $\eta_{j1} \times \eta_{j2}$ <0.

2. Central Jet veto: For a pure VBF process, no jets with $p_T > 40$ GeV are expected in the rapidity gap region between two reconstructed jets. Therefore we discard events if there be any jets in central region.

3. Lepton veto(LV): Since the signal has a pure hadronic topology, events with any lepton are vetoed out.

4. Selection of $\not{p}'_T$: Events are required to have at least $\not{p}'_{\rm T}$ >100 (170) GeV for 8 (14) TeV energy.

5. Dijet invariant mass M_{jj} : The invariant mass of two leading jets is expected to be very large and hence we demand, M_{jj} >1400 (1800) GeV for 8 TeV (14 TeV) energy.

Process	8 TeV		14 TeV	
	Production CS[pb]	After cuts CS[fb]	Production CS[pb]	After cuts CS[fb]
W+2jets(VBF)	76.5	4.5	167.9	6.3
W+2jets	18700	5.8	45900	18.7
W+3jets	10260	< 1	21000	13
Z+2jets(VBF)	19	6	43.2	6.7
Z+2jets	6000	16.5	14000	11.2
Z+3jets	2772	8.3	7300	17.8
tbW	140	< 1	611	< 1
Total Background		41.1		74
hjj(VBF)	1.73	7.3	4.3	8.7
hjj	6.7	1.2	24.5	1.3
Signal		8.5		10

Table 8.7: Event summary of the signal and backgrounds for the final state with two jets and $\not{p}_T$ via VBF channel for 8 TeV and 14 TeV LHC energies. In the second column the cross sections corresponding to production and after all cuts are shown for signal and background processes respectively for 8 TeV energy. The third column presents the same for 14 TeV energy.

We notice that $\not{p}_T$ and M_{jj} cuts are extremely useful to suppress the backgrounds with a marginal effect in the signal cross section. We have also checked that the background contribution due to QCD is negligible because of a strong $\not{p}_T$ and a large di-jet invariant mass cut(M_{jj}); this is why results for QCD are not presented here. In our simulation, the rejection efficiencies due to the central jet veto for QCD Wjj and QCD Zjj are about 20% for both energies. Note that this efficiency depends crucially on the detector effects like calibrations, electronic noise, pile up effects etc. [315], which are not taken into account in this analysis. In Table 8.7 we present the event summary for signal and all background processes subjected to the above set of cuts. The first column represents the production cross section at the leading order obtained from `MadGraph` [10]. The contribution due to the pure VBF type and non-VBF type of processes are shown separately. In the subsequent columns, the cross sections subject to all cuts are presented. Notably, there exists a non negligible possibility that W/Z+3jet channel may contribute to the background cross section, if the third jet is not detected. Here we present our results for both the 8 TeV and 14 TeV energies. At 8 TeV energy, the total signal cross section turns out to be 8.5 fb, consisting of 14 % contribution from ggF and the rest due to VBF process. At 8 TeV energy, for $\mathscr{L}$=20 fb^{-1}, it is possible to observe signal with S/$\sqrt{B}$ ∼5.9 leading to a detection of invisible BR ∼84% or above assuming $\sigma_{SM} = \sigma_{BSM}$ in Eq. 8.2.5. On the other hand, for 14 TeV energy, results are more encouraging where one can find a signal with a better sensitivity yielding S/$\sqrt{B}$ ∼ 6.3 (20) for 30 (300) fb^{-1} integrated luminosity which predicts a measurement of BR $\geq$ 0.79(0.25). In our estimation the signal purity S/(S+B) is approximately 40% lower than the results obtained by the Ref. [37]. As mentioned earlier, we use a more reliable method of jet reconstruction by using FastJet [8] with anti $-$ K$_t$ algorithm [7], and consider an additional W/Z+3jets background. It is to be noted that in our calculation we used LO cross sections for both signal and backgrounds. However the K-factor for the signal is ∼0.95 [319] and for W/Z+jets it is also very close to 1(∼1.1) [320, 321]. Therefore, inclusion of K-factors in the above calculation will not alter the conclusions significantly. Note however that we have not taken systematic uncertainities into account.

8.2.4 Invisible Higgs signal via ZH

Here we study the signature of the invisible decay of Higgs via the ZH channel, where Z can decay both leptonically and hadronically, $Z \to \ell\bar{\ell}, b\bar{b}$. It is well known from an experimental point of view that the leptonic channel is comparatively cleaner than the hadronic channel consisting of b-jets. However we simulate both these channels to find the detectability of an invisible Higgs decay. In the following, we describe our simulation for both the final states.
(a) $\underline{Z \to \ell\bar{\ell}}$
Here the final states consist of two leptons with opposite charge and same flavor and with a considerable amount of missing transverse momentum due to the Higgs decay into invisible particles.

The main dominant SM backgrounds are expected from the following processes,

1. ZZ production with one Z decaying to neutrinos and the other Z decaying leptonically. Clearly, this background has exactly identical characteristics to the signal.
2. WZ production followed by the leptonic decays of both the W and Z, giving rise to $\ell\nu_\ell\bar{\ell}\ell$ where one of the leptons is lost.
3. WW production with both W bosons decaying leptonically, $W \to \ell\nu_\ell$.
4. Top pair production, $t\bar{t} \to WWb\bar{b} \to l\nu_l\bar{l}\bar{\nu}_l b\bar{b}$ which may appear signal-like if the b-jets escape detection.

The Higgs being heavier in comparison to the particles in the background processes other than the top quark, gives rise to a harder $\not{p}_T$. Therefore, by demanding a large $\not{p}_T$ one can efficiently reduce backgrounds. In the signal topology, an added advantage is that the invariant mass of two leptons peaks around the mass of the Z boson. Hence requiring the di-lepton invariant mass to be around the mass of the Z boson, it is possible to suppress backgrounds partially except for the ZZ process. Since the Z boson and the Higgs are more likely to be produced back to back, the transverse mass of the di-lepton system and the $\not{p}_T$, defined as,

$$M_T^{l\bar{l}} = \sqrt{p_T^{ll}\not{p}_T\left(1-\cos\phi(\mathrm{E_T^{ll}},\not{p}_T)\right)}, \tag{8.2.7}$$

has a softer distribution for all background processes. Therefore, demanding a large value for this variable enables us to eliminate backgrounds substantially.

As before, we use `MadGraph` [10] to generate both the signal and background processes which are subsequently passed through `PYTHIA6` [6] for event generation including showering. We apply the following set of cuts in our simulation for the event selection and as well as suppressing the background events.

1. Select leptons with $p_T^\ell > 10$ GeV and $|\eta_l| < 3$. The isolation of lepton is ensured by looking at the total transverse energy $E_T^{ac} \leq 20\%$ of the p_T of lepton, where E_T^{ac} is the scalar sum of the transverse energies of jets within a cone of size $\Delta R(l,j) \leq 0.2$ between the jet and the lepton.
2. Since final states are hadronically quiet, vetoing events consisting jets, with $p_T > 30$ GeV and $|\eta| < 4$ are useful in eliminating certain fraction of backgrounds.
3. Azimuthal angle between two leptons, $\cos\phi_{\ell\bar{\ell}} > 0$ and transverse mass between two leptons and $\not{p}_T$, $M_T^{l\bar{l}} > 150$ (200) GeV for 8 (14) TeV energies.

Process	8 TeV		14 TeV	
	Production C.S[pb]	After Cuts C.S[fb]	Production C.S[pb]	After Cuts C.S[fb]
ZZ	4.79	6.7	10.1	17.6
WZ	12.6	1.8	26.7	3.8
WW	33.8	0.3	69.4	2.3
$t\bar{t}$	115	0.1	480	0.95
Total Bg		8.9		24.7
ZH	0.3	2.3	0.64	5.6

Table 8.8: Event summary for the dilepton+$\not{p}_T$ final states. In the second and third columns, the cross sections for signal and backgrounds before and after selection cuts, as described in the text, are presented for 8 TeV and 14 TeV center of mass energies respectively. We assume that the invisible branching fraction is 100 %.

4. Missing transverse momentum, $\not{p}_T$ >100 GeV.
5. Di-lepton invariant mass, $|M_Z - m_{\ell\ell}| < 10$ GeV.

For 14 TeV LHC energy, the strategy of simulation is not significantly different as no additional effects occur. The same set of cuts with similar thresholds are used with the only exception of $M_T^{\ell\ell}$ where 200 GeV is used instead of 150 GeV. In Table 8.8, we display cross sections for both signal and backgrounds for 8 and 14 TeV energies before and after cuts. In each column, numbers on left stand for the production cross sections corresponding to energies as shown in the respective columns. For both energies, we find that M_T^{ll} and $\not{p}_T$ play a very useful role in suppressing the backgrounds. The kinematics of ZZ process is identical to that of the signal process although there is a moderate mass difference (35 GeV) between the Z and the Higgs boson, resulting in a similar effect of cuts on both signal and ZZ background. As a consequence, ZZ turns out to be the dominant irreducible background. This channel was studied extensively in an earlier study for 14 TeV LHC energy [39]. Here we have revisited the analysis for 14 TeV LHC energy and performed an optimization of cuts. The numbers on the right hand side of each column show the final cross sections after being multiplied by acceptance efficiencies. For 8 TeV energy with an integrated luminosity of $\mathscr{L}$=20 fb^{-1} we find S/$\sqrt{B} \sim 3.5$ which implies a hint of the invisible Higgs signal. However, for 14 TeV energy with $\mathscr{L}$=50 fb^{-1} one can observe the invisible signal with signal significance of $\sim$8. Note that the estimations are based on LO cross sections. However, we note that the K-factors for vector boson production and $t\bar{t}$ are 1.6-1.7 [268, 322] while for the signal process it is 1.3 [122, 125, 126] respectively. Hence we do not expect any major changes in our results. Note again, that a study of systematic errors is beyond the scope of this work.

(b)$Z \to b\bar{b}$

In this section we explore the possibility of detecting invisible Higgs decay channel by identifying two b-jets arising from Z boson decay. We analyze this channel following two methods. In the first method, b-jets are identified by using the standard jet clustering algorithm and in the second method, the jet substructure technique [35] is used to reconstruct . However, in both cases the dominant SM backgrounds arise from:

1. irreducible background from ZZ production with one Z decaying to neutrinos and the other Z decaying to b quarks.
2. The production of Z boson in association with two b quarks and the Z boson decaying to neutrinos, $(Zb\bar{b} \to \nu\bar{\nu}b\bar{b})$. A generator level cut of $p_T^b \geq 10\ GeV$ was used to while generating

these events.

3. WZ production with the W decaying leptonically, and the Z decaying to b-quarks and the lepton is lost, $(WZ \to l\nu_l b\bar{b})$.
4. $t\bar{t}$ production where two b-jet from top decays are identified and rest of the event objects are lost.
5. W boson produced in association with b quarks ($Wb\bar{b}$) where W decays leptonically and the lepton is not identified.

The event topology of this channel is not significantly different from the di-lepton final state as discussed above, and hence we apply similar type of cuts. Absence of any detectable hard lepton in the final state leads us to apply a lepton veto to reduce backgrounds, in particular from $t\bar{t}$, WZ and $Wb\bar{b}$ production. As before, $M_T^{b\bar{b}}$, the transverse mass between two b-jets and $\not{p}_T$ distributions of the backgrounds are soft. Therefore, selection of signal events corresponding to large values of these kinematic variables helps to remove significant fraction of the backgrounds. Moreover, we construct another useful variable, R_T, to remove large amount of the QCD. [19]. This variable is defined as,

$$R_T = \frac{p_{T_{b_{j_1}}} + p_{T_{b_{j_2}}}}{H_T}, \tag{8.2.8}$$

where H_T is the scalar sum of the transverse momenta of all detected jets including all non-tagged jets. Since one expects less non-tagged jet activity in the signal, R_T would tend to have larger values (~ 1) as compared to the events arising from QCD and other backgrounds. Naturally, requiring R_T to have a large value(~ 1), leads to a substantial suppression of backgrounds, particularly for those due to QCD processes.

We simulate as before the signal and backgrounds using `MadGraph` [10] applying the following set of selection cuts:

1. Select b-jets by performing a matching between b quarks and jets using matching cone $\Delta R = 0.3$ and finally multiply a b-tagging efficiency of 0.6 [265] for each of the b-jets. In the jet substructure method we employ mass drop techniques described in [35] to find the subjets which are also identified as a b-like jets by flavor matching.
2. Veto events with leptons, where $p_T^l > 10$ GeV and $|\eta_l| < 3$.
3. Select dijet events with both jets b-like and ensure that $|M_{b\bar{b}} - M_Z| < 30$ GeV.
4. $\not{p}_T > 70$ GeV.
5. $M_T(b\bar{b}, \not{p}_T)$ >200 GeV.
6. $R_T > 0.9$.

In Table 8.9 we present the final results of the simulation for both methods for 8 TeV energy. The second column presents the total production cross sections corresponding to each processes and subsequent columns show cross sections after applying the above set of cuts. However, in both cases, for an integrated luminosity of $\mathscr{L} = 20$ fb^{-1} the best we can achieve is S/$\sqrt{B} \sim 2$. In Table 8.10 as before, we present results for 14 TeV LHC energy. Here also we find that we can achieve a modest S/$\sqrt{B} \sim 4$ with an integrated luminosity of $\mathscr{L}$=100 fb^{-1}. However, for a very high luminosity option, e.g $\mathscr{L}$=300 fb^{-1}, for a moderate value of signal events, one can expect

Process	Production C.S[pb]	After Cuts C.S [fb] b jet cluster	After cuts C.S[fb] b jet substructure
ZZ	4.79	2.26	1.92
WZ	12.6	0.38	0.36
$\nu\bar{\nu}b\bar{b}$	16	3.1	1.33
$t\bar{t}$	115	0.48	0.52
W$b\bar{b}$	50.5	0.54	0.16
Background		6.76	4.29
ZH	0.3	0.8	0.72

Table 8.9: Event summary for the final states with b jet pairs and $\not{p}'_T$ for 8 TeV energy. The last two columns show the final cross sections after all cuts as described in the text.

Process	Production C.S[pb]	After Cuts C.S [fb] b jet cluster	After cuts C.S[fb] b jet substructure
ZZ	10	5.56	2.47
WZ	26.7	3.5	1.44
$\nu\bar{\nu}b\bar{b}$	47.3	12.9	3.04
$t\bar{t}$	476	3.92	0.16
W$b\bar{b}$	112	4.2	1.08
Background		30.	8.19
ZH	0.64	2.	1.1

Table 8.10: Same as Table 8.9, but for 14 TeV LHC energy.

to observe an invisible BR of Higgs ∼75% or more. Note that because of low b-jet acceptance efficiency and irreducible ZZ backgrounds this final state yields a marginal sensitivity. As we see jet substructure method does not give substantially better results because of the fact that the Z boson is not sufficiently boosted. Like the dilepton scenario as explained before, our results do not change significantly with the inclusion of higher order cross sections by using appropriate K factors for Wbb, Zbb [323, 324],tt [268] and for the signal [122, 125, 126].

8.2.5 Summary

Recent discovery of a Higgs like resonance by both the experimental groups: CMS and ATLAS has now spurred a series of investigations to determine whether it is 'a' Higgs boson and if so it is 'the SM' Higgs boson. Assuming that it is 'a' Higgs boson the current experimental information still does not rule out the possibility of BSM physics. Many BSM models predict decay of the Higgs in the invisible channel along with the usual SM decay modes. Such invisible decay modes, if confirmed or ruled out, will allow us to indirectly probe BSM physics. In this note we revisit the possibility of looking for a Higgs boson decaying invisibly, for two production channels of the Higgs : the vector boson fusion channel (VBF) as well as the associated production of Higgs with Z (ZH), for two different LHC energies: 8 and 14 TeV. In the ZH case, we also investigate the possibility of using the $Z \to b\bar{b}$ channel.

In Table 8.11 we summarize the lower limits of BR_{inv} that can be probed for various channels and for different energy and luminosity options. We find that for the Z(→ bb)H channel we fail to set any limits for 8 TeV with 20 fb^{-1} and 14 TeV with 30 fb^{-1} luminosity. We note that in the VBF channel the sensitivity is more than 5σ for both the energies : 8 and 14 TeV for large

Process	8 TeV(20 fb^{-1})	14 TeV(30 fb^{-1})	14 TeV(100 fb^{-1})
VBF	0.34	0.32	0.17
$Z(\to l^+l^-)H$	0.58	0.32	0.18
$Z(\to b\bar{b})H$(substructure)	–	–	0.5
$Z(\to b\bar{b})H$(b-jet cluster)	–	–	0.55

Table 8.11: The 95 % exclusion limits for BR_{inv} corresponding to various channels at 8 and 14 TeV LHC energies and luminosities.

invisible branching ratios (> 0.8) for integrated luminosity of 20 fb^{-1} and 30 fb^{-1}, whereas at 14 TeV with 300 fb^{-1} one can reach an invisible branching ratio as low as 0.25. In the ZH channel with dileptonic decay of the Z, the sensitivity with the planned luminosity of 20 fb^{-1} is limited at 8 TeV and rises to 8σ at 14 TeV with 50 fb^{-1}. With the $b\bar{b}$ final state, with 20fb^{-1} we can only reach $S/\sqrt{B} \sim 2$ at 8 TeV energy, where as with high luminosity ($\sim$ 300 fb^{-1}) and at 14 TeV energy we can probe the invisible decay at 5σ level, for an invisible branching ratio above 0.75. As observations indicate that the determination of an invisible branching fraction of the Higgs at the LHC is difficult to achieve, specially for small invisible branching ratios, an electron-positron linear collider with the associated production of the Higgs along with a Z boson can provide an extremely clean channel in this regard [325, 326].

Chapter 9

Supersymmetry with third generation squarks

9.1 Motivation for third generation squarks

As was emphasized earlier, the focus of early SUSY searches at the LHC was on the production of the gluino and the squarks of the first two generations driven by strong interaction processes. After the 7 TeV run, the non-observation of the gluino and the first two generation of squarks in the sub-TeV range, and the miniscule cross section of the gluino and the squark pair productions at the TeV mass range prompted experimentalists and theorists to look for signatures beyond this narrow range. The attention therefore switched to the search for third generation squarks, and the emphasis shifted from a specific model scenario like CMSSM to a more phenomenological approach. While this was driven by experimental considerations, the motivation for third generation squarks also has a sound theoretical ground. The argument of naturalness and the connection of the Higgs mass has certainly played a significant role in this regard.

The idea of naturalness [201, 209, 256, 327–330] stems from the fact that the most important particle responsible for the cancellation of the quadratic divergences in the one loop Higgs self energy corrections are the light stops. As noted earlier in section 2.7.2, the quadratic divergence to the Higgs one loop potential is dominated by the top quark, and it requires the stops to cancel these divergences. The remnant of the divergence is logarithmic and vanishes in the limit of exact SUSY, i.e when the mass of the top and the stop are equal. We noted in section 8, that although the tree level mass of the lightest Higgs boson is bounded by the mass of the Z boson, loop corrections dominated by stop-top loops can significantly increase the Higgs mass up to 140 GeV. The fact that the Higgs boson has been discovered to have a mass of 125 GeV thus necessarily requires large positive loop corrections to the tree level MSSM Higgs mass.

It must be noted here that there is a little hierarchy problem with the measurements of the Higgs mass. To have a Higgs mass of 125 GeV the induced loop corrections would require the light stops to be 300 GeV $-$ 1TeV, thus contributing to $m^2_{H_u}$ and introducing some fine tuning.

In MSSM, the argument of naturalness is summarized by the tree level electroweak symmetry breaking condition (in the moderate $\tan\beta$ regime),

$$-\frac{m_Z^2}{2} \propto |\mu|^2 + m^2_{H_u} - m^2_{H_d} \tag{9.1.1}$$

where we have renamed H_2 as H_u and H_1 as H_d, to denote the Higgs doublet that provides masses to the up type and down type squarks respectively. In general the contribution from m_{H_u}

is dominant, although if the sbottom masses and the trilinear coupling A_b is large, the contribution from $m^2_{H_d}$ to the above can also be significant. If sparticles are too heavy the quantity on the right hand side needs to be fine tuned against one another to achieve the correct electroweak symmetry breaking. Since the mass of the EW gauginos are controlled by μ, they are expected to be light. Since the loop contributions to $\delta m_{H_u^2}$ have contributions from the stop and the gluino, they are also not expected to be heavy. The rest of the sparticle spectrum including the sleptons, squarks of the first two generations do not contribute much to fine tuning and can be heavy.

In a natural theory(of EWSB) one expects the parameters of the theory to be comparable to each other and to the value of the electroweak VEV. In a SUSY theory the key observables as pointed that contribute to this argument are μ and m_{H_u}. As argued earlier the requirement of a tolerable μ for fine tuning (where the measure of the fine tuning is defined in Eq. 2.4.8) requires the Higgsinos to be light. The radiative corrections to $m_{H_u^2}$ are dominated by top stop loops and is given by,

$$\delta m_{H_u^2} = -\frac{3}{8\pi^2} y_t^2 (m^2_{Q_3} + m^2_{u_3} + |A_t|^2) log\left(\frac{|\Lambda|}{TeV}\right) \tag{9.1.2}$$

where Q_3 and u_3 the left and right handed third generation squarks. This equation thus provides a guideline to the amount of fine tuning in the theory.

The third contributor to the fine tuning is the gluino which induces a large loop correction in the stop mass and thus induces a large 2 loop correction to the Higgs mass. Again the requirement of a modest fine tuning requires the gluino to be less than 1 TeV.

To summarize, the requirement of naturalness indicates the following constraints on the sparticle spectrum [201, 329–331] .

- The stops and the sbottoms to be below 1 TeV.
- The two Higgsinos, i.e the lightest chargino and the two lighter neutralino should be light.
- The gluino should not be significantly heavy (1-1.5 TeV).

Fig. 9.1 from [201] depicts the various level of fine tuning as a function of X_t/A_t for a common stop mass $m_{Q_3} = m_{u_3} = m_{\tilde{t}}$, $\tan\beta = 20$. The left panel shows the contours of fine tuning for the Higgs mass, while the right panel presents contours for the light stop mass. The red/blue band corresponds to a Higgs mass of 124-126 GeV.

A wide range of works probing the naturalness aspect and the collider signatures has been conducted in the recent times and is likely to continue in the future [44, 327, 328, 332–349]. The collaborations ATLAS and CMS has also probed third generation squarks in a variety of final states. The limits quoted in this thesis are at the time of these works and are updated as more data is analyzed.

Here we summarize some of the studies conducted by phenomenological groups, ATLAS and CMS for sbottoms and stops.

Studies on the prospect of an sbottom search at the LHC, although not neglected in literature, are rather sparse. Some of the earliest studies of sbottom phenomenology at colliders were performed in [350–353]. A study on the possibility of determining the sbottom spin at the LHC using angular correlations was performed in [354]. It should be noted that the sbottom pair production cross section is at par with that of stop and hence sbottom search should be conducted with the same priority as stop searches. In fact, differing topologies in various scenarios (leptons, b-jets etc.) can be used to distinguish between stop and sbottom and can provide useful information

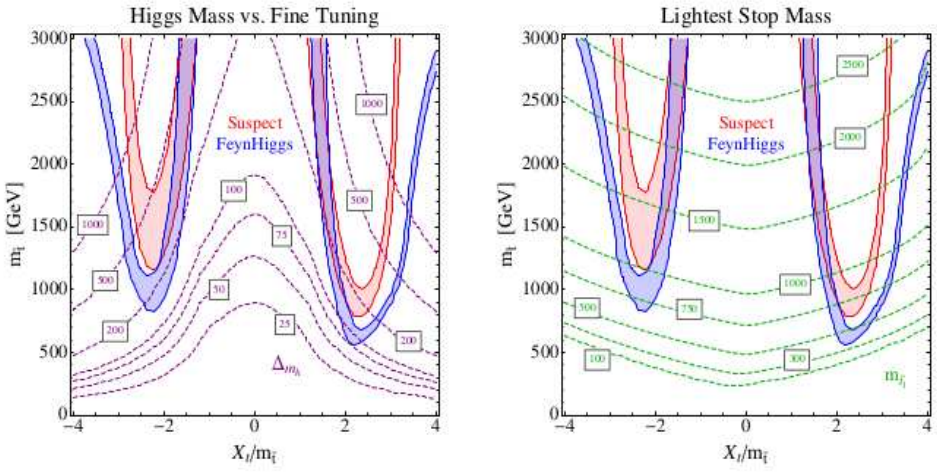

Figure 9.1: Fine tuning contours for m_h (left panel), and for stop (right panel) assuming a common stop mass from [201]. The red/blue band corresponds to a Higgs mass of 124-126 GeV.

about the nature of SUSY parameter space in question. Hence sbottom search at the LHC can be complementary to stop quark searches. Study of the prospect of a SUSY signal in a scenario where the sbottom is the NLSP has been performed in the literature in the channel $\tilde{b}_1 \to b\tilde{\chi}_1^0$ in the context of both LHC and ILC [43, 355–358].

Recently the CMS collaboration ruled out sbottom mass up to 500 GeV with 4.98 fb^{-1} of 7 TeV data assuming the branching ratio BR($\tilde{b}_1 \to b\tilde{\chi}_1^0$) to be 100% and the LSP mass of about 175 GeV [359]. This exclusion was also crucially dependent on the LSP mass and there was no exclusion limit for the LSP mass of about 200 GeV or higher.

However, in a large part of the MSSM parameter space the sbottom is not the NLSP. As a consequence, the branching ratios (BR) to channels other than $\tilde{b}_1 \to b\tilde{\chi}_1^0$ may be significant. Recently both the ATLAS and CMS collaborations have also searched for sbottoms in the leptonic channel in the decay mode $\tilde{b}_1 \to t\tilde{\chi}_1^{\pm}$ and in the hadronic mode with b-tagged jets in the $\tilde{b}_1 \to b\tilde{\chi}_1^0$ channel and have constrained a narrow region of parameter space assuming specific mass relations among $\tilde{b}_1$, $\tilde{\chi}_1^0$ and $\tilde{\chi}_1^{\pm}$ [40, 360]. For the leptonic channel the $\tilde{b}_1$ exclusion limits are $\sim$ 360-370 GeV for a $\tilde{\chi}_1^{\pm}$ mass $\sim$ 180-190 GeV, and a $\tilde{\chi}_1^0$ mass of 50 GeV. For the hadronic mode the exclusion limits are given in a model with gluino decaying into sbottom pairs with further decay into b-jets and lightest neutralino. The search excludes gluino masses around 1.1 TeV for sbottom masses in the range $\sim 400 - 800$ GeV and a $\tilde{\chi}_1^0$ mass of 60 GeV.

Most of the studies on third generation squarks, especially in the context of colliders have focused on the decay of lighter stop($\tilde{t}_1$) and sbottom($\tilde{b}_1$), $\widetilde{t}_1 \to t\chi_1^0$ and $\widetilde{b}_1 \to b\chi_1^0$ respectively. It has been observed that the feasibility of these channels depend critically on the mass difference

$$\Delta m = m_{\widetilde{t}_1(\widetilde{b}_1)} - m_{\chi_1^0}, \tag{9.1.3}$$

since it determines the hardness of the final state particles. A large value of Δm leads to large jet momentum and a sizable missing transverse momentum ($\not{p}_T$), both of which are imperative to suppress the SM backgrounds. Interestingly in the large Δm scenario, the use of jet-substructure and top tagging is also an important tool to suppress backgrounds [266, 361]. To alleviate the

problem of low mass differences shape analysis with various kinematic variables have also been considered [346].

As noted earlier the non-observation of a light sparticle in strongly interacting sector, i.e, a gluino and/or a squark of first two generation, in the sub-TeV regime along with the observation of a light Higgs have prompted ATLAS and CMS to perform dedicated searches for the third generations squarks. Note that, the limits on the masses of the squarks of first two generations using the generic SUSY searches are not applicable to the case of third generation squarks. The dedicated searches look for third generation squarks produced directly via QCD processes as well as those produced indirectly in gluino decays, in a plethora of final states coming from a variety of decay channels of $\tilde{t_1}$ assuming specific mass relationships among $\widetilde{g}$, $\widetilde{t}_1$, $\chi_1^{\pm}$ and the χ_1^0, assumed to be the lightest SUSY particle(LSP). The principle decay channels studied are $\widetilde{t}_1 \rightarrow t\chi_1^0$ and $\widetilde{t}_1 \rightarrow b\chi_1^{\pm}$, with leptons and b jets in the final state from top quark decay. ATLAS searched for $\tilde{t}_1$ in the decay channel, $\tilde{t}_1 \rightarrow t\chi_1^0$, from direct stop pair production using 8 TeV LHC data with 13 fb^{-1} luminosity and ruled out $m_{\tilde{t}_1}$ between 225 GeV- 575 GeV for an LSP mass up to 175 GeV [362]. ATLAS also probed $\tilde{t}_1$ in the channel $\widetilde{t}_1 \rightarrow b\chi_1^{\pm} \rightarrow b\chi_1^0 ff'$ assuming $\Delta m = m_{\chi_1^{\pm}} - m_{\chi_1^0}$ to be 5 GeV and 20 GeV. For $\Delta m = 5$ GeV they ruled out stop masses of about 600 GeV in a corridor of lightest neutralino mass [41]. With the use of the kinematic variable M_{T2}, ATLAS also excluded $m_{\tilde{t}_1}$ in the range of 150 GeV-450 GeV for the channel $\widetilde{t}_1 \rightarrow b\chi_1^{\pm}$, where the chargino is nearly degenerate with the $\tilde{t}_1$ state [363]. Similarly, CMS searched for $\tilde{t}_1$ in the channels $\widetilde{t}_1 \rightarrow t\chi_1^0$ and $\widetilde{t}_1 \rightarrow b\chi_1^{\pm}$, and excluded it with a mass between 160 GeV -430 GeV for a LSP mass up to 150 GeV [364].

In the following set of works, the emphasis is to probe various signatures of third generation squarks [44, 49].

9.2 Probing the left handed lightest sbottom in the four lepton channel

9.2.1 The left handed sbottom parameter space

In this work we consider the possibility of a light third generation of squarks, in particular we focus on a light sbottom and investigate the viability of its signal at the LHC with 14 TeV c.m. energy. We do not confine ourselves to a particular SUSY breaking scenario and perform our study without assuming any relations among the soft SUSY breaking parameters at the electroweak scale.

In this work we consider the decay of sbottom to the channels $\tilde{b}_1 \rightarrow b\tilde{\chi}_2^0$ and $\tilde{b}_1 \rightarrow t\tilde{\chi}_1^{\pm}$. The subsequent decays of $\tilde{\chi}_2{}^0 \rightarrow \tilde{\chi}_1{}^0 Z$ and $\tilde{\chi}_1{}^{\pm} \rightarrow \tilde{\chi}_1{}^0 W$ can now produce a number of hard leptons in the final state. A sample Feynman diagram is shown in Fig. 9.2.

The merits of considering the leptonic final state in particular, the 4 lepton channel is that it is rather clean and has minimal background. As we shall demonstrate below, it is possible to discover a SUSY signal for a substantial range of sbottom mass at 14 TeV LHC.

If no specific mechanism for the SUSY breaking is assumed then the total number of unknown parameters (the so called soft SUSY breaking terms) reaches a huge number (105) and it is almost impossible to carry out any phenomenological analysis with such a large number of free parameters. Many of these parameters in particular the intergenerational mixing terms and the complex phases are rather constrained from various measurements of both Charge-Parity (CP) conserving and CP-violating observables in K, B and D decays as well as lepton flavor violating decays [222]. It is then phenomenologically useful to make a few assumptions (which are indeed supported by experiments) like no new source of CP violation, diagonal sfermion mass matrices and tri-linear

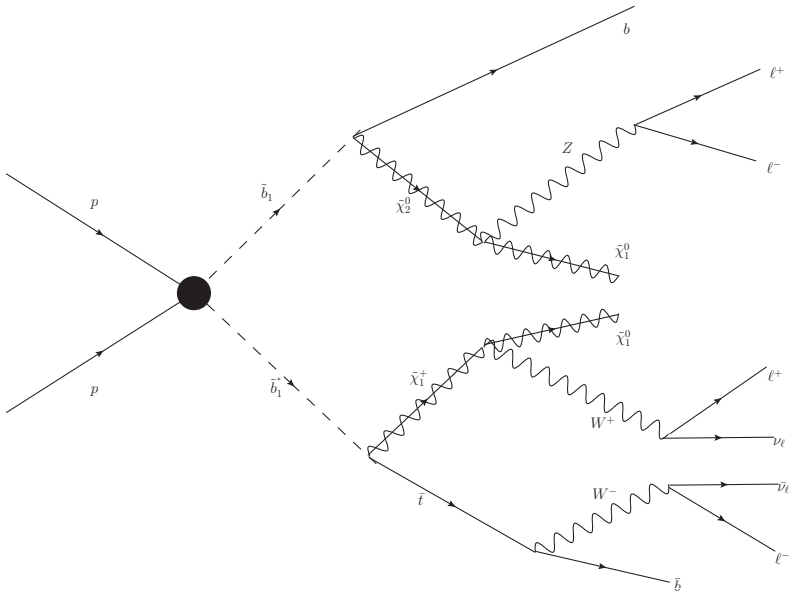

Figure 9.2: A sample Feynman diagram for the process $pp \to b\bar{b}\ell^+\ell^+\ell^-\ell^- + \not{p}'_{\mathrm{T}}$ in MSSM.

couplings etc. to reduce the number of free parameters. This rather simplified version of MSSM is called a phenomenological MSSM (pMSSM) [365]which has 22 free parameters. These parameters include

- The gaugino (bino, wino and gluino) mass parameters M_1, M_2 and M_3.
- The Higgs mass parameters m_{H_u}, m_{H_d}(which can be traded as μ and M_A) and the ratio of the Vacuum Expectation Values (VEV) of the two Higgs doublet namely $\tan\beta$.
- Common first and second generation sfermion mass parameters $m_{\tilde{Q}}, m_{\tilde{U}}, m_{\tilde{D}}, m_{\tilde{L}}, m_{\tilde{E}}$ and the third generation sfermion mass parameters $m_{\tilde{Q}_3}, m_{\tilde{t_R}}, m_{\tilde{b_R}}, m_{\tilde{L}_3}, m_{\tilde{\tau_R}}$.
- The common first and second generation tri-linear couplings A_u, A_d and A_e. The third generation tri-linear couplings A_t, A_b and A_τ.

In this work we take the pMSSM as our model framework and consider the constraints on the parameters coming only from the LEP exclusion limits [66], theoretical considerations like correct electroweak symmetry breaking, electric and color neutral LSP etc. and the lightest Higgs mass in the range 123 -128 GeV.

In Fig. 9.3 we show the production c.s. of a sbottom pair at the 14 TeV LHC. The cross sections are calculated using PROSPINO [17] in the limit where 1st two generation squarks are ~ 5 TeV, the gluino mass is around ~ 1.2 TeV and the stop mass is around 400 GeV. The Renormalization and Factorizations scales are set to the their default values in PROSPINO and the CTEQ6L parton distribution function has been used for the c.s. calculation. It can be seen that the cross section falls sharply from $\sim$ 10pb at 300 GeV to $\sim$ 10fb at 1TeV. It must be noted that the NLO cross section depends on the squark and gluino masses to some extent. In our scenario the first two generation of squarks and the gluino is decoupled from the thrid generation squarks.

The direct decay of sbottom to the LSP is always kinematicaly favored, and for right-handed squarks it can dominate if $\tilde{\chi}_1^0$ is bino like. This is generally the case with models like CMSSM

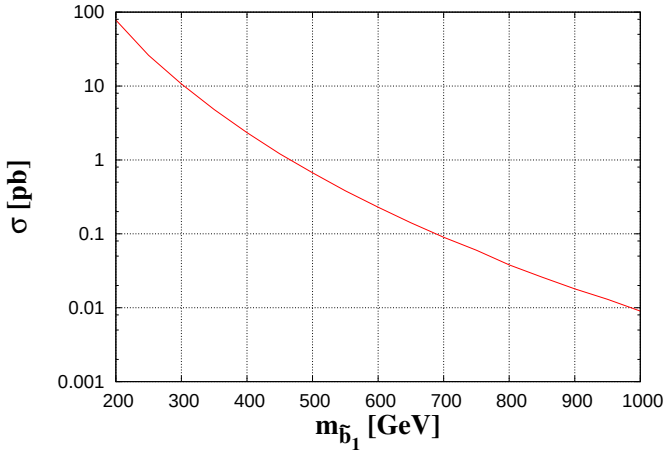

Figure 9.3: The central value of the Next to Leading Order (NLO) c.s. for the sbottom pair production at the 14 TeV LHC.

which has a large right handed component in the third generation mixing matrix. The bino co-annihilation case where the bino can co-annihilate with the NLSP sbottom is also an important scenario and has been considered in [43]. The interplay of sbottom and stop in the context of natural SUSY has been discussed in [356], where the authors argue that direct searches on sbottom can set limits on the stop sector from below causing a tension between naturalness which sets the stop scale from above and direct searches which constrain it from below.They also suggest that the limits on direct searches should depend on the admixture of left and right handed components of sbottom. The left handed nature of sbottom has been searched by CMS in [360], for 7 TeV LHC where they investigate the channel $\tilde{b}_1 \to t\tilde{\chi}_1^{\pm}$ in the dilepton + b-jets channel. This motivates us to investigate the scope of MSSM to admit a large left handed sbottom and ways to detect such a scenario. If the sbottom is left handed then it may prefer to decay strongly into heavier charginos or neutralinos instead, for example $\tilde{b}_1 \to b\tilde{\chi}_2^0$ and $\tilde{b}_1 \to t\tilde{\chi}_1^{\pm}$. This is because the relevant squark-quark-wino couplings are much bigger than the squark-quark-bino couplings. Squark decays to higgsino-like charginos and neutralinos are less important for sbottom (than stop) because of its relatively smaller Yukawa coupling. A light left-handed sbottom can be achieved by a large splitting between the left-handed and the right-handed components ($m_{\tilde{Q}_3}$ and $m_{\tilde{b_R}}$), in particular a light left-handed component ($m_{\tilde{Q}_3}$) and a heavy right-handed component ($m_{\tilde{b_R}}$). This ensures that once diagonalized the lighter sbottom remains predominantly left handed while the heavier sbottom remains mostly right handed. The sbottom mixing matrix in such a scenario is diagonal with the mixing angle $\theta_b \sim 0$. For our purpose therefore, the relevant parameters are the third generation squark mass parameters ($m_{\tilde{Q}_3}, m_{\tilde{t_R}}, m_{\tilde{b_R}}$), the tri-linear couplings A_t and A_b, the SU(2) and U(1) gaugino mass parameters (M_1 and M_2) and the Higgs sector parameters μ and $\tan\beta$.

To show that the situation we are considering is not a very fine tuned parameter space we vary the four parameters $m_{\tilde{Q}_3}, m_{\tilde{t_R}}, m_{\tilde{b_R}}$ in the range [100,3000] GeV and A_t in the range [-3000, 3000] GeV and calculate the branching ratios of sbottom to different channels. We keep $\tan\beta = 10$, $M_1 = 150\,\text{GeV}$ and $M_2 = 250\,\text{GeV}$ in the scan.

The first two generation squarks, and the three slepton generations are fixed at 5 TeV along with $M_3 = 1\text{TeV}$, and $A_u = A_d = A_\tau = 100\,\text{GeV}$ as they are irrelevant for our study. The μ parameter is set to 1000 GeV which implies that the lighter neutralino is gaugino like. We generate the physical

mass spectrum using the spectrum generator SuSpect [14]. A different set of choices for M_1 and M_2 do not significantly alter the collider results significantly as long as $\chi_2^0 \to \tilde{\chi}_1^0 Z$ is kinematicaly allowed as can be observed in the next section.

We choose $A_b = 0$ GeV in our scan but other values do not change the result in a significant manner. Fig 9.4 shows the maximum values of the branching ratios for the channels $\tilde{b}_1 \to b\chi_2^0$ and $\tilde{b}_1 \to t\chi_1^{\pm}$ as a function of the sbottom mass when we vary the parameters in the ranges mentioned above. It can be seen that significant branching ratios to these channels are allowed.

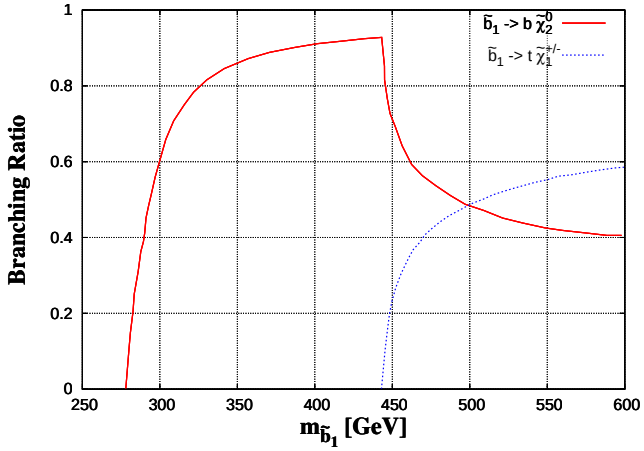

Figure 9.4: Maximum branching ratios of $\tilde{b}_1 \to b\chi_2^0$ (red/continuous) and $\tilde{b}_1 \to t\chi_1^{\pm}$ (blue/dotted) as a function of $\tilde{b}_1$ mass.

9.2.2 Signal and Background

We choose a few benchmark points to carry out the collider analysis. The parameters for these benchmark points along with the relevant BRs are shown in Table. 9.3.

	A_t	$m_{\tilde{Q}_3}$	$m_{\tilde{t}_R}$	$m_{\tilde{b}_R}$	$m_{\tilde{t}_1}$	$m_{\tilde{b}_1}$	$m_{\tilde{\chi}_1^0}$	$m_{\tilde{\chi}_2^0}$	$m_{\tilde{\chi}_1^{\pm}}$	BR($\tilde{b}_1 \to b\chi_2^0$)	BR($\tilde{b}_1 \to t\chi_1^{\pm}$)
P1	-2060	308	1922	1041	392	350	153	272	272	86 %	—
P2	-2335	401	1907	2626	470	450	153	272	272	71%	24 %
P3	-2680	492	2232	1904	573.1	550	152	271	271	44.5%	54.5%
P4	-2680	492	2232	1904	573.1	550	254	377	377	95%	-

Table 9.1: Masses of some of the sparticles for three benchmark points. In all the cases the other pMSSM parameters are fixed to values as described in the text.

In these parameter points the decay of sbottom proceeds mostly through the channels $\tilde{b}_1 \to b\chi_2^0$ and/or $\tilde{b}_1 \to t\chi_1^{\pm}$ following the deacys $\tilde{\chi}_2^0 \to \tilde{\chi}_1^0 Z \to l^+l^-\tilde{\chi}_1^0$ and $\tilde{\chi}_1^{\pm} \to \tilde{\chi}_1^0 W^{\pm} \to l^{\pm}\nu_l\tilde{\chi}_1^0$ from both sides which finally yield a 4-leptons + 2 b-jets + $\not{p}_T$ signal in the final state.

A look at the spectrum and the decay branching ratios point out that in absence of a sufficient mass gap for the top decay to open up, the principal decay mode is $\tilde{b}_1 \to b\tilde{\chi}_2^0$. When the mass difference is sufficient for the top channel the branching ratio is fairly equally divided between the two channels. This feature is also demonstrated in Fig 9.4.

As mentioned earlier, in order to show that a different choice of M_1 and M_2 do not change our results significantly as long as the decay $\tilde{\chi}_2^0 \to \tilde{\chi}_1^0 Z$ opens up we choose the benchmark point P4 in Table 9.3 in which M_1 and M_2 are changed to 250 GeV (from 150 GeV in P1 - P3) and 350 GeV (from 250 GeV in P1 - P3) respectively.

We mentioned earlier that the signal cross sections falls sharply with increasing $\tilde{b}_1$ mass. In particular, for an sbottom of 550 GeV (P-3) the NLO cross section reduces to 385 fb which, because of the very low branching ratio for the leptonic decay modes of Z, yields a miniscule final cross section. However since the background is miniscule and we are optimistic about high luminosity options for a 14 TeV LHC, this channel still offers some hope even for such high sbottom mass.

In our simulation of events, we have used PYTHIA6 [6] for both the signal as well as the backgrounds. We construct jets using the FastJet [8] package employing the anti-k_T [7] algorithm with a cone size $\Delta R = 0.5$. We use the CTEQ6L [13] parton density function from the LHAPDF [12] package. The scale is set at $Q^2 = \hat{s}$. We then use the following selection criteria for the final events:

1. We demand four isolated leptons (electron and muon) with the transverse momentum $p_T^\ell \geq 25$ GeV and the pseudo-rapidity $|\eta| \leq 2.5$. Isolation of leptons are ensured by demanding the total transverse energy $p_T^{AC} \leq 10\%$ of p_T^ℓ. Here p_T^{AC} is the scalar sum of transverse momenta of jets close to leptons satisfying $\Delta R(\ell, j) \leq 0.2$ with a jet p_T threshold of 30 GeV and $|\eta| \leq 3$. We ensure that the sum total charge of the 4 lepton system is 0 to avoid contamination from background.

2. Jets are selected with $p_T^j \geq 30$ GeV and $|\eta| \leq 3$. We demand at least 2 jets with b tags. The b-tagging is implemented by performing a matching of the jets with b quarks assuming a matching cone $\Delta R(b, j) = 0.3$.

3. In addition we demand $\not{p}_T > 50\,\text{GeV}$.

The effects of the above selection cuts are summarized in Table. 9.4. The potential SM backgrounds in our case are $t\bar{t}$, ZZ, WZ, and QCD. In Table. 9.4 we show only the non-vanishing background which in our case is the $t\bar{t}$.

Process	Production c.s. (pb)	Simulated Events	4 isolated ℓ	2 b-tagged jets	$\not{p}_T > 50$ GeV	$\frac{S}{\sqrt{B}}$ (50 fb^{-1})
P1	4.75	0.5M	5.1	1.4	1.1	26
P2	1.22	0.1M	1.5	0.5	0.4	10
P3	0.39	0.1M	0.5	0.2	0.2	4
P4	0.39	0.1M	0.6	0.2	0.2	4
tt	918	40M	2.8	0.09	0.09	

Table 9.2: Efficiency of the selection cuts for the signal in the three benchmark points and the top background for 14 TeV LHC. The cross-sections after each of the cuts (column 4 - 6) are given in femtobarns. Efficiency for 2 b-tagging has been multiplied in the 5th column. The significance has been quoted at a projected luminosity of 50 fb^{-1} in the last column.

The second column represents raw production c.s. for $\tilde{b}_1\bar{\tilde{b}}_1$ calculated at NLO using PROSPINO [17]. We have used the top pair production cross section at 14 TeV as quoted in Ref [366]. The third column represents the number of events simulated for each of the processes. From the fourth column the cumulative effects of the selection cuts are shown. In demanding b-jets we assume an optimistic b-tagging efficiency of 70% for each b-jet [367]. We find that even for the signal the

requirement of four isolated hard leptons with vanishing total lepton charge of the system leaves a small signal cross-section. On the other hand, this takes care of all the other backgrounds with the exception of $t\bar{t}$. The transverse momentum distribution of the 3rd hardest isolated (and $|\eta| < 2.5$) lepton is shown in the left panel of Fig.9.5 where a clear distinction can be made between the signal and the background. The lepton multiplicities for both the signal (benchmark-2) and $t\bar{t}$ background are also shown in the right panel of Fig. 9.5. Note that, though in the parton level a 3rd hard lepton is not expected from $t\bar{t}$ events, in real situation such leptons can come from the hadron decays for example, semileptonic decays of B hadrons.

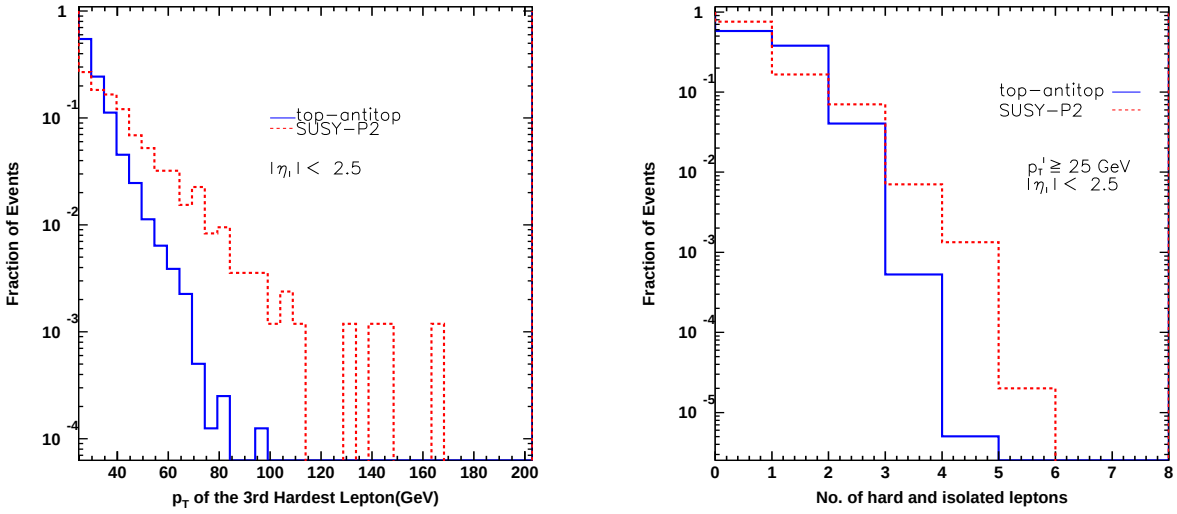

Figure 9.5: The P_T distribution of the 3rd hardest isolated (and $|\eta| < 2.5$) lepton (left panel) and the lepton multiplicities (right panel) for both the signal (benchmark-2) and the top background.

The demand of two b-like jets in addition to the four isolated hard leptons also removes a significant fraction of the top background. Since the $\not{p}_T$ is rather soft in the signal due to a low mass difference between $\tilde{\chi}_2^0$ and $\tilde{\chi}_1^0$, only a low $\not{p}_T$ cut could be used in selecting events. Our results are summmarized in the last column of Table. 9.4. The signal significance is obtained in terms of Gaussian statistics, given by the ratio $S/\sqrt{B}$ of signal and background events for a particular integrated luminosity. We project our significance ($S/\sqrt{B}$) at 50 fb^{-1} at 14 TeV LHC. We find that for low sbottom masses (up to 450 GeV) a reasonable significance ($S/\sqrt{B} \geq 5$) can be achieved at relatively low luminosities ($\sim$ 20 fb^{-1}). For masses of $\sim$ 500 GeV a higher luminosity of 50 fb^{-1} will be required. For even higher masses the sbottom production c.s. is miniscule and it will require at least 100 fb^{-1} luminosity to get any hint of a signal at LHC. As noted earlier we find that the change in LSP mass does not significantly change our signal significance. This can be seen in the event summary given in Table 9.4.

9.2.3 Summary and Conclusion

In this work we probed the prospect of a light sbottom search in the 4 lepton + jets (with two b-tagged jets) + $\not{p}_T$ channel in the context of pMSSM at 14 Tev LHC. We considered the scenario where the lighter sbottom is predominantly left handed and can decay into the second lightest

neutralino or lighter chargino which eventually yields 4 leptons and b jets. We find that in pMSSM there is a large part of parameter space where such a scenario is feasible and can be useful to look for sbottom signatures. We also find that such a parameter space is compatible with a Higgs mass of 125 GeV and is in tune with the ongoing motivation for a light third generation scenario.

Additionally we analyzed the signal and background for such regions of parameter space and found that it is possible to discover a substantial range of sbottom masses. In particular we find that for sbottom masses ~ 450 GeV it is possible to find a viable signal at the level of $S/\sqrt{B} \geq 5$ even at 20 fb^{-1} luminosity. For masses ~ 550 GeV and higher it will require higher luminosity LHC options which is achievable in the near future. It has to be noted that the channel has minimal background and the discovery reach is only cross section limited. We have demonstrated that as long as the studied decay channel is kinematically allowed our signal significance primarily depends on the signal cross section. Hence in our study the LSP mass plays a less significant role as compared to the NLSP sbotttom searches at the LHC which rely on a significant mass splitting between the sbottom and the LSP. In order to show this we calculated the signal using two different values of LSP mass viz. 152 GeV and 254 GeV.

9.3 Probing the flavor violating decay of the stop quark

In this work we turn our attention to stop quark. The LHC constraints on the third generation squarks, stops($\tilde{t}_{1,2}$) and sbottoms($\tilde{b}_{1,2}$) are weaker because of the lower production cross-section for a squark pair of a single flavor and are weakened even further when there is a small mass difference between the squark and the neutralino. The negative results in the initial searches for the gluino and first two generations of squarks, together with the discovery of the Higgs boson has prompted the consideration of natural SUSY as an attractive framework for phenomenological studies.

When the lighter stop becomes next to lightest SUSY particle(NLSP), the stop searches at colliders are quite different and become challenging. In this scenario, the dominant decay modes are via the flavor changing decays and the four body decay [368–370],

$$\tilde{t}_1 \rightarrow c\chi_1^0 \tag{9.3.1}$$

$$\rightarrow b f f' \chi_1^0. \tag{9.3.2}$$

Stop pair production followed by these decays leads to final states containing a heavy quark pair $c\bar{c}$ or $b\bar{b}$ respectively and are given by:

$$pp \rightarrow \tilde{t_1}\tilde{t_1^*} \rightarrow c\bar{c} + 2\chi_1^0, \tag{9.3.3}$$

$$pp \rightarrow \tilde{t_1}\tilde{t_1^*} \rightarrow b\bar{b} + 2\chi_1^0 + 2 f f'. \tag{9.3.4}$$

The flavor violating decay mode yields precisely two jets and missing transverse momenta($\not{p}_T$) due to the presence of χ_1^0. The relative decay rates into the above two channels are extremely sensitive to the model parameters [370, 371]. The signal sensitivity for the four body decay channels has been studied for different parameters [372].

For very low values of Δm (Eq. 9.1.3) it is rather difficult to obtain a reasonable signal sensitivity. In this case, the strategies have been to look at the mono-jet + $\not{p}_T$ [333, 334] and mono-photon+$\not{p}_T$ final state [373, 374]. The experimental limits on these channels come from reinterpretation of the monojet searches in ATLAS and CMS [375, 376]. With the available data at 7 TeV, lighter stops of mass below about 200 GeV are excluded for the above mentioned decay channels.

Thus the limits on the mass of the lightest stop from these channels are rather weak. This is because the final state objects are soft due to the low value of Δm leading to a lower acceptance of signal events. Therefore, it is a challenging task to probe these channels for very low Δm cases.

In this work we explore the possibility to find a signal for $\tilde{t_1}$ in the flavor violating decay, Eq. 9.3.3, resulting in a di-jet $+\not{p}_T$ signature. Note that the flavor violating decay mode is also important in the dark matter context in the stop co-annihilation scenario [370]. The correct relic density abundance in this case crucially depends on Δm. In analyzing this signal we apply different types of kinematic selection cuts which are described in the following sections. For the case of flavour violating decay mode, the presence of c-quarks can be exploited by tagging c-jets. It is known that tagging c-jets is not easy because of the low mass of c quark and the low decay length of the charmed mesons. However, development of a strategy to tag the c-jets, even with a modest efficiency will be helpful to suppress the SM backgrounds by an enormous amount and hence needs to be pursued.

9.3.1 CMSSM and PMSSM

We simulate the signal (Eq.9.3.2) for the parameter space of our interest in the context of both CMSSM and the phenomenological MSSM (pMSSM) with 19 parameters [365]. The CMSSM has been the most popular model of SUSY breaking in the context of collider phenomenology and experimental searches over the last two decades. This is primarily driven by the economy of the model which requires 4 parameters and a sign, as compared to the cornucopia of over 100 parameters in the MSSM. These parameters defined at the GUT scale, include the common scalar mass(m_0), the common gaugino mass($m_{1/2}$) and the common trilinear coupling A_0, along with $\tan\beta$, the ratio of vacuum expectation values(VEV) of the two Higgs doublets and the sign of μ, the Higgsino mass parameter, at the weak scale. The sparticle spectrum at the electroweak scale is obtained by renormalization group running from the GUT scale to the electroweak scale.

It is a well known fact the Higgs mass receives a substantial quantum correction resulting an enhancement of its mass from its tree level values which is bounded by mass of Z boson, viz, $M_H^2 \leq M_Z^2 \cos^2 2\beta$. In order to accommodate the Higgs mass of 125 GeV in the CMSSM framework one necessarily requires heavy scalars and a large trilinear coupling A_t. Loop corrections can increase the tree level Higgs mass up to $\sim$ 140 GeV, due to stop-top loops and a large value of the trilinear coupling A_t [194, 195]. However it has also been noted that such large trilinear coupling introduces a significant amount of fine tuning in the theory. On the other hand a large A_0 results in a large splitting in the stop mass matrix. This means that lighter stops are accessible at LHC energies even in CMSSM [195]. Hence it is worth investigating, in the CMSSM, the available parameter space, which provides $m_H \simeq 125$ GeV and where we have imposed various experimental and theoretical constraints as described below.

9.3.2 Constraining CMSSM

With this goal, we perform a numerical scan of the relevant part of the CMSSM parameter space, varying the range of parameters such as,

$$m_0 : [0-3 \ \text{TeV}], m_{1/2} : [0-1 \ \text{TeV}], A_0 : [-2 : -10 \ \text{TeV}], \tag{9.3.5}$$

and setting the top quark mass to be 172.9 GeV. We generate 5×10^5 random parameter points for a fixed value of $\tan\beta$. We fix the sign of the Higgsino mass parameter μ to be positive. We use

the SusPect [14] spectrum generator to generate the masses of the supersymmetric particles for a fixed set of input parameters along with SuperIso [16] for the calculations of the branching ratios of rare B-meson decays.

We refer to a point in the CMSSM parameter space as allowed if it survives the following constraints:

(i) The lightest Higgs boson mass M_H falls in the window 122.5 GeV $< M_H <$ 129.5 GeV. Note that this range also includes a 1.5 GeV theoretical uncertainty over and above the 95% C.L. uncertainties quoted by the ATLAS and CMS collaborations [1, 2].

(ii) The branching ratio ($\mathscr{B}$) of the radiative decay $B \to X_s\gamma$ satisfies the following 95 % C.L. bound [26],

$$2.6 \times 10^{-4} < \mathscr{B}(B \to X_s\gamma) \quad < 4.5 \times 10^{-4} \, .$$

(iii) The branching ratio of $B_s \to \mu^+\mu^-$ [178, 179] lies in the 95 % C.L. allowed range

$$1.5 \times 10^{-9} < \mathscr{B}(B_s \to \mu^+\mu^-) < 4.3 \times 10^{-9} \, .$$

Fig 9.6 - 9.7 show the results of our numerical study. A point is green if it satisfies only the constraint (i) but none of the other two. The blue colour is used to mean that the point satisfies both the constrains (i) and (ii) but not (iii). If a point is allowed by all of the three constraints above then the point is plotted in magenta. Note that all the points (except the red points in the $m_0 - m_{1/2}$ plane) have been checked to satisfy the requirements of electroweak symmetry breaking, electric and colour neutral LSP, the LEP lower bounds on the masses and other theoretical consistencies e.g., absence of tachyonic states and so on. Moreover, we also show the allowed values of $m_{\tilde{t}_1}$ for a wide range of $m_{1/2}$ and A_0 values (in the second row).

From these figures it is quite clear that even in the CMSSM, there exists regions in the parameter space where a light stop below a TeV scale is allowed

9.3.3 Stop decay and benchmarks

While it is certainly interesting to find a large region of parameter space pertaining to lighter stops and allowed by the Higgs mass constraint, the specific mass relations in CMSSM ties our hands to a large extent. In the context of natural SUSY it is enough to consider only the third generation squarks (stops and sbottoms), the third generation trilinear couplings along with charginos and neutralinos. The rest of the spectrum is mostly unimportant and can be decoupled from this set. This rather simplified approach, in the framework of the phenomenological MSSM (pMSSM) brings out the relevant physics with the minimal number of input parameters.

The parameter space of our interest is guided by the region where the flavor violating decay $\widetilde{t}_1 \to c\chi_1^0$, is kinematically dominant for relatively small mass differences corresponding to Eq. 9.1.3. The decay width is given by [368, 369],

$$\Gamma = \frac{1}{2}\alpha|\varepsilon|^2 m_{\tilde{t}_1}\left[1 - \frac{m^2_{\chi_1^0}}{m^2_{\tilde{t}_1}}\right]^2 , \tag{9.3.6}$$

where the loop factor ε is directly proportional to A_b^2 and $\tan^2\beta$ with α being the strong coupling constant [1].

A competing decay mode to the two body is the four body decay($\tilde{t}_1 \to b\chi_1^0 f f'$) [368, 369, 371], dominantly via an off shell chargino into fermions. The two body decay mode, which is

[1] For an exact one-loop calculation of this decay width see [369].

quadratically dependent on tanβ and A_b dominates over the four body decay for moderate to high tanβ. In the large tanβ scenario, the two body decay mode dominates over the four body decay mode, for similar mass differences as compared to lower tanβ.

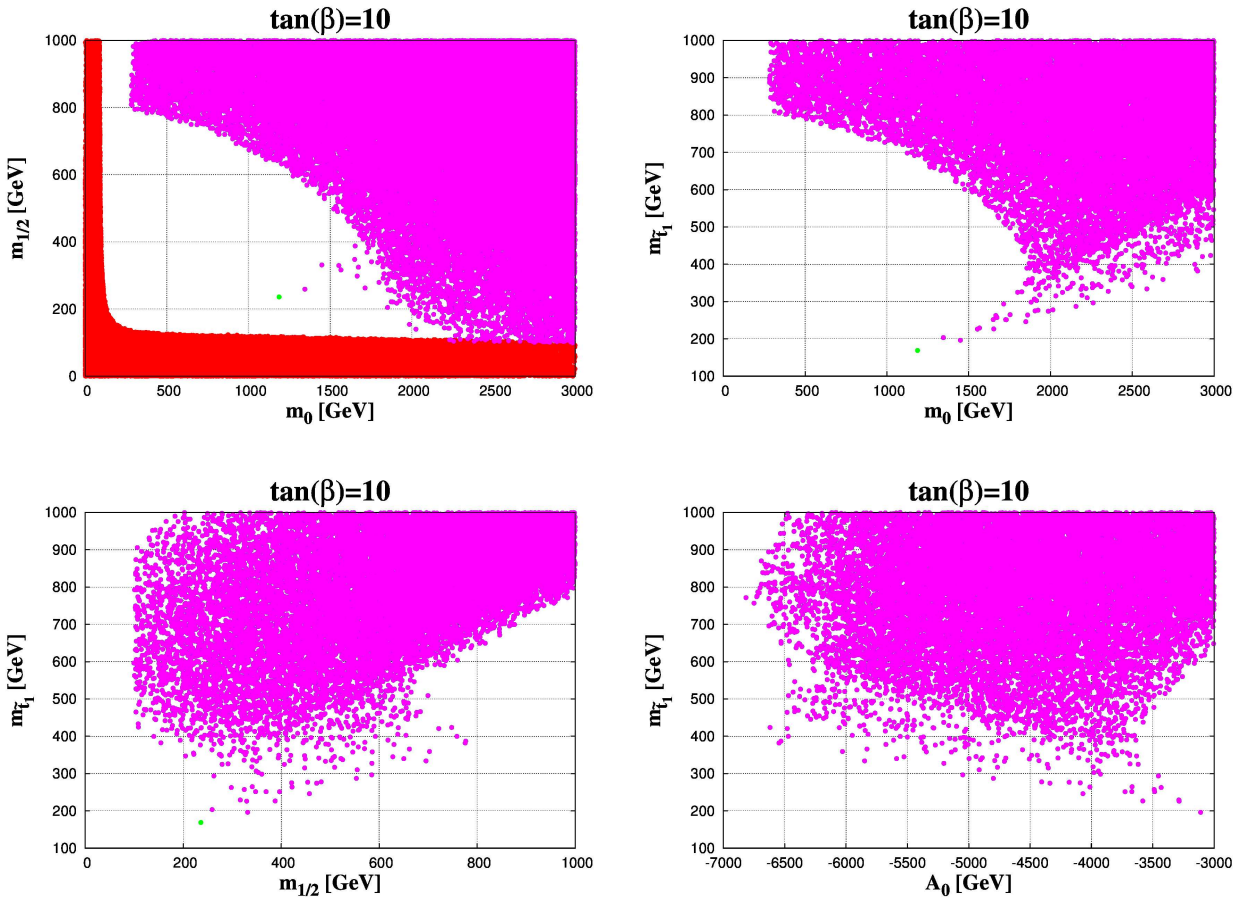

Figure 9.6: The allowed parameter points in the $m_0 - m_{1/2}$ (top left panel), $m_0 - m_{\tilde{t}_1}$ (top right panel), $m_{1/2} - m_{\tilde{t}_1}$ (middle left panel), $A_0 - m_{\tilde{t}_1}$ (middle right panel), in the CMSSM scenario for tan$\beta = 10$.

We choose two benchmark points in the CMSSM and four points in the 19 parameter pMSSM for our collider analysis. The representative points are shown in Tables 9.3 and 9.4, indicating the relevant branching ratios and other sparticle masses. All points in CMSSM (P1,P2) and three points in pMSSM(P3,P4,P5) are chosen to have tan$\beta = 10$. We choose one additional benchmark point with tanβ=30 in pMSSM(P6).

For the pMSSM benchmarks in Table 9.4, we set the first two generation of squarks and all slepton generations to 5 TeV and the gluino to 1.5 TeV as they are irrelevant for our study. The parameter M_2 is set to 900 GeV. The trilinear couplings with the exception of A_t are all set to zero. The pseudoscalar mass m_A is set to 500 GeV. All the benchmark points have been checked against the constraints mentioned in Sec. 9.3.2.

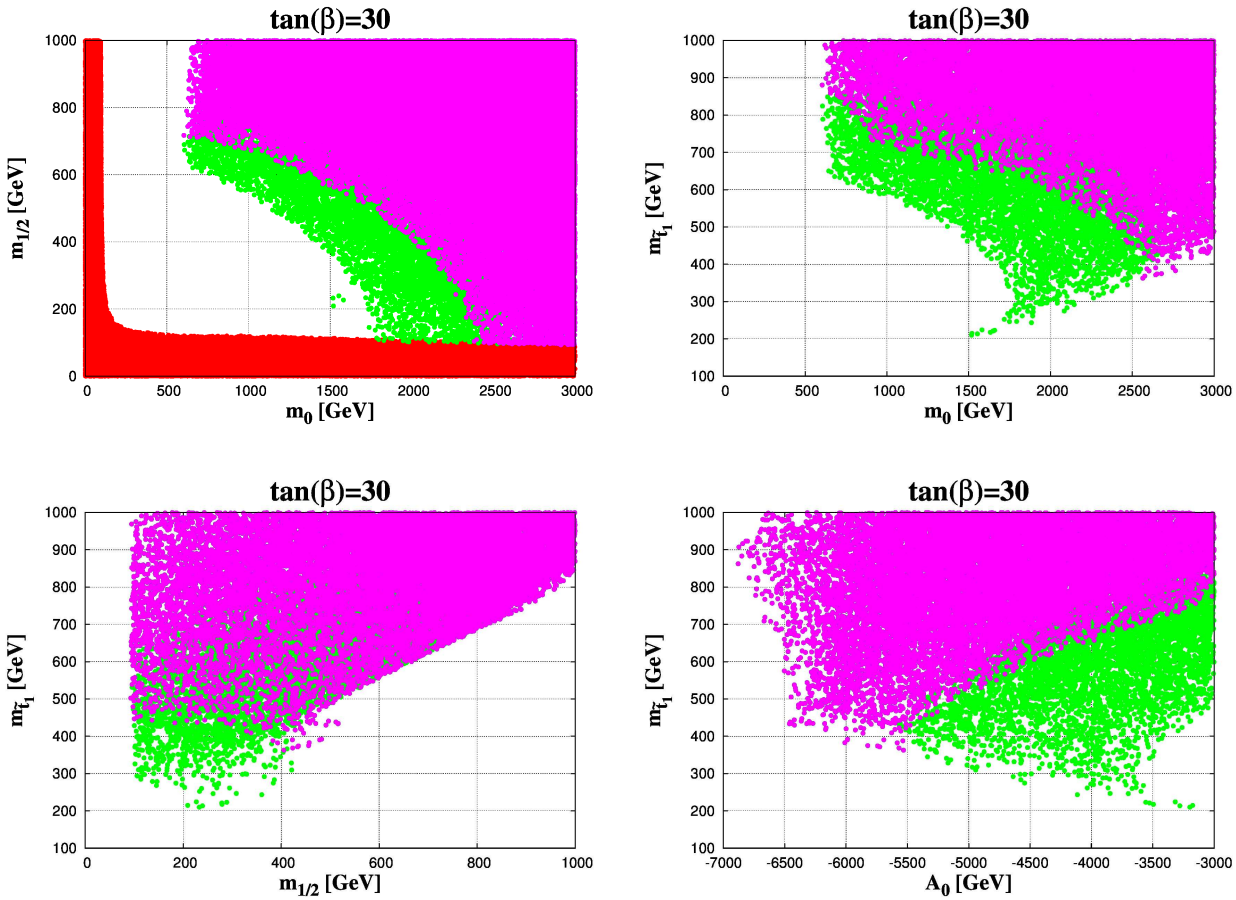

Figure 9.7: The allowed parameter points in the $m_0 - m_{1/2}$ (top left panel), $m_0 - m_{\tilde{t}_1}$ (top right panel), $m_{1/2} - m_{\tilde{t}_1}$ (middle left panel), $A_0 - m_{\tilde{t}_1}$ (middle right panel), in the CMSSM scenario for $\tan\beta = 30$.

9.3.4 Signal and background

We simulate the collider signatures of the stop pair production (Eq .9.3.3) for the benchmark points as shown in Tables 9.3 and 9.4 in the dijet + $\not{p}_T$ scenario and the corresponding SM background at the LHC.

As pointed earlier, the final state objects like jets and $\not{p}_T$ are expected to be soft because of low Δm making it difficult to obtain a reasonable acceptance after suppressing the SM backgrounds. The signal cross section is rather small at 8 TeV and falls to $\sim$ 50 fb for a stop mass of 500 GeV. Most of the search strategies proposed have taken recourse to monojet + $\not{p}_T$ or monophoton + $\not{p}_T$ searches, where a hard QCD jet is used along with a large $\not{p}_T$ [334]. It was demonstrated in [334] that with this strategy it is possible to use this channel for stop discovery, for stop masses up to $\sim$ 300 GeV at 14 TeV LHC, with 100 fb^{-1} luminosity.

Corresponding to the signal the principal SM backgrounds that can mimic the signal process are:

- **QCD** : The final state is swamped by the QCD dijet events, since the QCD cross section at hadron colliders is enormous. The $\not{p}_T$ source in this case comes from semileptonic B-decays. There are non physics sources due to mismeasurement of jets, detector noise which are out of

	$tan\beta$	m_0	$m_{1/2}$	A_0	m_H	$m_{\tilde{t}_1}$	$m_{\chi_1^0}$	Δm	Br($\tilde{t}_1 \to c\chi_1^0$) %	Br($\tilde{t}_1 \to bff'\chi_1^0$) %
P1	10	1848	457.6	-4069	126.0	241	198	43	74	25
P2	10	2589	695	-5849	126	331	306	25	97	2

Table 9.3: Masses and branching ratios of some of the particles in the CMSSM scenario. All energy units in GeV. sgn(μ) is set to be positive.

	A_t	$tan\beta$	μ	M_1	m_H	$m_{\widetilde{Q_3}}$	$m_{\tilde{t}_R}$	$m_{\tilde{b}_R}$	$m_{\tilde{t}_1}$	$m_{\chi_1^0}$	Δm	BR($\widetilde{t_1} \to c\chi_1^0$) %	BR($\tilde{t}_1 \to bff'\chi_1^0$) %
P3	-1900	10	800	280	123.0	380	1500	2000	355	285	70	98	2
P4	-2800	10	800	425	124.6	450	1800	1800	458	432	26	96	3
P5	-2800	10	800	510	126.6	530	1800	1800	548	517	31	95	4
P6	-2800	30	800	425	128	500	1800	1800	520	432	88	98	2

Table 9.4: Masses of some of the sparticles for the benchmark points in the pMSSM scenario. In all cases , the remaining parameters are as described in the text. All energy units are in GeV.

the scope of this study.

- **Z($\to \nu\bar{\nu}$) + jets** : This makes up the irreducible part of our background that looks exactly like the signal. Although the principal part of this background is Z + 2 jets, contribution from higher jet multiplicities are not negligible if some of the jets are not identified.
- **W($\to l\bar{\nu}$) + jets** : This process contributes dominantly to the background when the lepton is not identified. Since the cross section for W + jets is rather large this also contributes significantly to the background.
- $t\bar{t}$: This is primarily dominant when either the leptons from the W decay and/or some of the final state jets are not identified leading to the same configuration as the signal.
- **WW** : This process contributes to the background when one W decays hadronically while the other leptonically.
- **WZ** : This again contributes substantially to the background when W decays leptonically and Z decays hadronically with the lepton not being identified, or when Z decays to $\nu\bar{\nu}$ and W hadronically.
- **ZZ** : This irreducible background mimics the signal in the situation Z($\to \nu\bar{\nu}$)Z($\to q\bar{q}$).

We simulate the signal and the background processes $t\bar{t}$, WW,WZ,ZZ using PYTHIA6 [6]. For the background processes W/Z+jets, parton level events are generated using ALPGEN [9] and subsequently passed on to PYTHIA6 for showering and hadronization. Jets are reconstructed using FastJet [8] with anti-k_T [7] algorithm setting a size parameter R=0.5. Jets are selected with the following criteria,

$$p_T^j \geq 30(60)\ \text{GeV}\ \forall\ 8(13)\ \text{TeV},\ |\eta| \leq\ 3. \tag{9.3.7}$$

MLM matching [11] is performed while showering parton level events using PYTHIA for W/Z+ jets with a matching cone of ΔR =0.7 and a jet p_T threshold of 30 GeV within $|\eta| \leq 2.5$. We use

CTEQ6L [13] as parton density function(PDF) from the LHAPDF [12] package and set $Q^2 = \hat{s}$. Leptons are selected with,

$$p_T^l \geq 10\ GeV,\ |\eta| \leq 2.5, \tag{9.3.8}$$

which are used to veto events.

In order to suppress these backgrounds, in particular the large QCD di-jet background, we use kinematic variable,

$$\alpha_{\mathrm{T}} = \mathrm{p}_{\mathrm{T}}^{\mathrm{j_2}}/\mathrm{m}_{\mathrm{T}}^{\mathrm{jj}}, \tag{9.3.9}$$

where $\mathrm{p}_{\mathrm{T}}^{\mathrm{j_2}}$ is the transverse momentum of the second hardest jet and $\mathrm{m}_{\mathrm{T}}^{\mathrm{jj}}$ is the transverse mass of the two jet system [46]. It can be observed that for pure dijet events, without any hard $\not{\mathrm{p}}_{\mathrm{T}}$ like QCD, the jets are back to back in the transverse plane. Therefore the minimum value of m_T^{jj} in the limit when jet masses can be ignored turns out to be $2p_T^j$ and thus the distribution of α_{T} has a sharp end point at 0.5. However for dijet events in association with a significant amount of $\not{\mathrm{p}}_{\mathrm{T}}$, as is the case for the signal in Eq. 9.3.3, the two jets are not back to back, leading to large values of α_T. We present the α_T distribution for signal and background in Fig. 9.8 subject to the jet selection cuts (Eq. 9.3.7) along with lepton veto. The signal process is for P2 in Table 1 with $m_{\tilde{t}_1}, m_{\chi_1^0}$ masses of 331 and 306 GeV respectively. It can be seen in the figure, that as predicted, the QCD process has a sharp fall at ≈ 0.5 and therefore we impose a selection cut [46],

$$\alpha_T > 0.55. \tag{9.3.10}$$

In addition we also use the kinematic variable M_{T2} [47, 377] defined as,

$$\mathrm{M_{T2}}(\mathrm{j_1}, \mathrm{j_2}, \not{\mathrm{p}}_{\mathrm{T}}) = \min\left[\max\{\mathrm{M_T}(\mathrm{j_1}, \chi), \mathrm{M_T}(\mathrm{j_2}, \chi)\}\right], \tag{9.3.11}$$

the minimization being performed over $\not{\mathrm{p}}_{\mathrm{T}}^1 + \not{\mathrm{p}}_{\mathrm{T}}^2 = \not{\mathrm{p}}_{\mathrm{T}}$ where $\not{\mathrm{p}}_{\mathrm{T}}^1, \not{\mathrm{p}}_{\mathrm{T}}^2$ are all possible partitions of invisible transverse momentum($\not{\mathrm{p}}_{\mathrm{T}}$), which is due to the presence of LSP for signal and neutrinos for SM backgrounds. Here χ is the invisible particle whose mass (M_χ) is an unknown parameter. The kinematic variable transverse mass(M_T) between the jet and the accompanying missing particle is,

$$M_T^2 = M_j^2 + M_\chi^2 + 2(E_T^j E_T^\chi - \vec{p}_T^{\,j}.\vec{p}_T^{\,\chi}), \tag{9.3.12}$$

where $\vec{p}_T^{\,j}$ is the transverse momentum vector of the jet and E_T^j the corresponding energy, while $\vec{p}_T^{\,\chi}$ is the missing transverse momentum ($\not{\mathrm{p}}_{\mathrm{T}}$) vector.

Since the maximum value of M_T is restricted to the mass of the parent particle, M_{T2} is also expected to be bounded by the respective parent particle mass. Here M_{T2} is calculated by setting M_χ=0 without any loss of generality [48]. This assumption is clearly valid for SM processes where the missing momentum is mainly due to neutrinos. Furthermore, we found no significant difference to the population of events near the end points for the signal with massive χ when we make this assumption. However, there may be a difference in acceptance for the two cases which we will consider as a systematic uncertainty in the acceptance efficiency. In the SUSY processes where the parent particle($\widetilde{\mathrm{t}}_1$) is heavier than SM particles, the tail in the M_{T2} distribution is expected to extend up to a larger value. This variable thus provides an excellent handle to suppress the remainder of the background rates.

In Figure 9.9, the signal and background distributions for $\mathrm{M_{T2}}$ are displayed for 8 (left) and 13(right) TeV LHC energies. The distribution is subject to a di-jet criteria along with a lepton veto with jet and lepton selection criteria(Eq.9.3.7 and 9.3.8) . The signal distribution displayed in the figure corresponds to the benchmark P2 in Table 9.3.

We observe that for the signal process at 8 TeV the tail extends beyond the background processes and further reaches beyond the stop mass while for the background the end point of the distributions correspond to lower values of M_{T2}. As the missing energy in Z+jets comes from Z decaying to a pair of neutrinos from the same side of the configuration, the M_{T2} distribution is not expected to have an end point at the Z mass which is reflected in this plot [48].

Similarly in case of $t\bar{t}$ and in signal, the distribution extends beyond the end point which is expected to be at the parent particle mass. The contribution of events in this region is dominantly due to the jets from hard radiations, in particular from final state radiations [48]. This phenomena is more evident at 13 TeV energy where objects are kinematically heavily boosted. By observing the distributions, we apply a cut at,

$$M_{T2} > 130 \text{ GeV}(250 \text{ GeV}) \text{ for } 8(13) \text{ TeV}. \tag{9.3.13}$$

This fact can be exploited to suppress backgrounds when the signal is in unfavourable condition kinematically (eg. for small Δm). For example, for very small Δm, $\tilde{t}_1$ mostly decays invisibly, and hence M_{T2} constructed out of this hard $\not{p}_T$ and jets originating from initial and final state radiation(ISR/FSR) which are un-correlated with the $\not{p}_T$ has a much larger tail. For larger values of Δm, the longer tail is not observed due to the fact that $\tilde{t}_1$ will have both visible and the invisible (LSPs) decay products for which the momenta are correlated. In Fig.9.10 we present the distribution for these two cases, with Δm =10 and 140 GeV. Clearly M_{T2} gives some handle to recover sensitivity for the low Δm scenario. It is to be noted here also that for the case $\Delta m = 140$ GeV, the decay $\tilde{t}_1 \to bW\chi_1^0$ may open up, competing with the flavor violating decay mode. Clearly the flavour violating decay mode with very low Δm have some benefits due to ISR/FSR effects. However, it is clear that these effects have a dependence on the models employed in the event generators. Therefore, in order to understand its effect in our signal sensitivity in a more precise manner one needs to do more detailed investigation which is postponed to a future work.

Finally, considering signal and background characteristics, we use the following cuts to suppress the backgrounds.

- **Lepton Veto (LV) :** In the signal process leptonic activity is absent. However background processes like $t\bar{t}$, W+jets, WW,WZ contain a significant fraction of leptons from W/Z decays accompanied by $\not{p}_T$. The use of lepton veto thus helps to suppress the backgrounds efficiently. Leptons are selected using cuts described in Eq. 9.3.7.

- **2 jets (2J) :** We select exclusively dijets with the jet p_T thresholds as described in Eq. 9.3.8. Note that after the lepton veto, the $t\bar{t}$ background contribution is expected to be rich in hadronic activity and have more than 2 jets in the event. Hence a strict imposition of the dijet criteria is expected to reduce the background coming from the $t\bar{t}$, W/Z + jet processes.

- **b-jet veto (bJV) :** This veto is extremely efficient in suppressing the top background. The b-jet identification is implemented by performing a matching of the jets with b quarks assuming a matching cone $\Delta R(b, j) = 0.2$.

- $\alpha_T \geq 0.55$ as discussed in Eq. 9.3.10.

- $M_{T2} \geq$ 130 GeV (250 GeV for 13 TeV) as given by Eq. 9.3.13.

- $\not{p}_T/H_T \leq 0.9$ **:** For signal processes we expect this ratio to be less than 1, while in background processes this is expected to be close to 1. The difference in azimuthal angle between

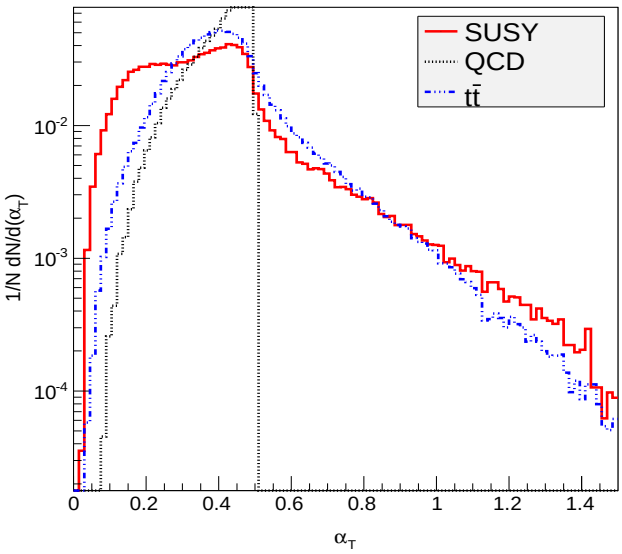

Figure 9.8: α_T distribution for signal and background at 8 TeV LHC energy. The signal corresponds to P2 from Table 9.3.

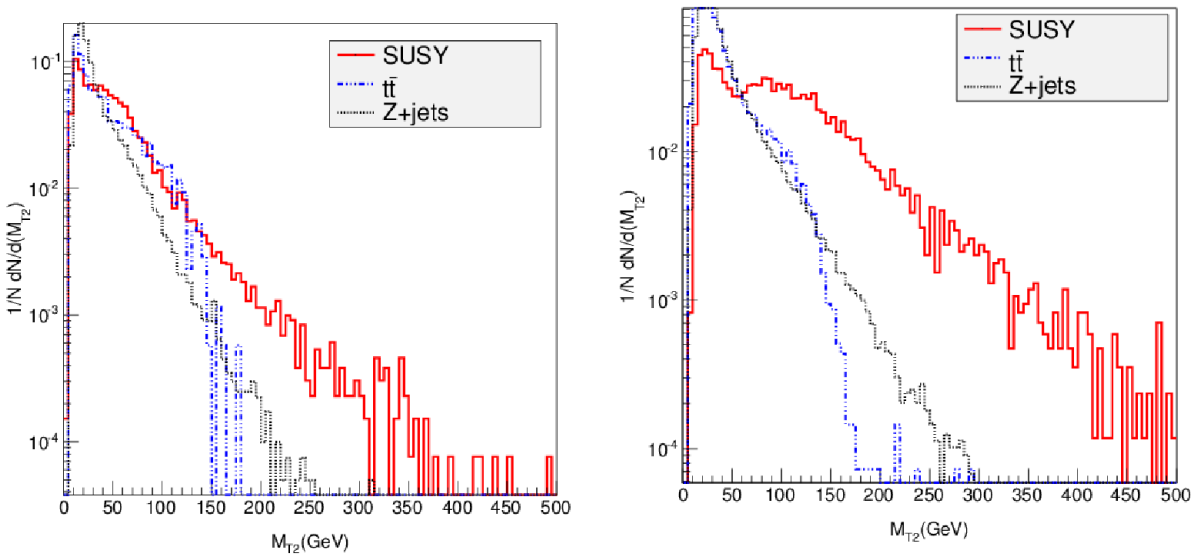

Figure 9.9: M_{T_2} distribution for signal and background for 8 TeV(left) and 13 TeV(right). The signal corresponds to P2 in Table 9.3.

Proc	$m_{\tilde{t}_1}, m_{\chi_1^0}$ GeV	C.S	LJV+2J+bJV	α_T ≥ 0.55	$M_{T2} \geq$ 130	$\frac{\not{p}_T}{H_T}$ ≤ 0.9	C.S	C.S (c-like)
P1	241,198	6330	1996.2	262.3	4.7	2.1	2.1	0.45
P2	331,306	1060	227.4	28.1	2.3	0.9	0.9	0.1
P3	355,285	700	262	46	0.6	0.25	0.25	0.12
P4	458,432	150	33.1	4.2	0.3	0.14	0.14	0.01
P5	548,517	45	11.5	1.42	0.1	0.04	0.04	0.007
P6	520,432	63	23.5	4.1	0.085	0.04	0.04	0.02
tt-5-200		85000	6063.4	80.24	8.9	0.46	0.46	0.17
$t\bar{t}$-200-500		9500	13.9	3.9	1.5	0.38	0.38	1
$t\bar{t}$-500- ∞		130	2.1	0.005	0.003	0.003	0.003	< 1
qcd-300-500		1.3×10^6	37512.7	< 1	< 1	< 1	< 1	< 1
WW		35000	7462.2	380.2	2.94	0.84	0.84	0.14
WZ		13000	2547.8	189.3	3.1	0.76	0.76	0.21
ZZ		5400	1050.1	78.12	1.62	0.3	0.3	0.02
$Z(\rightarrow \nu\bar{\nu})$+2jet		10^5	71215.2	6877.4	67.07	29.4	29.4	< 1
$Z(\rightarrow \nu\bar{\nu})$+3 jet		16500	5349.6	637.0	9.9	4.5	4.5	0.13
$Z(\rightarrow \nu\bar{\nu})$+4 jet		4240	361.4	41.3	0.75	0.6	0.6	< 1
$W(\rightarrow l\nu)$+2jet		5.8×10^5	117335.6	10752.1	63.4	35.3	35.3	2.1
$W(\rightarrow l\nu)$+3jet		10^5	14100.0	1240.8	9.1	6.1	6.1	< 1
$W(\rightarrow l\nu)$+4jet		16300	785.6	68.9	1.5	1.1	1.1	< 1

Table 9.5: The cross sections(fb) for signal and backgrounds after each cuts. The last two columns present normalized cross section(fb) after all cuts without and with identification of c-like jets respectively. All energy units are in GeV.

the two jet system and missing energy in signal and background being primarily responsible for this behaviour. We find that this selection is extremely effective in suppressing the $t\bar{t}$ background.

At the end, we explore the possibility of an improvement by somehow tagging charm jets which are a part of the signal. The identification of charm jet is quite challenging. Recently however, attempts have been made to measure W + c jets cross-section where c-jets are identified [378]. Note that the channel $\tilde{t}_1 \rightarrow c\chi_1^0$, has been recently searched by ATLAS by trying to identify charm jets in the final state [379]. Although the method we employ is rather simplified, it still points out that charm like jet identification can prove to be extremely effective in this case. To identify charm jets we match jets with charm quarks, using a matching cone of R=0.2. To find the presence of charm jets one can further check the presence of D-meson among the jet constituents, which we postpone to a future work.

Simulating the signal and background processes using the selection cuts as described above, we present results for 8 and 13 TeV LHC energies in Tables 9.5 and 9.6 respectively. The first three columns present the processes(Proc), the masses of the lightest stop($m_{\tilde{t}_1}$) and LSP($m_{\chi_1^0}$) and the cross section(C.S) respectively. We compute the next to leading order signal cross section using PROSPINO [17]. The subsequent columns display the cumulative effects of cuts. In the penultimate column the cross sections after all cuts are presented. The top and the QCD backgrounds are simulated by slicing the entire phase space into $\hat{p}_T$ bins, where $\hat{p_T}$ is the transverse momenta of the produced partons in the partonic frame. In both Tables we notice that the combined effects of lepton veto, b-jet veto and the dijet criteria (LV+2J+bJV) reduces the top background by an enormous amount ($\sim 95\%$) while reducing the signal process by about a third. As pointed out earlier, the α_T cut successfully isolates the entire QCD background as expected. For the sake

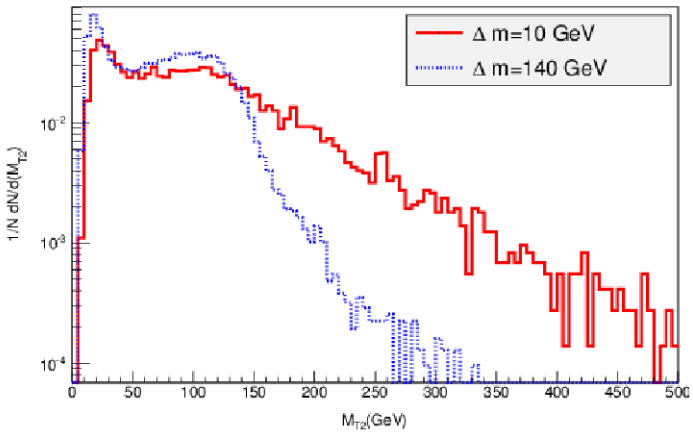

Figure 9.10: M_{T2} distribution for two values of Δm of 10 GeV for solid(red) and 140 GeV for broken(blue) for a $m_{\tilde{t}_1}$ of 240 GeV at 13 TeV LHC energy.

of simplicity we have quoted numbers corresponding to only one $\hat{p}_T$ bin for QCD. The rest of the backgrounds, particularly from top and the WW/WZ/ZZ are also suppressed by a significant amount, costing a significant fraction of signal cross section as well. The M_{T2} cut, as pointed out, removes a substantial fraction of $t\bar{t}$, WW/WZ/ZZ as well as W/Z+jets processes. Clearly the M_{T2} cut plays an important role in isolating backgrounds efficiently. Finally the cut $\not{p}_T/H_T$ suppresses the WW/WZ/ZZ backgrounds and brings it down to a negligible level. Even after a huge suppression of the irreducible backgrounds W/Z+2,3 jets, the remaining fraction is non negligible because of the large production cross section. Note that even after suppressing the SM backgrounds substantially, since signal cross section is miniscule, the prospects of discovering a signal at 8 TeV LHC is very limited. In the last column cross sections are presented requiring that out of the two jets in the final state one is a c-like jet. As mentioned earlier, c-like jets are identified by naively matching partonic c-quarks and reconstructed jets. Clearly, it shows that identification of c-like jets does help in reducing the background to a large extent. This happens as the signal is likely to have a larger fraction of identified charm jets than the background.

At 13 TeV the results improve significantly as can be seen from Table 9.6. The larger stop pair production cross section significantly helps in enhancing the event rates. On the other hand an increased boost in the system helps to effectively use the M_{T2} variable by applying a much larger cut value of 250 GeV to isolate the backgrounds. As can be observed from the right panel of Fig 9.9, a cut of 250 GeV is extremely effective in suppressing the irreducible Z+jets background. We observe from the last column of Table 9.6 that at 13 TeV energy, the signal and background cross sections are comparable as compared to 8 TeV where the background cross sections are dominant.

Table 9.7 summarizes cross sections of the signal and background after all cuts for 8 and 13 TeV LHC energy. The $t\bar{t}$ cross section has been multiplied in the table by a k factor of 2 to take into account NLO effects [268]. Note that the k-factors for W/Z + jets processes are very close to 1 [320, 321], and hence do not change our results significantly. From Table 9.7 we find that at 8 TeV the total background is 70.6 fb in which the dominant contribution comes from W/Z + jets, while the signal cross section varies from 2.1 fb for P1 to 0.04 fb in P6. Therefore for P1 with 20 fb^{-1} luminosity we obtain $S/\sqrt{B} = 1.1$, while the significance drops substantially with the increase of $m_{\tilde{t}_1}$. At 13 TeV the total background cross section turns out to be 2.6 fb while

Proc	$m_{\tilde{t}_1}, m_{\chi_1^0}$ GeV	C.S	LJV+2J+bJV	α_T ≥ 0.55	$M_{T2} \geq$ 250	$\frac{\not{p}_T}{H_T}$ ≤ 0.9	C.S	C.S (c-like)
P1	241,198	24100	3113.2	311.6	8.1	4.4	4.4	0.45
P2	331,306	4800	440.2	82.0	5.8	3.2	3.2	0.18
P3	355,285	3280	725.5	83.27	1.95	0.7	0.7	0.14
P4	458,432	820	84.7	16.8	1.63	0.75	0.75	0.03
P5	548,517	290	34.2	6.2	0.5	0.29	0.29	0.023
P6	520,432	400	121	17.8	0.29	0.1	0.1	0.04
tt-5-200		291,000	18690.2	2011.1	0.15	0.15	0.15	< 1
$t\bar{t}$-200-500		39800	492.2	85.2	< 1	< 1	< 1	< 1
$t\bar{t}$-500-∞		900	12.4	0.13	< 1	< 1	< 1	< 1
WW		69800	11858.3	376.2	0.14	< 1	< 1	< 1
WZ		26300	4144.9	231.5	0.5	0.15	0.15	< 1
ZZ		10900	1812.6	128.9	0.46	0.06	0.06	< 1
$Z(\rightarrow \nu\bar{\nu})$+2jet		241,800	34572.5	2643.4	12.4	1.3	1.3	< 1
$Z(\rightarrow \nu\bar{\nu})$+3 jet		48000	14282.9	115.9	3.15	0.45	0.45	< 1
$Z(\rightarrow \nu\bar{\nu})$+4 jet		11200	3477.7	294.1	3.1	0.35	0.35	< 1
$W(\rightarrow l\nu)$+2jet		1,185,000	76017.1	3529.8	8.4	< 1	< 1	< 1
$W(\rightarrow l\nu)$+3jet		229,000	27524.6	1490.2	3.0	< 1	< 1	< 1
$W(\rightarrow l\nu)$+4jet		47200	6278.9	400.1	1.2	< 1	< 1	< 1

Table 9.6: Same as Table 9.5 but for 13 TeV LHC.

the signal cross section varies from 4.4 fb in P1 to 0.1 fb in P6. Thus for the points P1 and P2 we obtain $S/\sqrt{B} = 6.1$ and 4.4 respectively for 5 fb^{-1} which implies that P1 is discoverable while an evidence of a signal can be obtained even with low luminosity options for P2. With 100 fb^{-1} luminosity we find that the benchmarks P3 and P4 have significance values of 4.7 and 4.3 respectively.

With this strategy we attempt to explore the sensitivity in Δm for various values of $m_{\tilde{t}_1}$ at a given luminosity. We present our findings in Fig. 9.11 where the accessible region below the curves are shown in the $m_{\tilde{t}_1} - \Delta m$ plane for two luminosity options 5 fb^{-1} and 100 fb^{-1} with $S\sqrt{B} \geq 5$. This plot is presented with the assumption of $BR(\tilde{t}_1 \rightarrow c\chi_1^0) = 100\%$. We find that even for low luminosity a light stop up to a mass of $\sim$ 350 GeV could be explored for $\Delta m = 20 GeV$. As mentioned earlier this search strategy is very sensitive to lower values of Δm and it is reflected in the figure. For a luminosity of 100 fb^{-1} we find that a light stop up to a mass of 450 GeV can be probed for Δm as low as 35 GeV. The solid horizontal line demarcates the kinematic region $m_{\tilde{t}_1} < m_t + m_{\chi_1^0}$, over which the the decay $\tilde{t}_1 \rightarrow t\chi_1^0$ opens up and dominates.

9.3.5 Implications for dark matter

In scenarios with a small stop-neutralino mass splitting and a bino($\tilde{B}$) LSP, stop-coannihilation can play an important role in determining the relic dark matter abundance. This is the case especially for small Δm, i.e, where the decay $\tilde{t}_1 \rightarrow c\tilde{\chi}_1^0$ is dominant. Hence it is important to investigate the implications of our studies for probing the stop coannihilation scenario at the LHC.

The relic density crucially depends on the stop-neutralino mass difference as well as on other parameters that will be discussed in the next paragraph. For the benchmarks considered, the value of the relic density as shown in Table 9.8 is either above (P1,P3,P6) or below (P2,P4,P5) the central value for PLANCK $\Omega_{DM}h^2 = 0.1199$ [380]. However it is well known that the value of the relic density in coannihilation scenarios depends critically on the NLSP-LSP mass difference, hence

	P1	P2	P3	P4	P5	P6	Total Bg
$m_{\tilde{t}_1}, m_{\tilde{\chi}_1^0}$(GeV)	241,198	331,306	355,285	458,432	548,517	520,432	
8 TeV	2.1	0.9	0.25	0.14	0.04	0.04	70.6
$S/\sqrt{B}(20\,fb^{-1})$	1.1	0.5	0.13	0.07	0.02	0.02	
13 TeV	4.4	3.2	0.7	0.75	0.29	0.1	2.6
$S/\sqrt{B}(30$ fb$^{-1})$	15	11	2.4	2.5	1	0.3	

Table 9.7: The signal and backgrounds cross sections(cs) for benchmark points. The signal significances($S/\sqrt{B}$) for different energies and luminosities are also shown.

a small decrease (increase) in the stop-neutralino mass difference will lead to a large decrease (increase) in the value of the relic density. We have therefore searched for modified benchmarks for which the relic density was in agreement with the central value of PLANCK. For this, we vary only the mass of the lightest neutralino by changing M_1, while keeping all other parameters of each benchmark P1-P6 to their value at the EWSB scale. The modified benchmarks, P1'-P6', with the corresponding stop and neutralino masses are listed in Table 9.8. The relic density is calculated using micromegas3 [381]. Furthermore, their position in the $\Delta m - m_{\tilde{t}_1}$ plane is displayed in Figure 9.11. We find that for the benchmark points that satisfy the PLANCK constraint our search strategy works very well indeed. We achieve reasonable sensitivity for stop masses below 400 GeV with an integrated luminosity $\mathscr{L} = 100$ fb^{-1} at 13 TeV LHC as can be seen in Fig. 9.11. In fact the 5σ significance contours for $\mathscr{L} = 5$ fb^{-1} even covers the relevant Δm for stop masses below 280 GeV.

A few comments are in order to ascertain the generality of this result since the relic density depends not only on the stop-neutralino mass difference but also on the nature of the neutralino LSP, the nature of $\tilde{t}_1$ (whether it is dominantly LH or RH), and on the value of M_A. First note that the mass splittings associated with the modified benchmarks of Table 9.8 are typical of scenarios where the LSP is a bino, and these are precisely the ones where stop coannihilation plays an important role in obtaining a low enough relic density. Second, the mass splitting required to satisfy the PLANCK constraint - for a given stop mass - should depend on whether the stop is LH (P3'-P6') or RH (P1'-P2'). The reason is the following: co-annihilation processes such $\tilde{\chi}_1\tilde{t}_1 \to tg, th$ have a larger cross-section for a RH stop than for a LH stop of the same mass since the coupling to the bino LSP is proportional to the top hypercharge (which is larger for the RH top/stop), hence one would expect the required Δm to be larger for a RH stop. Furthermore the QCD processes involving pairs of squarks $\tilde{t}_1\tilde{t}_1 \to tt, \tilde{t}_1\tilde{b}_1 \to tb...$ which are more important for LH stops involve two Boltzmann suppression factors [2], therefore the mass splitting required is smaller. However since the Boltzmann factor varies rapidly with Δm, in the end there is only a few GeV differences between the case of the RH and LH stop. For example for benchmark P2', the required mass splitting would be $\Delta m = 29$GeV for a dominantly LH stop instead of $\Delta m = 37$GeV for a RH one. Finally, the pseudoscalar mass, M_A, can also be a relevant parameter. For P1' and P2' it is set by CMSSM boundary conditions and is rather high hence plays no role in neutralino annihilation while for P3'-P6', it is set to 500 GeV. A higher value of M_A- which would not affect our collider search strategy and the relevant branching ratios of $\tilde{t}_1 \to c\chi_1^0$, would imply smaller mass differences than the ones listed in Table 9.8- hence would easily be covered by our search strategy. We can therefore safely conclude that the channel investigated here can probe the stop-coannihilation scenario for stop masses up to at least 400 GeV.

[2] The Boltzmann factor is $e^{-\Delta m}/T_f$ for each coannihilating particle and T_f is the freeze-out temperature.

	P1	P2	P3	P4	P5	P6
$m_{\tilde{t}_1}, m_{\tilde{\chi}_1^0}$ (GeV)	241,198	331,306	355,285	458,432	548,517	520,432
Ωh^2	0.17	0.04	1.9	0.04	0.06	0.59
	P1'	P2'	P3'	P4'	P5'	P6'
$m_{\tilde{t}_1}, m_{\tilde{\chi}_1^0}$ (GeV)	241,205	331,294	355,315	458,420	548,508	520,479
Ωh^2	0.119	0.119	0.119	0.119	0.119	0.119
$\Delta m\ (GeV)$	36	37	40	38	40	41

Table 9.8: Relic density for the benchmarks P1-P6 and the modified benchmarks P1'-P6'

9.3.6 Conclusion

In this study we perform a comprehensive analysis of the collider search prospects of the flavor violating decay of the stop quark, namely $\tilde{t}_1 \to c\chi_1^0$. Such a scenario is well motivated in the context of natural SUSY as well as from the dark matter perspective of stop co-annihilation. It had been earlier observed that this channel is rather difficult to probe due to the low mass difference between the stop quark and the lightest neutralino. The principle background to this channel arises from QCD, $t\bar{t}$ and Z($\nu\bar{\nu}$)/W($\to l\nu$)+jets final state. We use the kinematic variables α_T and M_{T2} to effectively suppress these at 8 and 13 TeV LHC. At 8 TeV, the level of background is still high and we are limited by low stop pair production cross section. We find that our strategy is far more effective at 13 TeV due to the increase in cross section and efficient use of the kinematic variables. We observe that it is possible to discover light stop quarks up to a mass of $\sim$ 450 GeV with 100 fb^{-1} luminosity at 13 TeV LHC energy for low values of Δm and even for the case when the $\tilde{t}_1$ and χ_1^0 are almost degenerate. We observe that for very low Δm case, the loss of acceptance because of soft visible particles in the final states is compensated by ISR/FSR effects through M_{T2} selection. Note the fact that the backgrounds are expected to have some uncertianties from statistical and systematic effects, which have not been taken into account. It requires a detailed and careful further investigation. Also note, that in our case, as mentioned earlier our conclusions are crucially based on ISR effects. At the PYTHIA level where this is only taken care at the leading log level, some uncertainties are expected to appear in the final result.

The result improves significantly when one attempts identifying charm jets both at 8 and 13 TeV LHC. We also show the discoverable region in $m_{\tilde{t}_1} - \Delta m$ plane assuming the branching ration of $\tilde{t}_1 \to c\chi_1^0$ to be 100%. This is an useful information in the context of DM via stop co-annihilation. Our analysis shows that a good region of the parameter space relevant for the stop - coannihilation scenario can be probed at 13 TeV LHC energy.

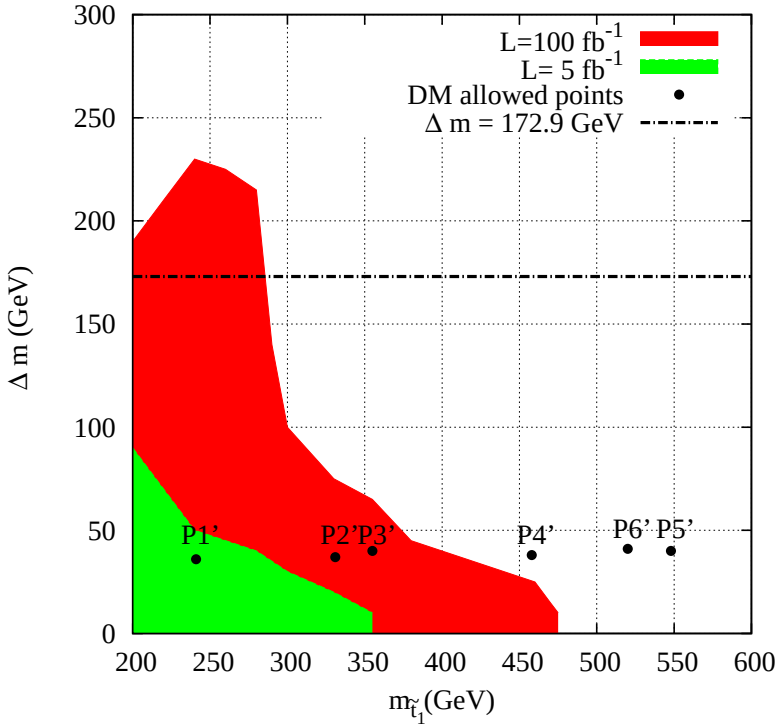

Figure 9.11: The 5 σ significance contours for $\mathscr{L} = 5$ fb^{-1} {green(light solid)}, and for $\mathscr{L} = 100 \ \ fb^{-1}$ {red(dark solid)} luminosity assuming $\tilde{t}_1 \to c\chi_1^0$ to be 100 % for 13 TeV LHC energy. The black (broken) line corresponds to $m_t = 172.9\ GeV$ and is the kinematic limit for $\tilde{t}_1 \to t + \chi_1^0$. The dark matter allowed points P1'-P6' corresponding to Table 9.8 are denoted by the black (solid) dots.

Chapter 10

Conclusion

In this thesis, the signatures of SUSY at the LHC in various scenarios were investigated. The attempt has been to explore various techniques in order to suppress the huge SM backgrounds in order to dig out a signal for SUSY.

We introduced the use of event shape variables in generic SUSY searches at the LHC for the first time. It was shown that the strategy, based on the use of transverse thrust (T) (Eq. 7.2.2), the variable R_T (Eq. 7.2.3) and the transverse mass of two leading jets M_T^{jj} (Eq. 7.2.4), the SM backgrounds could be reduced to negligible levels, retaining a significant amount of SUSY signal. It was shown that with the use of these variables one could probe gluino masses up to 1.35 TeV when $m_{\tilde{g}} \sim m_{\tilde{q}}$, and about 1.2 TeV for $m_{\tilde{g}} \ll m_{\tilde{q}}$ at 8 TeV LHC energy with 5 fb^{-1} luminosity. In the context of the CMSSM parameter space this search strategy was shown to be more effective than the ones currently employed by CMS and ATLAS, for regions of high m_0 and low $m_{1/2}$. It was also noted that this search strategy was not limited to the CMSSM but worked well for a variety of scenarios which yielded hard multijets as SUSY signatures. It should also be mentioned that at 14 TeV LHC, this strategy is expected to work even better because of high multiplicity of hard jets.

We also constrained the SUSY parameter space taking collider search data, flavor and dark matter bounds in the context of CMSSM. We argued that it is too early to write CMSSM off with the existing constraints, and it still remains a viable SUSY breaking model. However, it was observed that the high $\tan\beta$ scenario is highly constrained from the $B_s \to \mu^+\mu^-$ data.

The Higgs boson was observed to much fanfare, and although only more data and measurements of coupling and spin will finally confirm its true nature, the newly observed particle has been deconstructed within the context of BSM physics. We studied the consequences of the Higgs boson in the context of SUSY, in particular the signatures of the Higgs from the decay of sparticles. We used the method of jet substructure to probe a Higgs signature from heavy neutralino decays. It was shown that in the framework of CMSSM chargino ($\chi_1^{\pm}$) and neutralino (χ_2^0) masses up to 400 GeV could be observed in this decay mode with 100 fb^{-1} luminosity at 14 TeV center of mass energy at the LHC. We also investigated the prospect of the Higgs decaying invisibly to a pair of lightest stable neutralino in SUSY, which gives rise to an invisible decay width. The signatures of an invisible Higgs decay was studied in the Higgs production modes of vector boson fusion and associated production of Higgs with the Z boson. It was observed that one could probe an invisible branching ratio greater than 25 % at 14 TeV LHC with 300 fb^{-1} luminosity at the LHC.

The absence of a SUSY signal for the gluino and the first two generation squarks in the sub-TeV regime have prompted the consideration of third generation squarks (stops and sbottoms) as the focal point of SUSY searches at the LHC. The prospects of third generation squarks were studied

and it was observed that it is possible to discover a large part of the third generation parameter space at 13/14 TeV LHC. We studied the phenomenology of left handed sbottoms and observed that in this scenario a light sbottom up to a mass of 450 GeV could be discovered in the 4 lepton + $\not{p}_T$ channel. We also probed the flavor violating decay of the stop squark ($\tilde{t}_1 \rightarrow c\chi_1^0$) and observed that with the efficient use of certain kinematic variables light stops up to a mass of 450 GeV could be observed in this decay mode.

We conclude this thesis with the following observations and a wish list for the future,

- SUSY is still the most attractive candidate for a BSM theory. Although the early LHC run did not find a signature for SUSY, it has to be remembered that we have only skimmed the surface, and a vast region of the SUSY parameter space still remain unexplored.
- Most of the early limits on SUSY assumed specific mass relations between various sparticles. These limits are therefore highly model dependent and must be interpreted with caution.
- Some of the most interesting regions of SUSY and models like compressed SUSY require efficient kinematic variables to suppress the background. It may well be the case that we may have missed SUSY signals in the rubble of the background.
- Motivations of natural SUSY and the parameter space pertaining to third generation squarks are likely to be the focal point of SUSY phenomenology in the future. Additionally a large part of the elctroweak gaugino sector and the sleptons also remain unexplored and must be given due priority.
- LHC will continue to guide the direction at which SUSY phenomenology will proceed.
- Indirect constraints and dark matter should also be a guiding principle to look for SUSY signatures.

Bibliography

[1] **CMS** Collaboration, S. Chatrchyan et al., "Observation of a new boson at a mass of 125 GeV with the CMS experiment at the LHC," Phys.Lett. **B716** (2012) 30–61, arXiv:1207.7235 [hep-ex].

[2] **ATLAS** Collaboration, G. Aad et al., "Observation of a new particle in the search for the Standard Model Higgs boson with the ATLAS detector at the LHC," Phys.Lett. **B716** (2012) 1–29, arXiv:1207.7214 [hep-ex].

[3] A. Djouadi, "The Anatomy of electro-weak symmetry breaking. I: The Higgs boson in the standard model," Phys.Rept. **457** (2008) 1–216, arXiv:hep-ph/0503172 [hep-ph].

[4] H. Baer, V. Barger, A. Lessa, and X. Tata, "Capability of LHC to discover supersymmetry with $\sqrt{s} = 7$ TeV and $1\,fb^{-1}$," JHEP **1006** (2010) 102, arXiv:1004.3594 [hep-ph].

[5] B. Altunkaynak, M. Holmes, P. Nath, B. D. Nelson, and G. Peim, "SUSY Discovery Potential and Benchmarks for Early Runs at $\sqrt{s} = 7$ TeV at the LHC," Phys.Rev. **D82** (2010) 115001, arXiv:1008.3423 [hep-ph].

[6] T. Sjostrand, S. Mrenna, and P. Z. Skands, "PYTHIA 6.4 Physics and Manual," JHEP **0605** (2006) 026, arXiv:hep-ph/0603175 [hep-ph].

[7] M. Cacciari, G. P. Salam, and G. Soyez, "The Anti-k(t) jet clustering algorithm," JHEP **0804** (2008) 063, arXiv:0802.1189 [hep-ph].

[8] M. Cacciari, G. P. Salam, and G. Soyez, "FastJet User Manual," Eur.Phys.J. **C72** (2012) 1896, arXiv:1111.6097 [hep-ph].

[9] M. L. Mangano, M. Moretti, F. Piccinini, R. Pittau, and A. D. Polosa, "ALPGEN, a generator for hard multiparton processes in hadronic collisions," JHEP **0307** (2003) 001, arXiv:hep-ph/0206293 [hep-ph].

[10] J. Alwall, M. Herquet, F. Maltoni, O. Mattelaer, and T. Stelzer, "MadGraph 5 : Going Beyond," JHEP **1106** (2011) 128, arXiv:1106.0522 [hep-ph].

[11] S. Hoeche, F. Krauss, N. Lavesson, L. Lonnblad, M. Mangano, et al., "Matching parton showers and matrix elements," arXiv:hep-ph/0602031 [hep-ph].

[12] D. Bourilkov, R. C. Group, and M. R. Whalley, "LHAPDF: PDF use from the Tevatron to the LHC," arXiv:hep-ph/0605240 [hep-ph].

[13] **CTEQ** Collaboration, H. Lai et al., "Global QCD analysis of parton structure of the nucleon: CTEQ5 parton distributions," Eur.Phys.J. **C12** (2000) 375–392, arXiv:hep-ph/9903282 [hep-ph].

[14] A. Djouadi, J.-L. Kneur, and G. Moultaka, "SuSpect: A Fortran code for the supersymmetric and Higgs particle spectrum in the MSSM," Comput.Phys.Commun. **176** (2007) 426–455, arXiv:hep-ph/0211331 [hep-ph].

[15] A. Djouadi, M. Muhlleitner, and M. Spira, "Decays of supersymmetric particles: The Program SUSY-HIT (SUspect-SdecaY-Hdecay-InTerface)," Acta Phys.Polon. **B38** (2007) 635–644, arXiv:hep-ph/0609292 [hep-ph].

[16] F. Mahmoudi, "SuperIso: A Program for calculating the isospin asymmetry of B in the MSSM," Comput.Phys.Commun. **178** (2008) 745–754, arXiv:0710.2067 [hep-ph].

[17] W. Beenakker, R. Hopker, and M. Spira, "PROSPINO: A Program for the production of supersymmetric particles in next-to-leading order QCD," arXiv:hep-ph/9611232 [hep-ph].

[18] R. Ellis, W. Stirling, and W. R.K., "QCD and Collider Physics," Cambridge University Press. 2nd Ed. 2003 .

[19] M. Guchait and D. Sengupta, "Event-shape selection cuts for supersymmetry searches at the LHC with 7 TeV energy," Phys.Rev. **D84** (2011) 055010, arXiv:1102.4785 [hep-ph].

[20] R. M. Chatterjee, M. Guchait, and D. Sengupta, "Probing Supersymmetry using Event Shape variables at 8 TeV LHC," Phys.Rev. **D86** (2012) 075014, arXiv:1206.5770 [hep-ph].

[21] "Search for supersymmetry with the razor variables at cms," Tech. Rep. CMS-PAS-SUS-12-005, CERN, Geneva, 2012.

[22] "Search for new phenomena using large jet multiplicities and missing transverse momentum with atlas in 5.8 fb^{-1} of $\sqrt{s} = 8$ tev proton-proton collisions," Tech. Rep. ATLAS-CONF-2012-103, CERN, Geneva, Aug, 2012.

[23] "Search for squarks and gluinos with the atlas detector using final states with jets and missing transverse momentum and 5.8 fb^{-1} of $\sqrt{s}$=8 tev proton-proton collision data," Tech. Rep. ATLAS-CONF-2012-109, CERN, Geneva, Aug, 2012.

[24] M. Guchait, D. Roy, and D. Sengupta, "Probing a Mixed Neutralino Dark Matter Model at the 7 TeV LHC," Phys.Rev. **D85** (2012) 035024, arXiv:1109.6529 [hep-ph].

[25] D. Ghosh, M. Guchait, S. Raychaudhuri, and D. Sengupta, "How Constrained is the cMSSM?," Phys.Rev. **D86** (2012) 055007, arXiv:1205.2283 [hep-ph].

[26] **Heavy Flavor Averaging Group** Collaboration, D. Asner et al., "Averages of b-hadron, c-hadron, and τ-lepton Properties," arXiv:1010.1589 [hep-ex].

[27] M. Misiak, H. Asatrian, K. Bieri, M. Czakon, A. Czarnecki, et al., "Estimate of Bbar gt; X(s) gamma) at O(alpha(s)2)," Phys.Rev.Lett. **98** (2007) 022002, arXiv:hep-ph/0609232 [hep-ph].

[28] **LHCb** Collaboration, R. Aaij et al., "Strong constraints on the rare decays $B_s \to \mu^+\mu^-$ and $B^0 \to \mu^+\mu^-$," Phys.Rev.Lett. **108** (2012) 231801, arXiv:1203.4493 [hep-ex].

[29] A. J. Buras, "Minimal flavour violation and beyond: Towards a flavour code for short distance dynamics," Acta Phys.Polon. **B41** (2010) 2487–2561, arXiv:1012.1447 [hep-ph].

[30] "Search for squarks and gluinos using final states with jets and missing transverse momentum with the atlas detector in âĹŽs = 7 tev proton-proton collisions," Tech. Rep. ATLAS-CONF-2012-033, CERN, Geneva, Mar, 2012.

[31] K. Nakamura and P. D. Group, "Review of particle physics," Journal of Physics G: Nuclear and Particle Physics **37** no. 7A, (2010) 075021. http://stacks.iop.org/0954-3899/37/i=7A/a=075021.

[32] **WMAP Collaboration** Collaboration, E. Komatsu et al., "Seven-Year Wilkinson Microwave Anisotropy Probe (WMAP) Observations: Cosmological Interpretation," Astrophys.J.Suppl. **192** (2011) 18, arXiv:1001.4538 [astro-ph.CO].

[33] S. Akula, P. Nath, and G. Peim, "Implications of the Higgs Boson Discovery for mSUGRA," Phys.Lett. **B717** (2012) 188–192, arXiv:1207.1839 [hep-ph].

[34] D. Ghosh, M. Guchait, and D. Sengupta, "Higgs Signal in Chargino-Neutralino Production at the LHC," Eur.Phys.J. **C72** (2012) 2141, arXiv:1202.4937 [hep-ph].

[35] J. M. Butterworth, A. R. Davison, M. Rubin, and G. P. Salam, "Jet substructure as a new Higgs search channel at the LHC," Phys.Rev.Lett. **100** (2008) 242001, arXiv:0802.2470 [hep-ph].

[36] "Combination of standard model higgs boson searches and measurements of the properties of the new boson with a mass near 125 gev," Tech. Rep. CMS-PAS-HIG-12-045, 2012.

[37] Y. Bai, P. Draper, and J. Shelton, "Measuring the Invisible Higgs Width at the 7 TeV LHC," JHEP **1207** (2012) 192, arXiv:1112.4496 [hep-ph].

[38] D. Ghosh, R. Godbole, M. Guchait, K. Mohan, and D. Sengupta, "Looking for an Invisible Higgs Signal at the LHC," Physics Letters B **725** (2013) , arXiv:1211.7015 [hep-ph].

[39] R. Godbole, M. Guchait, K. Mazumdar, S. Moretti, and D. Roy, "Search for 'invisible' Higgs signals at LHC via associated production with gauge bosons," Phys.Lett. **B571** (2003) 184–192, arXiv:hep-ph/0304137 [hep-ph].

[40] **ATLAS** Collaboration, G. Aad et al., "Search for top and bottom squarks from gluino pair production in final states with missing transverse energy and at least three b-jets with the ATLAS detector," arXiv:1207.4686 [hep-ex].

[41] "Search for direct stop production in events with missing transverse momentum and two b-jets using 12.8 $fb-1$ of pp collisions at sqrts = 8 tev with the atlas detector," Tech. Rep. ATLAS-CONF-2013-001, CERN, Geneva, Jan, 2013.

[42] **CMS** Collaboration, S. Chatrchyan et al., "Search for new physics in events with same-sign dileptons and b jets in pp collisions at $\sqrt{s} = 8$ TeV," arXiv:1212.6194 [hep-ex].

[43] M. Adeel Ajaib, T. Li, and Q. Shafi, "Searching for NLSP Sbottom at the LHC," Phys.Lett. **B701** (2011) 255–259, arXiv:1104.0251 [hep-ph].

[44] D. Ghosh and D. Sengupta, "Searching the sbottom in the four lepton channel at the LHC," arXiv:1209.4310 [hep-ph].

[45] K. ichi Hikasa, "Heavy higgs production in ee colissions.," Physics Letters B **164** no. 4, (1985) 385 – 390. http://www.sciencedirect.com/science/article/pii/0370269385903466.

[46] L. Randall and D. Tucker-Smith, "Dijet Searches for Supersymmetry at the LHC," Phys.Rev.Lett. **101** (2008) 221803, arXiv:0806.1049 [hep-ph].

[47] A. Barr, C. Lester, and P. Stephens, "m(T2): The Truth behind the glamour," J.Phys. **G29** (2003) 2343–2363, arXiv:hep-ph/0304226 [hep-ph].

[48] A. J. Barr and C. Gwenlan, "The Race for supersymmetry: Using m(T2) for discovery," Phys.Rev. **D80** (2009) 074007, arXiv:0907.2713 [hep-ph].

[49] G. Belanger, D. Ghosh, R. Godbole, M. Guchait, and D. Sengupta, "Probing the flavor violating scalar top quark signal at the LHC," arXiv:1308.6484 [hep-ph].

[50] S. Glashow, "Partial Symmetries of Weak Interactions," Nucl.Phys. **22** (1961) 579–588.

[51] S. Weinberg, "A Model of Leptons," Phys.Rev.Lett. **19** (1967) 1264–1266.

[52] A. Salam, "Weak and electromagnetic interactions - in Elementary particle theory: relativistic groups and analyticity," N. Svartholm, ed p. 367. Almqvist and Wiksell, 1968. Proceedings of the eighth Nobel symposium. .

[53] G. 't Hooft and M. Veltman, "Regularization and Renormalization of Gauge Fields," Nucl.Phys. **B44** (1972) 189–213.

[54] D. J. Gross and F. Wilczek, "Ultraviolet behavior of non-abelian gauge theories," Phys. Rev. Lett. **30** (Jun, 1973) 1343–1346. http://link.aps.org/doi/10.1103/PhysRevLett.30.1343.

[55] H. D. Politzer, "Reliable perturbative results for strong interactions?," Phys. Rev. Lett. **30** (Jun, 1973) 1346–1349. http://link.aps.org/doi/10.1103/PhysRevLett.30.1346.

[56] S. L. Adler and W. A. Bardeen, "Absence of higher-order corrections in the anomalous axial-vector divergence equation," Phys. Rev. **182** (Jun, 1969) 1517–1536. http://link.aps.org/doi/10.1103/PhysRev.182.1517.

[57] F. Englert and R. Brout, "Broken Symmetry and the Mass of Gauge Vector Mesons," Phys.Rev.Lett. **13** (1964) 321–323.

[58] P. W. Higgs, "Broken symmetries, massless particles and gauge fields," Phys.Lett. **12** (1964) 132–133.

[59] P. W. Higgs, "Broken Symmetries and the Masses of Gauge Bosons," Phys.Rev.Lett. **13** (1964) 508–509.

[60] G. Guralnik, C. Hagen, and T. Kibble, "Global Conservation Laws and Massless Particles," Phys.Rev.Lett. **13** (1964) 585–587.

[61] P. W. Higgs, "Spontaneous Symmetry Breakdown without Massless Bosons," Phys.Rev. **145** (1966) 1156–1163.

[62] T. Kibble, "Symmetry breaking in nonAbelian gauge theories," Phys.Rev. **155** (1967) 1554–1561.

[63] J. Goldstone, "Field theories with Âń superconductor Âż solutions," Il Nuovo Cimento **19** no. 1, (1961) 154–164. http://dx.doi.org/10.1007/BF02812722.

[64] J. Goldstone, A. Salam, and S. Weinberg, "Broken symmetries," Phys. Rev. **127** (Aug, 1962) 965–970. http://link.aps.org/doi/10.1103/PhysRev.127.965.

[65] **ALEPH Collaboration, CDF Collaboration, D0 Collaboration, DELPHI Collaboration, L3 Collaboration, OPAL Collaboration, SLD Collaboration, LEP Electroweak Working Group, Tevatron Electroweak Working Group, SLD Electroweak and Heavy Flavour Groups** Collaboration, "Precision Electroweak Measurements and Constraints on the Standard Model," arXiv:1012.2367 [hep-ex].

[66] **Particle Data Group** Collaboration, J. Beringer et al., "Review of particle physics," Phys. Rev. D **86** (Jul, 2012) 010001.

[67] B. W. Lee, C. Quigg, and H. B. Thacker, "Strength of weak interactions at very high energies and the higgs boson mass," Phys. Rev. Lett. **38** (Apr, 1977) 883–885. http://link.aps.org/doi/10.1103/PhysRevLett.38.883.

[68] D. A. Dicus and V. S. Mathur, "Upper bounds on the values of masses in unified gauge theories," Phys. Rev. D **7** (May, 1973) 3111–3114. http://link.aps.org/doi/10.1103/PhysRevD.7.3111.

[69] M. S. Chanowitz, "Strong W W scattering at the end of the 90's: Theory and experimental prospects," arXiv:hep-ph/9812215 [hep-ph].

[70] M. Veltman, "Second Threshold in Weak Interactions," Acta Phys.Polon. **B8** (1977) 475.

[71] W. J. Marciano and S. S. D. Willenbrock, "Radiative corrections to heavy-higgs-scalar production and decay," Phys. Rev. D **37** (May, 1988) 2509–2514. http://link.aps.org/doi/10.1103/PhysRevD.37.2509.

[72] S. Dawson and S. Willenbrock, "Unitarity constraints on heavy higgs bosons," Phys. Rev. Lett. **62** (Mar, 1989) 1232–1235. http://link.aps.org/doi/10.1103/PhysRevLett.62.1232.

[73] T. P. Cheng, E. Eichten, and L.-F. Li, "Higgs phenomena in asymptotically free gauge theories," Phys. Rev. D **9** (Apr, 1974) 2259–2273. http://link.aps.org/doi/10.1103/PhysRevD.9.2259.

[74] B. Pendleton and G. G. Ross, "Mass and Mixing Angle Predictions from Infrared Fixed Points," Phys.Lett. **B98** (1981) 291.

[75] C. T. Hill, "Quark and Lepton Masses from Renormalization Group Fixed Points," Phys.Rev. **D24** (1981) 691.

[76] M. A. B. Bég, C. Panagiotakopoulos, and A. Sirlin, "Mass of the higgs boson in the canonical realization of the salam-weinberg theory," Phys. Rev. Lett. **52** (Mar, 1984) 883–886. http://link.aps.org/doi/10.1103/PhysRevLett.52.883.

[77] J. Bagger, S. Dimopoulos, and E. Masso, "RENORMALIZATION GROUP CONSTRAINTS IN TWO HIGGS THEORIES," Phys.Lett. **B156** (1985) 357.

[78] M. J. Duncan, R. Philippe, and M. Sher, "THEORETICAL CEILING ON QUARK MASSES IN THE STANDARD MODEL," Phys.Lett. **B153** (1985) 165.

[79] K. S. Babu and E. Ma, "Probing the desert with boson and fermion masses," Phys. Rev. Lett. **55** (Dec, 1985) 3005–3005. http://link.aps.org/doi/10.1103/PhysRevLett.55.3005.

[80] M. Lindner, M. Sher, and H. W. Zaglauer, "Probing vacuum stability bounds at the fermilab collider," Physics Letters B **228** no. 1, (1989) 139 – 143. http://www.sciencedirect.com/science/article/pii/0370269389905406.

[81] M. Sher, "Precise vacuum stability bound in the standard model," Phys.Lett. **B317** (1993) 159–163, arXiv:hep-ph/9307342 [hep-ph].

[82] G. Altarelli and G. Isidori, "Lower limit on the Higgs mass in the standard model: An Update," Phys.Lett. **B337** (1994) 141–144.

[83] J. Casas, J. Espinosa, and M. Quiros, "Improved Higgs mass stability bound in the standard model and implications for supersymmetry," Phys.Lett. **B342** (1995) 171–179, arXiv:hep-ph/9409458 [hep-ph].

[84] M. Sher, "Electroweak higgs potential and vacuum stability," Physics Reports **179** no. 5 - 6, (1989) 273 – 418. http://www.sciencedirect.com/science/article/pii/0370157389900616.

[85] G. Isidori, G. Ridolfi, and A. Strumia, "On the metastability of the standard model vacuum," Nucl.Phys. **B609** (2001) 387–409, arXiv:hep-ph/0104016 [hep-ph].

[86] G. W. Anderson, "New cosmological constraints on the higgs boson and top quark masses," Physics Letters B **243** no. 3, (1990) 265 – 270. http://www.sciencedirect.com/science/article/pii/0370269390908492.

[87] P. Arnold and S. Vokos, "Instability of hot electroweak theory: Bounds on m_h and m_t," Phys. Rev. D **44** (Dec, 1991) 3620–3627. http://link.aps.org/doi/10.1103/PhysRevD.44.3620.

[88] J. Espinosa and M. Quiros, "Improved metastability bounds on the standard model Higgs mass," Phys.Lett. **B353** (1995) 257–266, arXiv:hep-ph/9504241 [hep-ph].

[89] G. Degrassi, S. Di Vita, J. Elias-Miro, J. R. Espinosa, G. F. Giudice, et al., "Higgs mass and vacuum stability in the Standard Model at NNLO," JHEP **1208** (2012) 098, arXiv:1205.6497 [hep-ph].

[90] M. Veltman, "The Infrared - Ultraviolet Connection," Acta Phys.Polon. **B12** (1981) 437.

[91] C. F. Kolda and H. Murayama, "The Higgs mass and new physics scales in the minimal standard model," JHEP **0007** (2000) 035, arXiv:hep-ph/0003170 [hep-ph].

[92] "Experimental observation of isolated large transverse energy electrons with associated missing energy at s=540 gev," Physics Letters B **122** no. 1, (1983) 103 – 116. http://www.sciencedirect.com/science/article/pii/0370269383911772.

[93] "Observation of single isolated electrons of high transverse momentum in events with missing transverse energy at the {CERN} pp collider," Physics Letters B **122** no. 5âĂŞ6, (1983) 476 – 485. http://www.sciencedirect.com/science/article/pii/0370269383916052.

[94] **D0 Collaboration** Collaboration, "Search for high mass top quark production in $p\overline{p}$ collisions at $\sqrt{s} =$ 1.8 tev," Phys. Rev. Lett. **74** (Mar, 1995) 2422–2426. http://link.aps.org/doi/10.1103/PhysRevLett.74.2422.

[95] **CDF Collaboration** Collaboration, "Observation of top quark production in $\overline{p}p$ collisions with the collider detector at fermilab," Phys. Rev. Lett. **74** (Apr, 1995) 2626–2631. http://link.aps.org/doi/10.1103/PhysRevLett.74.2626.

[96] **CDF Collaboration, D0 Collaboration** Collaboration, T. Aaltonen et al., "Higgs Boson Studies at the Tevatron," arXiv:1303.6346 [hep-ex].

[97] **CMS Collaboration** Collaboration, S. Chatrchyan et al., "Combined results of searches for the standard model Higgs boson in pp collisions at $\sqrt{s} = 7$ TeV," Phys.Lett. **B710** (2012) 26–48, arXiv:1202.1488 [hep-ex].

[98] **ATLAS Collaboration** Collaboration, G. Aad et al., "Combined search for the Standard Model Higgs boson in pp collisions at $\sqrt{s} = 7$ TeV with the ATLAS detector," Phys.Rev. **D86** (2012) 032003, arXiv:1207.0319 [hep-ex].

[99] H. M. Georgi, S. L. Glashow, M. E. Machacek, and D. V. Nanopoulos, "Higgs bosons from two-gluon annihilation in proton-proton collisions," Phys. Rev. Lett. **40** (Mar, 1978) 692–694. http://link.aps.org/doi/10.1103/PhysRevLett.40.692.

[100] D. Graudenz, M. Spira, and P. M. Zerwas, "QCD corrections to Higgs-boson production at proton-proton colliders," Phys. Rev. Lett. **70** (Mar, 1993) 1372–1375. http://link.aps.org/doi/10.1103/PhysRevLett.70.1372.

[101] M. Spira, A. Djouadi, D. Graudenz, and P. Zerwas, "Higgs boson production at the LHC," Nucl.Phys. **B453** (1995) 17–82, arXiv:hep-ph/9504378 [hep-ph].

[102] R. Harlander and P. Kant, "Higgs production and decay: Analytic results at next-to-leading order QCD," JHEP **0512** (2005) 015, arXiv:hep-ph/0509189 [hep-ph].

[103] **LHC Higgs Cross Section Working Group** Collaboration, S. Dittmaier et al., "Handbook of LHC Higgs Cross Sections: 1. Inclusive Observables," arXiv:1101.0593 [hep-ph].

[104] S. Dawson, "Radiative corrections to Higgs boson production," Nucl.Phys. **B359** (1991) 283–300.

[105] A. Djouadi, M. Spira, and P. Zerwas, "Production of Higgs bosons in proton colliders: QCD corrections," Phys.Lett. **B264** (1991) 440–446.

[106] R. V. Harlander and W. B. Kilgore, "Next-to-next-to-leading order Higgs production at hadron colliders," Phys.Rev.Lett. **88** (2002) 201801, arXiv:hep-ph/0201206 [hep-ph].

[107] C. Anastasiou and K. Melnikov, "Higgs boson production at hadron colliders in NNLO QCD," Nucl.Phys. **B646** (2002) 220–256, arXiv:hep-ph/0207004 [hep-ph].

[108] V. Ravindran, J. Smith, and W. L. van Neerven, "NNLO corrections to the total cross-section for Higgs boson production in hadron hadron collisions," Nucl.Phys. **B665** (2003) 325–366, arXiv:hep-ph/0302135 [hep-ph].

[109] R. Cahn and S. Dawson, "Production of Very Massive Higgs Bosons," Phys.Lett. **B136** (1984) 196.

[110] R. Godbole and S. Rindani, "The equivalent vector boson approximation for intermediate mass higgs boson production," Zeitschrift Physik C Particles and Fields **36** no. 3, (1987) 395–401. http://dx.doi.org/10.1007/BF01573934.

[111] R. Godbole and S. Rindani, "The equivalent vector boson approximation for intermediate mass higgs boson production," Zeitschrift fÃijr Physik C Particles and Fields **36** no. 3, (1987) 395–401. http://dx.doi.org/10.1007/BF01573934.

[112] G. Altarelli, B. Mele, and F. Pitolli, "Heavy higgs production at future colliders," Nuclear Physics B **287** no. 0, (1987) 205 – 224. http://www.sciencedirect.com/science/article/pii/0550321387901039.

[113] T. Han, G. Valencia, and S. Willenbrock, "Structure-function approach to vector-boson scattering in *pp* collisions," Phys. Rev. Lett. **69** (Dec, 1992) 3274–3277. http://link.aps.org/doi/10.1103/PhysRevLett.69.3274.

[114] T. Figy, C. Oleari, and D. Zeppenfeld, "Next-to-leading order jet distributions for Higgs boson production via weak boson fusion," Phys.Rev. **D68** (2003) 073005, arXiv:hep-ph/0306109 [hep-ph].

[115] M. Ciccolini, A. Denner, and S. Dittmaier, "Strong and electroweak corrections to the production of Higgs + 2jets via weak interactions at the LHC," Phys.Rev.Lett. **99** (2007) 161803, arXiv:0707.0381 [hep-ph].

[116] P. Bolzoni, F. Maltoni, S.-O. Moch, and M. Zaro, "Higgs production via vector-boson fusion at NNLO in QCD," Phys.Rev.Lett. **105** (2010) 011801, arXiv:1003.4451 [hep-ph].

[117] R. V. Harlander, J. Vollinga, and M. M. Weber, "Gluon-Induced Weak Boson Fusion," Phys.Rev. **D77** (2008) 053010, arXiv:0801.3355 [hep-ph].

[118] T. Figy and D. Zeppenfeld, "QCD corrections to jet correlations in weak boson fusion," Phys.Lett. **B591** (2004) 297–303, arXiv:hep-ph/0403297 [hep-ph].

[119] E. L. Berger and J. M. Campbell, "Higgs boson production in weak boson fusion at next-to-leading order," Phys.Rev. **D70** (2004) 073011, arXiv:hep-ph/0403194 [hep-ph].

[120] S. L. Glashow, D. V. Nanopoulos, and A. Yildiz, "Associated production of Higgs bosons and Z particles," Phys. Rev. D **18** (Sep, 1978) 1724–1727. http://link.aps.org/doi/10.1103/PhysRevD.18.1724.

[121] Z. Kunszt, Z. Trocsanyi, and W. Stirling, "Clear signal of intermediate mass higgs boson production at {LHC} and {SSC}," Physics Letters B **271** no. 1, (1991) 247. http://www.sciencedirect.com/science/article/pii/037026939191308I.

[122] T. Han and S. Willenbrock, "QCD correction to the pp $\to$ WH and ZH total cross sections," Physics Letters B **273** no. 1, (1991) 167 – 172. http://www.sciencedirect.com/science/article/pii/0370269391905728.

[123] R. Hamberg, W. van Neerven, and T. Matsuura, "A Complete calculation of the order $\alpha - s^2$ correction to the Drell-Yan K factor," Nucl.Phys. **B359** (1991) 343–405.

[124] M. Ciccolini, S. Dittmaier, and M. Kramer, "Electroweak radiative corrections to associated WH and ZH production at hadron colliders," Phys.Rev. **D68** (2003) 073003, arXiv:hep-ph/0306234 [hep-ph].

[125] H. Baer, B. Bailey, and J. F. Owens, "$O(\alpha_s)$ Monte Carlo approach to $W+$ Higgs-boson associated production at hadron supercolliders," Phys. Rev. D **47** (Apr, 1993) 2730–2734. http://link.aps.org/doi/10.1103/PhysRevD.47.2730.

[126] J. Ohnemus and W. J. Stirling, "Order-α_s corrections to the differential cross section for the WH intermediate-mass Higgs-boson signal," Phys. Rev. D **47** (Apr, 1993) 2722–2729. http://link.aps.org/doi/10.1103/PhysRevD.47.2722.

[127] R. Raitio and W. W. Wada, "Higgs Boson Production at large transverse momentum in QCD," Phys.Rev. **D19** (1979) 941.

[128] J. N. Ng and P. Zakarauskas, "QCD -parton calculation of conjoined production of Higgs bosons and heavy flavors in $p\overline{p}$ collisions," Phys. Rev. D **29** (Mar, 1984) 876–886. http://link.aps.org/doi/10.1103/PhysRevD.29.876.

[129] Z. Kunszt, "Associated production of heavy higgs boson with top quarks," Nuclear Physics B **247** no. 2, (1984) 339 – 359. http://www.sciencedirect.com/science/article/pii/0550321384905534.

[130] J. Gunion, "Associated top-anti-top-higgs production as a large source of {WH} events: implications for higgs detection in the lÎ¡ÎşÎş final state," Physics Letters B **261** no. 4, (1991) 510 – 517. http://www.sciencedirect.com/science/article/pii/0370269391904653.

[131] W. J. Marciano and F. E. Paige, "Associated production of higgs bosons with pairs," Phys. Rev. Lett. **66** (May, 1991) 2433–2435. http://link.aps.org/doi/10.1103/PhysRevLett.66.2433.

[132] S. Dittmaier, . Kramer, Michael, and M. Spira, "Higgs radiation off bottom quarks at the Tevatron and the CERN LHC," Phys.Rev. **D70** (2004) 074010, arXiv:hep-ph/0309204 [hep-ph].

[133] S. Dawson, C. Jackson, L. Reina, and D. Wackeroth, "Exclusive Higgs boson production with bottom quarks at hadron colliders," Phys.Rev. **D69** (2004) 074027, arXiv:hep-ph/0311067 [hep-ph].

[134] L. Reina and S. Dawson, "Next-to-leading order results for t anti-t h production at the Tevatron," Phys.Rev.Lett. **87** (2001) 201804, arXiv:hep-ph/0107101 [hep-ph].

[135] W. Beenakker, S. Dittmaier, M. Kramer, B. Plumper, M. Spira, et al., "Higgs radiation off top quarks at the Tevatron and the LHC," Phys.Rev.Lett. **87** (2001) 201805, arXiv:hep-ph/0107081 [hep-ph].

[136] S. Dawson, C. Jackson, L. Orr, L. Reina, and D. Wackeroth, "Associated Higgs production with top quarks at the large hadron collider: NLO QCD corrections," Phys.Rev. **D68** (2003) 034022, arXiv:hep-ph/0305087 [hep-ph].

[137] J. Baglio and A. Djouadi, "Higgs production at the lHC," JHEP **1103** (2011) 055, arXiv:1012.0530 [hep-ph].

[138] S. Dittmaier, S. Dittmaier, C. Mariotti, G. Passarino, R. Tanaka, et al., "Handbook of LHC Higgs Cross Sections: 2. Differential Distributions," arXiv:1201.3084 [hep-ph].

[139] "Combined measurements of the mass and signal strength of the higgs-like boson with the atlas detector using up to 25 fb^{-1} of proton-proton collision data," Tech. Rep. ATLAS-CONF-2013-014, CERN, Geneva, Mar, 2013.

[140] **CMS** Collaboration, S. Chatrchyan et al., "Observation of a new boson with mass near 125 GeV in pp collisions at sqrt(s) = 7 and 8 TeV," JHEP **06** (2013) 081, arXiv:1303.4571 [hep-ex].

[141] N. ArkaniâĂŞHamed, S. Dimopoulos, and G. Dvali, "The hierarchy problem and new dimensions at a millimeter," Physics Letters B **429** no. 3âĂŞ4, (1998) 263 – 272. http://www.sciencedirect.com/science/article/pii/S0370269398004663.

[142] L. Randall and R. Sundrum, "Large mass hierarchy from a small extra dimension," Phys. Rev. Lett. **83** (Oct, 1999) 3370–3373. http://link.aps.org/doi/10.1103/PhysRevLett.83.3370.

[143] N. Arkani-Hamed, A. G. Cohen, and H. Georgi, "Electroweak symmetry breaking from dimensional deconstruction," Phys.Lett. **B513** (2001) 232–240, arXiv:hep-ph/0105239 [hep-ph].

[144] N. Arkani-Hamed, A. G. Cohen, T. Gregoire, and J. G. Wacker, "Phenomenology of electroweak symmetry breaking from theory space," JHEP **0208** (2002) 020, arXiv:hep-ph/0202089 [hep-ph].

[145] N. Arkani-Hamed, A. Cohen, E. Katz, and A. Nelson, "The Littlest Higgs," JHEP **0207** (2002) 034, arXiv:hep-ph/0206021 [hep-ph].

[146] P. Ramond, "Dual Theory for Free Fermions," Phys.Rev. **D3** (1971) 2415–2418.

[147] A. Neveu and J. Schwarz, "Quark Model of Dual Pions," Phys.Rev. **D4** (1971) 1109–1111.

[148] Y. Golfand and E. Likhtman, "Extension of the Algebra of Poincare Group Generators and Violation of p Invariance," JETP Lett. **13** (1971) 323–326.

[149] D. Volkov and V. Akulov, "Is the Neutrino a Goldstone Particle?," Phys.Lett. **B46** (1973) 109–110.

[150] J. Wess and B. Zumino, "Supergauge transformations in four dimensions," Nuclear Physics B **70** no. 1, (1974) 39 – 50. http://www.sciencedirect.com/science/article/pii/0550321374903551.

[151] A. Salam and J. Strathdee, "Supergauge Transformations," Nucl.Phys. **B76** (1974) 477–482.

[152] S. Coleman and J. Mandula, "All possible symmetries of the *s* matrix," Phys. Rev. **159** (Jul, 1967) 1251–1256. http://link.aps.org/doi/10.1103/PhysRev.159.1251.

[153] R. Haag, J. T. Lopuszanski, and M. Sohnius, "All possible generators of supersymmetries of the s-matrix," Nuclear Physics B **88** no. 2, (1975) 257 – 274. http://www.sciencedirect.com/science/article/pii/0550321375902795.

[154] P. Fayet and S. Ferrara, "Supersymmetry," Phys.Rept. **32** (1977) 249–334.

[155] S. Dimopoulos and H. Georgi, "Softly Broken Supersymmetry and SU(5)," Nucl.Phys. **B193** (1981) 150.

[156] N. Sakai, "Naturalness in Supersymmetric Guts," Z.Phys. **C11** (1981) 153.

[157] R. K. Kaul, "Gauge Hierarchy in a Supersymmetric Model," Phys.Lett. **B109** (1982) 19.

[158] M. Drees, R. Godbole, and P. Roy, "Theory and Phenomenology of sparticles," World Scientific , 2004 .

[159] H. Baer and X. Tata, "Weak Scale Supersymmtery," Cambridge University Press, 2006 .

[160] J. Wess and J. Bagger, "Supersymmetry and Supergravity," Princeton University Press, 2nd ed. 1992 .

[161] S. Weinberg, "The Quantum Theory of Fields: Vol. 3, Supersymmetry," Cambridge University Press, 2000 .

[162] L. O'Raifeartaigh, "Spontaneous Symmetry Breaking for Chiral Scalar Superfields," Nucl.Phys. **B96** (1975) 331.

[163] E. Cremmer, B. Julia, J. Scherk, P. van Nieuwenhuizen, S. Ferrara, and L. Girardello, "Super-higgs effect in supergravity with general scalar interactions," Physics Letters B **79** no. 3, (1978) 231 – 234. http://www.sciencedirect.com/science/article/pii/0370269378902307.

[164] E. Cremmer, B. Julia, J. Scherk, S. Ferrara, L. Girardello, and P. van Nieuwenhuizen, "Spontaneous symmetry breaking and higgs effect in supergravity without cosmological constant," Nuclear Physics B **147** no. 1, (1979) 105 – 131. http://www.sciencedirect.com/science/article/pii/0550321379904176.

[165] A. H. Chamseddine, R. Arnowitt, and P. Nath, "Locally supersymmetric grand unification," Phys. Rev. Lett. **49** (Oct, 1982) 970–974. http://link.aps.org/doi/10.1103/PhysRevLett.49.970.

[166] L. Hall, J. Lykken, and S. Weinberg, "Supergravity as the messenger of supersymmetry breaking," Phys. Rev. D **27** (May, 1983) 2359–2378. http://link.aps.org/doi/10.1103/PhysRevD.27.2359.

[167] P. Nath, R. Arnowitt, and A. Chamseddine, "Gauge hierarchy in supergravity {GUTS}," Nuclear Physics B **227** no. 1, (1983) 121 – 133. http://www.sciencedirect.com/science/article/pii/0550321383901451.

[168] N. Ohta, "Grand unified theories based on local supersymmetry," Progress of Theoretical Physics **70** no. 2, (1983) 542–549, http://ptp.oxfordjournals.org/content/70/2/542.full.pdf+html.

[169] A. Bailn and B. Love, "Supersymmetric Gauge Field Theory and String Theory," Taylor and Francis,1994 .

[170] T. Ortin, "Gravity and Strings," Cambridge University Press, 2004. .

[171] J. Terning, "Modern Supersymmetry: Dynamics and Duality," Oxford University Press, 2009. .

[172] M. Misiak and M. Steinhauser, "NNLO QCD corrections to the B X(s) gamma matrix elements using interpolation in m(c)," Nucl.Phys. **B764** (2007) 62–82, arXiv:hep-ph/0609241 [hep-ph].

[173] E. Lunghi and J. Matias, "Huge right-handed current effects in B gt;K*(K pi)l+l- in supersymmetry," JHEP **0704** (2007) 058, arXiv:hep-ph/0612166 [hep-ph].

[174] A. Freitas and U. Haisch, "Anti-B gt; X(s) gamma in two universal extra dimensions," Phys.Rev. **D77** (2008) 093008, arXiv:0801.4346 [hep-ph].

[175] S. Descotes-Genon, D. Ghosh, J. Matias, and M. Ramon, "Exploring New Physics in the C7-C7' plane," JHEP **1106** (2011) 099, arXiv:1104.3342 [hep-ph].

[176] W. de Boer, H. Grimm, A. Gladyshev, and D. Kazakov, "Higgs limit and b $>$ s γ constraints in minimal supersymmetry," Phys.Lett. **B438** (1998) 281–289, arXiv:hep-ph/9805378 [hep-ph].

[177] W. de Boer, M. Huber, A. Gladyshev, and D. Kazakov, "The b $>$ X(s)γ rate and Higgs boson limits in the constrained minimal supersymmetric model," Eur.Phys.J. **C20** (2001) 689–694, arXiv:hep-ph/0102163 [hep-ph].

[178] **LHCb** Collaboration, R. Aaij et al., "Measurement of the $B_s^0 \to \mu^+\mu^-$ branching fraction and search for $B^0 \to \mu^+\mu^-$ decays at the LHCb experiment," arXiv:1307.5024 [hep-ex].

[179] **CMS** Collaboration, S. Chatrchyan et al., "Measurement of the $B_s^0 \to \mu^+\mu^-$ branching fraction and search for $B^0 \to \mu^+\mu^-$ with the CMS Experiment," arXiv:1307.5025 [hep-ex].

[180] C. Bobeth, T. Ewerth, F. Kruger, and J. Urban, "Analysis of neutral Higgs boson contributions to the decays $\bar{B}(s) \to \ell^+\ell^-$ and $\bar{B} \to K\ell^+\ell^-$," Phys.Rev. **D64** (2001) 074014, arXiv:hep-ph/0104284 [hep-ph].

[181] R. L. Arnowitt, B. Dutta, T. Kamon, and M. Tanaka, "Detection of $B_s \to \mu^+\mu^-$ at the Tevatron run II and constraints on the SUSY parameter space," Phys.Lett. **B538** (2002) 121–129, arXiv:hep-ph/0203069 [hep-ph].

[182] F. Jegerlehner and A. Nyffeler, "The Muon g-2," Phys.Rept. **477** (2009) 1–110, arXiv:0902.3360 [hep-ph].

[183] M. Davier, A. Hoecker, B. Malaescu, and Z. Zhang, "Reevaluation of the Hadronic Contributions to the Muon g-2 and to alpha(MZ)," Eur.Phys.J. **C71** (2011) 1515, arXiv:1010.4180 [hep-ph].

[184] **Muon G-2 Collaboration** Collaboration, G. Bennett et al., "Final Report of the Muon E821 Anomalous Magnetic Moment Measurement at BNL," Phys.Rev. **D73** (2006) 072003, arXiv:hep-ex/0602035 [hep-ex].

[185] J. L. Lopez, D. V. Nanopoulos, and X. Wang, "Large (g-2)-mu in SU(5) x U(1) supergravity models," Phys.Rev. **D49** (1994) 366–372, arXiv:hep-ph/9308336 [hep-ph].

[186] A. Czarnecki and W. J. Marciano, "Muon anomalous magnetic moment: A harbinger for "new physics"," Phys. Rev. D **64** (Jun, 2001) 013014. http://link.aps.org/doi/10.1103/PhysRevD.64.013014.

[187] W. de Boer, M. Huber, C. Sander, A. Gladyshev, and D. Kazakov, "A Global fit to the anomalous magnetic moment, b > X(s) γ and Higgs limits in the constrained MSSM," arXiv:hep-ph/0109131 [hep-ph].

[188] M. Drees and M. M. Nojiri, "The Neutralino relic density in minimal $N = 1$ supergravity," Phys.Rev. **D47** (1993) 376–408, arXiv:hep-ph/9207234 [hep-ph].

[189] G. Bertone, D. Hooper, and J. Silk, "Particle dark matter: Evidence, candidates and constraints," Phys.Rept. **405** (2005) 279–390, arXiv:hep-ph/0404175 [hep-ph].

[190] **CDF Collaboration** Collaboration, D. e. a. Acosta, "Search for the supersymmetric partner of the top quark in dilepton events from $p\overline{p}$ collisions at $\sqrt{s} = 1.8$ TeV," Phys. Rev. Lett. **90** (Jun, 2003) 251801. http://link.aps.org/doi/10.1103/PhysRevLett.90.251801.

[191] **ATLAS Collaboration** Collaboration, G. Aad et al., "Search for new phenomena in final states with large jet multiplicities and missing transverse momentum at sqrt(s)=8 TeV proton-proton collisions using the ATLAS experiment," arXiv:1308.1841 [hep-ex].

[192] "Search for strong production of supersymmetric particles in final states with missing transverse momentum and at least three b-jets using 20.1 fb^{-1} of pp collisions at sqrt(s) = 8 tev with the atlas detector.," Tech. Rep. ATLAS-CONF-2013-061, CERN, Geneva, Jun, 2013.

[193] B. Bhattacherjee, A. Dighe, D. Ghosh, and S. Raychaudhuri, "Do new data on B $\to \tau\nu$ decays point to an early discovery of supersymmetry at the LHC?," Phys.Rev. **D83** (2011) 094026, arXiv:1012.1052 [hep-ph].

[194] H. Baer, V. Barger, and A. Mustafayev, "Implications of a 125 GeV Higgs scalar for LHC SUSY and neutralino dark matter searches," Phys.Rev. **D85** (2012) 075010, arXiv:1112.3017 [hep-ph].

[195] S. Akula, B. Altunkaynak, D. Feldman, P. Nath, and G. Peim, "Higgs Boson Mass Predictions in SUGRA Unification, Recent LHC-7 Results, and Dark Matter," Phys.Rev. **D85** (2012) 075001, arXiv:1112.3645 [hep-ph].

[196] J. L. Feng, K. T. Matchev, and D. Sanford, "Focus Point Supersymmetry Redux," Phys.Rev. **D85** (2012) 075007, arXiv:1112.3021 [hep-ph].

[197] S. Heinemeyer, O. Stal, and G. Weiglein, "Interpreting the LHC Higgs Search Results in the MSSM," Phys.Lett. **B710** (2012) 201–206, arXiv:1112.3026 [hep-ph].

[198] O. Buchmueller, R. Cavanaugh, A. De Roeck, M. Dolan, J. Ellis, et al., "Higgs and Supersymmetry," Eur.Phys.J. **C72** (2012) 2020, arXiv:1112.3564 [hep-ph].

[199] P. Draper, P. Meade, M. Reece, and D. Shih, "Implications of a 125 GeV Higgs for the MSSM and Low-Scale SUSY Breaking," Phys.Rev. **D85** (2012) 095007, arXiv:1112.3068 [hep-ph].

[200] J. Cao, Z. Heng, D. Li, and J. M. Yang, "Current experimental constraints on the lightest Higgs boson mass in the constrained MSSM," Phys.Lett. **B710** (2012) 665–670, arXiv:1112.4391 [hep-ph].

[201] L. J. Hall, D. Pinner, and J. T. Ruderman, "A Natural SUSY Higgs Near 126 GeV," JHEP **1204** (2012) 131, arXiv:1112.2703 [hep-ph].

[202] J. Ellis and K. A. Olive, "Revisiting the Higgs Mass and Dark Matter in the CMSSM," Eur.Phys.J. **C72** (2012) 2005, arXiv:1202.3262 [hep-ph].

[203] H. Baer, V. Barger, and A. Mustafayev, "Neutralino dark matter in mSUGRA/CMSSM with a 125 GeV light Higgs scalar," JHEP **1205** (2012) 091, arXiv:1202.4038 [hep-ph].

[204] L. Maiani, A. Polosa, and V. Riquer, "Probing Minimal Supersymmetry at the LHC with the Higgs Boson Masses," New J.Phys. **14** (2012) 073029, arXiv:1202.5998 [hep-ph].

[205] T. Cheng, J. Li, T. Li, D. V. Nanopoulos, and C. Tong, "Electroweak Supersymmetry around the Electroweak Scale," arXiv:1202.6088 [hep-ph].

[206] J.-J. Cao, Z.-X. Heng, J. M. Yang, Y.-M. Zhang, and J.-Y. Zhu, "A SM-like Higgs near 125 GeV in low energy SUSY: a comparative study for MSSM and NMSSM," JHEP **1203** (2012) 086, arXiv:1202.5821 [hep-ph].

[207] F. Brummer, S. Kraml, and S. Kulkarni, "Anatomy of maximal stop mixing in the MSSM," JHEP **1208** (2012) 089, arXiv:1204.5977 [hep-ph].

[208] C. Balazs, A. Buckley, D. Carter, B. Farmer, and M. White, "Should we still believe in constrained supersymmetry?," arXiv:1205.1568 [hep-ph].

[209] J. L. Feng and D. Sanford, "A Natural 125 GeV Higgs Boson in the MSSM from Focus Point Supersymmetry with A-Terms," Phys.Rev. **D86** (2012) 055015, arXiv:1205.2372 [hep-ph].

[210] A. Fowlie, M. Kazana, K. Kowalska, S. Munir, L. Roszkowski, et al., "The CMSSM Favoring New Territories: The Impact of New LHC Limits and a 125 GeV Higgs," Phys.Rev. **D86** (2012) 075010, arXiv:1206.0264 [hep-ph].

[211] P. Athron, S. King, D. Miller, S. Moretti, and R. Nevzorov, "Constrained Exceptional Supersymmetric Standard Model with a Higgs Near 125 GeV," Phys.Rev. **D86** (2012) 095003, arXiv:1206.5028 [hep-ph].

[212] M. W. Cahill-Rowley, J. L. Hewett, A. Ismail, and T. G. Rizzo, "The Higgs Sector and Fine-Tuning in the pMSSM," Phys.Rev. **D86** (2012) 075015, arXiv:1206.5800 [hep-ph].

[213] J. Cao, Z. Heng, J. M. Yang, and J. Zhu, "Status of low energy SUSY models confronted with the LHC 125 GeV Higgs data," JHEP **1210** (2012) 079, arXiv:1207.3698 [hep-ph].

[214] A. Arbey, M. Battaglia, A. Djouadi, and F. Mahmoudi, "The Higgs sector of the phenomenological MSSM in the light of the Higgs boson discovery," JHEP **1209** (2012) 107, arXiv:1207.1348 [hep-ph].

[215] P. Nath, "SUGRA Grand Unification, LHC and Dark Matter," arXiv:1207.5501 [hep-ph].

[216] J. Ellis, F. Luo, K. A. Olive, and P. Sandick, "The Higgs Mass beyond the CMSSM," arXiv:1212.4476 [hep-ph].

[217] M. Chakraborti, U. Chattopadhyay, and R. M. Godbole, "Implication of Higgs at 125 GeV within Stochastic Superspace Framework," arXiv:1211.1549 [hep-ph].

[218] A. Chakraborty, B. Das, J. L. Diaz-Cruz, D. K. Ghosh, S. Moretti, et al., "The 125 GeV Higgs signal at the LHC in the CP Violating MSSM," arXiv:1301.2745 [hep-ph].

[219] A. Dighe, D. Ghosh, K. M. Patel, and S. Raychaudhuri, "Testing Times for Supersymmetry: Looking Under the Lamp Post," arXiv:1303.0721 [hep-ph].

[220] **CMS Collaboration** Collaboration, "Search for supersymmetry with the razor variables at CMS,".

[221] **ATLAS Collaboration** Collaboration, "Search for squarks and gluinos using final states with jets and missing transverse momentum with the ATLAS detector in âĹŽs = 7 TeV proton-proton collisions,".

[222] S. P. Martin, "A Supersymmetry primer," arXiv:hep-ph/9709356 [hep-ph].

[223] A. Djouadi, "The Anatomy of electro-weak symmetry breaking. II. The Higgs bosons in the minimal supersymmetric model," Phys.Rept. **459** (2008) 1–241, arXiv:hep-ph/0503173 [hep-ph].

[224] S. Akula, D. Feldman, P. Nath, and G. Peim, "Excess Observed in CDF $B_s^0 \to \mu^+\mu^-$ and SUSY at the LHC," Phys.Rev. **D84** (2011) 115011, arXiv:1107.3535 [hep-ph].

[225] C. Beskidt, W. de Boer, D. Kazakov, F. Ratnikov, E. Ziebarth, et al., "Constraints from the decay $B_s^0 \geq \mu^+\mu^-$ and LHC limits on Supersymmetry," Phys.Lett. **B705** (2011) 493–497, arXiv:1109.6775 [hep-ex].

[226] A. Akeroyd, F. Mahmoudi, and D. M. Santos, "The decay $B_s \geq \mu^+\mu^-$: updated SUSY constraints and prospects," JHEP **1112** (2011) 088, arXiv:1108.3018 [hep-ph].

[227] O. Buchmueller, R. Cavanaugh, A. De Roeck, M. Dolan, J. Ellis, et al., "Supersymmetry in Light of 1/fb of LHC Data," Eur.Phys.J. **C72** (2012) 1878, arXiv:1110.3568 [hep-ph].

[228] A. Arbey, M. Battaglia, and F. Mahmoudi, "Constraints on the MSSM from the Higgs Sector: A pMSSM Study of Higgs Searches, $B_s^0 \geq \mu^+\mu^-$ and Dark Matter Direct Detection," Eur.Phys.J. **C72** (2012) 1906, arXiv:1112.3032 [hep-ph].

[229] **CMS** Collaboration, S. Chatrchyan et al., "Search for neutral Higgs bosons decaying to τ pairs in pp collisions at $\sqrt{s} = 7$ TeV," Phys.Lett. **B713** (2012) 68–90, arXiv:1202.4083 [hep-ex].

[230] O. S. BrÃijning, P. Collier, P. Lebrun, S. Myers, R. Ostojic, J. Poole, and P. Proudlock, "LHC Design Report,".

[231] **ATLAS Collaboration** Collaboration, G. Aad et al., "The ATLAS Experiment at the CERN Large Hadron Collider," JINST **3** (2008) S08003.

[232] **CMS Collaboration** Collaboration, S. Chatrchyan et al., "The CMS experiment at the CERN LHC," JINST **3** (2008) S08004.

[233] **LHCb Collaboration** Collaboration, J. Alves, A. Augusto et al., "The LHCb Detector at the LHC," JINST **3** (2008) S08005.

[234] A. Collaboration, "Alice: Physics performance report, vol. ii," Journ of Physics G: Nuclear and Particle Physics **32** no. 10, (2006) 1295. http://stacks.iop.org/0954-3899/32/i=10/a=001.

[235] G. Corcella, I. Knowles, G. Marchesini, S. Moretti, K. Odagiri, et al., "HERWIG 6: An Event generator for hadron emission reactions with interfering gluons (including supersymmetric processes)," JHEP **0101** (2001) 010, arXiv:hep-ph/0011363 [hep-ph].

[236] J. Huth and a. et, "Toward a standardization of jet definitions," FNAL-C-90-249-E, published in the proceedings of the 1990 Summer Study on High Energy Physics, Research Directions for the Decade, Snowmass, Colorado (1990) .

[237] G. Sterman and S. Weinberg, "Jets from quantum chromodynamics," Phys. Rev. Lett. **39** (Dec, 1977) 1436–1439. http://link.aps.org/doi/10.1103/PhysRevLett.39.1436.

[238] R. K. Ellis, D. Ross, and A. Terrano, "The Perturbative Calculation of Jet Structure in e+ e- Annihilation," Nucl.Phys. **B178** (1981) 421.

[239] **JADE** Collaboration, W. Bartel et al., "Experimental Studies on Multi-Jet Production in e+ e- Annihilation at PETRA Energies," Z.Phys. **C33** (1986) 23.

[240] **JADE** Collaboration, S. Bethke et al., "Experimental Investigation of the Energy Dependence of the Strong Coupling Strength," Phys.Lett. **B213** (1988) 235.

[241] S. Catani, Y. L. Dokshitzer, M. Seymour, and B. Webber, "Longitudinally invariant K_t clustering algorithms for hadron hadron collisions," Nucl.Phys. **B406** (1993) 187–224.

[242] Y. L. Dokshitzer, G. Leder, S. Moretti, and B. Webber, "Better jet clustering algorithms," JHEP **9708** (1997) 001, arXiv:hep-ph/9707323 [hep-ph].

[243] D. E. Kaplan, K. Rehermann, M. D. Schwartz, and B. Tweedie, "Top Tagging: A Method for Identifying Boosted Hadronically Decaying Top Quarks," Phys.Rev.Lett. **101** (2008) 142001, arXiv:0806.0848 [hep-ph].

[244] B. Andersson, G. Gustafson, G. Ingelman, and T. Sjostrand, "Parton fragmentation and string dynamics," Physics Reports **97** no. 2, (1983) 31. http://www.sciencedirect.com/science/article/pii/0370157383900807.

[245] L. Evans and P. Bryant, "Lhc machine," Journal of Instrumentation **3** no. 08, (2008) S08001. http://stacks.iop.org/1748-0221/3/i=08/a=S08001.

[246] P. Harrison and C. L. Smith, "Hadroproduction of supersymmetric particles," Nuclear Physics B **213** no. 2, (1983) 223 – 240. http://www.sciencedirect.com/science/article/pii/0550321383905102.

[247] E. Reya and D. Roy, "Signature for Gluino Production at the $\bar{p}p$ Collider," Phys.Lett. **B141** (1984) 442.

[248] W. Beenakker, R. Hopker, M. Spira, and P. Zerwas, "Squark production at the Tevatron," Phys.Rev.Lett. **74** (1995) 2905–2908, arXiv:hep-ph/9412272 [hep-ph].

[249] W. Beenakker, R. Hopker, M. Spira, and P. Zerwas, "Gluino pair production at the Tevatron," Z.Phys. **C69** (1995) 163–166, arXiv:hep-ph/9505416 [hep-ph].

[250] W. Beenakker, R. Hopker, M. Spira, and P. Zerwas, "Squark and gluino production at hadron colliders," Nucl.Phys. **B492** (1997) 51–103, arXiv:hep-ph/9610490 [hep-ph].

[251] W. Beenakker, M. Kramer, T. Plehn, M. Spira, and P. Zerwas, "Stop production at hadron colliders," Nucl.Phys. **B515** (1998) 3–14, arXiv:hep-ph/9710451 [hep-ph].

[252] W. Hollik, M. Kollar, and M. K. Trenkel, "Hadronic production of top-squark pairs with electroweak NLO contributions," JHEP **0802** (2008) 018, arXiv:0712.0287 [hep-ph].

[253] W. Hollik and E. Mirabella, "Squark anti-squark pair production at the LHC: The Electroweak contribution," JHEP **0812** (2008) 087, arXiv:0806.1433 [hep-ph].

[254] M. L. Mangano, "Standard Model backgrounds to supersymmetry searches," Eur.Phys.J. **C59** (2009) 373–387, arXiv:0809.1567 [hep-ph].

[255] G. L. Kane, E. Kuflik, R. Lu, and L.-T. Wang, "Top Channel for Early SUSY Discovery at the LHC," Phys.Rev. **D84** (2011) 095004, arXiv:1101.1963 [hep-ph].

[256] L. Randall and M. Reece, "Single-Scale Natural SUSY," arXiv:1206.6540 [hep-ph].

[257] C. Rogan, "Kinematical variables towards new dynamics at the LHC," arXiv:1006.2727 [hep-ph].

[258] "Search for supersymmetry in hadronic final states using mt2 with the cms detector at 7 tev," Tech. Rep. CMS-PAS-SUS-12-002, CERN, Geneva, 2012.

[259] H. Baer, C.-H. Chen, M. Drees, F. Paige, and X. Tata, "Probing minimal supergravity at the cern lhc for large tanβ," Phys. Rev. D **59** (Feb, 1999) 055014. http://link.aps.org/doi/10.1103/PhysRevD.59.055014.

[260] **ATLAS** Collaboration, G. Aad et al., "Hunt for new phenomena using large jet multiplicities and missing transverse momentum with ATLAS in 4.7 fb^{-1} of $\sqrt{s} = 7$ TeV proton-proton collisions," JHEP **1207** (2012) 167, arXiv:1206.1760 [hep-ex].

[261] T. Li, J. A. Maxin, D. V. Nanopoulos, and J. W. Walker, "The Ultra-High Jet Multiplicity Signal of Stringy No-Scale F-SU(5) at the $\sqrt{s}$ = 7 TeV LHC," Phys.Rev. **D84** (2011) 076003, arXiv:1103.4160 [hep-ph].

[262] W. Beenakker, M. Klasen, M. Kramer, T. Plehn, M. Spira, et al., "The Production of charginos / neutralinos and sleptons at hadron colliders," Phys.Rev.Lett. **83** (1999) 3780–3783, arXiv:hep-ph/9906298 [hep-ph].

[263] A. I. AHMADOV and M. DEMIRCI, "Electroweak corrections to the neutralino pair production at cern lhc," International Journal of Modern Physics A **28** no. 17, (2013) 1350077, http://www.worldscientific.com/doi/pdf/10.1142/S0217751X13500772. http://www.worldscientific.com/doi/abs/10.1142/S0217751X13500772.

[264] S. Gori, P. Schwaller, and C. E. Wagner, "Search for Higgs Bosons in SUSY Cascade Decays and Neutralino Dark Matter," Phys.Rev. **D83** (2011) 115022, arXiv:1103.4138 [hep-ph].

[265] **CMS** Collaboration, "Performance of the b-jet identification in CMS," Tech. Rep. CMS-PAS-BTV-11-001, 2011.

[266] T. Plehn, M. Spannowsky, and M. Takeuchi, "How to Improve Top Tagging," Phys.Rev. **D85** (2012) 034029, arXiv:1111.5034 [hep-ph].

[267] K. A, "talk given in MB UE meeting, CERN, 17th June, 2011,".

[268] N. Kidonakis, "Top Quark Theoretical Cross Sections and pT and Rapidity Distributions," arXiv:1109.3231 [hep-ph].

[269] A. Denner, S. Heinemeyer, I. Puljak, D. Rebuzzi, and M. Spira, "Standard Model Higgs-Boson Branching Ratios with Uncertainties," Eur.Phys.J. **C71** (2011) 1753, arXiv:1107.5909 [hep-ph].

[270] G. Belanger, F. Boudjema, A. Cottrant, R. Godbole, and A. Semenov, "The MSSM invisible Higgs in the light of dark matter and g-2," Phys.Lett. **B519** (2001) 93–102, arXiv:hep-ph/0106275 [hep-ph].

[271] G. F. Giudice, R. Rattazzi, and J. D. Wells, "Graviscalars from higher dimensional metrics and curvature Higgs mixing," Nucl.Phys. **B595** (2001) 250–276, arXiv:hep-ph/0002178 [hep-ph].

[272] M. Battaglia, D. Dominici, J. Gunion, and J. Wells, "The Invisible Higgs decay width in the add model at the LHC," arXiv:hep-ph/0402062 [hep-ph].

[273] S. Gopalakrishna, S. J. Lee, and J. D. Wells, "Dark matter and Higgs boson collider implications of fermions in an abelian-gauged hidden sector," Phys.Lett. **B680** (2009) 88–93, arXiv:0904.2007 [hep-ph].

[274] A. Drozd, B. Grzadkowski, and J. Wudka, "Multi-Scalar-Singlet Extension of the Standard Model - the Case for Dark Matter and an Invisible Higgs Boson," JHEP **1204** (2012) 006, arXiv:1112.2582 [hep-ph].

[275] K. Ghosh, B. Mukhopadhyaya, and U. Sarkar, "Signals of an invisibly decaying Higgs in a scalar dark matter scenario: a study for the Large Hadron Collider," Phys.Rev. **D84** (2011) 015017, arXiv:1105.5837 [hep-ph].

[276] K. Belotsky, D. Fargion, M. Khlopov, R. Konoplich, and K. Shibaev, "Invisible Higgs boson decay into massive neutrinos of fourth generation," Phys.Rev. **D68** (2003) 054027, arXiv:hep-ph/0210153 [hep-ph].

[277] R. E. Shrock and M. Suzuki, "Invisible decays of Higgs bosons," Phys.Lett. **B110** (1982) 250.

[278] J. R. Espinosa, M. Muhlleitner, C. Grojean, and M. Trott, "Probing for Invisible Higgs Decays with Global Fits," arXiv:1205.6790 [hep-ph].

[279] D. Carmi, A. Falkowski, E. Kuflik, T. Volansky, and J. Zupan, "Higgs After the Discovery: A Status Report," arXiv:1207.1718 [hep-ph].

[280] P. P. Giardino, K. Kannike, M. Raidal, and A. Strumia, "Is the resonance at 125 GeV the Higgs boson?," arXiv:1207.1347 [hep-ph].

[281] B. A. Dobrescu and J. D. Lykken, "Coupling spans of the Higgs-like boson," arXiv:1210.3342 [hep-ph].

[282] "Coupling properties of the new higgs-like boson observed with the atlas detector at the lhc," Tech. Rep. ATLAS-CONF-2012-127, CERN, Geneva, Sep, 2012.

[283] **ALEPH , DELPHI, CERN-L3 , OPAL** Collaboration, "Searches for invisible Higgs bosons: Preliminary combined results using LEP data collected at energies up to 209-GeV,LEP Higgs Working Group for Higgs boson searches," arXiv:hep-ex/0107032 [hep-ex].

[284] J. Gunion, "Detecting an invisibly decaying Higgs boson at a hadron supercollider," Phys.Rev.Lett. **72** (1994) 199–202, arXiv:hep-ph/9309216 [hep-ph].

[285] D. Choudhury and D. Roy, "Signatures of an invisibly decaying Higgs particle at LHC," Phys.Lett. **B322** (1994) 368–373, arXiv:hep-ph/9312347 [hep-ph].

[286] O. J. Eboli and D. Zeppenfeld, "Observing an invisible Higgs boson," Phys.Lett. **B495** (2000) 147–154, arXiv:hep-ph/0009158 [hep-ph].

[287] V. Barger, M. Ishida, and W.-Y. Keung, "Total Width of 125 GeV Higgs Boson," Phys.Rev.Lett. **108** (2012) 261801, arXiv:1203.3456 [hep-ph].

[288] B. Di Girolamo, A. Nikitenko, L. Neukermans, K. Mazumdar, and D. Zeppenfeld, "Experimental observation of an invisible Higgs boson at LHC," tech. rep., 2001.

[289] H. Davoudiasl, T. Han, and H. E. Logan, "Discovering an invisibly decaying Higgs at hadron colliders," Phys.Rev. **D71** (2005) 115007, arXiv:hep-ph/0412269 [hep-ph].

[290] C. Englert, J. Jaeckel, E. Re, and M. Spannowsky, "Evasive Higgs Maneuvers at the LHC," Phys.Rev. **D85** (2012) 035008, arXiv:1111.1719 [hep-ph].

[291] A. Djouadi, A. Falkowski, Y. Mambrini, and J. Quevillon, "Direct detection of Higgs-portal dark matter at the LHC," arXiv:1205.3169 [hep-ph].

[292] S. Bansal, K. Mazumdar, and J. Singh, "Search for invisibly decaying Higgs boson at Large Hadron Collider," Pramana **74** (2010) 231–246.

[293] K. Griest and H. E. Haber, "Invisible decays of higgs bosons in supersymmetric models," Phys. Rev. D **37** (Feb, 1988) 719–728. http://link.aps.org/doi/10.1103/PhysRevD.37.719.

[294] **ALEPH Collaboration, DELPHI Collaboration, L3 Collaboration, OPAL Collaboration, SLD Collaboration, LEP Electroweak Working Group, SLD Electroweak Group, SLD Heavy Flavour Group** Collaboration, S. Schael et al., "Precision electroweak measurements on the *Z* resonance," Phys.Rept. **427** (2006) 257–454, arXiv:hep-ex/0509008 [hep-ex].

[295] H. K. Dreiner, J. S. Kim, and O. Lebedev, "First LHC Constraints on Neutralinos," Phys.Lett. **B715** (2012) 199–202, arXiv:1206.3096 [hep-ph].

[296] M. S. Carena, J. Espinosa, M. Quiros, and C. Wagner, "Analytical expressions for radiatively corrected Higgs masses and couplings in the MSSM," Phys.Lett. **B355** (1995) 209–221, arXiv:hep-ph/9504316 [hep-ph].

[297] S. Dawson, A. Djouadi, and M. Spira, "QCD corrections to SUSY Higgs production: The Role of squark loops," Phys.Rev.Lett. **77** (1996) 16–19, arXiv:hep-ph/9603423 [hep-ph].

[298] R. V. Harlander and M. Steinhauser, "Hadronic Higgs production and decay in supersymmetry at next-to-leading order," Phys.Lett. **B574** (2003) 258–268, arXiv:hep-ph/0307346 [hep-ph].

[299] R. Harlander and M. Steinhauser, "Effects of SUSY QCD in hadronic Higgs production at next-to-next-to-leading order," Phys.Rev. **D68** (2003) 111701, arXiv:hep-ph/0308210 [hep-ph].

[300] R. V. Harlander and M. Steinhauser, "Supersymmetric Higgs production in gluon fusion at next-to-leading order," JHEP **0409** (2004) 066, arXiv:hep-ph/0409010 [hep-ph].

[301] R. V. Harlander and F. Hofmann, "Pseudo-scalar Higgs production at next-to-leading order SUSY-QCD," JHEP **0603** (2006) 050, arXiv:hep-ph/0507041 [hep-ph].

[302] G. Degrassi and P. Slavich, "On the NLO QCD corrections to Higgs production and decay in the MSSM," Nucl.Phys. **B805** (2008) 267–286, arXiv:0806.1495 [hep-ph].

[303] G. Degrassi, S. Di Vita, and P. Slavich, "NLO QCD corrections to pseudoscalar Higgs production in the MSSM," JHEP **1108** (2011) 128, arXiv:1107.0914 [hep-ph].

[304] M. Muhlleitner, H. Rzehak, and M. Spira, "MSSM Higgs Boson Production via Gluon Fusion: The Large Gluino Mass Limit," JHEP **0904** (2009) 023, arXiv:0812.3815 [hep-ph].

[305] G. Degrassi and P. Slavich, "NLO QCD bottom corrections to Higgs boson production in the MSSM," JHEP **1011** (2010) 044, arXiv:1007.3465 [hep-ph].

[306] R. V. Harlander, F. Hofmann, and H. Mantler, "Supersymmetric Higgs production in gluon fusion," JHEP **1102** (2011) 055, arXiv:1012.3361 [hep-ph].

[307] C. Anastasiou, S. Beerli, S. Bucherer, A. Daleo, and Z. Kunszt, "Two-loop amplitudes and master integrals for the production of a Higgs boson via a massive quark and a scalar-quark loop," JHEP **0701** (2007) 082, arXiv:hep-ph/0611236 [hep-ph].

[308] U. Aglietti, R. Bonciani, G. Degrassi, and A. Vicini, "Analytic Results for Virtual QCD Corrections to Higgs Production and Decay," JHEP **0701** (2007) 021, arXiv:hep-ph/0611266 [hep-ph].

[309] R. Bonciani, G. Degrassi, and A. Vicini, "Scalar particle contribution to Higgs production via gluon fusion at NLO," JHEP **0711** (2007) 095, arXiv:0709.4227 [hep-ph].

[310] M. Muhlleitner and M. Spira, "Higgs Boson Production via Gluon Fusion: Squark Loops at NLO QCD," Nucl.Phys. **B790** (2008) 1–27, arXiv:hep-ph/0612254 [hep-ph].

[311] C. Anastasiou, S. Beerli, and A. Daleo, "The Two-loop QCD amplitude gg ; h,H in the Minimal Supersymmetric Standard Model," Phys.Rev.Lett. **100** (2008) 241806, arXiv:0803.3065 [hep-ph].

[312] A. Pak, M. Steinhauser, and N. Zerf, "Towards Higgs boson production in gluon fusion to NNLO in the MSSM," Eur.Phys.J. **C71** (2011) 1602, arXiv:1012.0639 [hep-ph].

[313] **CMS** Collaboration, "Search for new physics with a monojet and missing transverse energy in pp collisions at sqrt(s) = 7 tev," Tech. Rep. CMS-PAS-EXO-11-059, CERN, Geneva, 2011. http://cdsweb.cern.ch/record/1376675.

[314] **ATLAS** Collaboration, G. Aad et al., "Search for new phenomena with the monojet and missing transverse momentum signature using the ATLAS detector in $\sqrt{s} = 7$ TeV proton-proton collisions," Phys.Lett. **B705** (2011) 294–312, arXiv:1106.5327 [hep-ex].

[315] D. Cavalli, A. Djouadi, K. Jakobs, A. Nikitenko, M. Spira, et al., "The Higgs working group: Summary report," arXiv:hep-ph/0203056 [hep-ph].

[316] B. P. Kersevan, M. Malawski, and E. Richter-Was, "Prospects for observing an invisibly decaying Higgs boson in the t anti-t H production at the LHC," Eur.Phys.J. **C29** (2003) 541–548, arXiv:hep-ph/0207014 [hep-ph].

[317] **ATLAS** Collaboration, P. Gagnon et al., "Sensitivity to an invisibly decaying Higgs boson," Tech. Rep. ATL-PHYS-PUB-2009-061, ATL-COM-PHYS-2009-220, 2009.

[318] J. Pumplin, D. Stump, J. Huston, H. Lai, P. M. Nadolsky, et al., "New generation of parton distributions with uncertainties from global QCD analysis," JHEP **0207** (2002) 012, arXiv:hep-ph/0201195 [hep-ph].

[319] T. Figy, S. Palmer, and G. Weiglein, "Higgs Production via Weak Boson Fusion in the Standard Model and the MSSM," JHEP **1202** (2012) 105, arXiv:1012.4789 [hep-ph].

[320] C. Berger, Z. Bern, L. J. Dixon, F. Febres Cordero, D. Forde, et al., "Precise Predictions for W + 4 Jet Production at the Large Hadron Collider," Phys.Rev.Lett. **106** (2011) 092001, arXiv:1009.2338 [hep-ph].

[321] H. Ita, Z. Bern, L. Dixon, F. Febres Cordero, D. Kosower, et al., "Precise Predictions for Z + 4 Jets at Hadron Colliders," Phys.Rev. **D85** (2012) 031501, arXiv:1108.2229 [hep-ph].

[322] J. M. Campbell, R. K. Ellis, and C. Williams, "Vector boson pair production at the LHC," JHEP **1107** (2011) 018, arXiv:1105.0020 [hep-ph].

[323] J. M. Campbell and R. K. Ellis, "Radiative corrections to Z b anti-b production," Phys.Rev. **D62** (2000) 114012, arXiv:hep-ph/0006304 [hep-ph].

[324] J. M. Campbell, "W / Z + B, anti-B / jets at NLO using the Monte Carlo MCFM," arXiv:hep-ph/0105226 [hep-ph].

[325] M. Schumacher, "Investigation of invisible decays of the Higgs boson at a future e+ e- linear collider," Tech. Rep. LC-PHSM-2003-096, 2003.

[326] F. Richard and P. Bambade, "Strategy to measure the Higgs mass, width and invisible decays at ILC," arXiv:hep-ph/0703173 [HEP-PH].

[327] J. Berger, J. Hubisz, and M. Perelstein, "A Fermionic Top Partner: Naturalness and the LHC," JHEP **1207** (2012) 016, arXiv:1205.0013 [hep-ph].

[328] J. Cao, C. Han, L. Wu, J. M. Yang, and Y. Zhang, "Probing Natural SUSY from Stop Pair Production at the LHC," arXiv:1206.3865 [hep-ph].

[329] J. R. Espinosa, C. Grojean, V. Sanz, and M. Trott, "NSUSY fits," JHEP **1212** (2012) 077, arXiv:1207.7355 [hep-ph].

[330] H. Baer, V. Barger, P. Huang, D. Mickelson, A. Mustafayev, et al., "Post-LHC7 fine-tuning in the mSUGRA/CMSSM model with a 125 GeV Higgs boson," Phys.Rev. **D87** no. 3, (2013) 035017, arXiv:1210.3019 [hep-ph].

[331] M. Papucci, J. T. Ruderman, and A. Weiler, "Natural SUSY Endures," JHEP **1209** (2012) 035, arXiv:1110.6926 [hep-ph].

[332] N. Desai and B. Mukhopadhyaya, "Constraints on supersymmetry with light third family from LHC data," JHEP **1205** (2012) 057, arXiv:1111.2830 [hep-ph].

[333] B. He, T. Li, and Q. Shafi, "Impact of LHC Searches on NLSP Top Squark and Gluino Mass," JHEP **1205** (2012) 148, arXiv:1112.4461 [hep-ph].

[334] M. Drees, M. Hanussek, and J. S. Kim, "Light Stop Searches at the LHC with Monojet Events," Phys.Rev. **D86** (2012) 035024, arXiv:1201.5714 [hep-ph].

[335] T. Plehn, M. Spannowsky, and M. Takeuchi, "Stop searches in 2012," JHEP **1208** (2012) 091, arXiv:1205.2696 [hep-ph].

[336] Z. Han, A. Katz, D. Krohn, and M. Reece, "(Light) Stop Signs," JHEP **1208** (2012) 083, arXiv:1205.5808 [hep-ph].

[337] V. Barger, P. Huang, M. Ishida, and W.-Y. Keung, "Scalar-Top Masses from SUSY Loops with 125 GeV mh and Precise Mw," arXiv:1206.1777 [hep-ph].

[338] A. Choudhury and A. Datta, "New limits on top squark NLSP from LHC 4.7 fb^{-1} data," Mod.Phys.Lett. **A27** (2012) 1250188, arXiv:1207.1846 [hep-ph].

[339] C.-Y. Chen, A. Freitas, T. Han, and K. S. Lee, "New Physics from the Top at the LHC," arXiv:1207.4794 [hep-ph].

[340] S. Bornhauser, M. Drees, S. Grab, and J. Kim, "Light Stop Searches at the LHC in Events with two b-Jets and Missing Energy," Phys.Rev. **D83** (2011) 035008, arXiv:1011.5508 [hep-ph].

[341] S. Kraml and A. Raklev, "Same-sign top quarks as signature of light stops at the LHC," Phys.Rev. **D73** (2006) 075002, arXiv:hep-ph/0512284 [hep-ph].

[342] Z.-H. Yu, X.-J. Bi, Q.-S. Yan, and P.-F. Yin, "Detecting light stop pairs in coannihilation scenarios at the LHC," arXiv:1211.2997 [hep-ph].

[343] M. A. Ajaib, T. Li, and Q. Shafi, "Stop-Neutralino Coannihilation in the Light of LHC," Phys.Rev. **D85** (2012) 055021, arXiv:1111.4467 [hep-ph].

[344] K. Ghosh, K. Huitu, J. Laamanen, L. Leinonen, K. Huitu, et al., "Top jets as a probe of degenerate stop-NLSP LSP scenario in the framework of cMSSM," arXiv:1207.2429 [hep-ph].

[345] B. Dutta, T. Kamon, N. Kolev, K. Sinha, and K. Wang, "Searching for Top Squarks at the LHC in Fully Hadronic Final State," Phys.Rev. **D86** (2012) 075004, arXiv:1207.1873 [hep-ph].

[346] D. S. Alves, M. R. Buckley, P. J. Fox, J. D. Lykken, and C.-T. Yu, "Stops and MET: The Shape of Things to Come," arXiv:1205.5805 [hep-ph].

[347] D. Berenstein, T. Liu, and E. Perkins, "Multiple b-jets reveal natural SUSY and the 125 GeV Higgs," arXiv:1211.4288 [hep-ph].

[348] A. Chakraborty, D. K. Ghosh, D. Ghosh, and D. Sengupta, "Stop and sbottom search using dileptonic M_{T2} variable and boosted top technique at the LHC," arXiv:1303.5776 [hep-ph].

[349] D. Ghosh, "Boosted di-boson from a mixed heavy stop," arXiv:1308.0320 [hep-ph].

[350] A. Bartl, H. Eberl, S. Kraml, W. Majerotto, W. Porod, et al., "Search of stop, sbottom, tau sneutrino, and stau at an e+ e- linear collider with S**(1/2) = 0.5-TeV - 2-TeV," Z.Phys. **C76** (1997) 549–560, arXiv:hep-ph/9701336 [hep-ph].

[351] J. Hisano, K. Kawagoe, and M. M. Nojiri, "A Detailed study of the gluino decay into the third generation squarks at the CERN LHC," Phys.Rev. **D68** (2003) 035007, arXiv:hep-ph/0304214 [hep-ph].

[352] M. Drees, Y. G. Kim, M. M. Nojiri, D. Toya, K. Hasuko, et al., "Scrutinizing LSP dark matter at the CERN LHC," Phys.Rev. **D63** (2001) 035008, arXiv:hep-ph/0007202 [hep-ph].

[353] J. Hisano, K. Kawagoe, R. Kitano, and M. M. Nojiri, "Scenery from the top: Study of the third generation squarks at CERN LHC," Phys.Rev. **D66** (2002) 115004, arXiv:hep-ph/0204078 [hep-ph].

[354] A. Alves and O. Eboli, "Unravelling the sbottom spin at the CERN LHC," Phys.Rev. **D75** (2007) 115013, arXiv:0704.0254 [hep-ph].

[355] A. Belyaev, T. Lastovicka, A. Nomerotski, and G. Lastovicka-Medin, "Discovering Bottom Squark Co-annihilation at ILC," Phys.Rev. **D81** (2010) 035011, arXiv:0912.2411 [hep-ph].

[356] H. M. Lee, V. Sanz, and M. Trott, "Hitting sbottom in natural SUSY," JHEP **1205** (2012) 139, arXiv:1204.0802 [hep-ph].

[357] E. Alvarez and Y. Bai, "Reach the Bottom Line of the Sbottom Search," JHEP **1208** (2012) 003, arXiv:1204.5182 [hep-ph].

[358] M. A. Ajaib, I. Gogoladze, and Q. Shafi, "Higgs Boson Production and Decay: Effects from Light Third Generation and Vectorlike Matter," arXiv:1207.7068 [hep-ph].

[359] **CMS** Collaboration, CMS-PAS-SUS-11-022, "Search for supersymmetery in final states with missing transverse momentum and 0, 1, 2, or $\geq$ 3 b jets with CMS,".

[360] **CMS** Collaboration, S. Chatrchyan et al., "Search for new physics in events with same-sign dileptons and b-tagged jets in pp collisions at sqrt(s) = 7 TeV," JHEP **1208** (2012) 110, arXiv:1205.3933 [hep-ex].

[361] D. E. Kaplan, K. Rehermann, and D. Stolarski, "Searching for Direct Stop Production in Hadronic Top Data at the LHC," JHEP **1207** (2012) 119, arXiv:1205.5816 [hep-ph].

[362] "Search for direct top squark pair production in final states with one isolated lepton, jets, and missing transverse momentum in sqrt(s) = 8 tev pp collisions using 13.0 ifb of atlas data," Tech. Rep. ATLAS-CONF-2012-166, CERN, Geneva, Dec, 2012.

[363] "Search for a supersymmetric top-quark partner in final states with two leptons in sqrt(s) = 8 tev pp collisions using 13 ifb of atlas data," Tech. Rep. ATLAS-CONF-2012-167, CERN, Geneva, Dec, 2012.

[364] "Search for direct top squark pair production in events with a single isolated lepton, jets and missing transverse energy at sqrt(s) = 8 tev,".

[365] **MSSM Working Group** Collaboration, A. Djouadi et al., "The Minimal supersymmetric standard model: Group summary report," arXiv:hep-ph/9901246 [hep-ph].

[366] F. Kling, T. Plehn, and M. Takeuchi, "Tagging single Tops," arXiv:1207.4787 [hep-ph].

[367] **CMS** Collaboration, CMS-PAS-BTV-11-001, "Performance of the b-jet identification in CMS,".

[368] K.-i. Hikasa and M. Kobayashi, "Light scalar top quark at colliders," Phys. Rev. D **36** (Aug, 1987) 724–732. http://link.aps.org/doi/10.1103/PhysRevD.36.724.

[369] M. Muhlleitner and E. Popenda, "Light Stop Decay in the MSSM with Minimal Flavour Violation," JHEP **1104** (2011) 095, arXiv:1102.5712 [hep-ph].

[370] C. Boehm, A. Djouadi, and Y. Mambrini, "Decays of the lightest top squark," Phys.Rev. **D61** (2000) 095006, arXiv:hep-ph/9907428 [hep-ph].

[371] A. Djouadi, M. Guchait, and Y. Mambrini, "Scalar top quarks at the run II of the Tevatron in the high tan beta regime," Phys.Rev. **D64** (2001) 095014, arXiv:hep-ph/0105108 [hep-ph].

[372] S. P. Das, A. Datta, and M. Guchait, "Four-body decay of the stop squark at the upgraded Tevatron," Phys.Rev. **D65** (2002) 095006, arXiv:hep-ph/0112182 [hep-ph].

[373] M. Carena, A. Freitas, and C. Wagner, "Light Stop Searches at the LHC in Events with One Hard Photon or Jet and Missing Energy," JHEP **0810** (2008) 109, arXiv:0808.2298 [hep-ph].

[374] G. Belanger, M. Heikinheimo, and V. Sanz, "Model-Independent Bounds on Squarks from Monophoton Searches," JHEP **1208** (2012) 151, arXiv:1205.1463 [hep-ph].

[375] "Search for new phenomena in monojet plus missing transverse momentum final states using 1 fb-1 of pp collisions at sqrts=7 tev with the atlas detector," Tech. Rep. ATLAS-CONF-2011-096, CERN, Geneva, Jul, 2011.

[376] **CMS** Collaboration, S. Chatrchyan et al., "Search for dark matter and large extra dimensions in monojet events in pp collisions at $\sqrt{s} = 7$ TeV," JHEP **1209** (2012) 094, arXiv:1206.5663 [hep-ex].

[377] C. Lester and D. Summers, "Measuring masses of semiinvisibly decaying particles pair produced at hadron colliders," Phys.Lett. **B463** (1999) 99–103, arXiv:hep-ph/9906349 [hep-ph].

[378] "Measurement of associated charm production in w final states at sqrt(s) = 7 tev," Tech. Rep. CMS-PAS-SMP-12-002, CERN, Geneva, 2013.

[379] "Search for pair-produced top squarks decaying into a charm quark and the lightest neutralinos with 20.3 fb^{-1} of pp collisions at $\sqrt{s} = 8$ tev with the atlas detector at the lhc," Tech. Rep. ATLAS-CONF-2013-068, CERN, Geneva, Jul, 2013.

[380] **Planck** Collaboration, P. Ade et al., "Planck 2013 results. XVI. Cosmological parameters," arXiv:1303.5076 [astro-ph.CO].

[381] G. Belanger, F. Boudjema, A. Pukhov, and A. Semenov, "micrOMEGAs3.1 : a program for calculating dark matter observables," arXiv:1305.0237 [hep-ph].